St George's University of London

INSTITUTE FOR INFECTION & IMMUNITY

Mycobacterium tuberculosis infection suppresses the expression of host genes involved in lysosomal targeting in the macrophage

Rebecca Flynn

Thesis submitted for the Degree of Doctor of Philosophy
St George's University of London 2022

I declare the work presented in this thesis is my own work. Where published work of others has been consulted this has been fully acknowledged.

To Dad, sadly you couldn't see me complete this part of my journey though I could not have gotten here without you.

Acknowledgments

Firstly, I am extremely grateful to my supervisor Prof P Butcher for his invaluable advice, continuous support, and patience during my PhD. I would also like to thank Dr J Dhillon for her assistance at every stage of the research project, Dr K Laing and the 'Bugs' team for their help and support, and Dr A Nohturfft for his initial ideas and supervision. I would also like to express my thanks to Dr Olivier Neyrolles (French National Centre for Scientific Research) and Prof Graham Stewart (University of Surrey) for supplying the mutants used for this study. Finally, I would like to express my gratitude to my friends and family for their support and encouragement over the years.

Abstract

Mycobacterial modulation of phagosome maturation in infected cells is a widely studied area in host-pathogen interactions, yet there is still no definitive understanding of all the mechanisms involved. Infection with *M. tuberculosis* (*M.tb*) is well known for a resultant modulation of gene expression of the host cell. This study identified and investigated three macrophage genes suppressed during *M.tb* infection, involved in lysosomal trafficking pathways: *RILP, OSBPL1a* and *RIN2*, with the hypothesis that *M.tb* infection actively suppresses the expression in order to disrupt phagolysosome fusion resulting in pathogen survival.

Two approaches were taken, the first, co-localisation studies using constructed cell lines over-expressing *RILP, OSBPL1a* and *RIN2*. The second approach was to analyse host cell gene expression in response to *M.tb* mutants known to be trafficked to the lysosome. Fluorescence microscopy co-location studies in *RIN2* over-expressing transfected macrophage cell lines exhibited differential trafficking of *M.tb*. Gene expression of *M.tb* in response to *RILP, RIN2* and *OSBPL1a* over-expression revealed changes to notable genes associated with exposure to the phagosomal environment. Finally, macrophage infections with *M.tb* mutants known to be trafficked to the lysosome, revealed that a *moaC1* mutant was unable to suppress the expression of *RILP* and *OSBPL1a,* indicating an active role in *M.tb* survival by blocking phago-lysosomal maturation.

The intention of this study was to gain a better understanding of the mechanisms by which *M.tb* evades lysosomal destruction to aid in devising potential new host-directed and pathogen-directed strategies for treatment and prevention of the disease, tuberculosis.

Table of contents

List of tables and figures

List of abbreviations

Abbreviation	Meaning
ADC	Albumin dextrose complement
BCG	Bacillus Calmette-Guérin
CaMKII	calmodulin-dependent protein kinase II
CRs	complement receptors
DCs	Dendritic cells
EEA1	early endosome antigen1
FBS	Fetal bovine serum
FcγRs	Fc receptor
GO	Gene ontology
IRES	internal ribosome entry site
LAM	Lipoarabinomannan
LM	Lipomannan
MAMPs	microbe-associated molecular patterns
ManLAM	mannose-capped lipo-arabinomannan
MP	monocyte-derived macrophages
MRs	mannose receptors
NADPH	nicotinamide adenine dinucleotide phosphate
PAMPs	molecular patterns expressed by pathogens
PBCs	primary blood cells
PBMCs	primary blood monocytic cells
PDIM	phthiocerol dimycocerosates
PI(3)P	phosphatidylinositol 3-phosphate
PIMs	phosphatidylinositol mannosides
PMA	phorbol 12- myristate 13-acetate
PRRs	pattern recognition receptors
RNS	reactive nitrogen species
ROS	reactive oxygen species
SapM	secreted acid phosphatase
Sec	secretion pathway
T(1-7)SS	Type (1-7) secretion system
TACO	tryptophan-aspartate containing coat protein
Tat	twin-arginine translocation
TDM	Trehalose-6,6-dimycolate
TEM	transmission electron microscopy
TLRs	Toll-like receptors
Tn	transposon
V-ATPase	vacuolar H+ ATPases

Chapter 1 - Introduction

Mycobacterium tuberculosis (M.tb), one of the world's most formidable pathogens, in the latest report from WHO (2020), an estimated 10 million people fell ill and a total of 1.4 million people died of TB in 2019. *M.tb* has evolved to use macrophages as a natural habitat and evade the humoral component of the adaptive immune response, antibodies, as well as evading complement components. Within cells, *M.tb* deploys many mechanisms to circumvent macrophage defences, enabling it to escape from macrophage killing and to replicate within these phagocytes. In order for new strategies for the control of this intracellular pathogen to be developed, a better understanding of the fundamental biology of the interaction between *M.tb* and the host cell, is required. The research presented in this thesis directly addresses this area of fundamental cell biology and host-pathogen interaction by investigating components of both the bacteria and the host cell in order to derive molecular mechanisms underpinning this highly complex biological cross-talk process.

The Macrophage

Macrophages are one of the main lines of defence the body has against microorganisms. Macrophages are professional phagocytes and phenotypically diverse (Jakubzick et al., 2017); they migrate to and circulate within almost every tissue; their role is critical for the uptake and degradation of infectious agents and senescent cells. Despite this role, macrophages serve as the natural habitat of *M.tb*.

Phagocytic cells have a highly evolved system of pattern recognition receptors (PRRs) which recognise molecular patterns expressed by pathogens (PAMPs), or microbe-associated molecular patterns (MAMPs) specific to bacteria; these patterns are conserved and shared by a large number of infectious agents. Surface PRRs, including mannose receptors (MRs) and C-type lectins, function so as to recognise, and also bind the bacteria to the surface of the macrophage, thus facilitating phagocytosis. An example of a mannose receptor ligand is the mannose-capped lipo-arabinomannan (ManLAM) found of the surface of mycobacteria. Another family of receptors, the Toll-like receptors (TLRs) are specific to lipopeptides, lipopolysaccharides and flagellin (Weiss and Schaible, 2015).

Molecules called opsonins from the humoral host defence system also recognise antigens and bind to the bacterial cell surface, thus opsonising the bacteria. Opsonins are a group of molecules including complement, antibodies, fibronectin and mannose-binding

lectin. Opsonisation allows the bacteria to be recognised by a number of different receptors the most important for phagocytosis being the complement receptors (CRs), and by Fc receptors (FcγRs) of specific antibodies (Lohmann-Matthes et al., 1994). The subsequent signalling induces receptor-mediated phagocytosis.

Principles of phagocytosis

Despite the variety of receptors, there is a common phagocytosis pathway after the adherence of the microbe to the surface of the macrophage resulting from the recognition of a PAMP. Signalling from the phagocytic receptors results in actin polymerisation at the site of ingestion, thus, extending pseudopods around the bacteria. Sequentially adjacent receptors attach to the surface of the microbe, thus, the plasma membrane of the phagocytic cell is pulled around the microbe. This process leads to the extrusion of the plasma membrane and eventual internalisation, forming the phagosome (Stockinger et al., 2006). Post-internalisation, actin is shed from the phagosome, and the phagosome matures via a series of fusion and fission events with components of the endocytic pathway. This maturation involves a coordinated interaction between actin and tubulin-based cytoskeletons (Aderem and Underhill, 1999), and culminates in the fusion of the phagosome with a lysosome.

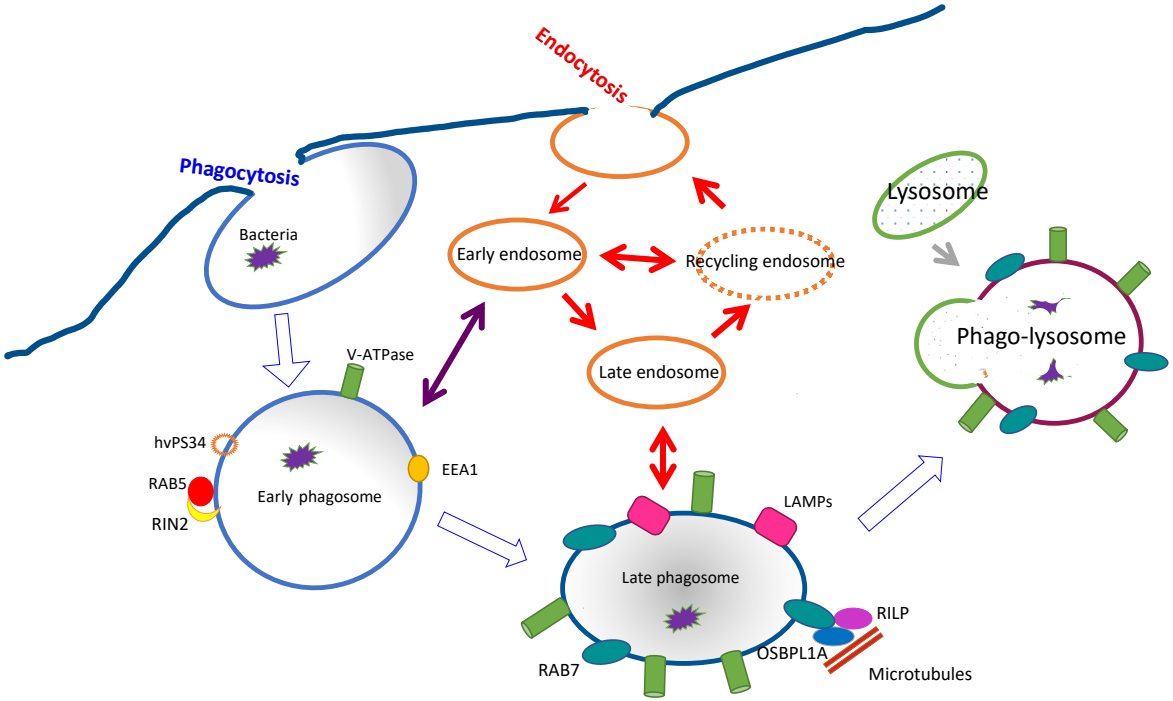

Figure 1.1- Phagosome maturation happens through a series of fusion and fission events with endosomes, the early phagosome acquires the small GTPase RAB5, early endosome antigen1 (EEA1), and the type III phosphatidylinositol (PI) 3-kinase hVps34. As maturation continues Rab5 is exchanged for RAB7 and the phagosome gets more acidic. RAB7 recruits RILP and OSBPL1A forming a heterotrimeric complex that is essential for the assembly of microtubule motor, this facilitates the fusion with lysosomes to form phago-lysosomes. Phago-lysosomes are acidic and contain a variety of degradative enzymes. (Uribe-Querol and Rosales, 2017).

The phagosomal stages can roughly be spilt into three: i) early phagosomes at around ten minutes' post-uptake; ii) late phagosomes, between ten to thirty minutes; and iii) after thirty minutes, phagolysosomes (Figure 1.1). These timings are dependent on the receptors initiating the uptake. For example, FcγR-mediated phagocytosis hastens the maturation of the phagosome compared to CR-mediated uptake. MR-mediated engulfment has been shown to not consistently result in immediate phagosome maturation (Kang et al., 2005).

Early phagosomes share many properties of early endosomes and are attained from fusion with sorting and recycling endosomes. They are mildly acidic (pH 6.1-6.5) and have little hydrolytic activity (Mukherjee et al., 1997). There are many proteins involved in the normal maturation of the phagosome; integral to this process is the small GTPase Rab5. Fusion between early endosomes and newly formed phagosomes is thought to rely on the presence of Rab5. This small GTPase forms complexes with RIN2 (Ras And Rab Interactor 2 protein) and the type III phosphatidylinositol (PI) 3-kinase hVps34, resulting in the generation of PI 3-phosphate (PI(3)P). (Sandri et al., 2012). Presence of PI(3)P is required for the recruitment of early endosomal antigen 1, mediating vesicle docking and fusion (Lawe et al., 2000). Phagosomes rapidly lose the characteristics of early endosomes, while attaining those of late endosomes. As the phagosomes mature, Rab5 is lost and replaced by small GTPase Rab7, permitting the fusion with Rab7-enriched late endosomes. Rab7 also forms a complex with Rab-interacting lysosomal protein (RILP) and Oxysterol Binding Protein Like 1A (OSBPL1a), which is essential for the assembly of the microtubule motors that move the phagosome towards the microtubule organising centre of the cell (Johansson et al., 2007a). The late phagosomes then fuse with lysosomes forming phago-lysosomes, which are the terminal degradation compartment of the endocytic pathway, and can be distinguished from endosomes, in part by the presence of lysosome-associated membrane protein (LAMP)-1 (Chang et al., 2002). Phago-lysosomes contain enzymes such as cathepsins, proteases, lipases and lysozymes, capable of degradation of microorganisms; they also contain scavenger molecules to recycle components from the bacteria.

Macrophage defence mechanisms against intracellular bacteria

As the phagosome matures the contained bacteria are subjected to a barrage of microbicidal mechanisms, and below the main strategies are described: i) vacuole acidification. ii) free radical generation. iii) antimicrobial peptides.

i) Acidification

During maturation from an early phagosome to a phago-lysosome the membrane amasses vacuolar H^+ ATPases (V-ATPase), which trans-locates protons in to the phagosome (Westman and Grinstein, 2021). The increase in the number of V-ATPase complexes results in a rise in the acidity of the phagosome; from a pH of 6.1-6.5 in early phagosomes, to a pH of 5.5-5.6 in late phagosomes, down to a pH of 4.5-5 in phago-lysosomes. This low pH is a hostile environment for most bacteria, as it disrupts normal metabolism in multiple ways, including disruption of membranes by hydrolysing lipids, impairing DNA replication by hydrolysing RNA and DNA, disruption of protein functional group ionization causing proteins to denature (Guan and Liu, 2020). The H^+ gradient across the membrane resulting from the V-ATPase also impairs trafficking of nutrients required for bacterial growth by limiting access to macro- and micro-nutrients (Marshansky and Futai, 2008).

ii) Free-radical formation

Phago-lysosomes accumulate both reactive oxygen species (ROS) and reactive nitrogen species (RNS). These radicals can damage proteins, lipids, and DNA and thus are efficient antimicrobial agents. V-ATPase also plays a role in the production of ROS, nicotinamide adenine dinucleotide phosphate (NADPH) oxidase transfers electrons from NADPH on to oxygen creating O_2^- which joins with the H^+ to form H_2O_2, this complex produces hydroxyl radicals (OH^-) or single oxygen molecules, both of which are highly reactive (Bogdan et al., 2000).

RNS are produced when L-arginine and oxygen react to give L-citrulline and $NO^·$, this reaction is catalysed by the enzyme nitric oxide synthase 2. $NO^·$ alone can have a detrimental effect on bacterial growth, it can also join with the ROS and form a wide variety of RNS such as peroxynitrite which is highly toxic (Flannagan et al., 2009).

iii) Antimicrobial proteins and peptides

The effector mechanisms of phagosomes that hinder bacterial growth include proteins and small peptides, which can roughly be broken down in to three groups - bacteriostatic, bactericidal and degradative enzymes. Bacteriostatic agents prevent growth of bacteria by limiting the bacteria's access to nutrients; one example of this would be the scavenger molecule, Lactoferrin, which sequesters iron, making it unavailable to the bacteria. Bactericidal agents such as defensins, disrupt the bacterial membrane causing permeabilization. Defensins bind to the cell surface and form multimeric ion-permeable channels; these allow the efflux of essential ions and nutrients from the bacteria. Degradative enzymes include an array of endopeptidases, exopeptidases and hydrolyses. These degrade various components of the bacteria such as carbohydrates, lipids and proteins, leading to the destruction of the bacteria (Flannagan et al., 2009).

Evasion of macrophage defence mechanisms by intracellular pathogens

Despite these highly effective defence mechanisms of the macrophage, a number of highly virulent intracellular bacteria have evolved mechanisms that enable them to circumvent these and thus survive and replicate. It is known that some pathogens can survive within phagocytes and even take advantage of the internalisation pathways to enter the cells (Sarantis and Grinstein, 2012). Intracellular bacteria colonize two distinct regions of the host cell, either the cytosol or vacuoles. The cytosolic bacteria escape from the endocytic pathway early on, to subsequently replicate in the cell cytosol, whereas the intravacuolar bacteria are able to inhabit and replicate within the host endomembrane system; this involves complex host-pathogen interactions. The vesicles containing the pathogen are modified and become unique organelles within the host cell (Mitchell et al., 2016). For example, vacuoles containing *Coxiella burnetti* resemble large, acidic, LAMP1 positive vacuoles. Similarly, *Salmonella enterica* reside in late endocytic acidic vesicles. Whereas vacuoles containing *Legionella pneumophila* resemble endoplasmic reticulum, *Chlamydia pneumonia* containing vacuoles have no notable

features, and initially *M.tb* vacuoles resemble early endosomes, the fate of *M.tb* after the initial infection is discussed later (see below) (Price and Vance, 2014).

The general strategies utilised for survival by intravacuolar bacteria involve: avoidance, blockage and adaptation to the phagolysosomal pathway, nutrient acquisition by disruption of host vesicle trafficking, enlargement of the vacuolar space and maintenance of the vacuole integrity.

Integrity of the vacuole

The ability of the bacteria to maintain the vacuoles in which they reside is essential for survival, as it prevents the bacteria from being recognised by the cytosolic innate immune sensors (e.g. NOD1 or NOD2 that recognise bacterial peptidoglycan) (Heim et al., 2019). The formation of the specialised vacuoles containing bacteria requires modulation of small host GTPases by the bacteria; this modulation of the small GTPases also contributes to vacuole stability. *Legionella* employs such a mechanism: it has an effector, LidA, which contributes to maintaining vacuole viability by recruiting the small GTPases Rab1 (Mitchell et al., 2016). Formation also relies on vesicle trafficking, which is dependent on the host cytoskeleton network (Amer and Swanson, 2002). Bacterial pathogens have been found to exploit effector proteins to remodel the cytoskeleton to their advantage. *Salmonella typimurium* has been shown to actively induce the formation of a mesh made of actin cytoskeleton around the vacuole it resides in; this was found to be necessary in order for the bacteria to replicate (Kühn et al., 2020).

Specialised secretion systems

As already discussed, bacteria must remain in the vacuole in order to be undetected in the cell; however, for survival the bacteria must exert actions beyond the vacuole. To do this many bacteria employ secretion systems, which allow proteins to be secreted out of the vacuole, that in turn modify the cytosolic environment. There are a number of secretion systems that have been identified: to date a minimum of 15 classes, all with varying functions (Costa et al., 2015; Denise et al., 2020; Green and Mecsas, 2016). Some secretion systems are common across many bacteria and are able to secrete a broad range of proteins, however, some are much more specific and found only in a small number of bacteria and simply secrete

one or two proteins. The different classes vary in the ability of the protein substrate to cross a single phospholipid membrane, or two or three membranes, in the case of three two would be bacterial and one host, thus, allowing proteins to be secreted out of the vacuole by the bacteria. Five of the currently identified secretion systems are able to transport protein substrates across three membranes directly from the cytoplasm: type I, III, IV, VI, and VII (Denise et al., 2020). These will be the focus of the following section.

The type I secretion system (T1SSs) is widely found in Gram-negative bacteria, it is composed of only three membrane proteins, making it one of the simplest of the secretion systems. It mediates the translocation of a large number of different proteins in one step; these proteins have a variety of purposes including nutrient acquisition and virulence (Kanonenberg et al., 2018).

The type III secretion system (T3SSs) also known an injectisome is found predominately in Gram-negative bacteria. It is formed of a series of rings spanning the inner and outer membranes and connects the bacteria to the cytosol with a hollow filament (Büttner, 2012). They secrete a wide variety of protein substrates across the inner and outer bacterial membranes and across a eukaryotic cell membrane in one step, allowing direct transfer from the bacteria in to the cytoplasm of the host cell, this makes them essential for virulence of many vacuole dwelling bacteria, including both *Salmonella enterica* and *Chlamydia* species, along with many other bacteria. Although their function is not uniform among different species, in general the proteins they secrete act as effectors remodelling cellular functions which aid the pathogen in establishing an infectious niche (Puhar and Sansonetti, 2014).

A number of intravacuolar Gram-negative bacteria employ the type IV secretion system (T4SS); like the T3SS it can span both the bacterial membranes and an additional host cell membrane. The T4SS is the only secretion system that is able to transport nucleic acid as well as proteins. This function is employed by *Neisseria gonorrhoeae* to mediate DNA uptake aiding in the acquisition of virulence genes (Hamilton and Dillard, 2006). It has been found to be essential for pathogenesis of *Legionella pneumophila*, employing it to translocate more than 200 effector proteins

into the host cell (Vogel et al., 1998), *and Coxiella burnetti* which also employs the ability to transport proteins to the host cytosol (Carey et al., 2011).

Type VI secretion systems (T6SS) are also found in intravacuolar Gram-negative bacteria, with *Salmonella* species harbouring five distinct types which are distributed among serotypes (Blondel et al., 2013). Interestingly T6SSs are capable of transporting proteins not only in to the host cell from within the vacuole, but also between bacteria in a contact-dependent manner (Russell et al., 2014).

Type VII secretion systems (T7SSs) are much more specialised and only found in bacteria with heavily lipidated cell walls such as *Mycobacteria* (Bunduc et al., 2020) *and Corynebacteria.* When first identified in *M. tuberculosis* in 2003 they were called ESX systems (Stanley et al., 2003), much work has focused on understanding both the structure and function of T7SSs, but there still remains a large number of questions. To date five T7SSs have been identified in *Mycobacteria*, ESX-1 to ESX-5; ESX-1 is considered important for virulence as it is lost in the attenuated strain of *M.bovis* - Bacillus Calmette-Guerin (BCG) (Brodin et al., 2006). ESX-3 and ESX-4 are the only T7SSs that are common across all *Mycobacteria* species;, ESX-4 appears to be oldest system and potentially the progenitor for the other 4, whereas ESX-3 is involved in metal ion acquisition and has been found to be critical for growth in vitro (Tufariello et al., 2016). ESX-5 appears to be the most recently evolved and plays a role in nutrient uptake and thus, necessary for growth (Ates et al., 2015)

Many studies cover the structure of the systems and research is ongoing as to how these T7SSs contribute to virulence and survival of the bacteria within the vacuole of the host cell. In this regard, ESX-1, ESX-3 and ESX-5 have been shown by knockout studies to be required for full virulence and viability of *M.tb* (Green and Mecsas, 2016; Rivera-Calzada et al., 2021).

Interference with phagosome maturation

To remain protected inside the specialised vacuole, bacteria must also prevent the compartment from being trafficked to the terminal phago-lysosome. Blocking of phagosome maturation has been shown to occur at different points. Some pathogens prevent acidification, others reduce the activity of the NADPH oxidase, while some prevent phagosome-lysosome fusion. *Streptococcus pyogenes* avoids acidification of its vacuole by blocking recruitment of V-ATPase. This process

is thought to be regulated by the transcription factor, Mga, which regulates the expression of surface proteins (Nordenfelt et al., 2012). *Salmonella typhimurium* is able to prevent NADPH oxidase from being trafficked towards vacuoles containing *Salmonella.* It is believed that the *Salmonella* pathogenicity island 2 effectors are responsible for this prevention (Wang et al., 2020).

One of the most studied pathogens that interferes with phagosome maturation is *M.tb*. The following sections will focus on the survival of *M.tb* inside host macrophages.

Mycobacteria tuberculosis

Goren et al., in 1976 first described the ability of *M.tb* to inhibit phago-lysosome fusion and acidification within the vacuolar compartment in which they reside (Goren et al., 1976). Since then there has been considerable work to identify the different mechanisms. *M.tb* have been shown to have a wide range of mechanisms to survive within macrophages, some unique and some shared with other pathogens. Here the current knowledge of those mechanisms will be covered in more detail.

Mycobacterial modulation of phagosome maturation is partially dependent on the cell wall structure. The cell wall is made up of two parts, the inner and outer. The inner section closest to the plasma membrane is called the cell wall core; it is composed of peptidoglycan covalently bonded to arabinogalactan, which in turn is attached to the mycolic acids. There are three classes of mycolic acids: alpha-mycolates, keto-mycolates and methoxymycolates. It is these mycolic acids which give the morphological trait of cording and are closely linked to virulence. The outer section of the wall is considered to be comprised of the signalling and effector molecules in amongst lipids and glycolipids, it is often called the mycomembrane (Daffé and Marrakchi, 2019). It is mainly composed of free lipids, with varying lengths of fatty acid chains, interspersed are the cell wall proteins, the phosphatidylinositol mannosides (PIMs), the phthiocerol dimycocerosates (PDIM), lipomannan (LM), and lipoarabinomannan (LAM). PIM has been shown to mediate early endosomal fusion to allow access to nutrients (Vergne et al., 2015). LAM has

been found to be important for the arrest in phagosome maturation. LAM binds to mannose receptors on macrophages, blocking calcium signalling via the Ca^{2+}/calmodulin-dependent protein kinase II (CaMKII) complex and inhibits PI(3) kinase (hVPS34), which as previously discussed is necessary for the generation of PI(3)P, which is required for vesicle docking and fusion (Brennan, 2003). This contributes to the *M.tb* containing vacuole resemblance to an early endosome (Rajaram et al., 2017) (Figure 1.2).

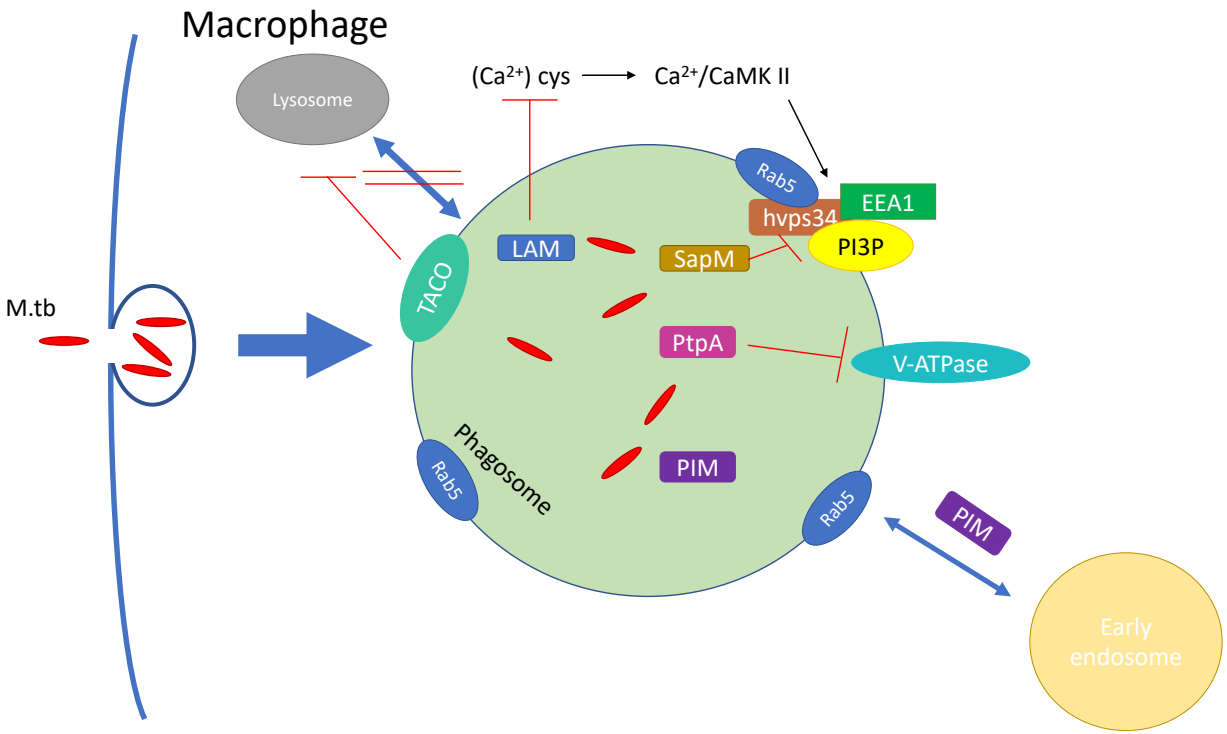

Figure 1.2 Phagosome maturation inhibition: LAM & SapM prevent the recruitment of EEA1. LAM also inhibits Ca^{2+}/ CaMKII signalling inhibiting in turn PI(3) kinase. ptpA blocks v-ATPase trafficking, PIM mediates early endosomal fusion to allow access to nutrients. TACO is retained on the phagosome preventing fusion with the lysosome. Figure modified from Peddireddy et al., (2017)

The bacteria influence the extra-phagosomal environment via secretion of virulence factors. This is made possible through multiple pathways: general secretion pathway (Sec) and twin-arginine translocation (Tat) pathway for protein export, and the more specialised, SecA2, and T7SSs as previously mentioned (Feltcher et al., 2010).

M.tb has been shown to secrete phosphatases such as secreted acid phosphatase (SapM), protein tyrosine phosphatase A and B (PtpA, PtpB), which dephosphorylate kinases and block v-ATPase trafficking respectively (Vergne et al., 2005)(Figure 1.2). During normal maturation, the phagosome becomes increasingly acidified but phagosomes containing the *M.tb* bacilli may become only mildly acidified (pH6.2) in comparison to normal phagosomes (pH 4.5 or lower). Currently three different strategies have been proposed. First, it was proposed that the bacilli-containing phagosomes were inhibited from fusion with proton-ATPase-containing vesicles, thus blocking the acidification. However, if this fusion does takes place, the complex is removed rapidly (Sturgill-Koszycki et al., 1994). Later *M.tb* was found to secrete phosphatase PtpA, which interacts with the H subunits of the H+ V-ATPase complex and prevents the assembly of the V-ATPase machinery (Wong and Jacobs, 2011). Mycobacterial cord factor Trehalose-6,6-dimycolate (TDM) interaction with the membrane-bound C-type lectin receptor (Mincle) has been shown to delay phagosomal maturation and acidification (Patin et al., 2017). The method of V-ATPase removal was also identified recently, Queval et al., 2017 found that *M.tb* induces the expression of cytokine-inducible SH2-containing protein, this targets directly a V-ATPase catalytic subunit A for ubiquitination and degradation.

The early endosomal marker Rab5 is retained on the vacuole containing the *M.tb*. Rab5 is thought to control the identity and functionality of the compartment, meaning its retention contributes to the arrest of maturation to late endosome. Maturation of the compartment is defined as the presence of Rab7, but the transition from Rab5 positive to Rab7 positive is much debated and no clear mechanism has been defined, although it is thought that the lipids in the cell wall plays a role, as mentioned above (Mottola, 2014). Research has shown the process

to be highly complex with a large number of effectors involved; one example of this is the secreted *M.tb* nucleoside diphosphate kinase (Ndk). It has been shown to have GTPase activating protein activity towards Rab5 and Rab7, suggesting an involvement in the retention of Rab5 (Sun et al., 2010). However, Ndk knockouts only show a slight reduction of survival suggesting that there are multiple strategies of preventing maturation of the phagosome (Spanò and Galán, 2018).

Rab5 is not the only protein retained by the *M.tb*-containing vacuole: tryptophan-aspartate containing coat protein (TACO) is recruited and retained on the phagosome membrane (Ferrari et al., 1999) (figure 2). TACO is an actin-binding protein, which associates with cholesterol within the plasma membrane. Normally the release of TACO is thought to trigger lysosomal fusion; however, its retention has been shown to activate calcium-calcineurin signalling blocking the fusion of lysosomes (Jayachandran et al., 2007).

Despite years of research there is still no definitive understanding of all the mechanisms involved in the arrest of phagosome maturation. The list of proteins implicated is long, however, their identification is mostly based on observational evidence and many of the mechanisms of action, not mentioned above are yet to be described. It is possible that some of the proteins are essential for intracellular persistence rather than involved in the disruption of trafficking. For example, mutants that cannot survive in the intravacuolar environment will be unable to maintain the vacuole, and thus phago-lysosome fusion with occur.

Is *M.tb* a true intra-vacuolar pathogen?

Recently an editorial hailed it as the 'escape room world champion' in an up to date review (Nguyen et al., 2019). Nguyen et al. discussed the multiple levels of escape mechanisms resulting in the pathogenicity of *M.tb*, beginning with the escape from lysosomal fusion, continuing with the shielding from humoral components of the immune system such as complement, then the breakout of the phagosome into the cytoplasm.

Over the years an increasing number of studies have reported that *M.tb* escapes the vacuole into the cytoplasm. This isn't a new question; as far back as 1984 Leake et al. reported this phenomenon, and it was also observed by electron

microscopy by multiple groups (McDonough et al., 1993; Myrvik et al., 1984). Other groups failed to reproduce these results and the vacuolar-escape research question remained controversial. As technology has improved this issue arose again, with the identification of cytosolic *M.tb* using in vitro 4 days post-infection human dendritic cells (DCs) using cryo-immunogold transmission electron microscopy (TEM) (van der Wel et al., 2007). A review by Welin and Lerm, (2012) covers the re-ignition of interest in this debate, which still continues. Welin and Lerm question if the cytosolic *M.tb* seen by TEM was due to the bacteria outgrowing their phagosome, or in fact membrane disruption during apoptotic cell death (de Chastellier, 2009). Many factors can influence experimental outcome of in-vitro infections: the cell lines used, the multiplicity of infection, the infection duration, the protocols followed for not only the infection but the preparation for imaging. Welin et al., 2011, found the presence of cytosolic *M.tb* in necrotic cells supporting the idea that the escape is a result of general membrane lysis during cell death, rather than a direct virulence strategy.

In more recent years the focus has turned to not only if the bacteria can escape the vacuole, but how. The technology to visualise the escape of the *M.tb* in real time at a single cellular level was developed by Simeone et al., (2012). This established a link between vacuole escape and cell death of the host. Repasy et al., (2013) demonstrated this was dose-dependent, greater cell death occurred with higher bacterial burden.

In light of this, the ability of the bacteria to escape from the vacuole does not negate the importance of its ability to modify the host environment and arrest phagosome maturation, as this potentially allows for the build-up of the bacterial burden in a protected environment.

In the past much of the research has been aimed at the post-transcriptional modulation of the host cell leading to the arrest of phagosome maturation. However, as technology has advanced the focus has shifted towards the functional genomics of the host-pathogen interaction.

Modulation of host cell gene expression

The basic premise of functional genomics, which includes whole genome level transcriptome data generated by microarray analysis or more recently by RNA

sequencing, is to generate novel information to generate new hypotheses as to the function of genes and gene products, thereby elucidating fundamental biological processes that were intractable prior to the genomic era.

Transcriptional profiling has become a powerful tool in deciphering the effect of a pathogen on gene expression of the host cell. High-throughput methods allow simultaneous identification and analysis of thousands of genes and their interactions during the infection process. A number of recent studies have used this tool to investigate the global changes to host gene expression post infection with *M.tb* (see Table 1.1).

M.tb is well known for manipulating gene expression of the host cell. Many examples of both up- and down-regulated genes post infection have been reported, although the follow-on experimental focus on differentially expressed genes has been on up-regulated genes. The majority of studies of host cell transcription are looking for biomarkers of disease in patient primary blood cells (PBCs), with the aim of contributing to diagnosis and distinguishing clinical groups (Jacobsen et al., 2007; Lesho et al., 2011; Maertzdorf et al., 2011; Ottenhoff et al., 2012).

Studies using either immortalised or naïve primary blood monocytic cells (PBMCs) are fewer in number and use lab strains of *M.tb* (as listed in Table 1.1). This research generally focuses on immune-related responses and intracellular signalling, again discussing only the up-regulated genes. Two studies have used cytokine gene arrays to look at human genes known for immunoregulation and identified a large number of up-regulated cytokines, for example, interleukin (Il)-1, Il-8, IFN-gamma and TNF-alpha (Ragno et al., 2001; Volpe et al., 2006).

Most recently Lee et al., (2019) used RNA-Seq to compare transcriptome differences in naïve bone-marrow-derived macrophages (BMDMs) and those infected with either H37Rv or H37Ra. This is the first of such studies using RNA-Seq. They studied the expression of over 9000 genes and found 750 genes significantly differentially expressed in both Rv and Ra infected cells, 131 only in Rv infected cells and 413 in Ra infected cells. Using this method they were also able to analyse the *M.tb* transcriptome in the same sample, highlighting the power of this new type of analysis. Lee et al. concluded their study with the identification of solute carrier family 7 member 2 (Slc7a2) as an important protein for suppressing intracellular

growth in macrophages. Slc7a2 was highly expressed in avirulent H37Ra infected macrophages compared with H37Rv infected macrophages; it is a cationic amino acid transporter which transports arginine. Arginine is required for NO production. As discussed previously, NO production is an important defence against intracellular bacterial infection, and its suppression in *M.tb* infected macrophages would aid in bacterial survival.

Host cell	*M.tb* Strains	# Replicates	Platform	GEO acc #	Reference	PMID
Patient PBCs	Clinical strains	-	AMADID 011412; Agilent Technologies		(Jacobsen et al., 2007)	17318616
Patient PBCs	Clinical strains	-	Affymetrix Human Genome 133 Plus 2.0		(Lesho et al., 2011)	21835698
Patient PBCs	Clinical strains	-	whole-genome 4x44 k human expression arrays	GSE28623	(Maertzdorf et al., 2011)	22046420
Patient PBCs	Clinical strains	-	Illumina HumanRef-8 V3 BeadChip		(Ottenhoff et al., 2012)	23029268
J774A.1	H37Ra, BCG, *M. smegmatis*	-	Affymetrix MOE430_2	GSE45675	(Zhang, 2013)	23824656
Mouse lung	H37Ra, H37Rv	-	Whole Mouse Genome 44 k microarrays		(Beisiegel et al., 2009)	19795415
Mouse lung	H37Rv	4	Agilent's mouse 44k microarrays		(Shepelkova et al., 2013)	23276693
THP-1	H37Rv	3	Panorama human cytokine gene arrays (Sigma-Genosys)		(Ragno et al., 2001)	11576227
U937	H37Rv	-	BioDoor 12800 microarray		(Xu et al., 2003)	12890386
Naïve PBMCs	H37Rv	-	Panorama human cytokine gene arrays (Sigma-Genosys)		(Volpe et al., 2006)	16895554
Naïve PBMCs	H37Rv	9	Human U133A oligonucleotide microarray chips		(Tailleux et al., 2008)	18167562
THP-1	H37Rv, clinical strains	-	HG-U133 Plus 2.0 array		(Wu et al., 2012)	22675550
Murine BMM	HN878, CDC1551	3	Affymetrix mouse GeneChip Gene ST 1.0	GSE31734	(Koo et al., 2012)	22280836
Naïve whole blood	H37Rv	-	Illumina HumanHT-12 V4.0 expression beadchip	GSE108363	(Both et al., 2018)	29330469
Murine BMDMs	H37Rv, H37Ra	2	Illumina HiSeq2500	PRJNA50644	(Lee et al., 2019)	30858471

Table 1.1 Summary of literature published on host cell transcription post M. tuberculosis infection.

Still the most complete study measuring both host cell and bacterial gene expression is that of Tailleux et al (2008) looking at the functional categories of genes with altered expression, with 9 biological replicates over three time points (4, 18 and 48 hours) using human peripheral blood monocytes differentiated with cocktails of cytokines into both macrophage and dendritic type cells. They report host cell lysosomal genes to be amongst those genes with the greatest altered expression. More recently, Zhang (2013) reported that the most down-regulated genes are involved in a variety of processes including cellular process pathways (e.g. phagosome and endocytosis), cell cycle, and metabolic processes. As down-regulated genes have been neglected in most studies to date and thus are poorly understood, the question arises as to whether the effect *M. tb* has on phagosome maturation is due to down-regulation of the host genes during the infection process.

Transcriptional adaptation of intracellular *M.tb*.

Just as the macrophage transcriptome reacts to infections, changes also occur in the transcriptome of the intracellular mycobacteria, however, the capture of the transcriptome of the bacteria during infection is difficult and possibly variable due to adverse bacterium-to-host ratio effects on infection outcome and low multiplicity of infection effects. Transcriptional profiling studies have provided a consensus model of bacterial transcriptional changes that infer the adaptations required for the *M.tb* to survive within the macrophage.

One of the first discoveries was the switch from aerobic to anaerobic respiration, along with the up-regulation of the dormancy regulon (dosR), found when comparing the intra-phagosomal transcriptome with the transcriptome of *M.tb* grown in standard broth (Schnappinger et al., 2003a). Since then many groups have built on this work, using a combination of sequencing, RNA-seq, microarrays and quantitative real-time PCR, all broadening the understand of intracellular *M.tb* (Cappelli et al., 2006; Dubnau et al., 2005; Fontán et al., 2008; Gerrick et al., 2018; Koo et al., 2012; Rachman et al., 2006).

The transcriptional changes that *M.tb* undergoes can be summarised into six main categories; lipid metabolism, respiratory state, growth rate, transcriptional regulation, nutrient acquisition, and virulence factors. Much is still unknown about the environmental cues or the mechanisms causing these changes, or their effect on the host (Waddell, 2010).

Transcriptional changes have shown *M.tb* able to switch to using fatty acids as a carbon source while inside phagosomes. This switch is characterised by the upregulation of multiple β-oxidation genes (*fadA, fadB, echA, fadE* and *fadD*) (Schnappinger et al., 2003a). It is suggested that these degradative enzymes are a key metabolic adaptation to intracellular life, and their induction could directly or indirectly result in virulence factor expression (Waddell, 2010). Along with switching carbon sources towards fatty acids and cholesterol inside phagosomes, transcription profiling also revealed that *M.tb* alternates between three respiratory states rather than the two first predicted. The first being aerobic growth during which aa_3-type oxidase, type 1 NADH dehydrogenase and cytochrome C reductase systems operate. As oxidative stress increases, these become downregulated, leading to the second intermediate state. During the intermediate state a less energy-efficient cytochrome bd oxidase and the nitrate transporter NarK2 are both up-regulated, suggesting a shift towards nitrate respiration. The final state is the complete shift to anaerobic respiration (Shi et al., 2005). These and many other discoveries have been made comparing the gene expression of intracellular to *in vivo* populations of *M.tb*, using transcriptional profiling, and while it remains a powerful tool there are limitations, and many of the mechanisms remain elusive.

A heterogeneous range of virulence factors have been identified using large pools of transposon mutants, identifying any gene which if disrupted causes attenuation of the bacteria (Shi et al., 2005). Due to the limitations of the methods employed for such studies, many of the genes or the transcribed proteins have unknown functions, or are generally required for growth, so it remains very difficult to elucidate which genes or proteins are directly involved specifically in counteracting the microbicidal host cell responses.

In the context of this thesis, both *M.tb* gene expression patterns associated with the intra-macrophage environments and the macrophage gene expression responses during stages of infection with *M.tb* are being used to interrogate host-pathogen interactions that underpin the diseases processes of tuberculosis. In doing so, mechanisms may be elucidated of this highly complex and multi-layered biological interaction.

Aims and Objectives

The aim of this research, therefore, was to explore the hypothesis that *M.tb* actively suppresses the expression of genes involved in phagolysosome biogenesis and trafficking. The intention was to gain a better understanding of the mechanisms by which *M.tb* evades lysosomal destruction and to aid in devising new strategies for treatment and for the prevention of disease.

This research built upon previously published microarray data from *M.tb* infected human macrophages and dendritic cells (Tailleux et al., 2008). The transcriptional data was re-analysed with a focus on known genes in phagolysosomal generation, function and remodelling of which there are about 200. Significant changes in gene expression (up or down) would imply a significant role in the *M.tb*-macrophage interaction. These were identified from the retrospective array data and the expression levels verified by qPCR. Experiments using validated qPCR assays to interrogate expression levels of selected genes were performed using models of infection of various macrophage-like cell lines and compared with published data, with the aim of establishing a tractable experimental model, which is comparable to the data obtained from PBMCs, to further investigate the phagolysosomal biogenesis hypothesis.

Further investigations of the selected genes consisted of a two-pronged approach. Firstly, stable cell lines were constructed over-expressing the selected host genes (downregulated during infection with *M.tb*), using the cells proven as the most appropriate model, closely mimicking the previously published data. This cell line was then infected with *M.tb* and assessed for bacterial killing efficiency and cell survival. Alongside this, they were stained by immunofluorescence post-infection for markers of phagosomal maturation, such as RAB7 and lysosomal marker LAMP1, to assess for phagosome-lysosome fusion. These were then studied using confocal microscopy with the hypothesis that over-expression of these normally down-regulated genes caused by *M.tb* infection counteracts the suppression by *M.tb,* allowing phagosomal maturation. Therefore, the cells transfected would stain for both mature phagosomal markers and potentially phagolysosome markers. Alongside this, gene expression analysis of the macrophage derived *M.tb* was measured to look for altered expression in response to the over-expressed proteins which act as surrogate markers for altered host-pathogen interactions.

The second approach involved investigating selected *M.tb* mutants obtained from a previously reported transposon (Tn) library. These mutant strains have been confirmed to be rapidly trafficked into acidified compartments (Brodin et al., 2010). They were used in place of the virulent lab strain in a previously established infection model, and qPCR assays were used to interrogate expression levels of the selected genes post-infection. With the genes mutated in the *M.tb* known, it was anticipated that this would lead to the identification of the bacterial genes involved in the down-regulation of the selected host-genes. Identifying *M.tb* genes associated with alterations to phagosome maturation and endosome trafficking inside macrophages will enable molecular mechanisms to be derived for such a complex biological interplay, for which to date very few candidate processes or gene products have been defined that explain this attributed virulence strategy on *M.tb*.

Chapter 2 - Materials and Methods

2.1 Cellular microarray data analysis

For the analyses of the microarray data taken from Tailleux (2008), the raw data were background-corrected and normalised using the Bioconductor GCRMA package as described in (Wu et al., 2004). These probe sets based on full-length cDNAs, assigned to a single gene and annotated as "grade A" according to Affymetrix annotation files, were used for further analyses. Probe IDs were replaced with gene symbols, and data for genes represented by more than one probe set were averaged. Genes with average expression values of less than one standard deviation (SD) under all four conditions were considered not expressed and excluded. In the remaining matrix (12,185 genes) values below 1 SD were set to 1 SD. Variances between pairs of triplicate data were then compared with an F test (R 'var.test' function); if the resulting p value was greater than 0.05, an unpaired Student's t test was performed; otherwise, Welch's t test was used (R 't.test' function). The p values returned by the t tests were corrected for multiple hypotheses testing using the false discovery rate method (R 'p.adjust' function). Log (base2) fold changes were set to zero when p values returned by p.adjust were greater than 0.05.

The resulting data set was saved as an R data frame in binary format for subsequent analyses. These analyses were performed using R studio Version 0.97.551. Gene ontology data were based on lists downloaded from the AmiGO gene ontology site (Carbon et al., 2009, http://amigo.geneontology.org/amigo). Lists of lysosomal genes were based on combined mouse and human annotations for the GO terms 'lysosome' (GO:0005764) and 'vacuole' (GO:0005773), which were extended based on reviews of the lysosomal proteome (Lübke et al., 2009; Schröder et al., 2010). The list of transcription factors was taken from the literature (Ravasi et al., 2010) and the list of vesicular transport genes was based on human annotations for the GO term 'vesicle-mediated transport' (GO:0016192). Gene expression correlation analyses and production of graphics were performed as described (Brignull et al., 2013).

2.2 Tissue culture methods

2.2.1 Cell lines

For this study three cell lines were used; J774 (murine monocyte macrophage cell line), RAW 264.7 (murine leukaemic monocyte macrophage cell line) and U937 (human leukemic monocyte lymphoma cell line)(Sundström and Nilsson, 1976).

2.2.2 Maintenance of cell lines

All tissue culture work was performed in laminar flow hoods and cells were incubated at 37°C with 5% CO_2. The U937 cells were cultured in RPMI 1640 medium containing Glutamax, 10% heat inactivated Fetal Bovine Serum (FBS). Cultures were established from frozen stocks, by centrifugation with subsequent resuspension at 1 to 2 X 10^5viable cells/ml and maintained at a cell density between 1 to 2 X 10^6 viable cells/ml. replacing the media every three to four days. Frozen stocks were stored in freezing media containing 30% FBS and 10% DMSO.

For the adherent cell lines J774 and RAW 264.7, the culture medium was Dulbecco's modified eagles containing 10% FBS. Re-feeding every two to three days as required until the cells reach confluency. Once confluent, the cells were sub-cultured at a ratio of 1:5 by scraping, aspirating and dispensing into new flasks. For infections, confluent cells were harvested and seeded in six-well plates at a density of 2 to 4x10^6 cells per well and grown for 24 hours prior to infection. Culture mediums were supplemented with 400ug/ml hygromycin and 500ug/ml G418 where appropriate.

2.2.3 Stimulation of U937 cells

For the U937 non-adherent cells, phorbol 12- myristate 13-acetate (PMA) was added to the six well plates at a concentration of 100ng per ml. Treatment of U937 cells with PMA stimulates the cells to differentiate and adhere to the surface of the tissue culture flasks, allowing excess un-phagocytosed bacteria to be washed off the adhered cells after infection. The cells were incubated for 24 hours at 37°C before infections were performed.

2.3 Mycobacterial strains and Culture media

2.3.1 Mycobacteria strains

All strains were treated as ACDP Hazard group 3 organisms; work was conducted in a Class 1 microbiological safety cabinet in containment level 3 conditions.

Table 2.1 Complete list of strains used in this study, the transposon mutants are referred to by the nomenclature Tn:: and the gene interrupted. The mutants were constructed by transposition of the IS1096-derived Tn5367 transposon into the M.tb *strain GC1237 (Brodin et al., 2010).These known mutants were provided for use in the study as a kind gift from Dr Olivier Neyrolles (French National Centre for Scientific Research) and Prof Graham Stewart (University of Surrey), following guidelines for safe and appropriate transfer of HG3 organisms to SGUL. For further details see Chapter 7 section 7.2.*

Strain	Origin
***M.bovis* BCG Pasteur strain (BCG)**	Gift from Tanya Parish (Queen Mary's hospital)
H37Rv *M. tuberculosis* (RV)	lab strains originally purchased from ATCC
H37Ra *M. tuberculosis* (RA)	
***M.tb* GC1237 (parent strain for the Tn mutants)**	Gift from Graham Stewart (University of Surrey)
Tn::*moaC1*	
Tn::*moaC1* complemented with pYUB412 derived cosmid.	
Tn::*moaD1*	
Tn::*Rv1506c*	
Tn::*lppM*	Gift from Olivier Neyrolles (University of Toulouse)
Tn::*pstS3*	
Tn::*Rv1503c*	
Tn::*Rv2295*	
Tn::*Rv3880c espL*	

2.3.2 Mycobacterial growth media

Mycobacteria were grown in 7H9 liquid medium – 2.35g Middlebrook 7H9 Broth Base in 450ml of distilled water and 2ml glycerol, autoclaved, allowed to cool to 45°C, then supplemented with Middlebrook albumin dextrose complement (ADC) growth supplement.

The mycobacterial cultures were set up from 1ml mid-log phase culture stocks, stored in 1.5ml cryovials in liquid nitrogen. These were added to 5ml of pre-warmed supplemented 7H9 in a 30ml universal (Passage 1, P1), and incubated at 37°C. The cultures were passaged every 7 days by transferring 2ml of freshly vortexed culture to a new 30ml

universal of sterile medium (P2). Cultures were only used up until passage number 5 (P5) to avoid mutations associated with continuous passage.

Mycobacteria were plated on Middlebrook 7H11 agar - 21g of Middlebrook agar in 900ml of distilled water plus 5ml glycerol, autoclaved, allowed to cool to 55°C, then 100ml of Oleic acid albumin dextrose complement (OADC) growth supplement was added. 10cm vented plates were poured and allowed to set, plates were dried upside down at 37°C overnight before use. Inoculated plates were incubated upside down in a sealed plastic bag at 37°C for 4 weeks.

2.3.3 Infections

The cell lines were infected with mid log phase *M. tuberculosis* strains at a multiplicity of infection (MOI) 20:1 (bacilli:cells). Prior to infection, the bacteria were centrifuged at 3000 rcf for 10 minutes and the pellet resuspended in supplemented RPMI. This was repeated, then the bacterial suspension was sonicated in five second bursts five times to disassociate the clumps but without disrupting the bacteria. The bacteria were counted using a Helber counting chamber. For the infection of U937 cells, RAW 264.7 cells, and J774 cells, the optimum MOI was found to be 20:1

The infections were performed in the six-well plates in 4ml of the appropriate media with 10% FBS. The plates were incubated for the desired time intervals with the maximum of 24 hours before the bacteria were removed by washing with pre-warmed media, fresh media was added, and the wells were then incubated up to a further 24 hours.

2.4 CFU counts

Enumeration of the bacteria on the surface of the cells (cell associated) and the intracellular bacteria were performed at various time points post-infection. For the cell associated count, the cells were washed twice with RPMI 1640 and the final wash was plated in serial dilutions on 7H11 with 10% added OADC agar plates. To measure the intracellular bacteria, after washing the cells were lysed using 0.25% sodium dodecyl sulfate (SDS). The lysate was sonicated (as above) and plated in triplicate serial dilutions on 7H11 with 10% added OADC agar plates. The mycobacterial colonies on the plates were counted after incubation at 37°C for four weeks. Triplicate plates were averaged, and CFU were calculated and plotted as the mean CFU per ml from triplicate wells.

2.5 Construction of transfection plasmids

As no commercial plasmids for RILP RIN2 or OSBPL1a were available, the plasmids were constructed for this project. The cDNA clones were purchased from the I.M.A.G.E consortium.

IRAK51K20 Image 5174974 – *RILP*

IRAK35D08 Image 3156682 – *RIN2*

IRAK198D21 Image 5264608 – *OSBPL1a*

The clones arrived in an *E. coli* culture stab and were used to inoculate agar plates containing Ampicillin (Amp) (100µg/ml) and incubated overnight at 37°C. Single colonies were then picked and 7ml Luria broth (LB) with Amp (100µg/ml) was inoculated. All cultures were propagated from a single colony and grown at 37°C at 220 rpm for aeration.

2.5.1 Extraction of Plasmid DNA

Plasmid extraction was performed using the NucleoSpin^{å} plasmid mini kit following the manufacturers guidelines. The saturated *E. coli* LB culture was pelleted at 37,500 rcf for 20 minutes at 20°C. All further centrifugation steps were performed in a microcentrifuge at 11,000 x g at RT. The *E. coli* pellet was re-suspended with 500µl Buffer A1 and decanted into a 1.5ml microfuge tube. 500µl of Buffer A2 was then added and mixed gently by inversion, and then incubated at RT for 5 minutes. After the incubation, 600µl of Buffer A3 was added and mixed by inversion until the blue sample turned colourless; this was then centrifuged for 10 minutes. The supernatant was pipetted into a NucleoSpin^{å} Plasmid Column in a collection tube, centrifuged for 1 minute and the flow-through discarded. The column was then washed with 500µl of buffer AW preheated to 50°C and centrifuged for 1 minute, discarding the flow-through. A further 600µl of Buffer A4 was added and again centrifuged for 1 minute, discarding the flow-through. The membrane was then dried by centrifugation for 2 minutes. The column was placed into a clean 1.5ml microcentrifuge tube and 50µl of buffer AE preheated to 70°C was added; the column was then incubated for 2 minutes at 70°C. The plasmid DNA was eluted by centrifugation for 1 minute. The final DNA concentration was measured with a Nanodrop N-1000 spectrophotometer.

2.5.2 Transformation of *E. coli*

Heat shock transformation was used to transform competent bacteria with plasmid DNA. The competent *E. coli* were thawed on ice for 20 minutes; once thawed the 3µl of DNA was mixed with 30µl of cells and gently mixed, and then incubated on ice for 20 minutes. Each tube was heat shocked by being submerged into a 42°C water bath for 45 seconds, then returned to the ice for 2 minutes. The bacteria were then plated on to an agar plate containing Amp (100µg/ml) and incubated at 37°C overnight. For new plasmids, an additional step was added prior to plating; 800µl of pre-warmed LB broth was added to the bacteria and grown in a shaking incubator for 45 minutes, before spinning down and removing 750µl of media. The pellet was re-suspended and the remaining 50µl was plated.

2.5.3 Restriction Digestion

Restriction enzyme digestions were used to cleave DNA plasmids. All restriction enzymes digests were performed according to the manufacturer's instructions (NEB, UK). A typical digest reaction consisted of 1µg of DNA, the corresponding amount of the appropriate 10x restriction enzyme digestion buffer and 10 U of restriction enzyme. The reaction was made up to 20µl using nuclease-free water. If more than one enzyme was used, the compatibility of the enzymes determined whether the reaction was either carried out simultaneously or sequentially. If the reaction buffers required differed, the reactions had to be performed sequentially and the buffer was changed between reactions using a gel extraction spin column. The reaction was mixed and incubated at 37°C overnight. The digested products were resolved by agarose gel electrophoresis to visualise and purify the fragments of interest.

2.5.4 Agarose Gel Electrophoresis

Linearised DNA products generated following restriction digest were resolved by electrophoresis. For a 1% w/v agarose gel, 1g of agarose was added to 100ml Tris-acetate-EDTA (TAE). This was heated until the agarose was dissolved and allowed to cool to approximately 50°C. Ethidium bromide (EtBr) was added to a final concentration of 0.5µg/ml, and the agarose poured into a gel tray with a well comb in place. This was left at RT for 30 minutes to solidify. A molecular weight ladder in BPB loading dye was loaded into the first well. The appropriate volume of 10x XC loading dye was added to the DNA samples

prior to loading into the rest of the wells. The gel was run at 100 volts for 20 minutes, and a UV light was used to visualise the DNA fragments.

2.5.5 Gel extraction

DNA was purified away from the agarose gel using the Qiagen Gel Extraction Kit as per the manufacturer's instructions. All centrifugation steps were carried out at 17,900 x g at RT. DNA bands were viewed using a UV light and the bands of interest were excised from the agarose gel using a scalpel. The gel slice was weighed and three volumes of Buffer QG were added to one volume of gel (100mg - 100µl). This was incubated at 50°C for 10 minutes to dissolve the gel. Once dissolved one gel volume of isopropanol was added to the sample and mixed. This mixture was pipetted into a QIAquick spin column and centrifuged for 1 minute, and flow-through discarded. Next, 500µl of buffer QG was added to the column and centrifuged for 1 minute, then 750µl of Buffer PE was added to wash the DNA, and the mixture was centrifuged for 1 minute. The flow-through was discarded and an additional 1-minute centrifugation was performed to dry the membrane. The purified DNA was eluted using 50µl of buffer EB into a clean 1.5ml microcentrifuge by centrifugation for 1 minute.

2.5.6 Dephosphorylation of plasmid DNA

Linearised DNA vectors required dephosphorylation of the 5' end. In each 25µl reaction 1pmol of DNA was added with 2.5µl of 10x Antarctic Phosphatase Reaction buffer, 1µl of Antarctic Phosphatase, made up to 25µl with purified H_2O. The reaction was incubated at 37°C for 15 minutes for 5' overhang and 60 minutes for 3' overhang or blunt ends. The reaction was stopped by heat-inactivation at 70°C for 5 minutes.

2.5.7 Ligation

The final step of plasmid construction is connecting the insert DNA into a compatible digested vector which was done by ligation. Ligation reactions were set up according to the manufacturers' instructions (NEB). A typical ligation reaction consisted of 100ng digested plasmid, with the insert added at a 1:5 molar ratio (plasmid: insert), 10x DNA ligase buffer and 5 U T4 DNA ligase. The reaction volume used was 10µl. The reaction was incubated at 18°C overnight and then stored at -20°C prior to use.

2.6 Construction of stable cell lines

2.6.1 Transfections using FuGeneÒ

Transfections were performed using FuGENE®HD Transfection reagent, a non-liposomal reagent. The protocol for use was taken from the FuGENE protocol database and was optimised for U937 cells. Cells were plated in six-wells plates at a density of $8x10^5$ cells per well with 3ml of medium. For each well, a solution of 1.7µg of DNA in 155µl of sterile deionised water plus 9.9µl of FuGENE reagent was mixed and incubated for 30 minutes at room temperature. 150µl of this mixture was added to the cells and mixed thoroughly. These were incubated for 48 hours at 37°C in a humidified 5% CO_2 incubator before the selection process began.

2.6.2 Electroporation of U937 cells

Electroporation of the U937s was performed using the Amaxa® Nucleofector® device using the cell line Nucleofector® Kit C, following the optimised protocol provided by the manufacturer. In brief, $1x10^6$ cells were used per sample, this was pelleted and the supernatant removed. The cells were resuspended in 100ml Nucleofector® solution. 2mg of DNA was added to the cell suspension, this was then transferred into the cuvette and the lid closed. The cuvette was inserted into the device and the program W-001 was selected and run. 500ml pre-warmed culture medium was added to the cuvette immediately after running the program and then the sample was transferred into a twelve-well plate and incubated at 37°C in a humidified 5% CO_2 incubator. Selective antibiotics were added 48 hours post transfection.

2.6.3 Maintenance of the stable cell lines

After transfections, cells were allowed to grow under non-selective conditions for 48 hours before the addition of either 500mg /ml G418 or 400mg/ml Hygromycin B as required. The use of selection medium was continued with frequent changes of medium to eliminate dead cells and debris. The cells were split as necessary until there was an outgrowth of resistant cells. These were then either used for assays or made into frozen stocks and stored in liquid nitrogen for future work.

2.7 DNA/RNA Extraction and cDNA preparation

2.7.1 Host RNA Extraction

Total RNA was extracted from the cells at the required time points post-infection using TRIZOL® reagent (Invitrogen), and further purified with a PureLink® RNA mini kit (Life Technologies) as described by the manufacturer, with an added on-column DNase treatment step to remove any remaining DNA. All centrifugation steps were carried out at room temperature (RT) at 12,000 x g. In short, the media was removed from the cells and 500 µl of TRIzol® was added and incubated at RT for 5 minutes to allow complete dislocation of nucleoprotein complexes, 100 µl of chloroform was added and shaken vigorously at RT for 15 seconds. This was incubated at RT for 3 minutes before centrifugation for 15 minutes, the resulting upper aqueous phase was transferred to a new microfuge tube. 70% Ethanol was added to obtain a final concentration of 35% and mixed thoroughly by vortexing. This solution was transferred on to the PureLink® mini column and spun for 15 seconds, flow-through was then discarded. 10 µl of Dnase1 and 80 µl of buffer were then added to the column and left at RT for 15 minutes where DNA-free RNA was required. Wash buffer was added to the spin column and the spin step was repeated. Flow-through was discarded and the column put into a new collection tube. Next, wash buffer II was added to the spin column, spun and flow-through discarded; this was repeated. The column was then dried by centrifugation for 1 minute and placed into a 1.5ml recovery tube and 50 µl RNase free water was added to the centre of the spin cartridge. This was incubated at RT for 1 minute before centrifugation for 2 minutes to elute the purified RNA.

The RNA quality was assessed using a NanoDrop® ND1000 Spectrophotometer (Thermo Scientific). Only samples with a good yield and purity (a 260nm/280nm ratio greater than 1.75) were retained for further experiments. After cDNA preparation was performed, the remaining RNA was stored at -70°C until required.

2.7.2 Intracellular Mycobacterial RNA extraction

RNA was extracted from phagocytosed mycobacteria as described by Monahan et al. (2001). Stimulated U937 cells were cultured and infected in 75cm^2 tissue culture flasks. At each time point, the liquid media was removed and the monolayer of cells washed with pre-warmed PBS. 10ml of 4M GTC solution was added to each flask and rocked to ensure the GTC covered all the surface. 500ml of 4 M GTC solution was prepared by adding 250g

guanidine thiocyanate to 200ml of distilled H_2O and dissolved overnight at 37ºC. Once dissolved, 2.5g N-lauroyl-sacosine, 12.5ml 1 M sodium citrate (pH 7), 5ml Tween 80, and 7.7g DTT were added and the solution mixed. The GTC lysate was decanted into 30ml universals with a scrapper, to ensure all the cells were removed from the surface. This was vortexed and pipetted up and down to reduce viscosity, before being centrifuged at 3000 rcf for 20minutes. The supernatant was gently removed with a Pasteur pipette and discarded; the pellet was re-suspended in TRIzol®. The suspension was aliquoted into 2ml ribolyser tubes, then ribolysed at 6.5 m/s for 45 seconds. The tubes were left to sit at RT for 10 minutes, after this 200 µl chloroform was added to the ribolyser tubes and mixed by shaking for 15 seconds, these were then left at RT for a further 10minutes. The preparations were centrifuged at 15, 000 rcf for 15 minutes. The aqueous phase was pipetted into fresh microfuge tubes, equal volumes of chloroform was added and mixed for 15 seconds. This was incubated at RT for 5 minutes before a second centrifugation at 15, 000 rcf for 15 minutes. Again the aqueous phase was removed into a clean microfuge tube. 70% Ethanol was added to obtain a final concentration of 35% and mixed thoroughly by vortexing before continuing with the PureLink® RNA mini kit protocol as previously described in the host RNA extraction section above.

2.7.3 cDNA synthesis

cDNA was synthesized using the Invitrogen high-capacity cDNA reverse transcription kit as per manufacturer's guidelines; 2µg of RNA was used for each 20-µl reaction. In short, a master mix of 2ml of 10x RT Buffer, 2ml of 25x RT random primers, 1ml of Multiscribe reverse transcriptase, and 3.2ml of H_2O per reaction was made, 10ml of the mix was added to 10ml of RNA, this was then incubated in a thermal cycler with a four step program.

Table 2.2 - Thermal cycler program used for qRT-PCR

	Step 1	Step 2	Step 3	Step 4
Temperature (°C)	25	37	85	4
Time (minutes)	10	120	5	¥

cDNA was stored for later use at -80°C.

2.7.4 Total Bacterial DNA extraction

DNA was extracted from the bacteria using the FastDNA™ spin kit for soil by MP Biomedicals. The DNA was isolated from 10ml 7H9 broth cultures; the cultures were centrifuged at 3000 x g for 10 minutes and the supernatant removed, the bacteria was re-suspended in a screw-top Eppendorf tube and spun at 15,000 rcf for 5 minute and the supernatant was removed. The bacteria were then heat killed by complete submergence in a water bath at 90°C for 45 minutes. The DNA was extracted by following the FastDNA™ spin kits manufacturers' protocol with some adjustments. All centrifugation steps were performed at 14,000 x g and at RT. In brief, the bacteria were re-suspended in 978ml sodium phosphate buffer (PBS) and transferred into the Lysing Matrix E tube, then 122ml of MT buffer was added. This was homogenized in the FastPrep instrument for 40 seconds at a speed of 6.0 and then centrifuged for 10 minutes. The supernatant was transferred to a clean 2ml Eppendorf and 250ml of protein precipitation solution was added and mixed by shaking. This was centrifuged for 5 minutes and the supernatant transferred into a clean 15ml tube. 1ml of the Binding Matrix suspension was added to the 15ml tube, this was then inverted by hand for 2 minutes to allow for binding of the DNA, and then left to settle for 3 minutes. 500ml of the supernatant was then removed, and the remaining amount was re-suspended. 600ml of the mixture was then added to a SPIN™ filter and centrifuged for 1 minute. The flow-through was discarded, the pellet on the filter was then re-suspended with 500ml of SEWS-M and again centrifuged for 1 minute. The flow-through was discarded and the filter was further spun for 2 minutes, again the flow-through was discarded and the filter was placed in a new catch tube. The filter was air-dried for 30 minutes at room temperature, then at 56°C for a further 30 minutes. The remaining Binding Matrix above the filter was re-suspended in 50ml of DES, this was incubated for 5 minutes at 55°C in a shaker set 1400rpm before a final centrifugation for 1 minute to elute the DNA.

2.7.5 DNA clean up

The DNA was cleaned following the recommended clean-up procedure; 430 µl of TE buffer was added, then the sample was loaded on to a Microcon YM-30 filter in a 1.5ml microfuge tube, this was spun at 8,000 xg for 10 minutes at RT, and the flow-through discarded. This step was repeated but with 480 µl of TE. The filter was then inverted into a fresh 1.5ml microfuge tube and spun for 1 minute at 8,000 x g at RT to collect the purified sample. The purified DNA was stored at -20°C until use.

2.7.6 Host DNA extraction

DNA was extracted from the U937 cells using the DNeasy Blood & tissue Qiagen kit following the manufactures' guidelines for cultured cells. In brief, the cells were pelleted by centrifugation for 5 minutes at 300 x g, re-suspended in 200ml of PBS with 20ml proteinase K added. 200ml of buffer AL was added and mixed by vortexing, this suspension was incubated at 56°C for 10 minutes. After incubation, 200ml of ethanol was added and vortexed, this mixture was pipetted into the DNeasy mini spin column. The column in a collection tube was centrifuged at 6,000 x g for 1 minute, the flow-through discarded and the column placed in a new collection tube. 500ml buffer AW1 was added to the column and again centrifuged at 6,000 x g for 1 minute, discarding the flow-through and the collection tube again after. With the column in a new tube, 500ml of buffer AW2 was added and then centrifuged for 3 minutes at 20,000 x g to dry the membrane, again the flow-through and the tube were discarded. The column was placed into a clean microfuge tube and 200ml of buffer AE was added, this was incubated for 1 minute at room temperature, then centrifuged for 1 minute at 6,000 x g to elute. DNA was stored at -20°C until required.

2.7.7 Bioanalyzer automated electrophoresis

Electrophoresis was performed using the Agilent 2100 Bioanalyzer system. The chips were prepared prior to each use; each chip was filled using the chip priming station with a mix of DNA dye concentrate and DNA gel matrix. The ladder was added to the well marked with the ladder symbol, and 1ml of DNA sample added to the remaining wells. The chip was then vortexed before being inserted in the Agilent 2100 Bioanalyzer to be read. The system automatically gives a quantitative assessment of size, the readout is either an electropherogram or a densitometry plot (gel-like image) for each sample.

2.7.8 TapeStation DNA analysis

DNA analysis of the mutants was performed on the Agilent 4200 TapeStation, as per the manufacturer's guidelines. The instrument takes strips of tubes each containing 3ml of D1000 sample buffer and 1ml of either Ladder or DNA sample. The tubes were sealed and vortexed before loading in the TapeStation. Each tube acts an electrophoresis gel, separating the DNA and fluorescently stains the DNA, so is imaged as you would any gel electrophoresis.

2.8 Protein extraction and quantification

2.8.1 Whole cell lysates

Lysates of the U937 cell lines were made using RIPA buffer; the culture medium was removed from the cells by centrifugation 2500 x g for 5 minutes, and washed twice with cold PBS. After the final spin, the cells were re-suspended in cold RIPA buffer 1ml to every $5x10^6$ cells. This was kept on ice for 5 minutes while mixing occasionally. The lysate was transferred to a micro-centrifuge tube, and centrifuged at 14, 000 x g for 15 minutes. The resulting whole cell lysate supernatant was removed from the cell debris pellet and transferred into a new tube, these were stored at -20°C before being used for Western blot analysis.

2.8.2 BCA assay

To determine the protein concentration of the cell lysates, a Pierce™ BCA assay kit was used. In short, a BCA working reagent (WR) was prepared, 50 parts BCA reagent A to 1 part BCA reagent B. Protein standards of known concentration (2000mg/ml to 25mg/ml) of Bovine Serum Albumin (BSA) were prepared; these formed a standard curve to determine the total protein amounts in the samples. 25ml of each standard and of the unknown samples were pipetted in triplicate on to a 96 well plate, 200ml of WR was added to each well and mixed. The plate was covered and incubated at 37°C for 30 minutes, allowed to cool to RT, and then absorbance was read at 595nm on a plate reader. A standard curve was plotted using the Blank corrected OD values of the BSA standards vs. its concentration in mg/ml; this was then used to determine the protein amounts in the unknown samples.

2.8.3 SDS-PAGE gel electrophoresis

The SDS-PAGE gel electrophoresis was performed using a Biorad vertical electrophoresis cell with hand-casted gels; 8% gels were prepared containing 14ml ddH_2O, 7.5ml 1.5 M Tris-HCL (pH 8.8), 8ml 30% Acrylamide, 300ml 10% SDS, 20ml Temed, and 150ml 10% APS. Gels were poured into gel apparatus, overlayed with 100% ethanol and left to set for 45 minutes. Once set, the stacking gel was prepared with 4.35ml ddH_2O, 1.9ml 0.5 M Tris-HCL (pH 6.8), 1ml 30% Acrylamide, 80ml 10% SDS, 20ml Temed, and 160ml 10% APS. The lane comb was inserted and left to set for 30 minutes, once set running buffer was added to the tank. The cell lysates were prepared by boiling for 5 minutes and added 2x

sample buffer with 5% b-mercaptoethanol and 0.02% bromophenol blue to each sample. These were loaded into the wells and run at 100v until the bromophenol blue dye front had run to the bottom of the gel.

2.8.4 Wet electro-blotting

The protein was transferred from the SDS-PAGE gel to a nitrocellulose membrane using wet electro-transfer. The gel was soaked in transfer buffer for 15 minutes then placed in the transfer sandwich of filter paper-gel-membrane-filter paper, which was then placed in the vertical tank filled with transfer buffer. The gel tank was run overnight at 30 volts, steeped in a bucket of ice. The transfer was checked by visualisation using ponceau red dye, the gel was soaked for 5 minutes and rinsed to visualise the bands, further rinsing completely removed the stain ready for Western blotting.

2.8.5 Near-Infrared Western blotting

The Licor Odyssey[å] system was used for immune-probing the blots; the Odyssey[å] blocking buffer was diluted 1:1 with PBS and IRDye[å] secondary antibodies were used. The membrane was rinsed in TBS-T for 5 minutes then diluted Odyssey[å] blocking buffer was added. This was incubated at RT for an hour with gentle agitation. The block was then removed and the blot was sealed in plastic with 2ml of primary antibody diluted Odyssey[å] blocking buffer and incubated as per the manufacturer's instructions. After incubation, the blot was washed three times for 5 minutes in TBS-T, once washed the secondary antibody diluted with Odyssey[å] blocking buffer was added, this was incubated for 1 hour with shaking at RT. The membrane was protected from light during both the incubation and washing steps. After incubation, the blot was washed four times for 5 minutes in PBS-T, followed by twice for 5 minutes in PBS. The membrane was then imaged using an Odyssey[å] imaging system.

2.9 Microscopy

2.9.1 Acid Fast Staining

Oil emersion light microscopy was used to calculate the number of infected U937 cells and average number of bacteria per cell. The U937 cells were grown in four well plates with coverslips at the bottom. The cells were adhered to the coverslips with the addition of 100ng/ml PMA. After 24 hours incubation, the cells were infected at a MOI of 20:1. At each

time point, the liquid culture was removed from the well and ice-cold 100% methanol was added to cover the cells to a depth of 2-3mm. This was left for 5 minutes to allow the cells to fix. The methanol was aspirated, the wells washed once with PBS and left to dry before staining. Staining was performed following the Kinyoun's cold staining procedure. The wells were flooded with Kinyoun's carbol fuchsin and left for 20 minutes at room temperature (RT). The wells were then rinsed gently with water to remove the excess stain. The wells were washed again with acid-alcohol (3% HCL in ethanol) for 3 minutes until all excess carbol fuchsin was removed, the wells were again rinsed and then the acid-alcohol decolourising was repeated for 1-2 minutes, then rinsed. The wells were counterstained by flooding with 2% Malachite green and left for 3-4 minutes at RT. The wells were rinsed and the slides removed from the bottom of the wells and fixed to slides and left to dry. The infected cells were examined on an oil emersion light microscope at 1000x magnification. A selection of images was also taken using a Zeiss Axioplan 2 upright microscope and the Axiocam HR digital CCD camera, using AxioVision 4.8 imaging software.

2.9.2 FITC labelling of Bacteria

The *M.tb* was labelled using fluorescein isothiocyanate (FITC), the bacteria were pelleted at 3000 rcf at RT for 15 minutes. The pellet was then re-suspended in 1ml of 0.1M sodium bicarbonate buffer. 0.2mg/ml in 1% DMSO of FITC stock solution was added to the cell suspension and vortexed. This was then incubated in the dark for 30 minutes at 37°C with regular shaking. The cells were washed with HBSS four times to remove any unbound dye and re-suspended in medium at the required concentration for infection assays.

2.9.3 Immunocytochemistry

U937 cells were set up at density of $1x10^4$ cells in 500µl medium per well in four well plates. The cells were stimulated with 100ng/ml of PMA and left for 24 hours to adhere. Cells were infected with the labelled bacteria as per the infection protocol and the staining performed at different time points as required. At the required time points, the cells were washed with PBS for 5 mins, then fixed with 4% paraformaldehyde for 15 minutes. This was washed off with PBS 500µl per cell, twice. The cells were permeabilised with 0.1% Triton-X 100 on ice for 4 minutes, and then washed with PBS. These were blocked with 10% species dependant normal serum in 1% BSA in complete PBS for 1 hour. This block was removed and the primary antibody added in 1% BSA in complete PBS and incubated according to the

manufacturers' instructions. This was washed with PBS six times for 5 minutes. Next, the appropriate secondary antibody was added in 1% BSA in complete PBS and incubated for 1 hour protected from light. This was then washed three times in complete PBS, and counter-stained with 1µg/ml DAPI in PBS for 10 minutes, washed three times and allowed to dry. This was then imaged using the confocal microscope. Table 2.3 is a complete list of all primary antibodies used in this work; table 2.4 is a complete list of the secondary antibodies used.

Image capture and analysis

Stained cells were observed with a Nikon A1R confocal microscope equipped with 60x oil CFI apochromat lambda s 1.4NA objective lens. Samples were excited at 405nm, 488nm, 561nm, and in the UV range. Images were acquired sequentially to avoid bleed-through signal. The transmission and detector gains were set to achieve the best signal to noise ratios and the laser powers were tuned to limit bleaching of fluorescence. Acquisition of the images was carried out using Nikon NIS-Elements C software and analysis was performed using package COLOC2 in Fiji. Pearsons R value and M1 co-localisation coefficient of *M.tb* and the various markers were calculated in the software.

Table 2.3 Primary anti-bodies used

Antibody	**Source**	**Reactivity**	**Application**	**Concentration**	**Incubation**
Anti-LAMP1 rat monoclonal	Abcam (ab25245)	Mouse, Human	Immunocytochemistry	1/1000	16 hours at 4°C
Anti-Rab5 rabbit polyclonal	Abcam (ab18211)	Mouse, Human	Immunocytochemistry	1□g/ml	Overnight at 4°C
Anti-RAB7 mouse monoclonal	Abcam (ab50533)	Mouse, Human	Immunocytochemistry	1□g/ml	Overnight at 4°C
Anti-RIN2 rabbit polyclonal	GeneTex (GTX117153)	Human, Mouse	Western blot	1/1000	Overnight at 4°C
Anti-ORP1 rabbit monoclonal	Abcam (ab131165)	Mouse, Human	Western blot	1/1000	Overnight at 4°C
Anti-Actin mouse monoclonal	Abcam (ab3280)	Mouse, Human	Western blot	0.5□g/ml	Overnight at 4°C
Anti-RILP rabbit polyclonal	Santa Cruz (sc-98331)	Mouse, Human	Western blot	1/1000	Overnight at 4°C
Anti-RILP goat polyclonal	Santa Cruz (sc-82746)	Mouse, human	Western blot	1/1000	Overnight at 4°C

Table 2.4 secondary anti-bodies used

Antibody	**Source**	**Fluorophore**	**Concentration**	**Incubation**
Donkey-anti-Rabbit	LI-COR	800CW	1/1000	1 hour at RT
Donkey-anti-Mouse	LI-COR	680RD	1/1000	1 hour at RT
Goat Anti-rabbit	abcam	405	1/1000	1 hour at RT
Goat Anti-mouse	abcam	594	1/1000	1 hour at RT
Donkey Anti-Rat	abcam	555	1/1000	1 hour at RT

2.10 SYBR Green Quantitative RT-PCR

Quantitative PCR reactions were performed in a Bio-Rad CFX96 thermocyler using a SYBR Green qPCR mastermix (Applied Biosystems®, Catalog number 4309155), each in a volume of 10µl containing 2µl of cDNA and 667nM of primers. Each sample was measured in triplicate, a non-template control was added to each plate where 2µl of water was used in place of the cDNA, and a minus RT was also included in the plate using the –RT control cDNA. Once the plate was loaded with cDNA sample, it was covered using an optical clear adhesive cover and spun to remove air bubbles. The plates were loaded into the CFX Connect™ real time RPC detection system. The thermal cycling was performed following the manufacturer's protocol for SYBR green in the CFX system.

Primers were designed using the Primer-Blast tool with the following criteria:

- 20 and 25 nucleotides long,
- GC content of greater than 50%,
- exon-exon junction spanning (where possible).

Where multiple isoforms existed, a common region was located using Clustal Omega, a multiple sequence alignment tool. Tables 2.5 and 2.6 give a complete list of primers designed for this study.

Table 2.5 A complete list of mouse primers generated for this study.

Target gene	Orientation	Primer sequence
Actb ***(house keeping gene)***	Forward Reverse	AGTACTCTGTGTGGATCGGTG AACGCAGCTCAGTAACAGTCC
Ctsc	Forward Reverse	TAACTGCTCGGTGATGGAAGC CACAATCTCGAAGCCTTGGTTG
Fuca1	Forward Reverse	GTTAACAGCTACAAGCCTGACC TCGTTGTAGAGCCAAGCAAGG
Lipa	Forward Reverse	GGCTGCACCATAGGTTTCATAG GGCAAGCGTCCCAATTGAAG
Mafb	Forward Reverse	ACATCACCTGGAGAACGAGAAG TTGACCTTGTAGGCGTCTCTC
Mmp10	Forward Reverse	ACCCTCAGGGACCAACTTATTC TTAGCTGGGCTTGTGGAGAAC
Naga	Forward Reverse	GTGGCTCAGGTACTGATGCTG GCCGTTCACTGATGCAGTTC
Osbpl1A	Forward Reverse	TGGTTCCATCAAGGTCCTAACC ACTGTACCAGATGCCTTGCC
Pgk1	Forward Reverse	TTCCTGTGCTCCTAAGTCAACC AGACGAGCTGAGATGCTGTG
Ppia	Forward Reverse	AGCCATGGAGCGTTTTGGGTCC AGGGACGCTCTCCTGAGCTACAG
Rilp	Forward Reverse	AACAGAGGAGGAAGATCAAGGC CTTGTCGTTGGAGAGCAGGAG
Rin2	Forward Reverse	GGAGAAGGAGGCTATTACTTGACC TAGTTCGGTTGGTGGTTCTCC

Table 2.6 A complete list of human primers generated for this study.

Target gene	Orientation	Primer sequence
CTSC	Forward	ACTGCACCTATCTTGACCTGC
	Reverse	CCAGCTTCTGAAGGTACACCAC
FUCA1	Forward	CGAGTCCTGTGTCTTGGAACTG
	Reverse	CCATAGCGGATGTTCCTCTTCC
IRF8	Forward	AGTTACAGAGATGGAGTGCGG
	Reverse	CAGTCTGGAAGGAGCTGACTC
LIPA	Forward	TGGTGTTCCATGAGAGCATTCC
	Reverse	TGACTTGGTGGTACACAGCTC
MAFB	Forward	CACTCCGTGTAGCTCCGTG
	Reverse	GGTTCATCTGCTGGTAGTTGC
MMP1	Forward	AGCTACACCTTCAGTGGTGATG
	Reverse	AGGTTAGCTTACTGTCACACGC
MMP10	Forward	AGAGGTGACTCCACTCACAT
	Reverse	GGTCTGTGAGTGAGTGATAG
MMP3	Forward	GTCACTTCAGCTCCTTTCCT
	Reverse	ATCTTGCGAAAGGCGGAACT
NAGA	Forward	CTGGCTGACTACGTTCACTCC
	Reverse	GCATGTCTACCTTCCACTCGG
OSBPL1A	Forward	TTGTCAGAAGCACTGGAGACG
	Reverse	AGCGCATCATAGAACTCGTCC
PKR	Forward	TACTGTGGACAAGAGGAAGGC
	Reverse	AGAGAATCATCACTGGTCTCAGG
RILP	Forward	GTTCCTCCCTACCCTTATCGC
	Reverse	CATGTCTCCCAGAGGCTTAGG
RIN2	Forward	ACGACTTCCAGAATTACCTCCG
	Reverse	TGACACACATCCTCAGTGGTG
STAT1	Forward	TCGACAGTCTTGGCACCTAAC
	Reverse	GTACCACTGAGACATCCTGCC
TBP (house keeping gene)	Forward	GACCATTGCACTTCGTGCC
	Reverse	TTCTTCACTCTTGGCTCCTGTG

For each qPCR run, standard curves with serial template dilutions were included, cycle thresholds were determined with instrument software and relative expression values calculated using the Pfaffl method as previously described (Pfaffl, 2001). Each run also included a house keeping gene for standardisation of the total RNA amount; this was *TBP* for the U937 experiments and *Actb* for the J774 experiments. The statistical analyses were performed and graphs were plotted using GraphPad Prism Version 7 software (San Diego, USA); a paired t test was performed to assess statistical significance.

2.11 Statistics

Statistical significance was assessed using statistical packages in GraphPad software Prism 7, t-tests or ANOVAs were performed as appropriate. Values of less than 0.05 were considered statistically significant, symbols were used on figures for ease (Table 2.7).

Table 2.7 Symbols used for statistical results.

Symbol	Meaning
ns	P > 0.05
*	P ≤ 0.05
**	P ≤ 0.01
***	P ≤ 0.001
****	P ≤ 0.0001

Chapter 3 - Results - Macrophage gene expression analysis during infection with *M.tb*: identification of endosome trafficking genes

3.1 Introduction

Inferred biological processes involved in *M.tb* survival during macrophage infection can be investigated through the re-examination of published transcriptome data, using gene functional categories that are associated with the hypothesis that *M.tb* evades phago-lysosome development by actively modifying host cell functions. It is hypothesised that this disruption may be reflected in host transcriptional alterations for the genes involved in such processes, revealed by functional genomics transcriptional data sets. The first step in defining relevant host genes in this proposed host-pathogen interaction begins with the interpretation and re-analyse of published transcriptome data, followed by the confirmation of expression pattern reproducibility in experimental macrophage cell lines necessary for further investigation. This chapter considers relevant transcriptional data sets and takes a functional category approach to data analysis to identity host genes for further study. The transcription patterns of genes of interest were then compared between previously published studies and macrophage cell line infection protocols established in this thesis. Comparisons between virulent and avirulent strains of *M.tb* were performed on the assumption that avirulent strains would not have the same suppressive effects on host cell endosome trafficking genes. Finally, it was established at what point after the infection the changes in transcription occurred.

3.2 Effects of *M. tuberculosis* infection on macrophage gene expression

As discussed in the introduction, *M. tuberculosis* has a global effect on gene expression in host cells. The aim of this study was to investigate the effect *M. tb* infection has on host cell gene expression, with a particular focus on those host genes that are suppressed in response to infection. Many studies of primary transcriptional data sets assume that only genes that are upregulated have significance in terms of virulence mechanisms, or at least only these ones are normally considered for further study. This thesis takes the view that suppression of genes is equally as biologically significant yet have

been neglected in previous studies. Given that the underlying hypothesis is one of *M.tb* moderated suppression of biological processes in the host macrophage (namely inhibition of endosome trafficking), suppressed genes are a relevant target for this study. It is also pertinent to this data analysis approach to gene selection that fold changes in expression levels are not always directly correlated with biological importance, yet many studies subsequently analysing whole genome transcriptome data choose only to investigate highly upregulated genes. This wrongly assumes that only large changes in mRNA levels can have biological significance; clearly that cannot be the only criteria for gene involvement in important biological consequences. Many genes have fundamentally major biological consequences with only minor changes in expression levels: cytokine genes are just one example, the presence of Interleukin-6 upregulates the expression of macrophage colony-stimulating factor receptors, which in turn triggers the differentiation of monocytes into macrophages (Chomarat et al., 2000). Many other factors involved in transcriptional, translational and post-translational gene expression control have fundamental effects on biological processes and the role of individual genes. Excluding genes because they are downregulated or display lower levels of change, will necessarily limit interrogation of the pathways in which they may be involved.

Tailleux et al., 2008 published comprehensive gene expression profiles from human monocyte-derived macrophages (MP) and dendritic cells (DC) taken from 9 independent healthy donors. The cells were infected with *M.tb* and the cellular RNA extracted after 1, 4, 18 and 48 hours. From this RNA microarray experiments were performed, using Human U133A oligonucleotide microarray chips; the raw data was then processed as per the method in chapter 2.

Accordingly, the cellular transcriptomes published by Tailleux et al., 2008, infected by *M. tb* for 48 hours were compared with non-infected cells and analysed to identify $\log_2$ fold changes of expression, p values <0.05, and also corrected for gene duplications. All the genes showing statistically significant changes in expression (p value less than 0.05) are plotted in Figure 3.1, comparing macrophage with dendritic cells.

Figure 3.1 shows a total of 686 genes downregulated post-infection in both dendritic cells and macrophages (bottom left quadrant, Fig 3.1). This is compared to 445 induced genes in both cell types (upper right quadrant, Fig.3.1). A gene encoding matrix metallopeptidase 1 (*MMP1*) is the most strongly induced. It clearly had the largest fold

change in both cell types, followed by *MMP10*. The most downregulated genes include coagulation factor XIII (*F13A1*), complement component 1 (*C1QA*), chemokine ligand 8 (*CCL8*) and transforming growth factor beta 1 (*TGFB1*). Figure 3.1 also reveals a strong correlation between the effect in both macrophage and dendritic cells (R= 0.81).

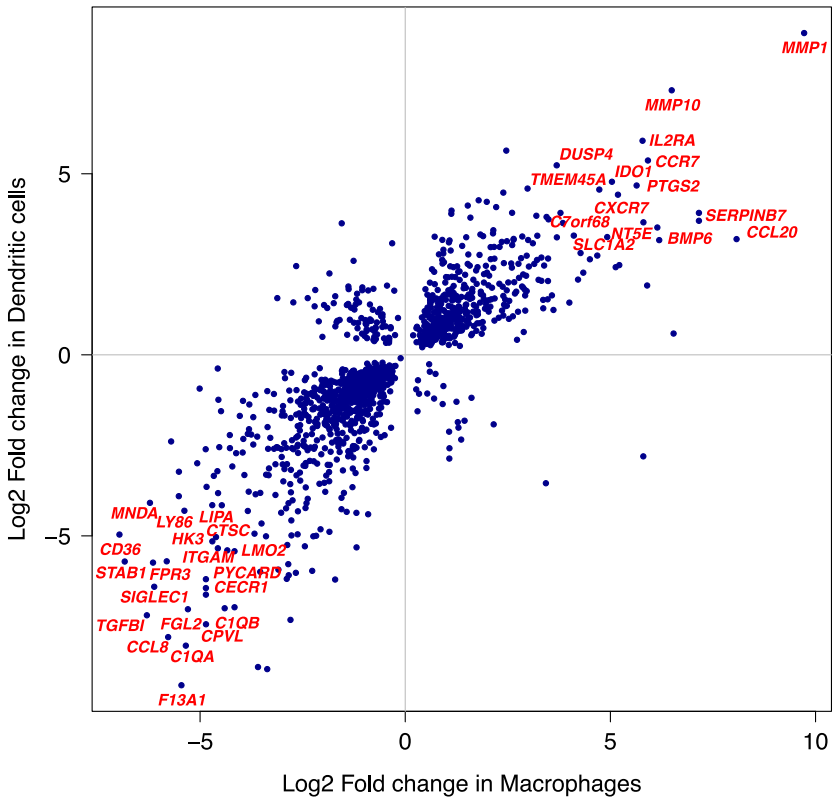

Figure 3.1 - Graphical representation of the fold changes of expression in macrophages and dendritic cells 48 hours post infection with M. tuberculosis; the genes with the greatest positive and negative fold changes are named in red. (Primary gene expression data from Tailleux et al 2008)

The categories of genes which were downregulated by the presence of *M. tuberculosis* were then investigated further. Gene Ontology (GO) enrichment analyses were performed on the genes downregulated at least 2-fold in both macrophages and dendritic cells. The analysis included results for criteria defined by the terms cellular compartment.

Table 3.1 Gene ontology analysis for cellular compartment, of the downregulated genes in macrophages and dendritic cells, in order of p value. The second column is the number of genes annotated in the human genes ascribed to the category; third column is the number of genes in the down regulated subset. The expected number is how many genes you would expect in each category if selected at random. Fold enrichment shows the fold change above the normal and finally the P-value to show the significance of the enrichment, with some genes falling into multiple categories. The categories of interest for this study are highlighted in yellow.

cellular compartment	#	#	expected	Fold Enrichment		raw P value
Cytoplasmic vesicle	2458	46	16.47	2.79	+	4.82E-11
intracellular vesicle	2461	46	16.49	2.79	+	5.02E-11
secretory granule	870	26	5.83	4.46	+	2.03E-10
vesicle	3940	59	26.4	2.23	+	2.83E-10
secretory vesicle	1032	26	6.92	3.76	+	6.71E-09
extracellular region	4381	60	29.36	2.04	+	6.93E-09
secretory granule lumen	321	15	2.15	6.97	+	7.38E-09
cytoplasmic vesicle lumen	324	15	2.17	6.91	+	8.31E-09
vesicle lumen	326	15	2.18	6.87	+	8.99E-09
cell periphery	6392	74	42.83	1.73	+	4.98E-08
extracellular space	3410	48	22.85	2.1	+	2.21E-07
lytic vacuole	731	19	4.9	3.88	+	5.82E-07
lysosome	731	19	4.9	3.88	+	5.82E-07
plasma membrane	5905	66	39.57	1.67	+	2.69E-06
vacuole	828	19	5.55	3.42	+	3.50E-06
cellular anatomical entity	18761	138	125.71	1.1	+	5.76E-06
membrane	9911	93	66.41	1.4	+	6.99E-06
cytoplasm	11989	106	80.33	1.32	+	7.80E-06
endomembrane system	4683	55	31.38	1.75	+	8.77E-06
Unclassified	1689	0	11.32	< 0.01	-	1.32E-05
cellular_component	18906	138	126.68	1.09	+	1.32E-05
extracellular exosome	2098	31	14.06	2.21	+	2.65E-05
ficolin-1-rich granule lumen	124	7	0.83	8.42	+	2.79E-05
extracellular vesicle	2120	31	14.21	2.18	+	3.05E-05
extracellular organelle	2121	31	14.21	2.18	+	3.08E-05
extracellular membrane-bounded organelle	2121	31	14.21	2.18	+	3.08E-05
intrinsic component of plasma membrane	1742	27	11.67	2.31	+	4.07E-05
cytoplasmic vesicle membrane	1175	21	7.87	2.67	+	4.27E-05

azurophil granule lumen	90	6	0.6	9.95	+	4.42E-05
ficolin-1-rich granule	185	8	1.24	6.45	+	4.61E-05
integral component of plasma membrane	1660	26	11.12	2.34	+	5.17E-05
vesicle membrane	1194	21	8	2.62	+	5.36E-05
azurophil granule	154	7	1.03	6.78	+	1.03E-04
primary lysosome	154	7	1.03	6.78	+	1.03E-04
integral component of membrane	5788	60	38.78	1.55	+	1.28E-04
intrinsic component of membrane	5947	61	39.85	1.53	+	1.46E-04
platelet dense granule lumen	14	3	0.09	31.98	+	1.83E-04
bounding membrane of organelle	2112	29	14.15	2.05	+	1.92E-04
vacuolar lumen	173	7	1.16	6.04	+	2.06E-04
complement component C1q complex	3	2	0.02	99.49	+	4.34E-04
specific granule membrane	91	5	0.61	8.2	+	4.57E-04
platelet dense granule	21	3	0.14	21.32	+	5.27E-04
collagen-containing extracellular matrix	427	10	2.86	3.5	+	7.02E-04
specific granule	160	6	1.07	5.6	+	8.66E-04
lipopolysaccharide receptor complex	5	2	0.03	59.7	+	9.04E-04
tertiary granule	164	6	1.1	5.46	+	9.80E-04
phagocytic cup	28	3	0.19	15.99	+	1.13E-03

As shown in Table 3.1., the results of Gene Ontology (GO) analysis for the most downregulated genes, ranked according to statistical probability, include genes associated with many types of vesicles, most noticeably cytoplasmic and intracellular vesicles (p value 4.82E-11 and 5.03E-11 respectively). Also included were genes associated with lysosome, primary lysosome and vacuole, with p values of 5.82E-07, 3.5E-06 and 1.03E-04 respectively, all highly significant. The data suggests that these genes are most relevant to the hypothesis linking downregulation and the arrest of phago-lysosome maturation and formation.

The same GO enrichment analysis was performed on the induced genes (Table 3.2). The results revealed lower significance values than the suppressed genes in Table 3.1, yet remained highly statistically significant. Negative regulation of biological processes and cellular processes categories were highly significantly induced with p values 1.68E-06 and 7.38E-06 respectively, supporting the assumption that *M.tb* suppresses functions in the macrophage rather than activating functions (see final discussion, Chapter 8).

Table 3.2 Gene ontology analysis for molecular function and biological process, of the upregulated genes in macrophages and dendritic cells, in order of p-value. The second column is the number of genes annotated in the human genes ascribed to the category; third column is the number of genes in the down regulated subset. The expected number is how many genes you would expect in each category if selected at random. Fold enrichment shows the fold change above the normal and finally the P- value to show the significance of the enrichment, with some genes falling into multiple categories. The categories of interest for this study are highlighted in yellow.

GO biological process	#	#	expected	Fold Enrichment	+/-	raw P value
cellular response to chemokine	90	7	0.31	22.56	+	4.19E-08
response to chemokine	90	7	0.31	22.56	+	4.19E-08
response to chemical	4001	33	13.79	2.39	+	2.42E-07
positive regulation of multicellular organismal process	1428	19	4.92	3.86	+	2.63E-07
response to organic substance	2657	26	9.16	2.84	+	3.73E-07
chemokine-mediated signalling pathway	81	6	0.28	21.49	+	5.38E-07
immune system process	2338	24	8.06	2.98	+	5.40E-07
cellular response to chemical stimulus	2566	25	8.85	2.83	+	7.55E-07
cell chemotaxis	208	8	0.72	11.16	+	7.56E-07
regulation of response to external stimulus	953	15	3.29	4.57	+	8.02E-07
response to external stimulus	2393	24	8.25	2.91	+	8.23E-07
leukocyte chemotaxis	147	7	0.51	13.81	+	9.93E-07
positive regulation of biological process	6162	41	21.24	1.93	+	1.45E-06
chemotaxis	513	11	1.77	6.22	+	1.62E-06
negative regulation of biological process	5234	37	18.04	2.05	+	1.68E-06
taxis	517	11	1.78	6.17	+	1.75E-06
regulation of cellular component movement	1028	15	3.54	4.23	+	2.03E-06
regulation of cell migration	895	14	3.09	4.54	+	2.13E-06
cellular response to organic substance	1994	21	6.87	3.05	+	2.38E-06
regulation of MAPK cascade	668	12	2.3	5.21	+	3.16E-06
regulation of multicellular organismal process	2618	24	9.03	2.66	+	4.06E-06
regulation of cell motility	953	14	3.29	4.26	+	4.37E-06
cell killing	119	6	0.41	14.63	+	4.51E-06
regulation of stress-activated MAPK cascade	193	7	0.67	10.52	+	5.64E-06
regulation of stress-activated protein kinase signaling cascade	196	7	0.68	10.36	+	6.22E-06
myeloid leukocyte migration	127	6	0.44	13.7	+	6.45E-06

cytokine-mediated signaling pathway	376	9	1.3	6.94	+	6.62E-06
response to stimulus	8054	47	27.77	1.69	+	7.04E-06
regulation of locomotion	997	14	3.44	4.07	+	7.28E-06
negative regulation of cellular process	4821	34	16.62	2.05	+	7.38E-06
regulation of response to stress	1317	16	4.54	3.52	+	8.95E-06
regulation of cell adhesion	748	12	2.58	4.65	+	9.79E-06
regulation of ERK1 and ERK2 cascade	299	8	1.03	7.76	+	1.02E-05
inflammatory response	508	10	1.75	5.71	+	1.05E-05
response to lipopolysaccharide	308	8	1.06	7.53	+	1.26E-05
positive regulation of cellular process	5664	37	19.53	1.89	+	1.31E-05
granulocyte chemotaxis	85	5	0.29	17.06	+	1.45E-05
regulation of p38MAPK cascade	42	4	0.14	27.63	+	1.87E-05
response to molecule of bacterial origin	326	8	1.12	7.12	+	1.88E-05
leukocyte migration	235	7	0.81	8.64	+	1.95E-05
immune response	1569	17	5.41	3.14	+	1.95E-05
response to lipid	807	12	2.78	4.31	+	2.06E-05
response to cytokine	811	12	2.8	4.29	+	2.16E-05
regulation of cell-cell adhesion	450	9	1.55	5.8	+	2.67E-05
granulocyte migration	98	5	0.34	14.8	+	2.80E-05
positive regulation of metabolic process	3741	28	12.9	2.17	+	3.33E-05
cellular response to cytokine stimulus	717	11	2.47	4.45	+	3.59E-05
regulation of cell population proliferation	1646	17	5.67	3	+	3.59E-05
peptidyl-threonine dephosphorylation	16	3	0.06	54.39	+	3.62E-05
positive regulation of cytokine production	471	9	1.62	5.54	+	3.79E-05
response to bacterium	726	11	2.5	4.4	+	4.01E-05
biological regulation	12355	59	42.59	1.39	+	4.48E-05
regulation of cell differentiation	1520	16	5.24	3.05	+	5.12E-05
cell surface receptor signalling pathway	2083	19	7.18	2.65	+	6.13E-05
response to other organism	1379	15	4.75	3.16	+	6.38E-05
response to external biotic stimulus	1382	15	4.76	3.15	+	6.54E-05
regulation of cellular process	11176	55	38.53	1.43	+	6.55E-05
positive regulation of platelet-derived growth factor production	2	2	0.01	> 100	+	6.95E-05
defense response	1405	15	4.84	3.1	+	7.87E-05
positive regulation of cell migration	526	9	1.81	4.96	+	8.73E-05

regulation of cell death	1597	16	5.51	2.91	+	9.16E-05
positive regulation of stress-activated MAPK cascade	128	5	0.44	11.33	+	9.48E-05
positive regulation of stress-activated protein kinase signalling cascade	130	5	0.45	11.16	+	1.02E-04
regulation of biological process	11639	56	40.12	1.4	+	1.02E-04
killing of cells of other organism	67	4	0.23	17.32	+	1.04E-04
response to biotic stimulus	1442	15	4.97	3.02	+	1.05E-04
positive regulation of ERK1 and ERK2 cascade	213	6	0.73	8.17	+	1.07E-04
mast cell activation	24	3	0.08	36.26	+	1.07E-04
regulation of platelet-derived growth factor production	3	2	0.01	> 100	+	1.16E-04
positive regulation of mesenchymal stem cell migration	3	2	0.01	> 100	+	1.16E-04
regulation of mesenchymal stem cell migration	3	2	0.01	> 100	+	1.16E-04
negative regulation of adherens junction organization	3	2	0.01	> 100	+	1.16E-04
positive regulation of cell motility	550	9	1.9	4.75	+	1.22E-04
regulation of localization	2716	22	9.36	2.35	+	1.22E-04
response to stress	3336	25	11.5	2.17	+	1.27E-04
positive regulation of cell differentiation	835	11	2.88	3.82	+	1.37E-04
positive regulation of T cell activation	225	6	0.78	7.74	+	1.43E-04
positive regulation of cellular component movement	563	9	1.94	4.64	+	1.45E-04
positive regulation of locomotion	566	9	1.95	4.61	+	1.51E-04
positive regulation of cell adhesion	451	8	1.55	5.15	+	1.74E-04
regulation of leukocyte cell-cell adhesion	336	7	1.16	6.04	+	1.75E-04
neutrophil chemotaxis	79	4	0.27	14.69	+	1.92E-04
cell migration	868	11	2.99	3.68	+	1.92E-04
regulation of T cell activation	344	7	1.19	5.9	+	2.01E-04
biological process involved in interspecies interaction between organisms	1536	15	5.3	2.83	+	2.10E-04
regulation of macrophage derived foam cell differentiation	31	3	0.11	28.07	+	2.15E-04
positive regulation of lipid metabolic process	154	5	0.53	9.42	+	2.19E-04
positive regulation of leukocyte cell-cell adhesion	246	6	0.85	7.07	+	2.29E-04
regulation of adherens junction organization	5	2	0.02	> 100	+	2.42E-04
regulation of cell communication	3300	24	11.38	2.11	+	2.44E-04
regulation of inflammatory response	356	7	1.23	5.7	+	2.47E-04

regulation of signalling	3316	24	11.43	2.1	+	2.55E-04
positive regulation of MAPK cascade	480	8	1.65	4.83	+	2.64E-04
regulation of signal transduction	2934	22	10.11	2.18	+	2.69E-04
cellular response to stimulus	6426	37	22.15	1.67	+	2.75E-04
homeostatic process	1585	15	5.46	2.75	+	2.94E-04
neutrophil migration	89	4	0.31	13.04	+	2.97E-04
regulation of lipid localization	166	5	0.57	8.74	+	3.06E-04

3.3 Distribution across the functional category of lysosomal biogenesis genes

Currently, there are 435 known lysosomal genes listed in The Human Lysosome Gene Database (hLGDB) (Brozzi et al., 2013) and 1483 genes listed as involved in vesicular transport for GO term vesicle-mediated transport (GO ID0016192). From the analysis of the published microarray data of Tailleux et al (2008), 686 genes in both these functional categories were found to be downregulated. This leads to the question: how prevalent is the downregulation of expression in all the lysosomal and vesicular transport genes? What is happening to the rest of the lysosomal and vesicular transport gene expression?

The fold changes calculated from the Tailleux data were plotted graphically, with the non-statistically significant values set to zero change; below the curve are three histograms (Figure 3.2). The three histograms represent set of genes from three different GO categories: lysosome, vesicular transport and immune response. The curve in the top half of the plots represents the log2 fold changes, with the highest fold change on the left and the most negative fold change on the right; the horizontal sections in the centre represent zero significant fold-change. Below the curves are histograms; on the y-axis is the number of genes which correspond to the fold change above, for example in dendritic cells there are 39 genes which have a log2 fold change of nearly -10. All the genes below the horizontal section of the plot display non-statistically significant fold change. Due to the bulk of previously published research focusing on the upregulation of genes relating to the immune response, this final GO category was also included for comparison (which also corroborates the GO results in table 3.2. above that small changes in cytokine and immune response genes are the norm and only a few show large log2 changes in differential expression).

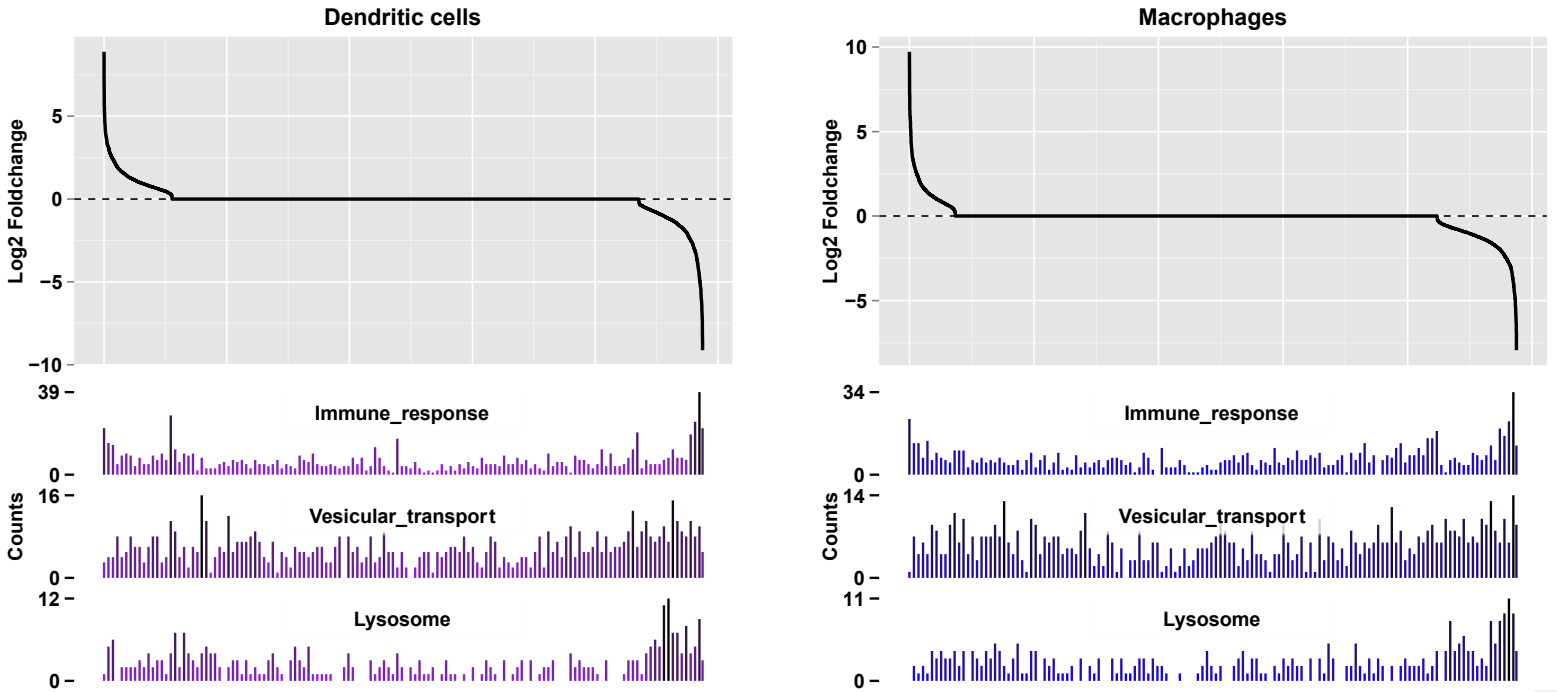

Figure 3.2 Barcode plots for dendritic cells and macrophages, showing the position of the lysosomal, vesicular transport, and immune response genes along the fold change curve. All fold changes that were deemed not to be statically significant were set to 0. The bars show the frequency of genes for each fold change.

Figure 3.2 shows a similar pattern for the dendritic cells and the macrophages. In both, there is clustering on the right in the lysosomal genes, meaning that a large number of genes are downregulated with proportionately only a few upregulated (in line with a blocking of phagosome maturation). The vesicular transport genes appear to be spread across up- and downregulation for both DC and macrophage plots, with a small bias towards downregulation. This small bias is harder to see because it is the largest category (1977 genes) so the sheer volume of genes included in the plot could mask any trends. As with the lysosomal category, the immune response-related genes cluster to the right, revealing a large number of downregulated genes. However, as predicted from the previously published data, there is a second cluster in the positive fold change section (Ragno et al., 2001; Volpe et al., 2006). The cluster on the left of both plots shows that there are also a number of upregulated genes. This could be a dynamic response of the host immunity to the infection.

These analyses support the hypothesis, illustrating that among the genes most downregulated post-*M. tuberculosis* infection are many genes with functions in lysosomal and vesicular transport pathways.

3.4 Are the changes in expression reproducible in immortalised cell lines?

A literature search revealed a number of published microarray studies of host cells infected with *M. tb* (see Introduction, chapter 1). These studies have used a variety of cell lines, with no indication of which is the most appropriate disease model. The Tailleux et al (2008) data set was collected from human primary macrophages and dendritic cells. Therefore, the present study went on to investigate whether the same altered expression could also be seen in immortalised cell lines using qRT-PCR for selected genes to compare gene expression patterns. Immortalised cell lines represent a more tractable experimental model in that they are easier to maintain in culture, can be grown to numbers where infection parameters can be measured, have higher transfection efficiencies and avoid the problem of variable genetic backgrounds seem in primary cells from different human donors.

Accordingly, cell line models of macrophage infection were established in two commonly used macrophage-like cell lines: J774 cells (mouse, semi adherent macrophage lineage cell line), and U937 cells (human, lung lymphoblast with monocytic like characteristics). The infection parameters were established so as to mimic the Tailleux et al.

(2008) method, sampling at a 48-hour infection period, after which RNA was extracted and cDNA prepared. Table 3.3 is a complete list of the genes that were tested using qRT-PCR. The housekeeping genes were included as a control to correct for differing amounts of mRNA.

Table 3.3 All genes tested using qRT-PCR, including those found to be downregulated, upregulated and housekeeping genes which should remain the same.

Gene symbol	Full Name	Summary
Actb	Actin beta	Actins are involved in cell motility, integrity and structure (housekeeping gene for J774 experiments)
CTSC	cathepsin C	A lysosomal cysteine proteinase, central coordinator of activation of serine proteinases
FUCA1	fucosidase alpha-L-1	A lysosomal enzyme involved in the degradation of fucose-containing glycoproteins and glycolipids
IRF8	Interferon regulatory factor 8	Transcription factor regulating expression of genes stimulated by type 1 IFNs
LIPA	lipase A lysosomal acid cholesterol esterase	A lysosomal enzyme catalysing the hydrolysis of cholesteryl esters and triglycerides
MAFB	v-maf avian musculoaponeurotic fibrosarcoma oncogene homolog B	A basic leucine zipper transcription factor involved in the regulation of haematopoiesis
MMP1	matrix metallopeptidase 1 (interstitial collagenase)	A secreted enzyme involved in the breakdown of interstitial collagens
MMP10	matrix metallopeptidase 10 (stromelysin 2)	A secreted enzyme which degrades proteoglycans and fibronectin
MMP3	matrix metallopeptidase 3 (stromelysin 1, progelatinase)	A secreted enzyme which degrades fibronectin, laminin, collagens III, IV, IX, and X, and cartilage proteoglycans
NAGA	alpha-N-acetylgalactosaminidase	A lysosomal enzyme which cleaves alpha-N-acetylgalactosaminyl moieties from glycoconjugates
OSBPL1A	oxysterol binding protein-like 1A	An intracellular lipid receptor involved in vesicular transport
PKR	eukaryotic translation initiation	A serine/threonine protein kinase that is activated by autophosphorylation after binding to dsRNA

	factor 2-alpha kinase 2	
RILP	Rab interacting lysosomal protein	A lysosomal protein that interacts with RAB7, a small GTPase that controls transport to endocytic degradative compartments
RIN2	Ras and Rab interactor 2	Binds with Rab5 and functions as a guanine nucleotide exchange factor for RAB5
STAT1	signal transducer and activator of transcription 1	Transcription factor mediates the expression of a variety of genes, thought to be important for cell viability in response to different cell stimuli and pathogens
TBP	TATA box binding protein	A transcription factor that recognizes promoters and initiates transcription (housekeeping gene for U937 experiments)

Where the human gene symbol (all uppercase) is used, the genes if possible were studied in both the mouse and human cell lines. Where the mouse symbol (first letter uppercase, the rest lowercase) is used, this gene was only studied in the mouse cell line.

qRT-PCR was performed using a selected set of lysosomal, vesicular transport genes, and transcription factors genes that showed the highest level of downregulation in the microarray data, plus the gene which gave the highest upregulation (*MMP1*) as a control. As *MMP1* is not expressed in mice, *MMP10* had to be used for the J774 cells being of murine origin. qRT-PCR results for mouse J774 cells and human U937 cells are presented in Fig 3.3 and Fig 3.4, respectively.

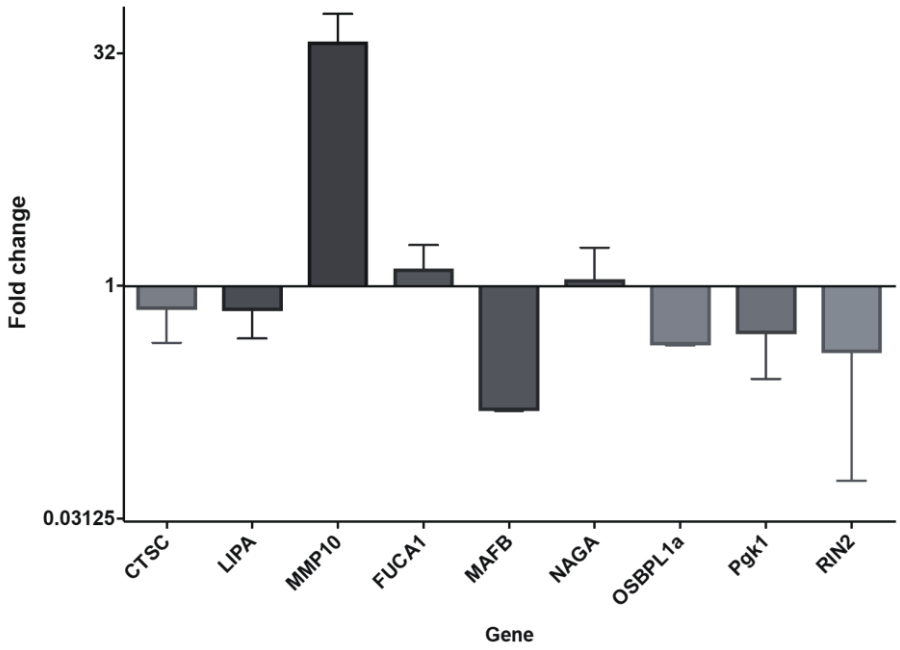

Figure 3.3 Log Fold change of gene expression comparing infected and non-infected J774s from multiple qPCR assays combined for selected set of genes representing GO categories of vesicular transport, lysosome, and transcription factors. RNA was extracted at 48 hours from M. tb naive J774 cells (control) and M. tb infected J774 cells. MMP10 was included as a positive control, as had been shown to be induced in M.tb infection.

Figure 3.3 shows that the genes downregulated in human infection are also downregulated in J774s the mouse cell line post-infection, the largest fold downregulation being in genes *MAFB, OSBPL1α* and *RIN2*. Genes *CTSC* and *LIPA* displayed a small downregulation. Genes *FUCA1* and *NAGA* do not show a clear up- or downregulation, as there is a large difference between the fold change values represented by the error bars, but they were shown to be downregulated in the microarray data (Fig 3.1). *MMP10* displays a large induction with a Log2 fold change >32; this supports the microarray result (as shown in Fig 3.1) , providing a robust positive control.

There is some debate around the use of murine models of *M. tb* infection. It has been suggested that only mice engineered to be genetically susceptible to TB should be used as a disease model (Apt and Kramnik, 2009). Additionally, mouse J774 cells have been

studied in parallel with primary macrophages by Audreu et al. (2017) and the primary cells responded faster and with greater regulatory changes than the J774 cells (Andreu et al., 2017). Accordingly, a human cell line may be better suited to replicate the microarray data generated from human primary blood derived macrophages and dendritic cells.

To investigate whether the same modulation of gene expression could be seen with an immortalised human cell line with monocytic like characteristics, the U937 cells were cultured, then differentiated using PMA prior to infection with *M. tb*. Again 48-hour infections were set up and RNA extracted and cDNA synthesised. qRT-PCR was performed for a selection of the most upregulated genes (Matrix metallopeptidases) and a selection of lysosomal, vesicular transport genes, and transcription factors, which were found to be downregulated in the microarray data.

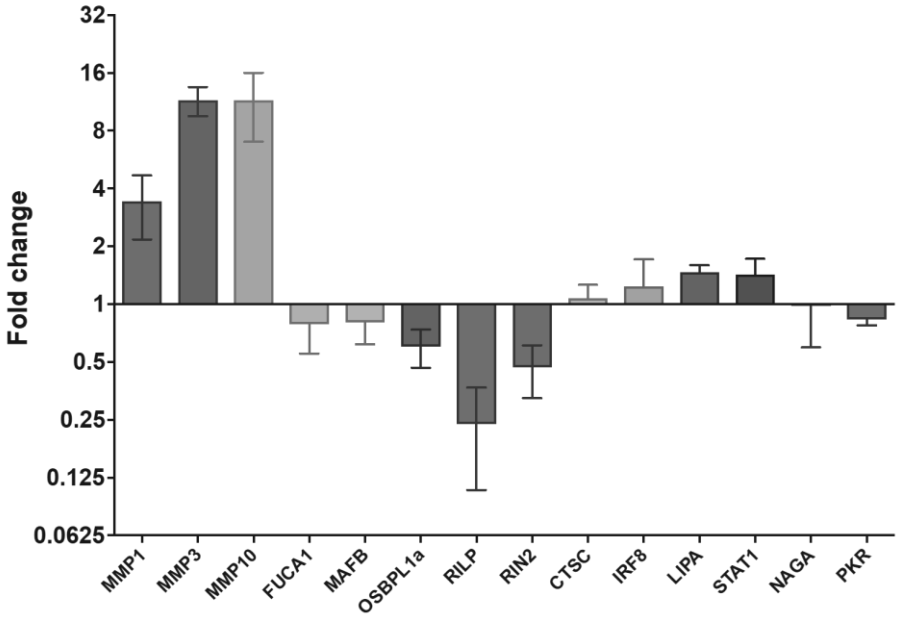

Figure 3.4 Log fold change of gene expression comparing non-infected and infected U937s, from multiple qPCR assays combined for selected genes identified as both up- and downregulated in the microarray data. RNA was extracted at 48 hours from M. tb naive U937 cells (control) and M. tb infected U937 cells.

The qRT-PCR results shown in Figure 3.4 corroborate the microarray data, revealing the downregulation of several of the vesicular transport genes, *RIN2, RILP* and *OSBPL1A* and

also the strong upregulation of the MMP genes, included as positive controls. This confirms that *M.tb* infected U937s display a similar regulation variation post-infection as the primary cell, making them a valid experimental model cell line for use in subsequent mechanistic studies.

3.5 Do we still see this downregulation in non-virulent strains?

There are global changes to host gene expression during the infection process, many of which will be pathogen non-specific and not due to the virulence of pathogen. Similarly, if there are possible distinct differences in the intracellular host-pathogen interaction as a result in differences in the virulence of the infecting strain, then it would be expected that changes in host responses would reflect any such altered processes.

Early literature compared virulent H37Rv and BCG strains (Armstrong and Hart, 1971), and found BCG is unable to replicate appreciably in the macrophage, however, both strains appear to inhibit fusion between the phagosomes and lysosomes initially, but over a period of time a difference becomes clear. Over the time course of the infection, the phagosomes containing the BCG began to show fusion with lysosomes. Due to limitations in the study, the cells were only sampled at 2, 5 and 15 days and the shift happened in this time frame. As the BCG were non-replicating, the number of viable bacteria reduced, and the number of phagosomes fused with lysosomes increased (84% of the population). The study makes suggestions that either fusion takes place with the loss of viability, or fusion results in loss of viability. This is supported in a more recent study of the BCG phagosome proteome (Lee et al., 2010), which reported a high level of concordance between proteins present in BCG and lysosomal proteins such as LAMP -1 and LAMP -2 on day 3 of infection; however, this study does not assess earlier time points. Many recent studies using BCG as a tool only focus on the very initial stages of the infection without mentioning this difference, and this appears not to have been studied further.

Further differences between virulent and non-virulent strains (BCG) were found in the ability to inhibit apoptosis of the host cell. Infection with BCG was found to readily induce apoptosis, whereas infections with virulent *M.tb* (H37Rv) apoptosis of the host cell is

inhibited (Riendeau and Kornfeld, 2003). This further highlights a difference in handling by the host cell.

Thus, the question is raised whether the downregulation seen in these vesicular transport genes (*RIN2, OSBPL1a* and *RILP*) is specific to the virulent strain of *M.tb*. Accordingly, U937 cells were infected with the two strains of bacteria: the virulent lab strain of *M.tb* H37Rv and the non-virulent *M. bovis* BCG. U937 cells were infected under identical conditions and MOIs for both strains where compared with an uninfected control, RNA was extracted and cDNA synthesised followed by qRT-PCR for *RIN2*, *OSBPL1a* and *RILP* and the data is shown in Figure 3.5.

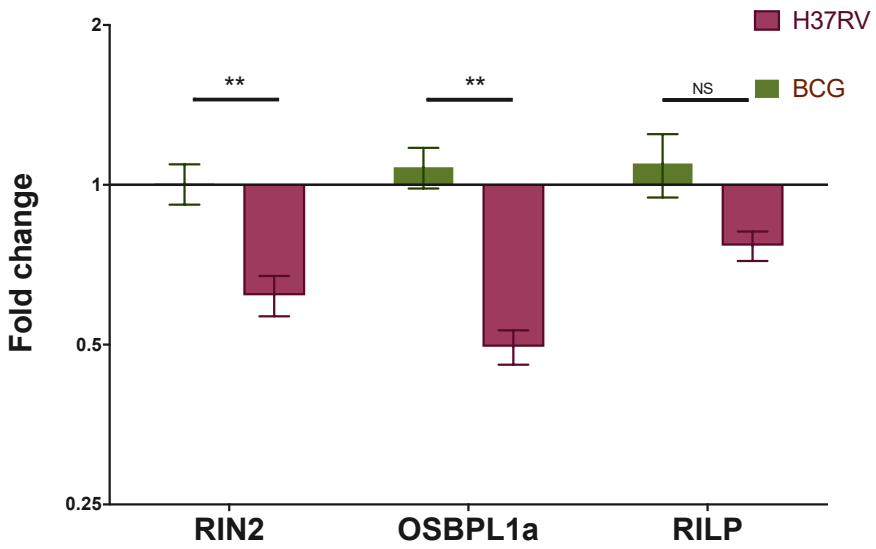

Figure 3.5 Log fold change of gene expression of RIN2, OSBPL1a and RILP in U937 cells at 48 hours post-infection comparing M. tb naive U937 cells with M. tb infected U937 cells (Red) and BCG infected U937cells (Green).

Figure 3. 5 shows a clear difference between the RNA expression of the three vesicular transport genes of interest post-infection with *M.tb* and *M. bovis* BCG. The *M.tb*

infected U937 cells display a downregulation of all three genes (similar, but not identical to data shown in Fig 3.4), whereas the BCG infected cells show little change in the RNA expression compared to the non-infected cells. This suggests that the downregulation of these genes (*RIN2, OSBPL1α* and *RILP*) could play a part in the bacterial survival mechanism leading to virulence and that the process by which this occurs is likely to involve endosome trafficking and phagolysosome maturation.

3.6 Conclusion

In summary, 686 genes were found to be downregulated in primary dendritic cells and macrophages, a large proportion of these genes are involved in lysosomal membrane and vascular processes (Table 1). This downregulation was then confirmed using qPCR in both mouse (Figure 3.3) and human-derived cell lines (Figure 3.4). Three genes of particular interest were revealed to be strongly down-regulated *RIN2, RILP, OSBPL1α*, and upon further investigation they were shown to be affected only when the virulent strain of *M.tb* was used for the infections (Figure 3.5). Together, the data supports the hypothesis that this cellular response to infection with *M. tuberculosis* involve processes ultimately leading to prevention of phago-lysosome fusion and bacterial survival.

3.7 Discussion

The aim of this chapter was to identify whether *M. tb* actively suppresses the expression of genes involved in phagosome-lysosome biogenesis by interfering with one or more host transcriptional pathways. Several published studies (Table 1.1) reveal many changes to host cell gene expression post *M. tb* infection. Re-analysis of the Tailleux et al (2008) data revealed downregulation of lysosomal genes, transcription factors and vesicular transport genes. Many genes identified were either hypothetical proteins and/or had unknown functions. The genes with known functions were further investigated by qRT-PCR to validate the array data using models of cell line infections. The qRT-PCR results confirmed the downregulation of several of the vesicular transport genes, *RIN2, RILP* and *OSBPL1A*. However, the downregulation of many of the other genes could not be replicated. This is most likely to be due to the limitations of using cells lines, but no alternative technology was available at the time of the study, so the use of cell lines was required.

A number of microarray studies have been published (Table 1.1), but most focus on the immune response. Only two studies looked at the downregulated genes, and even then, only in brief (Zhang, 2013; Tailleux et al, 2008). The genes involved in the lysosomal and vesicular transport pathways have been a neglected area of study until now but were found to be amongst the most strongly downregulated genes (Table 3.1).

The lysosomal genes downregulated include a number of enzymes; fucosidase alpha-L-1 (*FUCA1*), cathepsin C (*CTSC*), and lipase A lysosomal acid (*LIPA*). These all play a role in the degradation of infectious agents in the phago-lysosome. Suppression of these enzymes would be advantageous for the survival of the *M. tb* in the host cell. As the majority of studies have focused on which genes are induced rather than suppressed by *M. tb* infection, these findings are unsupported by existing literature at present.

Current literature suggests that *M. tb* is known not only for blocking phagolysosome fusion, but also for halting phagosome maturation (covered in section 1.5 of the introduction). A number of vesicular transport genes are involved in this process. Downregulation of these genes could explain the lack of maturation observed in infected phagosomes. *RIN2, RILP,* and *OSBPL1a* are all involved in phagosome targeting, and were found to be among the most downregulated genes in the experiments presented here. Previously, it has been observed that infection of *Mycobacterium bovis* disrupts the interaction of Rab7 and RILP, but the expression of the *RILP* was not investigated (Sun et al, 2007).

qRT-PCR was used to investigate the changes in expression for cross-platform validation. The qRT-PCR results confirmed the downregulation of several of the vesicular transport genes, *RIN2, RILP* and *OSBPL1A*, supporting the hypothesis that this cellular response to infection with *M. tb* that could be part of the bacterial survival mechanism. Figure 3.6 depicts the involvement of the three genes in the phagocytosis pathway.

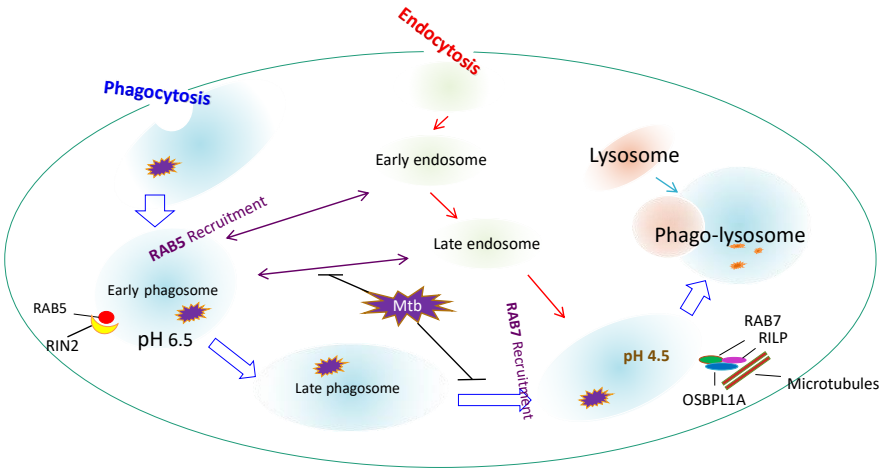

Figure 3.6 simplified diagram of phagocytosis in a macrophage, RIN2 is found to interact with RAB5 at the early phagosome stage, RILP and OSBPL1a form a complex with RAB7 at the late phagosome stage. Also in the diagram are the blocks found in phagocytosis of M.tb, there's no loss of RAB5 and no recruitment of RAB7, no acidification of the phagosome and finally no fusion of the phagosome and lysosome.

RIN2 was first identified in 2002 by Saito et al, descibed as a novel binding protein for Rab5, exhibiting unique biochemical properties. RIN2 is thought to function as an upstream activator and /or downstream effector of Rab5 in the endocytic pathway; it preferentially interacts with the GTP-bound form of Rab5 (Saito et al., 2002) . Rab proteins are a large family of small GTPases responsible for the control of various steps in the intracellular transport process; Rab5 is localised to early endosomes (Gutierrez, 2013). It regulates the fusion between phagosomes and early endosomes, as well as the homotypic fusion between early endosomes (Vieira et al., 2003). Once the early endosomes are associated with phagosomes, it is the role of Rab5 to recruit Early Endosomal Antigen-1 (EEA-1); this recruitment is considered critical for the maturation of phagosomes (Fratti et al., 2001). Rab5 is retained in phagosomes containing *M. tb* bacilli but the mechanism is as yet unknown. An obvious hypothesis is that *M. tb* is responsible by inducing a reduction in the expression of RIN2, supported by the data presented in this chapter.

GTP-bound Rab7 controls late endocytic transport. Rab7 simultaneously binds RILP and OSBPL1a to form a RILP-Rab7-OSBPL1A complex. This complex is required for the assembly of microtubule motors on endosomes via a series of connected events. After RILP and OSBPL1A are recruited to the Rab7, the RILP binds to the projecting arm of the p150 (Glued) dynactin subunit and recruits the dynein motor. Next, OSBPL1A transfers the dynein motor receptor Rab7-RILP to beta-III spectrin (a component of the cell membrane-cytoskeleton). After interacting with beta-III spectrin, dynein initiates the translocation of late endosomes to the microtubule minus ends (Johansson et al., 2007b). This process is essential for the fusion of phagolysosomes. It is therefore reasonable to suggest that the downregulation of both RILP and OSBPL1A post *M. tb* infection could be a survival mechanism employed by the bacteria. Blocking the recruitment of RILP has previously been implicated to be involved in arresting phagosome maturation (Sun et al., 2010, 2007), however, no other studies have discussed its downregulation. OSBPl1a has also been implicated in the regulation of cholesterol transport through the endo-lysosomal system (Zhao and Ridgway, 2017), which further adds to the hypothesis that its downregulation is advantageous to the bacteria; this will be discussed in more detail later.

In light of this*, RIN2*, *RILP* and *OSBPL1A* are good candidates for further investigation; they are all involved in phagosomal maturation and targeting, and all downregulated post *M. tb* infection. If these are over-expressed in U937 cell lines, do the phagosomes mature and fuse with the lysosomes, allowing killing of the bacteria, and if so by what mechanism is the *M. tb* working to suppress expression?

Chapter 4 - Cellular and Microbiological Validation of the *M.tb* infection model in U937 cells

4.1 Introduction

As previously discussed in chapter 3, there is some debate around the use of cell lines for studying host-pathogen interactions. An accepted general biological principle is that any experimental systems do not/cannot fully replicate the natural infection process. The reductive scientific approach necessarily requires models that are at least validated in some aspect of the process under investigation. Using this principle, the choice of macrophage-derived cell lines to study host-pathogen interactions needs to be validated both from a cellular and microbiological perspective. The use of human primary macrophages would be ideal, as physiologically, they are the most relevant. However, there are technical and ethical issues with the acquisition, maintenance and use of such cell lines. Primary macrophages potentially introduce genetic variation in the study, as they are pooled from different human donors, thus, making interpretation of results more complicated. Furthermore, primary cells are difficult to maintain in the laboratory and manipulate genetically (Hamm et al., 2002). While cell lines have their own set of drawbacks, these are outweighed by the benefits in this study. Chapter 3 has demonstrated that the downregulation of a selected set of genes (*RIN2 RILP, and OSBPL1a*) in primary macrophages and dendritic cells found in previously published studies (Tailleux et al., 2008) was reproducible in cell lines, as well as a limited number of positive control genes(e.g. MMPs). The use of murine cells was ruled out, due the question of validity (covered in chapter 3.4), Thp-1 cells died too soon after infection to allow for RNA extraction of the required volume at 48 hours, whereas U937 cells were more robust to infection, allowing greater volumes of RNA to be extracted.

However, in order to proceed using the human U937 cell line, the infection model needs to be further characterised, especially as it is intended to be used not only in transfection experiments as an over-expression cell line (Chapter 5 and 6), but also with different mutant strains of *M.tb* (Chapter 7). Thus, the aim of this chapter was to characterise the infection of U937 cells with *M.tb*, using both cell biology and microbiological approaches. The U937 cells were assayed for efficiency of infection, intracellular bacterial growth and survival, and finally bacterial intracellular trafficking using

confocal fluorescence microscopy and co-localisation of biomarkers for the phagosome-lysosome maturation pathways. These experiments thus provide appropriate and targeted, if not complete, validation of the use of U937 cell infection model for the proposed subsequent studies.

4.2 Coverslip assay of infection: efficiency of phagocytosis and intracellular growth

A coverslip-based assay was used to count the number of bacteria per U937 cell. This not only allowed an estimation of the number of cells infected at each time point and the number of bacteria per cell, but also the collection of representative images of the cells at different time points. The representative images are the control experiments for the later confocal studies.

Method: 24 hours prior to infection, the U937 cells were plated into four-well tissue culture plates containing sterile glass coverslips. The cells were plated at $0.5x10^6$ cells per ml, and simulated with PMA to a final concentration of 100 ng/ml. The U937s were then infected with H37Rv at a MOI of 20:1. The tissue culture plates were incubated in a humidified 37ºC incubator containing 5% CO_2 up to 48 hours. At each time point, the cells were washed with RPMI, then fixed using ice cold methanol and stained using Kinyoun's cold carbol-fuscin stain and counter-stained with 2 % malachite green. Experiments were performed in duplicate. After staining, the cover slips were removed from the wells and mounted onto microscope slides. At 24 hours, all remaining cells were washed with RPMI to remove any non-phagocytosed bacteria, followed by the addition of fresh media, and re-incubation at 37°C for the remaining time.

Results: Images from the cover slip assay of mycobacterial growth within U937 cells are shown in Figure 4.1. They are representative of the different time-points throughout the assay for both uninfected and infected cells across a 48 hour period. The images reveal that the macrophages differentiate over time, with the addition of PMA, starting as small spherical non-adherent cells and becoming larger adherent, less uniform cells. The infected cells exhibit more signs of differentiation than the uninfected cells, with the cell membranes becoming less defined and projections forming between the macrophages. Also, it is evident that there was a substantial decrease of cells at 48 hours for the *M.tb* infected cells. This was taken into account when looking at the viable counts later in this chapter.

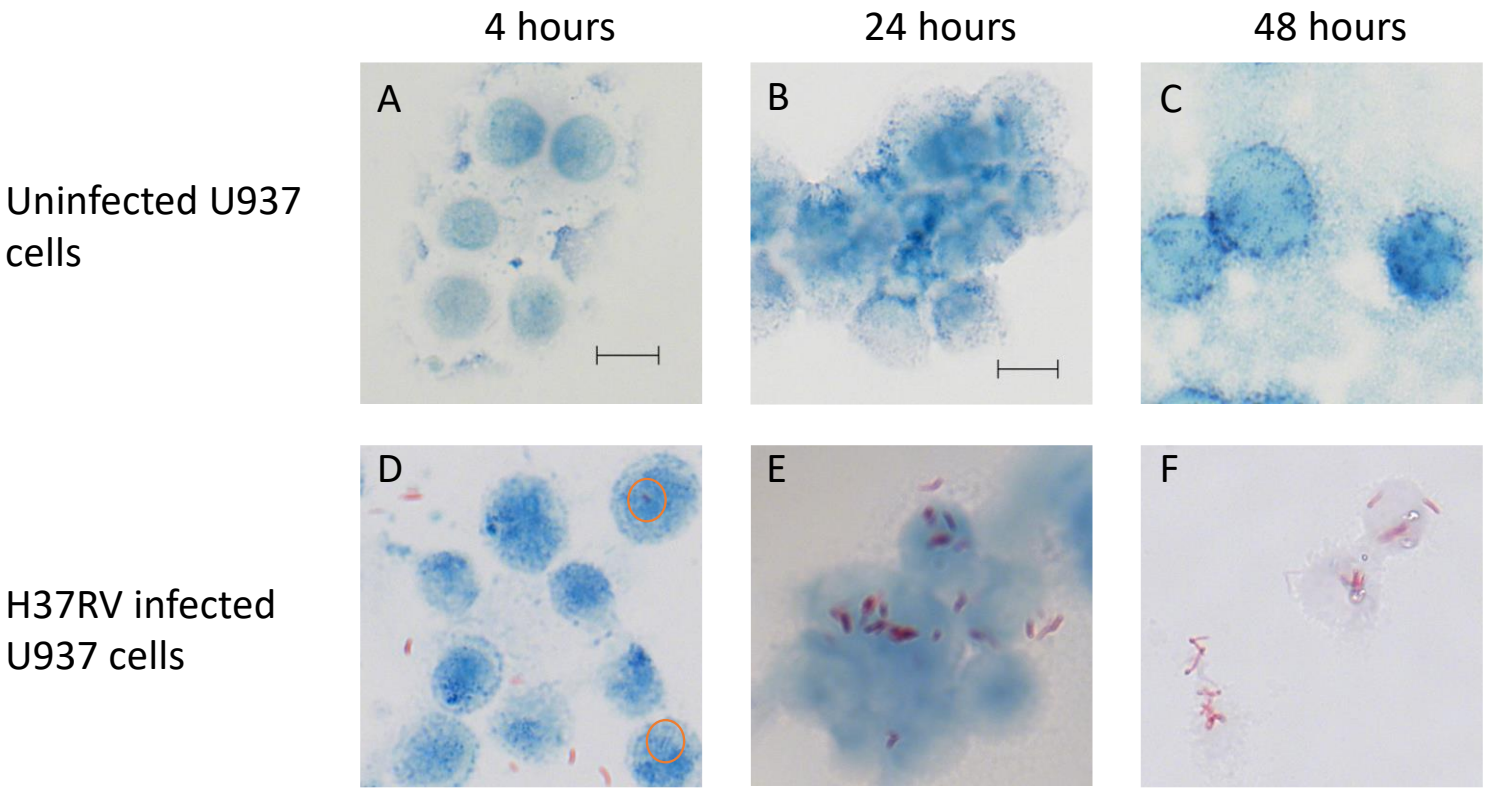

Figure 4.1- Representative images of naïve and H37Rv infected U937 cells after 4 hours, 24hours and 48hours, with the bacteria being washed off at 24 hours. Images were taken using a Zeiss Axioplan 2 upright microscope coupled with a Axiocam HR digital CCD camera. Magnification x 1000. The cells were stained using Kinyoun's carbol fuchsin and counter-stained with 2% malachite green. Single infecting bacillus are circled in the 4 hours image (D) for the infected U937 cells.

From Figure 4.1, bacteria were identified as the red stain within the malachite green counter-stained macrophages. At four hours (image D), a small number of cells contained one or two bacteria, but a large number of cells remained uninfected. After 24 hours (image E), more cells contained bacteria but still relatively small numbers compared with 48 hours (image F). At both 24 hours and 48 hours post-infection, some cells contained clumps of bacteria which could be due to phagocytosis of multiple bacteria or replication of the *M.tb* within the cell. Also, the loss of cells after 24 hours became more apparent, the infected U937s cells were lysing, thus releasing more bacteria for the neighbouring cells to phagocytose. The lysis of the U937s could explain the faint counter-stain in the 48-hour image of the infected cells in Figure 6F, where the bottom left hand corner of the image shows a lysed cell with the bacteria escaping.

A quantitative analysis of the infection rate and intracellular growth was conducted using the coverslip-based assay. For each time-point the number of intracellular *M.tb* were counted randomly in a minimum of 100 U937 cells across 2 different coverslips. This allowed the calculation of the mean percentage of U937 cells infected (Figure 4.2) and the mean number of *M.tb* per cell at each time-point throughout the infection (Figure 4.3). The average number of infected U937 cells at 4 hours was 40 %, which increased to 61 % and 66 % at 24 hours and 48 hours, respectively (Fig. 4.2). The small increase in the percentage of infected cells after washing of the cells at 24 hours could be explained by the incomplete removal of the initial bacterial inoculum, or the re-phagocytosis of the released bacteria from the lysed infected U937 cells.

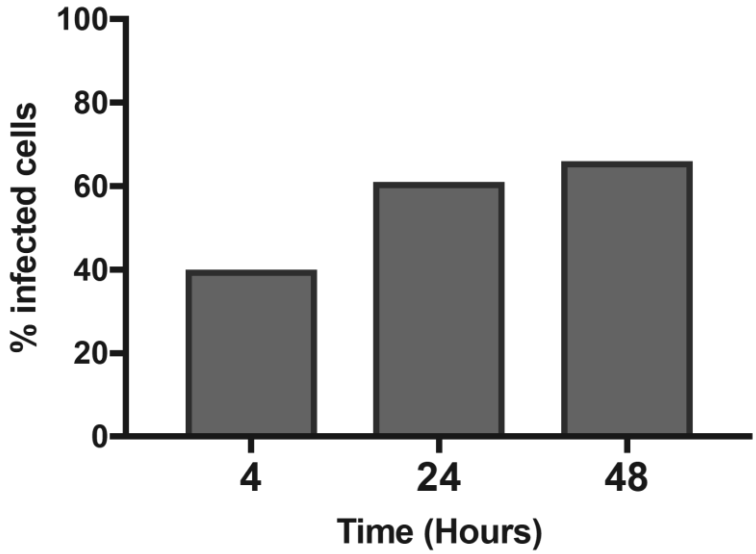

Figure 4.2 - Coverslip assay of infection rate: percentage of cells infected with H37Rv at 4, 24 and 48 hours post infection. The U937 cells were infected at a MOI of 20:1 and were washed to remove the excess bacteria at 24 hours. 100 cells were counted at each time point across 2 different coverslips.

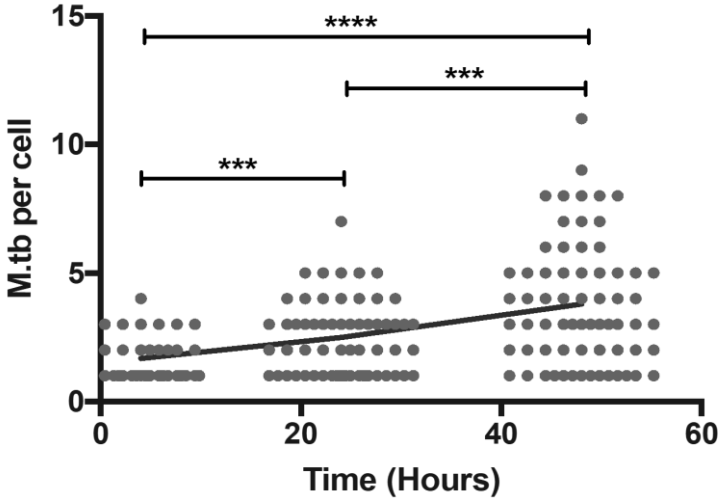

Figure 4.3 - Efficiency of phagocytosis as measured by coverslip assay of the average number of intracellular bacteria per infected U937 cell at 4, 24 and 48 hours post infection. The U937 cells were infected at a MOI of 20:1, Coverslips were set up in duplicate and 100 cells were counted across multiple fields of view on both slides and data combined.

Figure 4.3 illustrates the results of the coverslip assay of the number of intracellular bacteria in the infected U937 cells. The average number of bacteria per infected cell at 4 hours was 1.68 (SD 0.83, range 1-4 *M.tb*/cell). This number increased to 2.49 bacteria per cell at 24 hours (SD 1.41, range 1-7 *M.tb*/cell), then increased again at 48 hours to 3.79 bacteria per cell (SD 2.41, range 1-11 *M.tb*/cell). There was a statistically significant increase in the number of bacteria per cell over time (p-value <0.0001). There is also a significant increase between the individual time points, between 4 and 24 hours (p-value 0.0004), and between 24 and 48 hours (p-value 0.0003). An increase from 1.68 bacteria/cell at 4 hours to 3.79 bacteria/cell at 48 hours is approximately in line with a generation time of 24 hours, accounting for re-phagocytosis.

4.3 Viable counting for intracellular growth

Counting the intracellular *M.tb* throughout the infection process of the U937 cells doesn't directly indicate the viability of the bacteria. Thus, viable counts were used to measure the survival of *M.tb* phagocytosed by the U937 cells.

Method: The U937 cells were set up in six-well plates and stimulated with PMA then infected as before at a MOI 20:1, with a maximum infection time of 6 hours. After the infection, viable count at the time-points of 2, 6, 24 and 48 hours were measured. At each time-point the infected cells were washed to remove any residual bacteria and then lysed with sterile 0.25% SDS. The lysates were sonicated to disperse the bacteria and reduce the clumping, before being plated in triplicate serial dilution on 7H11 agar, followed by incubation at 37°C for four weeks before counting.

Results: Figure 4.4 illustrates the intracellular growth of H37Rv in U937 cells with a 20:1 MOI and a maximum infection time of 6 hours. Figure 4.4 shows that phagocytosis continued between 2 and 6 hours, however, no significant change in the number of viable bacteria were observed (p= 0.51). The bacteria appeared to grow after phagocytosis with viable counts increasing significantly from 6 hours to 24 hours (P-value 0.001). At 6 hours there was on average $5x10^5$ bacteria/ml of media, by 24 hours this had increased to around $2.5x10^6$ bacteria/ml, this can roughly be back calculated, taking into account the % of cells infected (60%, Figure 4.2) at 24 hours, as around 2 bacteria per infected cell, which is in line with the total counts (Figure 4.3). Between 24 and 48 hours the rate of growth slows but the

number of bacteria increases to $5x10^6$, approximating the doubling time of *M.tb* of 24 hours and accounting for re-phagocytosis due to partial cell lysis at 48 hours (Fig.4.1). Again this can be back calculated giving an average of 3.8 bacteria per cell, which almost exactly matches the observed 3.79 bacteria per cell (Figure 4.3). The increase in growth of the bacteria between 6 and 48 hours is significant (p-value 0.02), given that there is usually a lag phase for bacterial growth in the first 4 – 8 hours post-infection, followed by growth, the data are consistent with this infection phenomenon and validates the use of U937 cells and the experimental infection protocol for subsequent mechanistic studies.

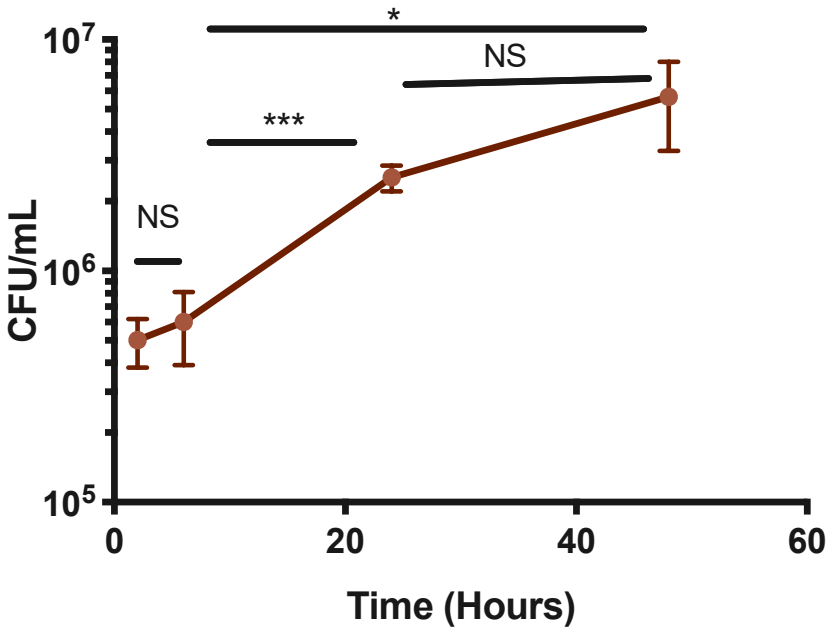

Figure 4.4 –Intra-macrophage growth of H37Rv infection in U937 macrophage like cell line. MOI 20:1. Expressed as CFU/ml of cell lysate. Each time point was plated in triplicate.

4.4 Confocal microscopy of U937 cells infected with *M.tb*

It is well known that *M.tb* affects phagosome maturation (Koul et al., 2004). When functioning correctly, the phagosome acquires the early endosomal markers Rab5 and EEA1 immediately after phagocytosis. As the phagosome matures it loses Rab5 and gains Rab7, a late endosomal marker and finally as they form phagolysosomes, acquire lysosomal markers such as Lamp1. However, phagosomes containing virulent *M.tb* have been shown not to acquire Rab7 and retain Rab5 (Fratti et al., 2003; Koh et al., 2018; Via et al., 1997).

In order for the U937 infection model to be valid, the cells need to display this phenomenon of phagosome maturation arrest *i.e.* retain the Rab5 marker and not acquire Rab7 or Lamp1. To test this, an immunofluorescence assay was set up to analyse trafficking of the *M.tb* within the cells and to look for co-localisation of the bacteria with either Rab5, Rab7 or Lamp1.

Method: Cells were set up as per the coverslip assay, stimulated using PMA and then infected with a MOI of 20:1, with an infection time of 24 hours with FITC stained H37Rv. After 24 hours, the cells were washed with 0.1M PBS then fixed with 4 % paraformaldehyde. The cells were permeabilised using 0.1 % Triton-X before blocking with 10 % of normal serum, which is dependent on the species of the secondary antibody, with 1 % BSA in 0.1M PBS. The cells were then incubated overnight at 4°C with the primary antibodies (Rab5, Rab7, Lamp1). Subsequently, Alexa dye conjugated secondary antibodies were used for immunostaining, and Dapi was used as a counter stain.

Results: Figure 4.5 shows representative images of the fluorescence co-localisation studies. For each primary antibody, the slides were set up in triplicate and all three coverslips were examined for the assay, totalling over 100 cells, and a representative image was taken for illustration purposes. The majority of the infected cells displayed co-localisation of the bacteria with Rab5 and did not exhibit any co-localisation with either Rab7 or Lamp1, as expected. Figure 4.5c illustrates co-localisation of *M.tb* with Rab5; this is evident from the yellow colour as a result of the merging of the green fluorescence-stained bacteria (image 4.5a) and the red fluorescence-stained Rab5 (image 4.5b). Figure 4.5d is the result for the co-localisation represented graphically in a scatterplot, where the intensity of the green fluorescence is plotted against the intensity of the red fluorescence for each pixel. The pixels in the scatterplot are pseudo-coloured to represent the frequency of green-red

pixel combinations (hot colours representing high values by convention). When co-localisation is present, the points of the scatterplot cluster around a straight line, thus confirming the visually apparent co-localisation. For further confirmation, a statistical quantification of the co-localisation was also performed, giving a Pearson's R value of 0.79 and a Manders tM1 value of 0.83. Mander's Colocalization coefficient splits the coefficients in to tM1 and tM2, one being high-colocalisation and zero being low. tM1 and tM2 represent how well each channel overlaps with the other (Li et al., 2004). Here, tM1 is used as it shows how well the bacteria (green) overlaps the Rab5 (red). This is useful as there is a larger amount of Rab5 than bacteria, the green overlaps well with the red but not all the red overlaps with the green, and this can skew the Pearson's R value, thus Mander's gives a more accurate result.

For both Rab7 and Lamp1, no co-localisation with the FITC-stained bacteria was observed (Figure 4.5 e-g, i-k). The scatterplots also confirmed this, as no linear relationship was seen between the two colours (Figure 4.5 h&l). Pearsons R values were -0.04 and -0.1 and the Manders tM1 values were 0.002 and 0.0, respectively.

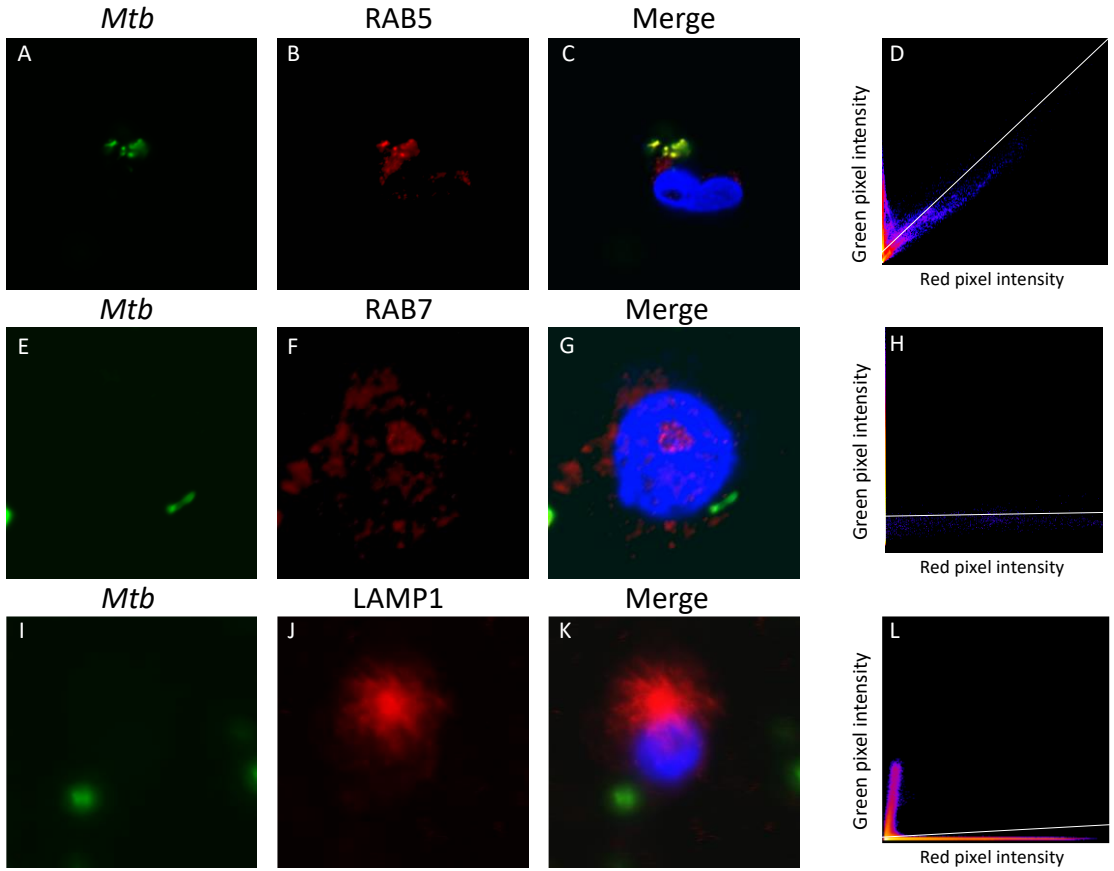

Figure 4.5 Confocal microscopy of U937 cells infected with M.tb H37Rv. Panels A, E and I, M.tb stained with FITC. Panels B, F, and J, stain endosomal markers (Rab5, Rab7 and Lamp1). Panels C, G, and K, merged images of the M.tb and endosomal marker. Panels D, H and L, co-localisation represented graphically in a scatterplot where the intensity of the green is plotted against the intensity of the red for each pixel. Over 100 cells were analysed across coverslips set up in triplicate.

4.5 Conclusion

In summary, this chapter covers the evaluation of the infection model of *M.tb* R37RV in the U937 human macrophage-like cell line. The infection rate was demonstrated to be 40 % of cells infected at 4 hours, increasing to over 61 % at 24 hours and 66 % at 48 hours (Figure 4.2). The infected cells were analysed to give the average number of bacteria per cell, which was 1.68, 2.49, and 3.79 at 4, 24, and 48 hours respectively (Figure 4.3). The growth of viable bacilli across the 48-hour period was also consistent with multiple previously published studies and correlated with the generally accepted approximate growth rate of 20 hours for *M.tb*. In addition, the U937 cells were confirmed to display the same phenomenon of phagosomal maturation arrest when infected with *M.tb* (Figure 4.5). This is in concordance with what has been consistently shown in publications for primary cells (Chandra et al., 2015; Clemens et al., 2000; Clemens and Horwitz, 1995; Via et al., 1997).

4.6 Discussion

The aim of this chapter was the characterisation of the use of U937 cells as an infection model. Traditionally, THP-1 a human monocytic leukemic cell line (Tsuchiya et al., 1982) was the preferred cell line for host pathogen studies of *M.tb* (Theus et al., 2004). Preliminary studies demonstrated greater THP-1 cell death compared with J774 and U937 cells, requiring a lower MOI for cell survival, while U937s appeared to be more robust and capable of surviving a higher MOI, implying greater infection rates at early time points. Several recent *M.tb* host-pathogen studies have also used U937 cells for host-pathogen studies, this also contributes to the validity or at least acceptance of their use as an infection model (Butler et al., 2017; Lavarti et al., 2016; Shen et al., 2017; Yang et al., 2017).

As is known with any population of cells, not all cells behave in an identical manner. This is clearly highlighted by both the coverslip assay images and analysis, where even at 24 hours with a MOI of 20:1, only around 60 % of the cells are infected, and of those cells infected, the number of bacteria per cell also varies greatly. This must be taken into account when looking at changes in expression of mRNA in the host; with 40 % the cells naïve to the *M.tb*, this could artificially supress the fold change results significantly, and potentially mask a meaningful result. Thus, the data generated needs to be considered as an average of the heterogenous cell population rather than an accurate measure of any one single cell. This is

also true for the interpretation of previous transcriptome data from cell models and is the technical limitation of such studies, only overcome by single cell analysis using microfluidic devices for visualisation (Ng et al., 2015) and single cell transcriptomes developed for eukaryotic cells (Cai et al., 2020; Ziegenhain et al., 2017), but these require cDNA library amplification that alters the true representation of mRNA profiles. Examining host-pathogen interactions at a single cell level and an individual intracellular bacteria level currently lies beyond available technological methods. However, confocal microscopy and biomarker co-localisation linked to single cell microfluidic separation provides the nearest experimental model to date.

Another factor to be taken into account in the described experiments in this chapter is the noticeable loss of cells at 48 hours. While for the RNA analysis this is rectified by correcting the results to a stably expressed housekeeping gene, this is harder to rectify when doing viable counts; nevertheless, this technical limitation of using U937 cells and sufficient MOI to make efficient measurements possible, will be taken into account when reporting further viable counts. Overall, as phagocytosis is a rapid process and the arrest in maturation of the phagosomes also appears to be almost immediate, the relevance of a 48 hour time point is questioned. The importance is on the maximum number of cells infected at the early time points, rather than longevity of the cells.

The confocal studies looked at a population of cells spread over different phases of infection. Thus, it was important to get an overview of the population before taking representative images for analysis, as this would provide an accurate picture. With co-localisation studies using confocal microscopy, there is a risk that markers could be merely in the same plane rather than co-localised. Although this could be true for small number of cells, it is unlikely that the majority of the cells analysed display the same characteristic. Z-stacks (3D visualisation of the cell built by taking images incrementally stepping through the sample using the focal drive) could be used to visually test co-location, however, the statistically quantification of co-localisation is designed for flat images; newer software has been developed to specifically analyse 3D microscopy data but was unavailable at the time of this study.

While the coverslip assay, viable counts and microscopy of trafficking events are basic assays, they provide evidence for the use of the U937 cell line for infections and transfections in the forthcoming chapters.

Chapter 5 – Transfection and generation of stable human macrophage cell line U937, for overexpression of genes involved in phagosome trafficking

5.1 Introduction and aims

This chapter covers two main areas; i) the construction of mammalian expression plasmids (vectors) to enable the overexpression of three target genes associated with human macrophage responses to infection with *M. tb* and ii) developing methods for efficient transfection into the human cell line, U937 and demonstration of efficient expression of target genes.

Bioinformatic analysis of previously published transcriptional data, as described in Chapter 3, identified the downregulation of three important vesicular transport genes that are known to be involved in phagosomal maturation following infection of human macrophages and dendritic cells with *M. tb*. These selected genes encode: Ras and Rab interactor 2 (*RIN2*), Rab-interacting lysosomal (*RILP*) and Oxysterol binding protein like 1A (*OSBPL1A*). Based on this analysis and extensive literature evidence (see Introduction Chapter 1) that *M. tb* displays a survival strategy within macrophages associated with the inhibition or delay in phago-lysosome fusion, it can be hypothesised that *RIN2, RILP and OSBPL1*A are suppressed in response to infection with *M.tb* as part of a complex multi-layered host-pathogen interaction leading to intracellular survival of *M.tb*. It is widely known that *M. tb* infection causes arrest of phagosome maturation in the host cell (Cambier et al., 2014; Ernst, 2000; Hestvik et al., 2005; Meena and Rajni, 2010).

In order to test this hypothesis, an experimental strategy was proposed which overexpressed these genes in human macrophage cell lines and subsequently monitored the effect on *M.tb* trafficking through the phagosome-lysosome (P-L) pathway. The supposition is that over-expression of *RIN2, RILP and OSBPL1A* essentially reverses the suppression induced by *M.tb* and thus the normal P-L pathway will be restored and *M.tb* will be found in P-Ls. Confocal tracking of *M.tb* location and bacterial viability will be measured as an indicator of the reversal of P-L inhibition, confirming the *M.tb* subversion mechanisms role that targets RIN2, RILP and OSBPL1A.

The first step of the strategy was to clone the genes which encode *RIN2, RILP* and *OSBPL1A* in expression vectors that could be transfected into experimental macrophage cell lines and subsequently to show that they are expressed prior to monitoring infection outcome. Accordingly, this chapter describes the generation of transfectant constructs with each gene individually over-expressed in U937 cell lines. The development of methods for transfecting human macrophage cells lines and establishing conditions that maintain stably transfected cells, which can subsequently be used for infection with *M.tb*, is described.

5.2 Propagation of plasmids containing cDNA for *RILP, RIN2 and OSBPL1A*

As these genes have been poorly studied, no commercial expression plasmids containing them and suitable for transfection were available for purchase. However, clones of human genes are available commercially. Accordingly, cDNA clones were ordered from the Integrated Molecular Analysis of Genomes and their Expression (I.M.A.G.E) consortium (Lennon et al., 1996), which holds a large collection of genes and cDNA clones for research purposes. The cDNA for the opening reading frames (ORF) predicted to code for *RIN2*, *RILP* and *OSBPL1A* were procured (see Table 5.1).

Table 5.1 Clone identification from the I.M.A.G.E consortium and their cloning vectors.

Gene name	IMAGE id number	Code	Vector
RILP	5174974	IRAK51K20	pCMV-SPORT6
RIN2	3156682	IRAK35D08	pCMV-SPORT6
OSBPL1a	5264608	IRAK198D21	pBluescriptR

The cDNA was in the form of a plasmid transfected into *E. coli* in a stab culture. The clones were sent in 2 different vectors, both of which were designed for cloning and expression (pBluescriptR: Bacterial expression only, pCMV-Sport6: Bacterial and mammalian expression) of a single gene, and in this case the gene encoding ampicillin resistance (Figure 5.1 & 5.2). The *RILP* cDNA clone is the complete coding sequence (cds) taken from human

pooled organ tissue, inserted into the cloning sites NotI and EcoRV of the pCMV-Sport6 vector. The *Rin2* cDNA clone is a synthetic construct of the full cds of the mouse gene, which is a homolog for the human gene and the only full cds of the gene *Rin2* available, the homolog has the same four conserved domain architectures and 91 % score for the pairwise alignment (details attached in appendices) so is predicted to function within the human cell. The source was an infiltrating ductal carcinoma in the mammary gland of a female mouse. The cDNA was cloned in the *Not*I and the *Sal*I cloning site of the pCMV-Sport6 vector (Figure 5.2). The *OSBPL1a* cDNA clone is the complete cds taken from human hippocampus tissue, inserted in the *Bam*HI and the *Sal*I-*Xho*I cloning sites of the pBluescriptR vector. It was noted that the cds for *OSBPL1a* were short compared to the longest cds in the locus, however, there were multiple transcript variants for this gene (Strausberg et al., 2002).

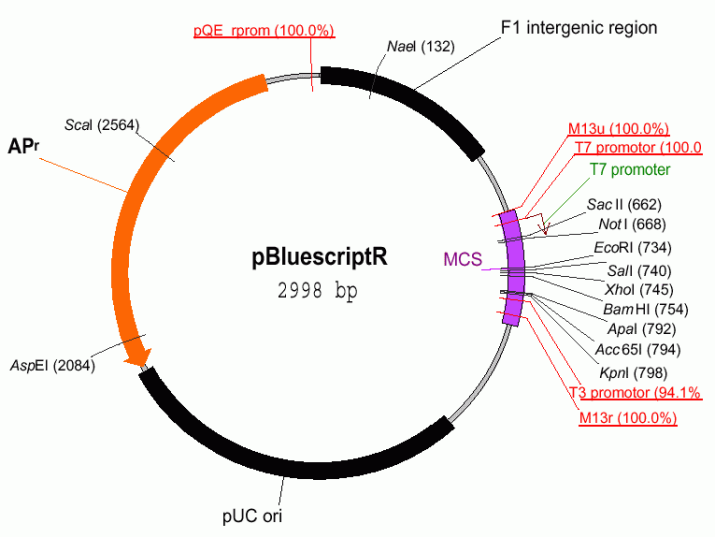

Figure 5.1 Plasmid map of the pBluescriptR vector with all the main features labelled.

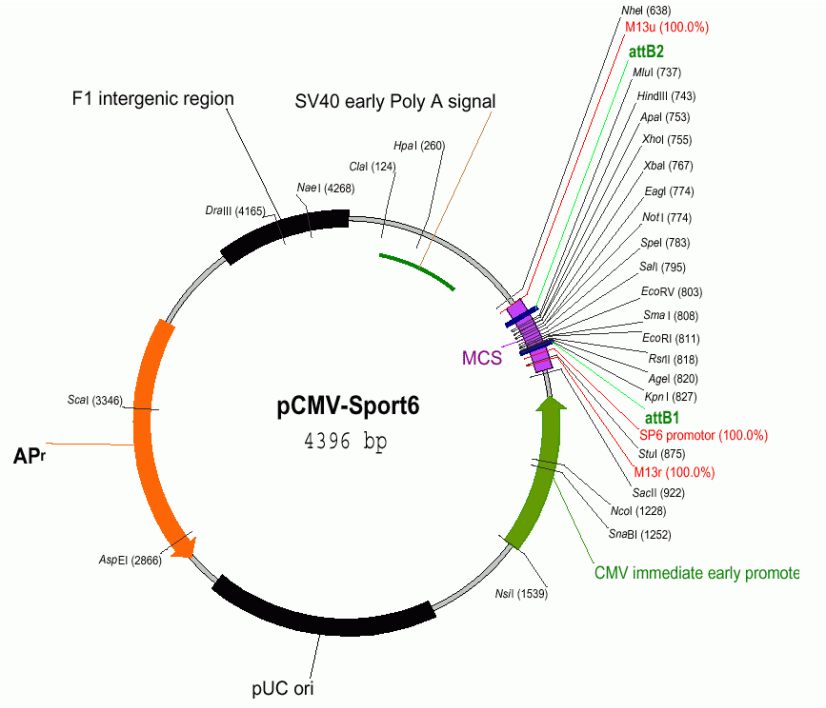

Figure 5.3 Plasmid map of pCMV-Sport6 vector, with all the main features labelled.

Confirmation of clone identity - *Methodology:* To check that the clones were as expected once they were propagated diagnostic digests were performed, to highlight any inconsistencies between the expected and the received clones. The culture was plated on to LB agar plates containing Ampicillin (100 µg/ml) and incubated overnight at 37°C. Single colonies were subsequently picked and grown in LB plus Ampicillin (100 µl g/ml) at 37°C under agitation, thus all cultures were propagated from a single colony. The plasmid was extracted using the NucleoSpin® plasmid mini kit following the manufacturer's guidelines and used to transform competent *E. coli* using the heat shock method (see Methods). The transformed *E. coli* were grown in LB broth and stored as 10 % glycerol stocks at -80°C for future use. NucleoSpin® plasmid preps were performed for the three plasmids containing the cloned inserts for *RILP*, *Rin2* and *OSPBL1α*. Once the plasmids were extracted their identification was confirmed using restriction endonuclease analysis, the plasmids were mapped and the restriction sites identified (Figure 5.3 – 5.5). Based on this, the enzymes were selected to cut multiple times within both the vector and insert, giving bands of

distinguishable different sizes (Table 5.2). Each plasmid had a different restriction map, thus, the fragment sizes were distinct to each plasmid, allowing for confirmation of their identity.

Table 5.2 Restriction characteristics of vectors.

Vector	Gene	Restriction enzyme	Fragment sizes (bp)
pCMV-Sport6	*RILP*	*SacI*	4218bp, 1272bp, 520bp
pCMV-Sport6	*Rin2*	*HindIII*	6104bp, 2464bp, 492bp
pBluescriptR	*OSBPl1a*	*SacI*	4806bp, 1104bp, 77bp

Results: The diagnostic digests confirmed that the plasmids had the expected restriction sites, confirming the identity of each gene. Confirmation of fragment lengths by agarose gel electrophoresis are shown in Figure 5.6.

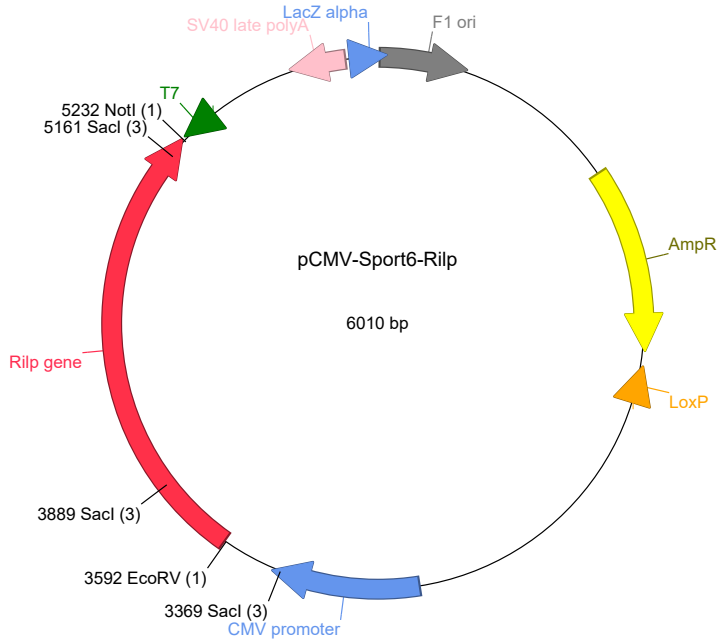

Figure 5.3 Plasmid map of pCMV-Sport6 vector containing RLIP cDNA (red); obtained from the I.M.A.G.E consortium.

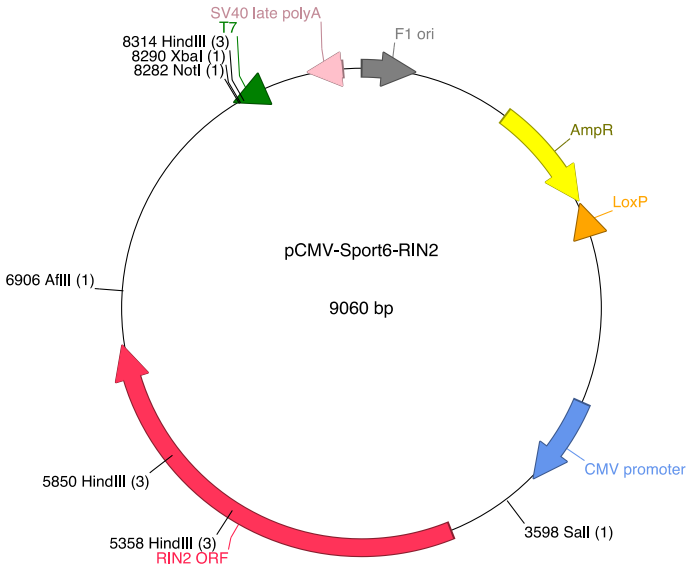

Figure 5.4 Plasmid map of pCMV-Sport6 vector continuing Rin2 cDNA (red); obtained from the I.M.A.G.E consortium.

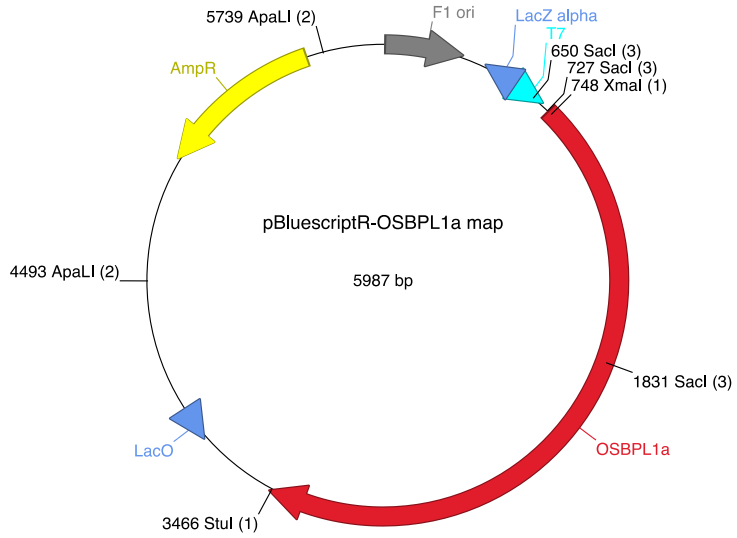

Figure 5.5 Plasmid map of the pBluescriptR vector and OSBPL1a cDNA insert (red) obtained from the I.M.A.G.E consortium

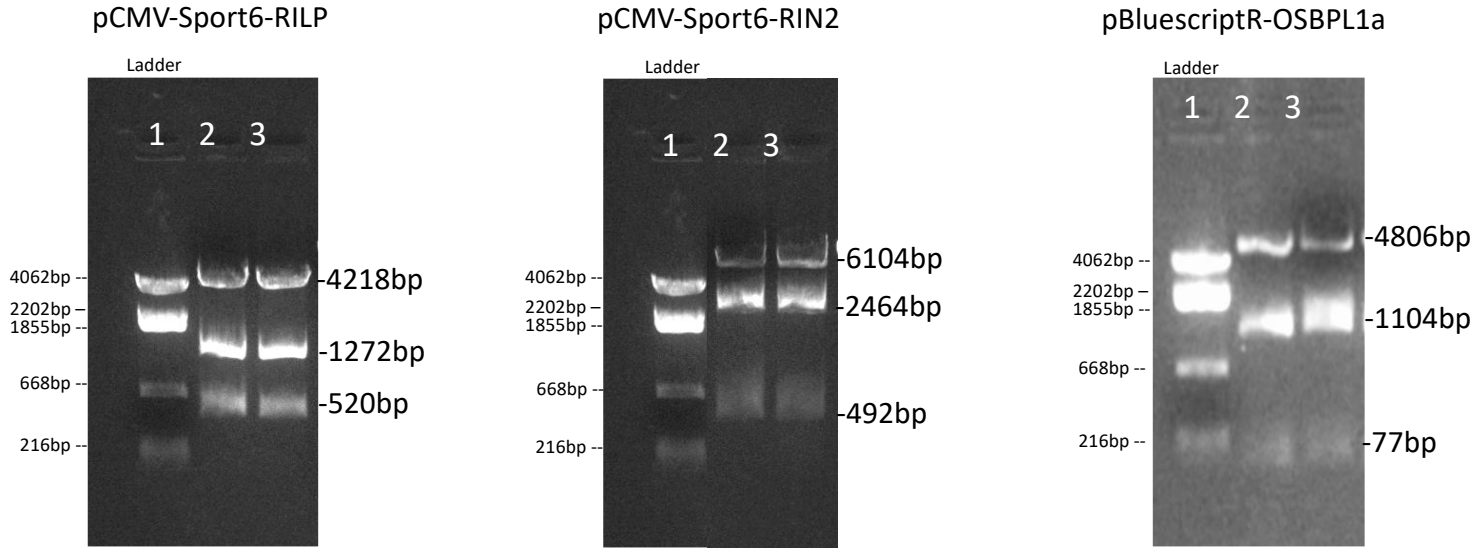

Figure 5.6 Restriction digests of the IMAGE plasmids – The three plasmids were digested with restriction enzymes SacI, HindIII and SacI as per Table 5.2. The digested fragments were then separated using agarose gel electrophoresis. Lane one is the 1KB ladder, lanes two and three are replicate digestions.

The cDNA was supplied in vectors capable of expression of a single mammalian gene, however, to co-express the gene of interest and a resistance gene, a multi-cistronic vector is required. The antibiotic resistance gene will be used to select the successful transfectants and maintain the stable cell lines. Multicistronic vectors have an internal ribosome entry site (IRES) element which allows initiation of translation from an internal region of the mRNA. The IRES acts as another ribosome recruitment site, thus resulting in co-expression of two proteins from a single mRNA. To allow the expression of the gene of interest and the antibiotic resistance gene, the cDNA was removed by restriction digest and cloned into two multicistronic vectors, one expressing a neomycin resistance gene (Figure 5.7) and one expressing a hygromycin resistance gene (Figure 5.8). These plasmids were chosen as they have been previously used to successfully stably transfect cell lines, most recently pIREShyg2 (Figure 5.8) was used by Kortüm et al., (2015) in a study of Lynch syndrome to stably transfect human colon cancer cells (HCT116). pIRESneo2 (Figure 5.7) is also a commonly used vector for constructing stable cell lines, its use dates back to 2002 and most recently five papers in 2017 (Allison et al., 2017; Chan et al., 2017; Kadlecova et al., 2017; Newman et al., 2017; Rack et al., 2017).

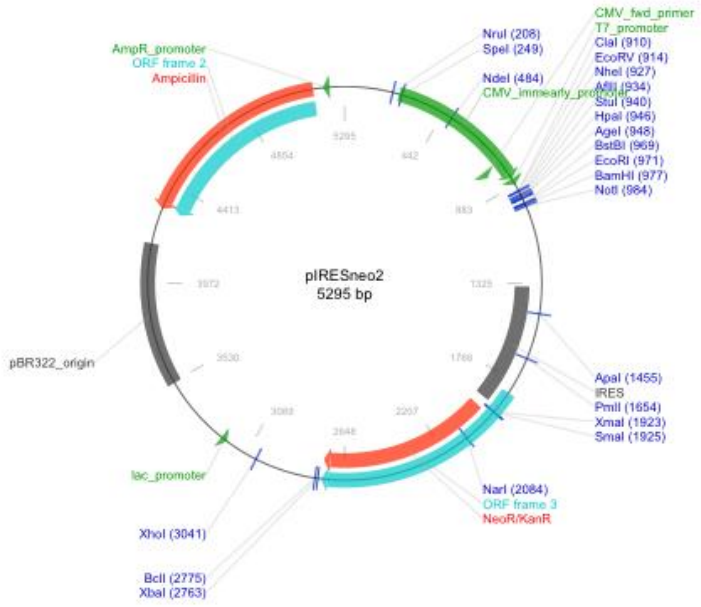

Figure 5.7 Plasmid map of multicistronic vector expressing neomycin resistance gene.

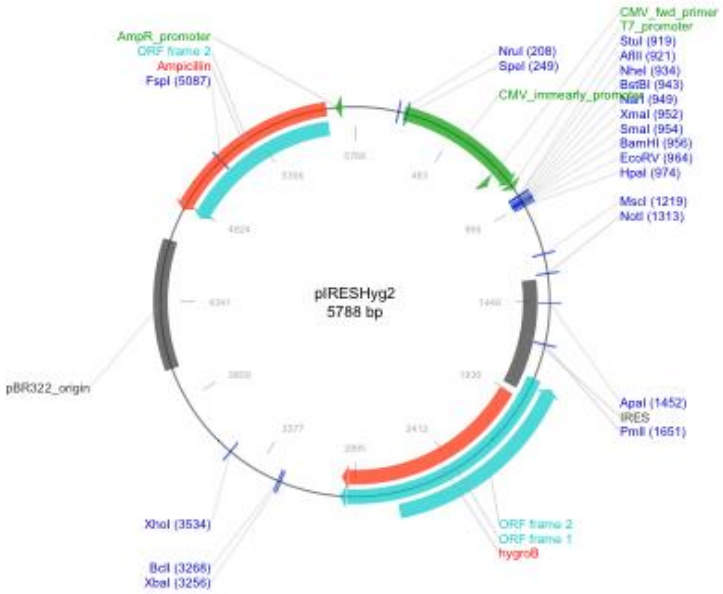

Figure 5.8 Plasmid map of multicistronic vector expressing hygromycin resistance gene.

5.3 Construction of the multi-cistronic expression vectors

This section covers the removal of the cDNA sections required from the plasmids obtained from the I.M.A.G.E consortium by restriction digest and ligation into multi-cistronic vectors for transfection into human cell line U937.

5.3.1 *RILP*

The plasmid pCMV-Sport6-*RILP* (Figure 5.3) obtained from the I.M.A.G.E consortium was digested with *Not*I and *Eco*RI to give two fragments, 5282 bp and 1651 bp, the larger fragment being the unsuitable vector and the smaller containing the *RILP* gene. The enzymes chosen were also used initially to insert the gene into the vector, so by using these the full gene was recovered. The fragments were separated using agarose gel electrophoresis, and the smaller fragment containing the gene was extracted from the gel (Figure 5.9), this will be ligated in to the multi-cistronic vector.

The new vector capable of expressing more than one gene was prepared for insertion of the *RILP* gene; pIRESneo2 (Figure 5.7), was cut using the same enzymes *Not*I and *Eco*RI giving two fragments, 5282 bp and 13 bp; these were separated on gels and the largest fragment extracted, giving a vector ready for ligation with the gene fragment from the previous step. The vector was then prepared by dephosphorylation and ligated with the fragment obtained from the digestion of pCMV-Sport6-*RILP,* containing the *RILP* gene, to form the new plasmid (Figure 5.10), pIRESneo2-*RILP* (pBF1).

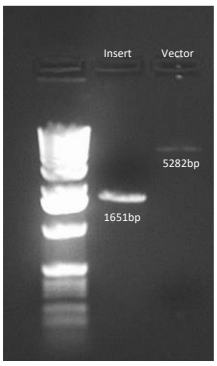

Figure 5.9- Gel electrophoresis of the vector and the insert containing the DNA of the RILP gene. Lane one contains a 1KB ladder.

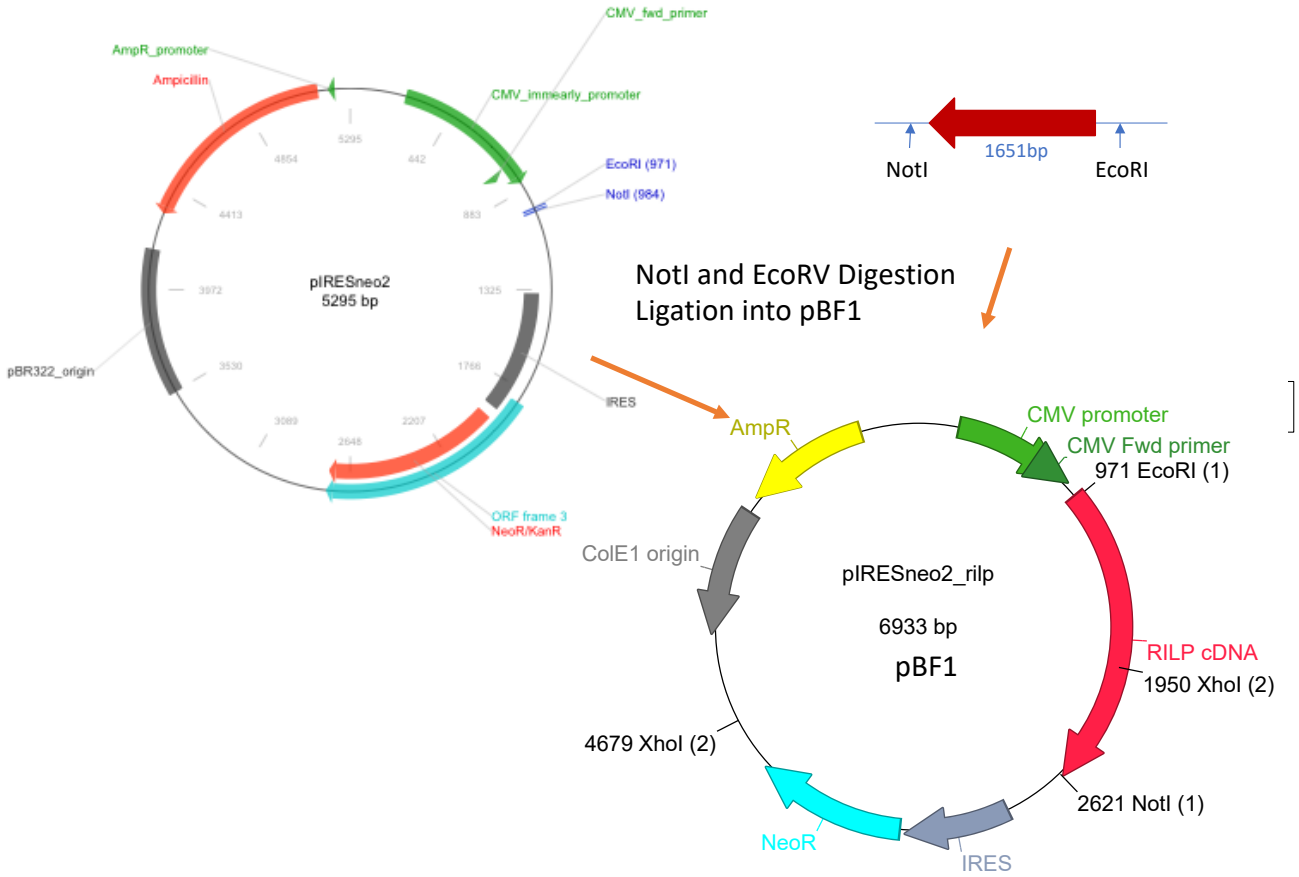

Figure 5.10 Plasmid map of the construction of the RLIP expression vector, A-vector containing mammalian expression promoter and neomycin resistance gene, B- Backbone from where the RILP gene was obtained, gene was removed using the Not1 and EcoRI restriction sites, C- the newly constructed expression vector containing the RILP gene (pBF1)

Following ligation, the integrity of pBF1 was confirmed by diagnostic digests, to ensure that construction was successful, by using an enzyme that cut once in the vector and once in the insert. The enzyme used was *Xho*l giving two fragments (4204bp and 2729bp). The digestion products were separated using gel electrophoresis and imaged (Figure 5.11). The imaging showed the expected bands and that the plasmid had been cut in two places. This shows that the insertion into the vector was successful, as one of the restriction sites was in the RILP cDNA, so two bands would only be seen after successful insertion.

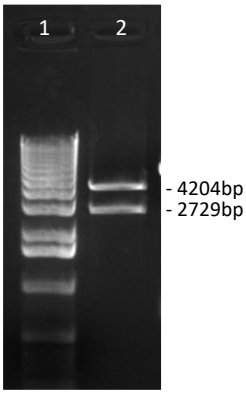

Figure 5.11- Gel electrophoresis of the fragments resulting from the digestion of pBF1 with Xhol. Lane one contains a 1KB ladder.

5.3.2 RIN2

To construct the required plasmid to express *Rin2* in mammalian cells and the antibiotic resistance gene, a different approach was taken due to the restriction enzyme locations. The UTR of the pCMV-Sport6-*RIN2* plasmid (Figure 5.4), obtained from the I.M.A.G.E consortium was removed and replaced with the IRES region and selectable gene, neomycin phosphotransferase (NeoR) from another vector, enabling the expression of both the *RIN2* gene and the NeoR gene. The pCMV-Sport6-*RIN2* plasmid was digested with *Xba*I and *AF*III to give two fragments, 7676 bp and 1384 bp, the smaller fragment containing the UTR (Figure 5.4). The fragments were separated using agarose gel electrophoresis and the largest fragment was extracted from the gel and retained.

The vector pIRESneo2 was cut using the same enzymes giving two fragments, 3466bp and 1829bp (Figure 5.7). These were separated on a gel and the smallest fragment

extracted, containing the IRES region and selectable gene, neomycin phosphotransferase (NeoR), which was used to replace the 3' UTR in the pCMV-Sport6-*Rin2* vector. The fragment sizes were confirmed by running a small amount of the extracted fragments on an agarose gel (Figure 5.12). Upon confirmation, the vector was then dephosphorylated, and the vector and insert ligated forming the new plasmid, pBF2 (Figure 5.13).

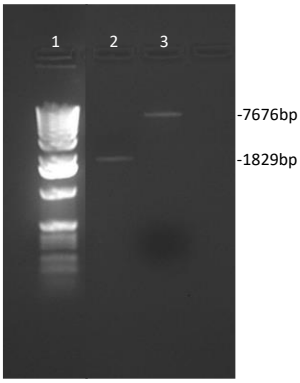

Figure 5.12 Gel electrophoresis of the vector and insert for confirmation of fragment length, lane 1 contains a 1KB ladder, lane 2 is the insert and lane 3 contains the vector.

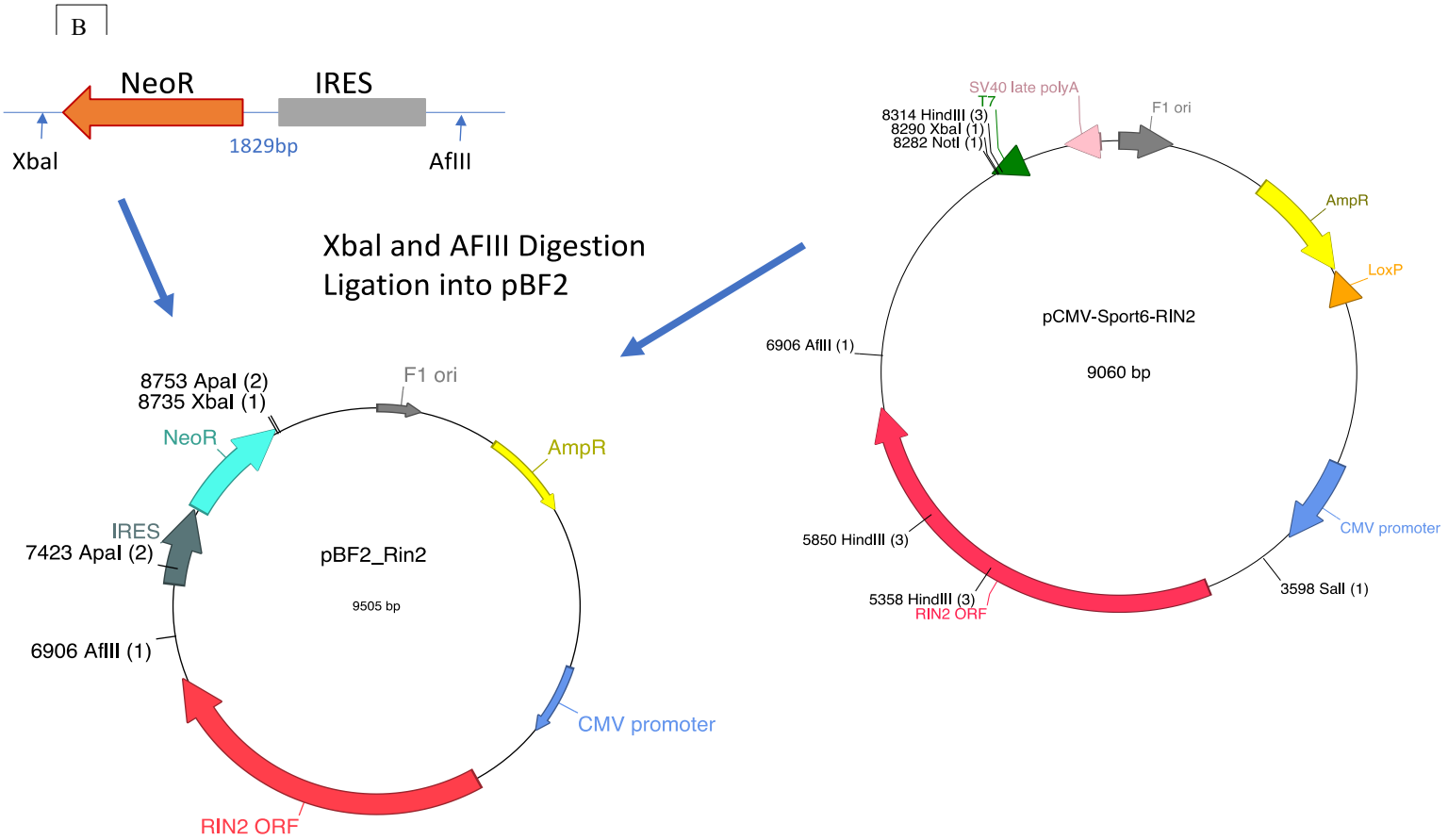

Figure 5.13 A-Backbone containing mammalian expression promoter and neomycin resistance gene, B- vector containing the Rin2 gene, UTR was removed using the BbaI and AFIII restriction sites. C- ligated vector and insert to form pBF2 expressing RIN2 gene and neoR.

To confirm the construction of the new plasmid, further diagnostic digests were performed, using an enzyme that cut once in the vector and once in the insert. The enzyme used was *ApaI,* giving two fragments (8175bp and 1330bp). The digestion products were separated using gel electrophoresis and imaged (Figure 5.14). The imaging showed the expected bands and that the plasmid had been cut in two places. This shows that the insert into the vector was successful.

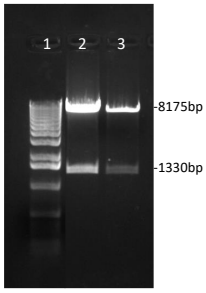

Figure 5.14 – Image of the gel electrophoresis of the digested fragments of pBF2 using ApaI. Lane one contains a 1KB ladder. Lane two and three are replicates of the digestions.

5.3.3 OSBPL1a

To create the required plasmid to express *OSBPL1a* and hygromycin resistance gene (Hyg) in mammalian cells, the pBluescriptR-OSBPL1a plasmid, obtained from the I.M.A.G.E consortium, was digested with *Xma*I, *Stu*I and *Apa*LI to give four fragments, 996bp, 1246bp, 1025bp and 2720bp (see Figure 5.5). The fragments were separated using gel electrophoresis and the largest fragment containing the *OSBPL1a* gene, was extracted from the gel this was retained as the insert.

The vector pIREShyg2 was cut using the enzymes *Xma*I and *Eco*RV giving two fragments, 5776bp and 834bp (Figure 5.8); these were separated by agarose gel electrophoresis and the largest fragment extracted and retained. The fragment sizes were confirmed by running a small amount of the extracted fragments on gel. Once confirmed, the vector was dephosphorylated, and the vector and insert were ligated together to form the new plasmid (Figure 5.15); this plasmid was given the name pBF3.

To confirm the construction of the new plasmid, further diagnostic digests were performed, using an enzyme that cut once in the vector and once in the insert. The enzyme used was *SpeI,* giving two fragments (6245bp and 2249bp). The digestion products were separated using gel electrophoresis and

imaged (Figure 5.16). The imaging showed the expected bands and that the plasmid had been cut in two places, implying that the vector was successfully constructed.

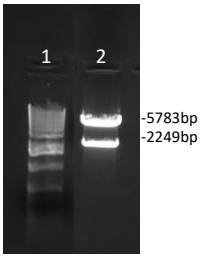

Figure 5.15 Image of the gel electrophoresis of the diagnostic digests of pBF3 with SpeI, lane 1 contains 1KB ladder, lane 2 the sample.

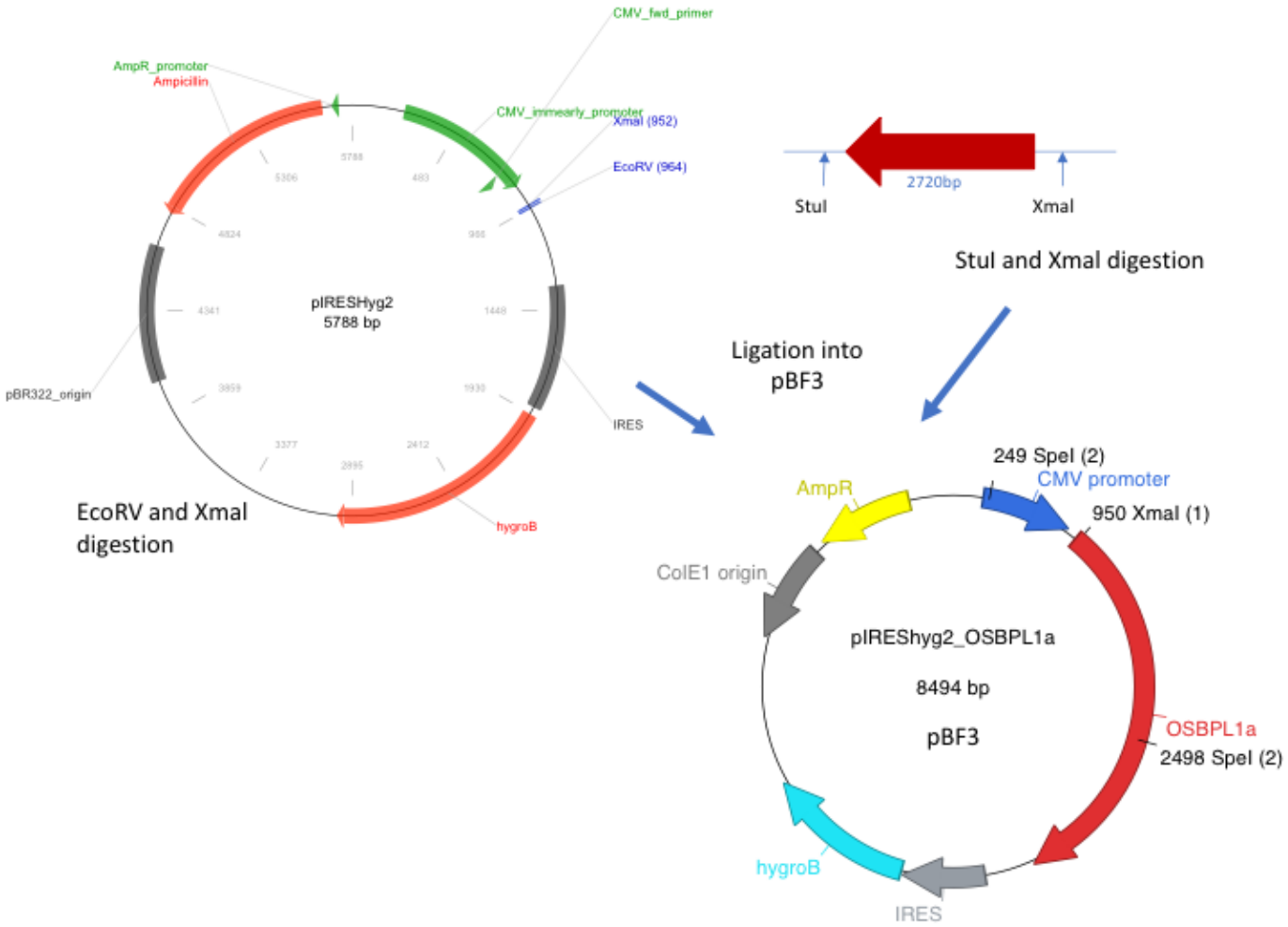

Figure 5.16 Plasmid map of the construction of the OSBPL1a expression vector, A-vector containing mammalian expression promoter and hygromycin resistance gene, B- Backbone from where the OSBPL1a gene was obtained, gene was removed using the StuI and XbaI restriction sites, C- the newly constructed expression vector containing the OSBPL1a gene (pBF3)

5.4 Sequence determination and alignment

The three newly constructed plasmids were sent for Sanger sequencing to confirm the insert was in the correct position and orientation. Standard primers for the CMV promoter were used to initiate the transcription. The resulting sequence was compared to the expected sequence using the online alignment tool, Clustal Omega. For each plasmid, the cDNA insertion site is highlighted in yellow and the cDNA from the I.M.A.G.E clones is highlighted in blue. All three sequences confirmed the correct insertion and orientation for the insert into the vector (Figures 5. 17 - 5.19).

pIRESneo2-*Rilp* (pBF1) expected sequence aligned with sequencing result

```
pIRESneo2       GAGCTCGGATCGATATCTGCGGCCTAGCTAGCGCTTAAGGCCTGTTAACCGGTCGTACGT
pBF1            NNNNNNNNNTNNATANCTGCGGCCTAGCTAGCGCTTAAGGCCTGTTAACCGGTCGTACGT
                     .    *  ***.*******************************************

pIRESneo2       CTCCGGATTCGaattcccgggatatcgtcGacCCACGCGTCCGACGGCTTCCTGGGGCGG
pBf1            CTCCNGNTTCGAATTCCCGGGAT--------------------ACGGCTTCCTGGGGCGG
                **** * ****************                     ******************

pIRESneo2       AACTGTTTCGCTTTTCCCCGTCCCAGTGGAGGGTGGGGTGGGGGGGTCGCAGCCCTAAGC
pBF1            AACTGTTTCGCTTTTCCCCGTCCCAGTGGAGGGTGGGGTGGGGGGGTCGCAGCCCTAAGC
                ************************************************************

pIRESneo2       CTCTGGGAGACATGGAGCCCAGGAGGGCGGCGCCCGGGGTGCCTGGCTGGGGGTCTCGGG
pBf1            CTCNGGGAGACATGGAGCCCANGAGGGCGGCGCCCGGGGTGCCTGNCTGGTGGTCTCGNG
                ***.**************** ********************** **** ******* *

pIRESneo2       AGGCCGCG
pBF1            AGGNNNCG
                ***   **
```

Figure 5.17 Alignment diagram of the expected sequence for pBF1 containing RILP gene compared with the sequencing result from sager sequencing.The cDNA insertion site is highlighted in yellow and the cDNA from the I.M.A.G.E clones is highlighted in blue

pIResneo2-*RIN2* (pBF2) expected sequence aligned with sequencing result

```
pIRESneo2   tgacctccatagaagacaccgggaccgatccagcctccggactctagcctaggccgcgga
pBf2        TGACNTNNNTNNNANACACCGGGACCGATCCAGCCTCCGGACTCTAGCCTNGGCCGCGGG
            **** *   *   * ********************************** ********.

pIRESneo2   gcggataacaatttcacacaggaaacagctatgaccattaggcctatttaggtgacacta
pBf2        ACGGATAACAATTTCACACAGGAAACAGCTATGACCATTAGGCCTATTTAGGTGACACTA
            .************************************************************

pIRESneo2   tagaacaagtttgtacaaaaaagcaggctggtaccggtccggaattcccgggatatcgtc
pBf2        TAGAACAAGTTTGTACAAAAAAGCAGGCTGGTACCGGTCCGGAATTCCCGGGATATCGTC
            ************************************************************
```

```
pIRESneo2   gacCCACGCGTCCGCGGACGCGTGGGCGGACGCGTGGGCTGGCCGCGGCAGGAAACCGGG
pBf2        GACCCACGCGTCCGCGGACGCGTGGGCGGACGCGTGGGCTGGCCGCGGCAGGAAACCGGG
            ************************************************************

pIRESneo2   CTGAAAGGAGATGAGTCCCCGGCATGCTGTAGAGCCTCGCTGGGGGAAATGTCAGAGTGG
pBf2        CTGAAAGGAGATGAGTCCCCGGCATGCTGTAGAGCCTCGCTGGGGGAAATGTCAGAGTGG
            ************************************************************

pIRESneo2   ACCATGGGCGCCCAAGGTCTGGACAAGCGAGGAAGTTTCTTTAAGCTCATTGACACGATC
pBf2        ACCATGGGCGCCCAAGGTCTGGACAAGCGAGGAAGTTTCTTTAAGCTCATTGACACGATC
            ************************************************************

pIRESneo2   GCCTCGGAGATCGGAGAACTGAAACGGGAGATGGTGCAGACAGATATCAGCCGGGAAAAT
pBf2        GCCTCGGAGATCGGAGAACTGAAACGGGAGATGGTGCAGACAGATATCAGCCGGGAAAAT
            ************************************************************

pIRESneo2   GGCCTGGAACCTTCTGAAACCCACAGAACCGGGAAATTGTCAGTCACGTATCACAGTGAT
pBf2        GGCCTGGAACCTTCTGAAACCCACAGAACCGGGAAATTGTCAGTCACGTATCACAGTGAT
            ************************************************************

pIRESneo2   GGAAAGAGTAATACAGCGGACCTTCCGTGCATGAAGTAGAATTCAGTATAGCCCTGGAAG
pBf2        GGAAAGAGTAATACAGCGGACCTTCCGTGCATGAAGTAGAATTCAGTATAGCCCTGGAAG
            ************************************************************
```

Figure 5.18 Alignment diagram of the expected sequence for pBF2 containing RIN2 gene compared with the sequencing result from sager sequencing. The cDNA insertion site is highlighted in yellow and the cDNA from the I.M.A.G.E clones is highlighted in blue

pIReshgy-*OSBPL1a* (pBF3) expected sequence aligned with sequencing result

```
pIREShgy  GAGCTCGGATCTGTACAGGCCTTAAGCCGGCGCGCTAGCGCTTCGAAGG--CCcgggcgg
pbf3      NNTNNNCNGATCTGNNAGGCCNTAAGCCGGCGCGCTAGCGCTTCGAAGGCGCCCGGGCGG
                       ***** ************************** *********

pIREShgy  gcgcggcgcgggagtcctgggccgctggcgggcaacgcctctgcccgacctcgctgggga
pbf3      GCGCGGCGCGGGAGTCCTGGGCCGCTGGCGGGCAACGCCTCTGCCCGACCTCGCTGGGGA
          ************************************************************

pIREShgy  aggctggcgctgctgcccggccggagccaggggcaggctgcgcaaaggtgacttagggag
pbf3      AGGCTGGCGCTGCTGCCCGGCCGGAGCCAGGGGCAGGCTGCGCAAAGGTGACTTAGGGAG
          ************************************************************

pIREShgy  accttgcgggccgccctgggtcgcgcctcccggatcggctcgcctcggctcgactggagg
pbf3      ACCTTGCGGGCCGCCCTGGGTCGCGCCTCCCGGATCGGCTCGCCTCGGCTCGACTGGAGG
          ************************************************************

pIREShgy  ggaggaggaggagcaggccgagcgcattcgcgctggagcttgcgaggagcgcagggtgga
pbf3      GGAGGAGGAGGAGCAGGCCGAGCGCATTCGCGCTGGAGCTTGCGAGGAGCGCAGGGTGGA
          ************************************************************

pIREShgy  gcgcgccagccggggtcctcggatctggcccaggtgaggaattttaaattggaacaagag
pbf3      GCGCGCCAGCCGGGGTCCTCGGATCTGGCCCAGGTGAGGAATTTTAAATTGGAACAAGAG
          ************************************************************

pIREShgy  caagaaaaaaacaaaatcttgtcagaagcactggagacgctggccactgaacatcatgaa
pbf3      CAAGAAAAAAACAAAATCTTGTCAGAAGCACTGGAGACGCTGGCCACTGAACATCATGAA
          ************************************************************

pIREShgy  ttagagcagtctctggtgaaaggctctccacccgccagcatccttagcgaggacgagttc
```

```
pbf3        TTAGAGCAGTCTCTGGTGAAAGGCTCTCCACCCGCCAGCATCCTTAGCGAGGACGAGTTC
            ************************************************************

pIREShgy    tatgatgcgctgtcagattccgagtccgaaaggt
pbf3        TATGATGCGCTGTCAGATTCCGAGTCCGAAAGGT
            **********************************
```

Figure 5.19 Alignment diagram of the expected sequence for pBF3 containing OSBPL1a compared with the sequencing result from sager sequencing. The cDNA insertion site is highlighted in yellow and the cDNA from the I.M.A.G.E clones is highlighted in blue

5.5 Transfections

Following confirmation of the insertion and orientation of the cloned inserts in plasmids pBF1 (*RILP*) , pBF2 (*RIN2*) and pBF3 (*OSBPL1a*), transfections were performed. U937s are known to be difficult to transfect (Sundström and Nilsson, 1976; Tietz and Berghoff, 2012), however, as they exhibit the closest expression profile compared with primary cells when infected with *M.tb*, it made them the most suitable cell line to use (characterisation presented in Chapter 4) . Either FuGENE HD Transfection reagent (Promega) or electroporation using the Amaxa Nucleofector device (Lonza) was used for the transfections. Both methods had been previously used to successfully transfect U937 cells (Jin et al., 2012; Martinet et al., 2003).

For the FuGENE protocol, 1.7 µg of DNA was used with $8x10^5$ U937 cells per reaction. Electroporation of the U937s was performed using the Amaxa Nucleofector device using the cell line Nucleofector Kit C, which was optimised for use with U937 cells, which used 2 µg of DNA per $1x10^6$ cells. The plasmids generated (pBF1, pBF2 and pBF3) and an empty vector were transfected into U937 cells. Following 48 hours incubation at 37°C, antibiotics 500 µg /ml G418 or 400 µg/ml Hygromycin B were used to select for successfully transfected cells. Cells were washed and re-suspended in fresh media every 3-4 days to remove any dead cells and debris. Selective pressure was kept on the cells until there was an out-growth of healthy cells. An out-growth of successfully transfected cells took up to 8 weeks, due to poor transfection efficiency. Up to three transfection reactions per plasmid were pooled to increase the number of viable cells. Once out growth occurred, 1ml aliquots were stored in liquid nitrogen.

5.7 Confirmation of successful transfections

The newly transfected U937s were then assessed in multiple ways to confirm the transfections. qPCR for the plasmid, was conducted not only to confirm the presence of the plasmid but also to estimate the copy number per cell using a single copy number control. Primers were designed to amplify a common section from all three plasmids found in the internal ribosome entry site (IRES), identified using an alignment of all three newly constructed plasmids produced using the online tool Clustal (Figure 5.20).

```
pBF2    CGGTGTGCGTTTGTCTATATGTGATTTTCCACCATATTGCCGTCTTTTGGCAATGTGAGG        7424
pBF1    CGGTGTGCGTTTGTCTATATGTGATTTTCCACCATATTGCCGTCTTTTGGCAATGTGAGG        3090
pBF3    CGGTGTGTGTTTGTCTATATGTGATTTTCCACCATATTGCCGTCTTTTGGCAATGTGAgg        4155
        ******* ************************************************

pBF2    GCCCGGAAACCTGGCCCTGTCTTCTTGACGAGCATTCCTAGGGGTCTTTCCCCTCTCGCC        7484
pBF1    GCCCGGAAACCTGGCCCTGTCTTCTTGACGAGCATTCCTAGGGGTCTTTCCCCTCTCGCC        3150
pBF3    gcccGGAAACCTGGCCCTGTCTTCTTGACGAGCATTcctaggGGTCTTTCCCCTCTCGCC  4215
        ************************************************************

pBF2    AAAGGAATGCAAGGTCTGTTGAATGTCGTGAAGGAAGCAGTTCCTCTGGAAGCTTCTTGA        7544
pBF1    AAAGGAATGCAAGGTCTGTTGAATGTCGTGAAGGAAGCAGTTCCTCTGGAAGCTTCTTGA        3210
pBF3    AAAGGAATGCAAGGTCTGTTGAATGTCGTGAAGGAAGCAGTTCCTCTGGAAGCTTCTTGA        4275
        ************************************************************

pBF2    AGACAAACAACGTCTGTAGCGACCCTTTGCAGGCAGCGGAACCCCCCACCTGGCGACAGG        7604
pBF1    AGACAAACAACGTCTGTAGCGACCCTTTGCAGGCAGCGGAACCCCCCACCTGGCGACAGG        3270
pBF3    AGACAAACAACGTCTGTAGCGACCCTTTGCAGGCAGCGGAACCCCCCACCTGGCGACAGG        4335
        ************************************************************

pBF2    TGCCTCTGCGGCCAAAAGCCACGTGTATAAGATACACCTGCAAAGGCGGCACAACCCCAG        7664
pBF1    TGCCTCTGCGGCCAAAAGCCACGTGTATAAGATACACCTGCAAAGGCGGCACAACCCCAG        3330
pBF3    TGCCTCTGCGGCCAAAAGCcacgtgTATAAGATACACCTGCAAAGGCGGCACAACCCCAG        4395
        ************************************************************

pBF2    TGCCACGTTGTGAGTTGGATAGTTGTGGAAAGAGTCAAATGGCTCTCCTCAAGCGTATTC        7724
pBF1    TGCCACGTTGTGAGTTGGATAGTTGTGGAAAGAGTCAAATGGCTCTCCTCAAGCGTATTC        3390
pBF3    TGCCACGTTGTGAGTTGGATAGTTGTGGAAAGAGTCAAATGGCTCTCCTCAAGCGTAGTC        4455
        ************************************************************ **
```

Figure 5.20 Alignment diagram of the three created plasmids, constructed using Clustal, primers used highlighted in yellow. Nucleotide positions should be given and the fragment identified on a plasmid map.

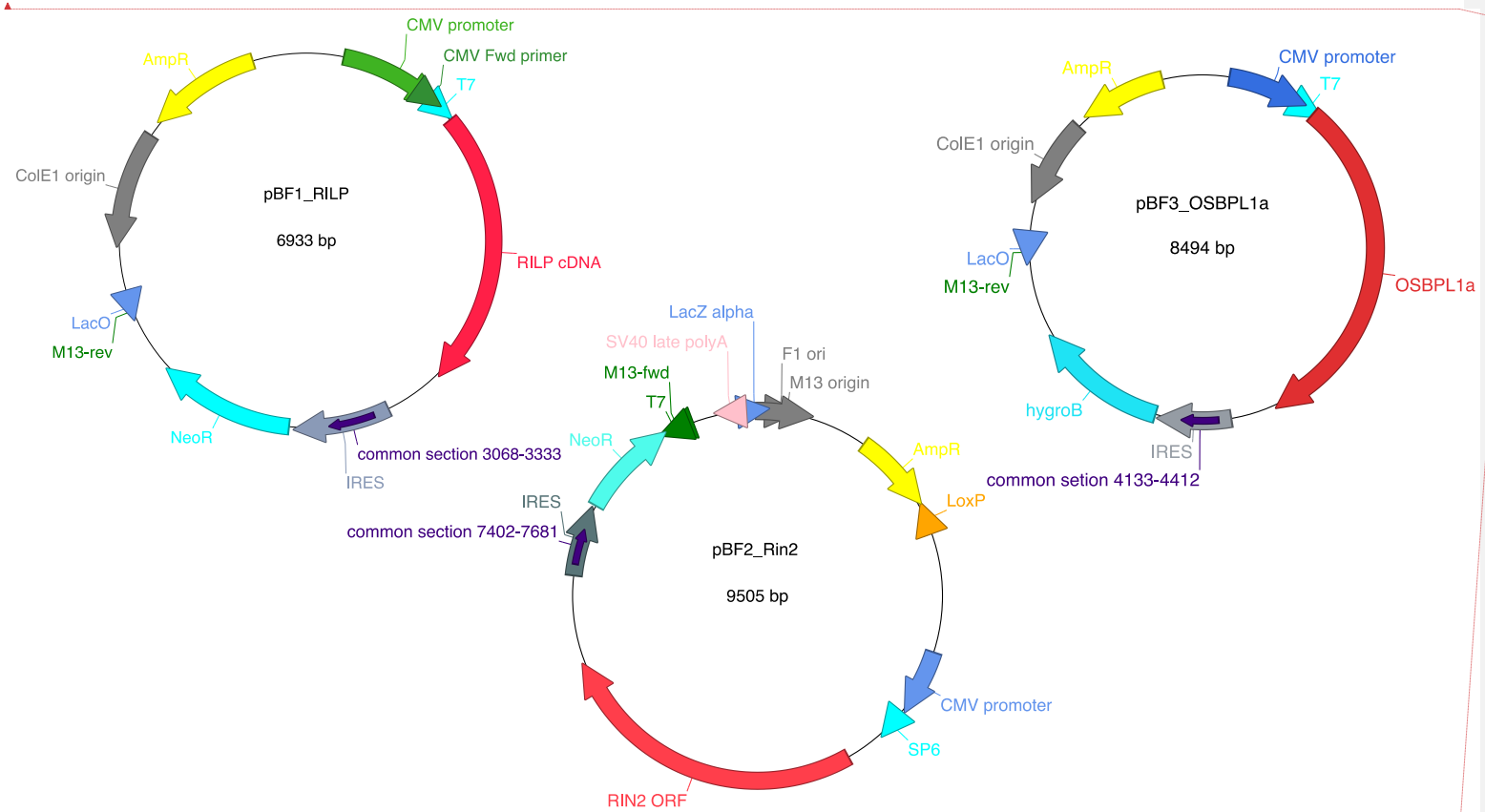

Figure 5.21 Diagram of all three constructed plasmids highlighting the common section used for qPCR.

Formatted: Font: (Default) +Body (Calibri)

Formatted: Font: (Default) +Body (Calibri)

Calibration curves were plotted for each of the plasmids and these were used to calculate the plasmid concentration in the extraction from the transfected U937s. This gave ng per uL of product and coupled with the number of cells per ul gave the ng per cell. This was then used to calculate copy number per cell using the equation:

$$number = (ng * number/mole) / (bp * ng/g * g/mole\ of\ bp)$$

where number/mole equals Avogadro's number 6.022×10^{23}, and the length of template is 280bp.

Table 5.3 – Estimation of plasmid number per cell.

Plasmid	Gene	ng/ul	cells per ul	ng/cell	copies per cell
pBF1	*RILP*	1×10^{-5}	10000	1×10^{-9}	3.31
pBF2	*RIN2*	2×10^{-5}	10950	1.83×10^{-9}	5.96
pBF3	*OSBPL1a*	1×10^{-5}	10550	9.48×10^{-10}	3.11

The results show that the plasmid number per cell is between 3 and 6 for the different plasmids (Table 5.3). The presence of multiple copies of the plasmids per cell confirms successful transfection of the U937 cells using all three of the plasmids. The next question that needed to be answered was if the proteins encoded within the constructs were overexpressed within the transfected cells.

5.8 Confirmation of overexpression

Transcription of the transfected genes will lead to overexpression of the encoded proteins within the cells, for which there must be a corresponding increase in mRNA levels. To confirm the overexpression of mRNA within the transfected cells, RT-qPCR was performed, comparing the native expression of *RILP*, *RIN2* and *OSBPL1a* in U937s with the expression in transfected U937s with pBF1, pBF2 and pBF3. Ratios were normalised to the house keeping gene TBP, this corrected for the input amount of mRNA in the different preparations. From the RT-qPCR data, a significant increase in expression of the genes within each transfected cell line was seen (Table 5.4 and Figure 5.22), compared with an alternate (empty vector control) transfected cell line; this confirmed the plasmids were expressing the desired genes (p-value <0.05). As the three cell lines were constructed to over-express different genes, the alternate transfected cell line acted as a control (called

pBF0 in the plots). This validates that the increase in gene expression is not due to the introduction of a plasmid into the cells, but rather the plasmid expressing the cloned gene.

Table 5.4- The fold changes of expression in the transfected cell lines for the genes of interest (biological replicates) as fold change compared to empty vector control

Plasmid	**gene**	**Fold change**			**Average fold change**
pBF1	*RILP*	2.40	4.40	3.10	3.30
pBF2	*RIN2*	1.60	1.70	1.70	1.67
pBF3	*OSBPl1a*	2.13	4.30	4.80	3.74

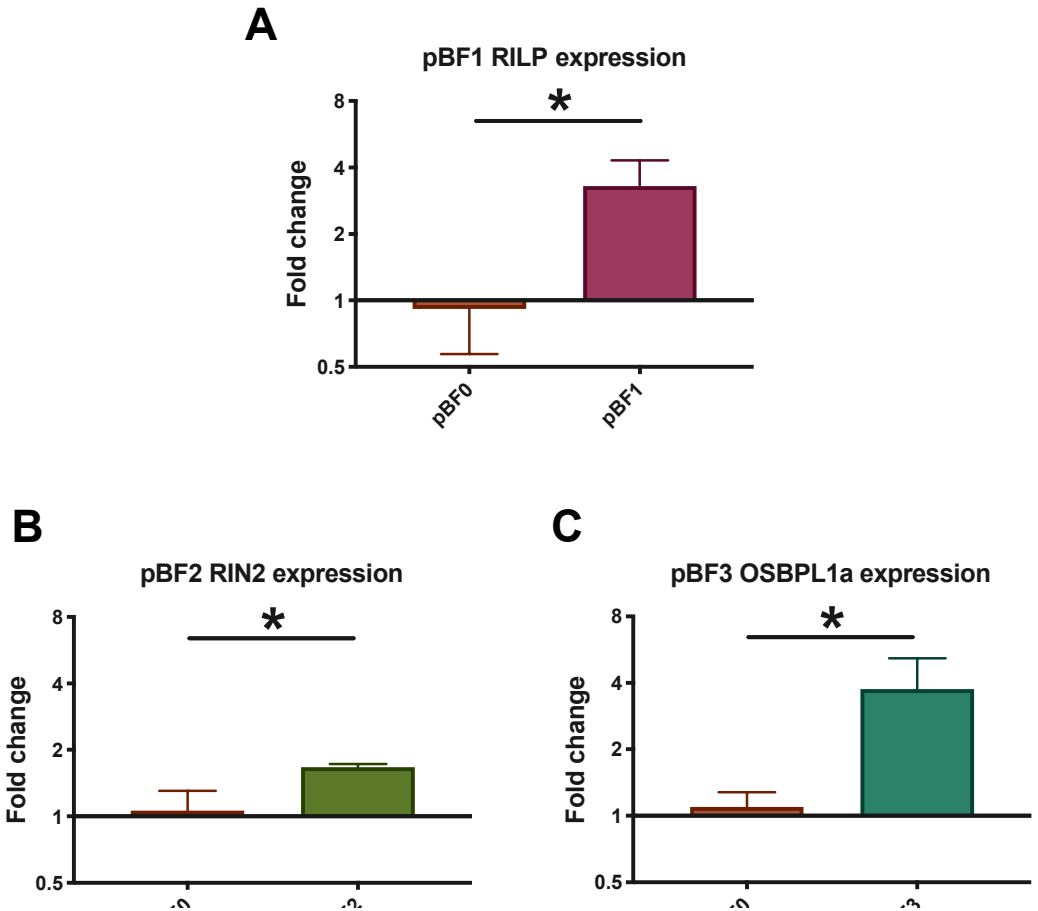

Figure 5.22 Relative RNA expression of the transfected cell lines when compared to U937s transfected with a different expression plasmid. The values were adjusted to TBP levels a house keeping gene to allow for differences in loading. Un-paired t tests were performed and the resulting p-values were: pBF1 vs pBF0 p-value= 0.0182, pBF2 vs pBF0 p-value= 0.0136, pBF3 vs pBF0 p-value=0.0328.

Western blot was then used to confirm that the over-expression of the mRNA corresponded to an increase in the protein levels. A loading control of ß-actin was used and lysate from a positive control, un-transfected U937s and the transfected U937s were compared with each other, using the appropriate antibody for the target protein.

After trying all the commercially available antibodies for both RILP and RIN2, expression of the proteins could not be observed using a sensitive fluorescence-based visualisation and electronic image scanning analysis (Odyssey system – see Methods). For RILP, a positive control of A549 cell lysate was used (as recommended by the antibody manufacturer), but still no protein was seen (Figure 5.23A). For RIN2, HepG2 cell lysate was used as the positive control (as recommended by the antibody manufacturer), but no protein was seen (Fig5.23 Panel B). For both RILP and RIN2 Western blots, a loading control antibody to beta-Actin was used to confirm the equivalent total cell protein loading was present in all. These experiments failed to demonstrate either the presence of RILP and RIN2 native proteins in the cell lysate blots or indeed any increase in protein level as a consequence of transfection and overexpression. This could result from antibodies with too poor sensitivity to the target proteins to be able to detect low levels of proteins. Poor specificity and avidity of purchased antibodies might reflect that these proteins have rarely been studied in the literature and high functioning reagents have not therefore been a priority for development for these two proteins – RILP and RIN2. Since purchasing the RILP antibody has been removed from sale, suggesting that its functionality was a problem.

For the U937s transfected with pBF3 carrying the gene for OSBPLa1, the antibodies were more successful. The Western blot revealed an increase in the expression of the protein and also a fainter smaller band just below, when comparing lanes 2&3 containing U937 lysate, to lanes 4-6 containing transfected U937-pBF3-OSBPL1a lysate (Figure 5.23c). This confirms that the transfection was successful and the plasmid functional. As previously mentioned, there are a number of transcript variants derived from alternate splicing or use of different promoters (Strausberg et al., 2002), resulting in a number of different isoforms. The antibody is designed to recognise a number of these isoforms ranging from 50-108KDa. The predominant isoform here is around 100KDa, but the smaller band seen around 95KDa appears to be only in the transfected cells. There are a number of possible explanations for this including; a misfolded protein, splice variant or some sort of degradation event having taken place. This smaller protein could be present in the non-transfected cells but at a lower

amount so therefore not visible on the Western blot. Further study would be required to determine which hypothesis is correct, however this was felt to be unnecessary. With a visible increase in the correct size protein (lane 4-6 - Figure 5.23c) after transfection, this would suggest that the protein encoded from the plasmid was the protein desired.

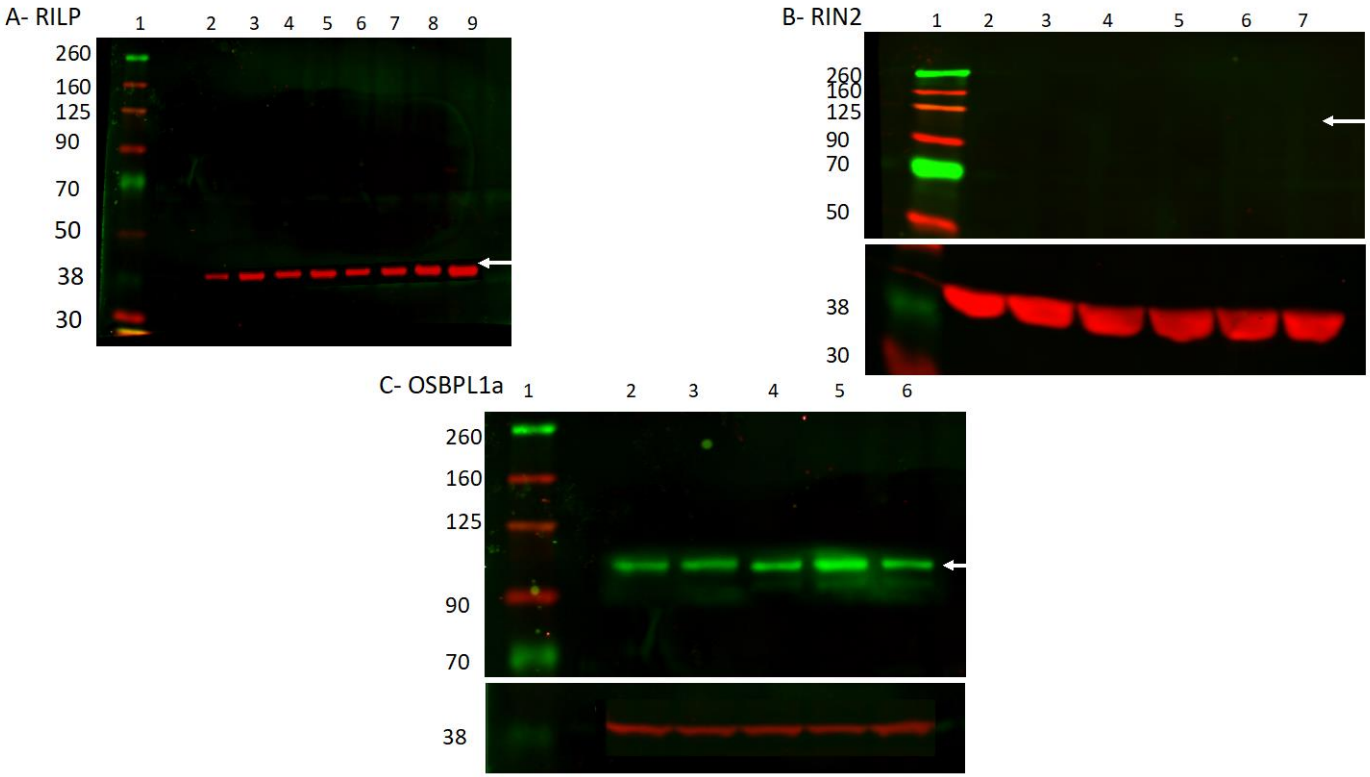

Figure 5.23- Imaging of Western blots using the Odyssey system and the Chameleon™,Duo ladder (Li-cor) and anti-Actin antibody (Red) as a loading control expected size 42KDa. Panel A - Example of Western blot with anti-RILP (Green) expected size 45KDa (White arrow)) and anti-Actin antibody (Red) , lanes 1&2 A549 cell lysate (positive control), lanes 3&4 U937 cell lysate, lanes 6-8 U937 pBF1-RILP(transfected cells) cell lysate. Only the loading control is visible. Panel B- Example of Western blot with anti-RIN2 (Green) expected size 100KDa (white arrow) and anti-Actin antibody (Red), lane 1 Ladder, lanes 2&3 HepG2 cell lysate (positive control), lanes 3&4 U937 cell lysate, lanes 6&7 U937 pBF2-RIN2 (transfected cells) cell lysate. Only the loading control is visible. Panel C – Example of Western blot with anti-OSBPL1a (Green) expected size 100KDa and anti-Actin antibody (Red) Lane 1 ladder, lanes 2&3 U937 lysate, lanes 4-6 U937 pBF3-OSBPL1a. Lanes 2-6 show a green band at around 100KDa with lanes 4-6 showing a faint band at round 95KDa.

5.9 Conclusion

In summary, cDNA was ordered from the I.M.A.G.E consortium for the three genes identified in Chapter 1: *RILP, RIN2* and *OSBPL1a* (Table 5.1). Three plasmids were then constructed from these clones by ligating the cDNA into multicistronic vectors for transfection into the human cell line, U937 (Figures 5.10, 5.13, 5.15). A summary of the plasmids constructed is given in Table 5.5.

Table 5.5 Summary of constructed plasmids

Plasmid name	Vector	cDNA insert	Resistance marker	Plasmid map
pBF1	pIRESneo2	*RILP*	neomycin	Figure 5.10
pBF2	pIRESneo2	*RIN2*	neomycin	Figure 5.13
pBF3	pIREShyg2	*OSBPL1a*	hygromycin	Figure 5.15
pBF0	pIREShyg2	n/a	hygromycin	Figure 5.8

A control plasmid was also constructed without the cDNA insert (pBF0). Once constructed, the identity of the expression vector plasmids was confirmed via both restriction mapping (Figures 5.11, 5.14, 5.16) and sequencing (Figures 5.17-19).

Plasmids were transfected into U937 cells, using either FuGENE® HD Transfection reagent (Promega) or electroporation using the Amaxa® Nucleofector® device (Lonza). The transfected cells took a prolonged period to outgrow the non-transfected cells. Once outgrowth was seen, the transfected cell lines were assessed by qPCR for plasmid vector to confirm that transfection was successful. The amount of plasmid per cell was calculated using qPCR for the plasmid and a single copy number gene; this showed that all the cell lines had on average of three to six copies of the plasmid per cell. The increase of RNA expression for the genes was also assessed using RT-qPCR with gene specific primers. This showed that there was a significant increase in expression of the desired genes in U937 compared with the control cells (p-values of <0.05). Western blotting to detect the increased expression of target genes was unsuccessful for RILP and RIN2 due to low antibody sensitivity. In all subsequent experiments, the RILP and RIN2 transfected U937 cells were assumed to be

over-expressing the target genes as shown by increases in mRNA alone (see the discussion section below). OSBPLa1 expression was detectable on Western blots and over-expression was detected in the transfected cells.

5.9 Discussion

The aim of this chapter was to construct cell lines which over-expressed the genes for RILP, RIN2 and OSBPL1a individually in U937 cells. This involved the construction of multicistronic plasmids, their stable transfection and confirmation of over-expression. The first challenge was the lack of availability of commercial plasmids expressing the genes of interest (*RIN2, RILP and OSBPL1a*). While the I.M.A.G.E consortium have a vast cDNA library, the only full cds they hold for *RIN2* is a synthetic construct of the mouse gene. The mouse *RIN2* is a homolog for the human gene, sharing four conserved domains and a 93 % sequence match when a BLASTP search was conducted (Figure 5.24). This provides evidence that the mouse gene is a suitable substitute for the unavailable human gene.

ras and Rab interactor 2 [Mus musculus] and [*Homo sapiens*]
Sequence ID: NP_083000.5Length: 858Number of Matches: 1
Range 1: 1 to 858GenPeptGraphicsNext MatchPrevious Match

Score	Expect	Method	Identities	Positives	Gaps
1388 bits(3593)	0.0	Compositional matrix adjust.	780/859(91%)	807/859(93%)	10/859(1%)

```
Query  95   LEPAETHSMVRHKDGGYSEEEDVKTCARDSGYDSLSNRLSILDRLLHTHPIWlqlslsee  154
            ++P    SMVRHKDGGYSE++D KTC RDSGYDSLSNRLSILDRLLHTHPIWLQLSLSEE
Sbjct  1    MDPFCILSMVRHKDGGYSEDKDGKTCPRDSGYDSLSNRLSILDRLLHTHPIWLQLSLSEE  60

Query  155  eaaevlqaqPPGIFLVHKSTKMQKKVLSLRLPCEFGAPLKEFAIKESTYTFSLEGSGISF  214
            EAAEVLQAQPPGIFLV KS+KMQKKVLSLRLPCEFGAPLKEF IKESTYTFSLEGSGISF
Sbjct  61   EAAEVLQAQPPGIFLVRKSSKMQKKVLSLRLPCEFGAPLKEFTIKESTYTFSLEGSGISF  120

Query  215  ADLFRLIAFYCISRDVLPFTLKLPYAISTAKSEAQLEELAQMGLNFWSSPADSKppnlpp  274
            ADLFRLIAFYCISRDVLPFTLKLPYAISTAK+E+QLEELAQ+GLNFWSS AD+KP N PP
Sbjct  121  ADLFRLIAFYCISRDVLPFTLKLPYAISTAKTESQLEELAQLGLNFWSSSADNKPLNSPP  180

Query  275  phrpLSSDGVCPASLRQLCLINGVHSIKTRTPSELECSQTNGALCFINPLFLKVHSQDLS  334
            PHRPL S G+CPASLRQLCLINGVHSIKTRTPSELECSQTNGALCFINPLFLKVHSQDLS
Sbjct  181  PHRPLPSAGICPASLRQLCLINGVHSIKTRTPSELECSQTNGALCFINPLFLKVHSQDLS  240

Query  335  GGLKRPSTRTPNANGTERTRSppprppppAINSLHTSPRLARTETQTSMPETVNHNKHGN  394
             G KRPSTRTPNANGTER RSPPPRPPPPAINSLHTSP L+RTE QTSMPETVNH+KHGN
Sbjct  241  TGPKRPSTRTPNANGTERPRSPPPRPPPPAINSLHTSPGLSRTEPQTSMPETVNHSKHGN  300

Query  395  VALpgtkptpipppRLKKQASFLEAEGGAKTLSGGRPG--------AGPELELGTagspg  446
            VAL GTKPTPIPPPRLKKQASFLEAE  AKTL+  RP            ELE+GTAG  G
Sbjct  301  VALLGTKPTPIPPPRLKKQASFLEAESSAKTLTARRPSRRSEPEPELELELEMGTAGHAG  360

Query  447  gappeaapgDCTRAppp-ssesrppCHGGRQRLsdmsistsssdslefdrsMPLFGYEAD  505
            GAPP  APGDCTRAPPP S    PPCHG RQRLSDMS+STSSSDSLEFDRSMPL+GYEAD
Sbjct  361  GAPPRDAPGDCTRAPPPGSESQPPPCHGARQRLSDMSLSTSSSDSLEFDRSMPLYGYEAD  420

Query  506  TNSSLEDYEGESDQETMAPPIkskkkrsssFVLPKLVKSQLQKVSGVFSSFMTPEKRMVR  565
            T SSLEDYEGESDQETMAPPIKSKKKR+SSFVLPKLVKSQL+K+SGVFSSFMTPEKRMVR
Sbjct  421  TTSSLEDYEGESDQETMAPPIKSKKKRNSSFVLPKLVKSQLRKMSGVFSSFMTPEKRMVR  480

Query  566  RIAELSRDKCTYFGCLVQDYVSFLQENKECHVSSTDMLQTIRQFMTQVKNYLSQSSELDP  625
            RIAELSRDKCTYFGCLVQDYVSFL+ENKECHVSSTDMLQTIRQFMTQVKNYLSQSSELDP
Sbjct  481  RIAELSRDKCTYFGCLVQDYVSFLKENKECHVSSTDMLQTIRQFMTQVKNYLSQSSELDP  540
```

```
Query  626  PIESLIPEDQIDVVLEKAMHKCILKPLKGHVEAMLKDFHMADGSWKQLKENLQLVRQRNP  685
            PIESLIPEDQIDVVLEKAMHKCILKPLKGHVEAMLKDFH ADGSWKQLKENLQLVRQRNP
Sbjct  541  PIESLIPEDQIDVVLEKAMHKCILKPLKGHVEAMLKDFHTADGSWKQLKENLQLVRQRNP  600

Query  686  QELGVFAPTPDFVDVEKIKVKFMTMQKMYSPEKKVMLLLRVCKLIYTVMENNSGRMYGAD  745
            QELGVFAPTPD +++EKIK+KFMTMQKMYSPEKKVMLLLRVCKLIYTVMENNSGRMYGAD
Sbjct  601  QELGVFAPTPDLMELEKIKLKFMTMQKMYSPEKKVMLLLRVCKLIYTVMENNSGRMYGAD  660

Query  746  DFLPVLTYVIAQCDMLELDTEIEYMMELLDPSLLHGEGGYYLTSAYGALSLIKNFQEEQA  805
            DFLPVLTYVIAQCDMLELDTEIEYMMELLDPSLLHGEGGYYLTSAYGALSLIKNFQEEQA
Sbjct  661  DFLPVLTYVIAQCDMLELDTEIEYMMELLDPSLLHGEGGYYLTSAYGALSLIKNFQEEQA  720


Query  806  ARLLSSETRDTLRQWHKRRTTNRTIPSVDDFQNYLRVAFQEVNSGCTGKTLLVRPYITTE  865
            ARLLSSE RDTLRQWHKRRTTNRTIPSVDDFQNYLRVAFQEVNSGCTGKTLLVRPYITTE
Sbjct  721  ARLLSSEARDTLRQWHKRRTTNRTIPSVDDFQNYLRVAFQEVNSGCTGKTLLVRPYITTE  780

Query  866  DVCQICAEKFKVGDPEEYSLFLFVDETWQQLAEDTYPQKIKAELHSRPQPHIFHFVYKRI  925
            DVCQ+CAEKFKV DPEEYSLFLFVDETWQQLAEDTYPQKIKAELHSRPQPHIFHFVYKRI
Sbjct  781  DVCQLCAEKFKVEDPEEYSLFLFVDETWQQLAEDTYPQKIKAELHSRPQPHIFHFVYKRI  840

Query  926  KNDPYGIIFQNGEEDLTTS  944
            K+DPYG+IFQNG EDLT S
Sbjct  841  KSDPYGVIFQNG-EDLTPS  858
```

Genes

Genes identified as putative homologs of one another during the construction of HomoloGene.

RIN2, *H.sapiens*
Ras and Rab interactor 2

Rin2, *M.musculus*
Ras and Rab interactor 2

Proteins

Proteins used in sequence comparisons and their conserved domain architectures.

NP_001229510.1
944 aa

NP_083000.5
858 aa

Conserved Domains

Conserved Domains from CDD found in protein sequences by rpsblast searching.

HCV_NS5a_C (pfam12941)
HCV NS5a protein C-terminal region.

SH2 (cl15255)
Src homology 2 (SH2) domain.

UBQ (cl00155)
Ubiquitin-like proteins.

SH2 (cl15255)
Src homology 2 (SH2) domain.

VPS9 (cl19569)
Vacuolar sorting protein 9 (VPS9) domain.

Figure 5.24 - alignment diagram of RIN2 human protein compared with Mouse protein, and diagram of the conserved domains.

As the vectors obtained from the I.M.A.G.E consortium were only designed to express single genes in mammalian cell lines, it was necessary to clone the cds for each gene into a multicistronic vector to enable the expression of a second gene (selectable marker). This resulted in a second round of cloning, restriction digests, and re-ligation. The sequence of a section of the final plasmids were then determined to confirm the position and orientation of the inserts. All the sequences were shown to be in the correct position and orientation; however, the alignment for the newly constructed plasmid, pBF1 (Figure 5.17), revealed some irregularities in the sequence compared with what was expected. In general, the sequencing was poor for this sample as the read length was very short when compared to the results for the other plasmids and contained more unknown residues (N) as well as a 20 bp deletion. The poor quality of reads could explain the differences seen, although there is also the possibility that there was an error in the expected sequence. The expected sequence was taken from the information on the cds clones available from the I.M.A.G.E consortium, variant forms of the vector pCMV-Sport6 are available, however the consortium do not indicate what version was used. The 20 bp deletion observed during alignment of the sequences was located within the multiple cloning site of the pCMV-Sport6 plasmid, rather than the ORF for RILP. Thus, it is unlikely that this deletion has any effect on the ability of the plasmid to express RILP.

The plasmids, once constructed, were then used to transfect U937 cells. The methods of FuGENE HD and Nucleofection were chosen because they had previously been used in published studies (for example: Jin et al., 2012; Martinet et al., 2003). Despite this, the efficiency of the transfections was found to be very low. It took prolonged periods of time in selective media to achieve any outgrowth of cells. Due to this and the fact that U937 cells grow in suspension requiring multiple cells to support growth, propagating a clonal population of cells from a single cell was impossible. This meant that the transfected cells varied in number of plasmids they contained. While this is not an issue for populations of cell assays as each cell had at least one copy (Table 5.3), it will be taken into consideration when single cells are to be analysed. Having multiple copies of the plasmid would increase this expression and amplify any effect. If clonal populations of cells had been achieved, the clonal population with the greatest increase in expression for the genes would have been selected for further work. Thus, such experimental limitations are acknowledged as unavoidable when attempting to study the functional role of rarely studied proteins, with

few efficient antibody reagents and difficult to transfect planktonic cell lines selected on the basis of showing the most appropriate gene expression patterns mimicking *M.tb* infection of macrophages. "Nothing is a beautiful as nature!" Science often requires a reductive approach and is accompanied by limitations, as seen here, and consideration of such limitations is essential.

The final section of this chapter covers the confirmation of the over-expression of the three genes encoding the proteins of interest (*RIN2, RILP,* and *OSBPL1a*). This was done in two ways; qRT-PCR of the mRNA to look for an increase in expression and Western blots to look for an increase in the amount of protein. The qRT-PCR revealed fold changes of expression between two and four, for all three cell lines (Figure 5.21). These results were statistically significant when compared with one of the alternate empty vector control transfected U937s for each gene. However, the Western blot was less successful in confirming the overexpression (Figure 5.23). As these proteins are not well studied, only a small number of commercial antibodies were available. While they have all been previously used for publications (Balaji et al., 2014; Cianciola et al., 2013; Luca et al., 2014), only the anti- OSBPL1a antibody showed sufficient sensitivity for the U937 cells used here. The Western blot showed an increase in the amount of protein (normalised to beta-actin control), and a fainter second band which could be due to a miss-folding of the protein or a different isoform. However, the experiments for both RILP and RIN2 failed to detect protein even with the suggested positive controls. An anti-actin control was also included and this provided evidence it was not a technical issue with the blot but rather an antibody issue, but with no alternatives commercially available, this limitation could not be overcome. This is not ideal as it could mean that the proteins are not over-expressed and thus further experiments would be flawed. The decision was taken to continue with the planned experiments for the stable transfected cell lines, despite the inability to visualise the increase in protein. The increase in mRNA indicates that the plasmids are functional, so without evidence to the contrary it is hypothesised that there will also be an increase in the protein. Studies have shown that there is a strong correlation between mRNA and proteins amounts (Koussounadis et al., 2015; Lu et al., 2007). Nevertheless, alterations in observed phenotypes of cellular responses and bacterial trafficking in these transfected cells (as described in subsequent chapters) does indicate that the transfected genes are being expressed at the protein and therefore functional level.

Chapter 6 – Host-pathogen gene interaction and phagosome arrest.

6.1 Introduction

This chapter covers the investigation into the effect of over-expressing the three vesicular transport genes, *RILP, RIN2* and *OSBPL1a,* in U937s, a macrophage-like cell line. The selection of these genes has been described in Chapter 3. In brief, the genes are all involved in phagosomal maturation and targeting, which are downregulated post *M.tb* infection. It is hypothesised that *RIN2, RILP and OSBPL1A* are actively suppressed in response to infection with *M.tb* as part of a complex multi-layered host-pathogen interaction leading to the arrest of phagosome maturation and subsequent pathogen survival. The theory is that over-expressing these genes will reverse the suppression by *M.tb*, thereby restoring the normal phagosome-lysosome pathway. To test this hypothesis, stable transfected cell lines were constructed (as described in Chapter 5) and have been used in this chapter in three ways; i) viable counts to look for altered bacterial killing; ii) trafficking analysis by immunofluorescence assays to look for altered trafficking; iii) gene expression analysis of the macrophage derived *M.tb* to look for altered expression in response to the over-expressed proteins which act as surrogate markers for altered host-pathogen interactions.

6.2 Viable counts

Viable counts were used to measure the survival of *M.tb* phagocytosed by U937 cells, as described in Chapter 4.3. This assay was to compare the survival of *M.tb* within the transfected U937 cells with the non-transfected U937 cells. The hypothesis is, if overexpression of these genes restores normal phagosome-lysosome fusion, then this would have an impact on *M.tb* survival within the cell.

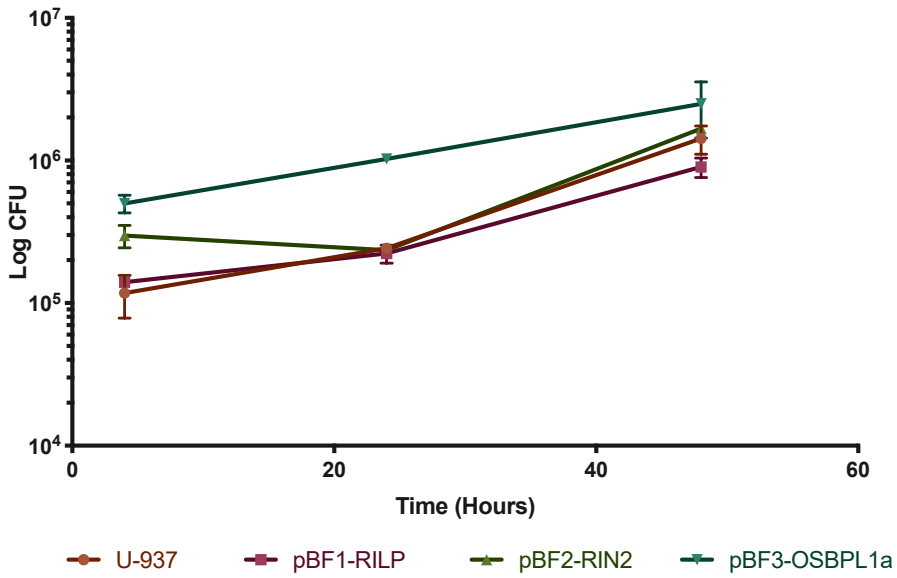

Figure 6.1 Graph of viable counting of H37Rv intracellular growth throughout a 20:1 infection in control non-transfected cells and three transfected U937 cell lines, these were set up in two biological replicates. Each time point was plated in duplicate (Error bars represent standard deviation, the error bar for pBF2-RIN2 at 24hours is not visible due to being the same size as the data point itself).

Figure 6.1 illustrates the intracellular growth of H37Rv in four different cell lines, one control cell line of non-transfected U937s, and three transfected cell lines; U937-pBF1 over-expressing RLIP, U937-pBF2 over-expressing *RIN2*, and U937-pBF3 over-expressing *OSBPL1a*. The *M.tb* in control cells shows a slight increase in growth rate between 24 and 48 hours compared to 4-24 hours. The CFU increases from $1\text{^}10^5$ to $2.5\text{^}10^5$ bacteria/ml from 4 to 24 hours, and from $2.5\text{^}10^5$ to $1.5\text{^}10^6$ bacteria/ml from 24 hours to 48 hours, this is in line with multiple published studies and 20 hour generation time (Gill et al., 2009). This is not seen to the same extent in the *M.tb* in the transfected cells. The intracellular growth of *M.tb* in the cells over-expressing RILP (U937-pBF1) follows the control cells most closely, displaying a slight increase in growth rate after 24 hours. The growth within the cells over-expressing OSBPL1a displays a steady increase in growth from 4 to 48hours. The intracellular growth of the *M.tb* in the cells over-expressing RIN2 was observed to deviate most from the control non-transfected cells, with the CFU counts dropping slightly at 24 hours from $3\text{^}10^5$ down to

2.3^10^5 bacteria/ml. However, no significant differences between the curves were seen upon statistical analysis of triplicate experiments (p-value=0.5). The same inoculum was used for all the infections, but at four hours there was a difference in the amount of phagocytosed bacteria. This suggested that there could be an increase in the phagocytic potential of the RIN2 and OSBPL1a cell lines.

6.3 Confocal microscopy to identify altered trafficking

As discussed in Chapter 4.4, infection with *M.tb* prevents both phagosomal maturation and acquisition of the late endosomal or lysosomal markers by the phagosome. The infected cells instead retain early endosomal markers, such as Rab5. To test if over-expressing RILP, RIN2 or OSBPL1a in the macrophages alters the trafficking of *M.tb*, an immunofluorescence assay was set up to analyse co-localisation of the bacteria with either Rab5, Rab7 or Lamp1 (according to Chapter 4.4). If maturation of the phagosome into the phagolysosome is arrested by suppression of these proteins, reintroduction of these on a plasmid for ectopic expression could potentially revert this effect and aid in maturation. If that is the case, then phagosomes containing bacteria will consequently acquire the late endosomal or lysosomal markers, Rab7 and Lamp1, respectively. For each primary antibody, the slides were set up in triplicate and all three coverslips were examined for the assay, totalling over 100 cells, and a representative image was taken for illustration purposes.

6.3.1 Confocal microscopy of infected U937-pBF1 overexpressing RILP

Figure 6.2 shows representative images of the results of the fluorescence co-localisation studies for the cell line over-expressing RILP. As can be seen from the images in Figure 6.2c, the infected U937-pBF1 cells exhibit the same behaviour as native infected U937 cells (see Chapter 4, Figure 4.10), where the *M.tb* co-localise with Rab5. Figure 6.2d confirms this graphically, as two distinct populations were observed. The population near the Y-axis is the red stained Rab5 that is seen below the nucleus in Figure 6.2c. The population that clusters around the straight line illustrates where the FITC stained *M.tb* and red stained Rab5 merge, as seen in the top left of image 6.2c. For further confirmation, a

statistical quantification of the co-localisation was performed, the Pearsons R value for the co-localisation of the green stained *M.tb* with the red stained Rab5 was 0.83 and the Manders' tM1 value was 0.59.

No co-localisation was seen between *M.tb* and the stained endosomal markers, Rab7 and Lamp1, respectively, (Figure 6.2, panels G and K). The graphical confirmation of no co-localisation is illustrated in Figure 6.2 panels H and I; the statistical quantification corroborates this. The statistics were as follows (Table 6.1);

Table 6.1 Statistical analysis of the co-localisation results for U937-pBF1 overexpressing RILP

	Pearson's R Value	**Manders' tM1**
***M.tb* and Rab5**	0.83	0.59
***M.tb* and Rab7**	0.29	0.0
***M.tb* and Lamp1**	-0.24	0.124

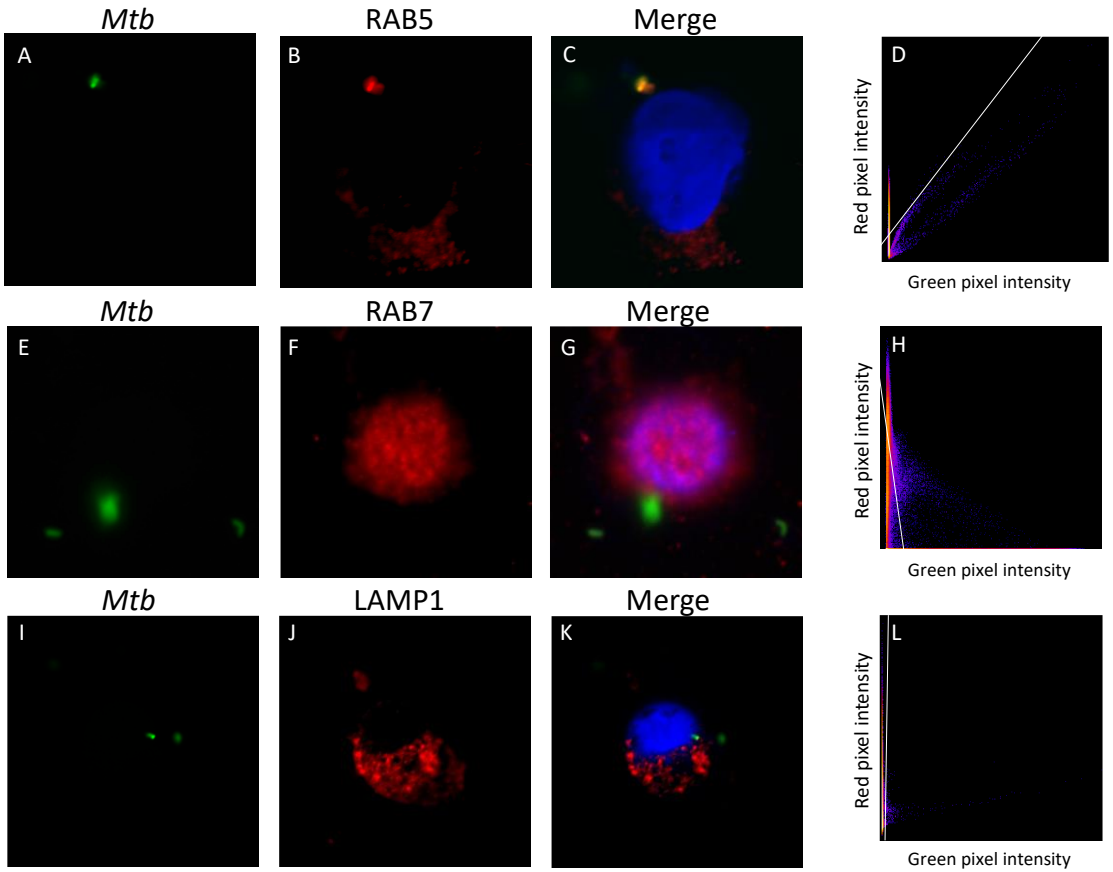

Figure 6.2 Confocal microscopy of U937-pBF1 cells over expressing RILP infected with M.tb H37Rv. Panels A,E and ,I, M.tb stained with FITC. Panels B, F, and J, stained endosomal markers (Rab5, Rab7 and Lamp1). Panels C, G, and K, merged images of the M.tb and endosomal marker. Panels D, H and L, co-localisation represented graphically in a scatterplot where the intensity of the red is plotted against the intensity of the green for each pixel.

6.3.2 Confocal microscopy of infected U937-pBF2 overexpressing RIN2

Figure 6.3 shows representative images of the fluorescence co-localisation studies of the cells over-expressing RIN2. As can be seen from the images in Figure 6.3c, the infected U937-pBF2 cells do not exhibit the same behaviour as native infected U937 cells (see Chapter 4, Figure 10). As illustrated in Figure 6.3, no co-localisation can be seen with Rab5, Rab7 or Lamp1; the graphical representation supported this, as did the statistical quantification. There was a suggestion of a co-localised population in the scatterplot for Rab5 (Figure 3 panel D), however, this was not seen in the image or confirmed with the statistical analysis. The statistics were as follows (Table 6. 2);

Table 6.2 Statistical analysis of the co-localisation results for U937-pBF2 overexpressing RIN2

	Pearson's R Value	**Manders' tM1**
***M.tb* and Rab5**	-0.15	0.345
***M.tb* and Rab7**	-0.05	0.125
***M.tb* and Lamp1**	-0.08	0.055

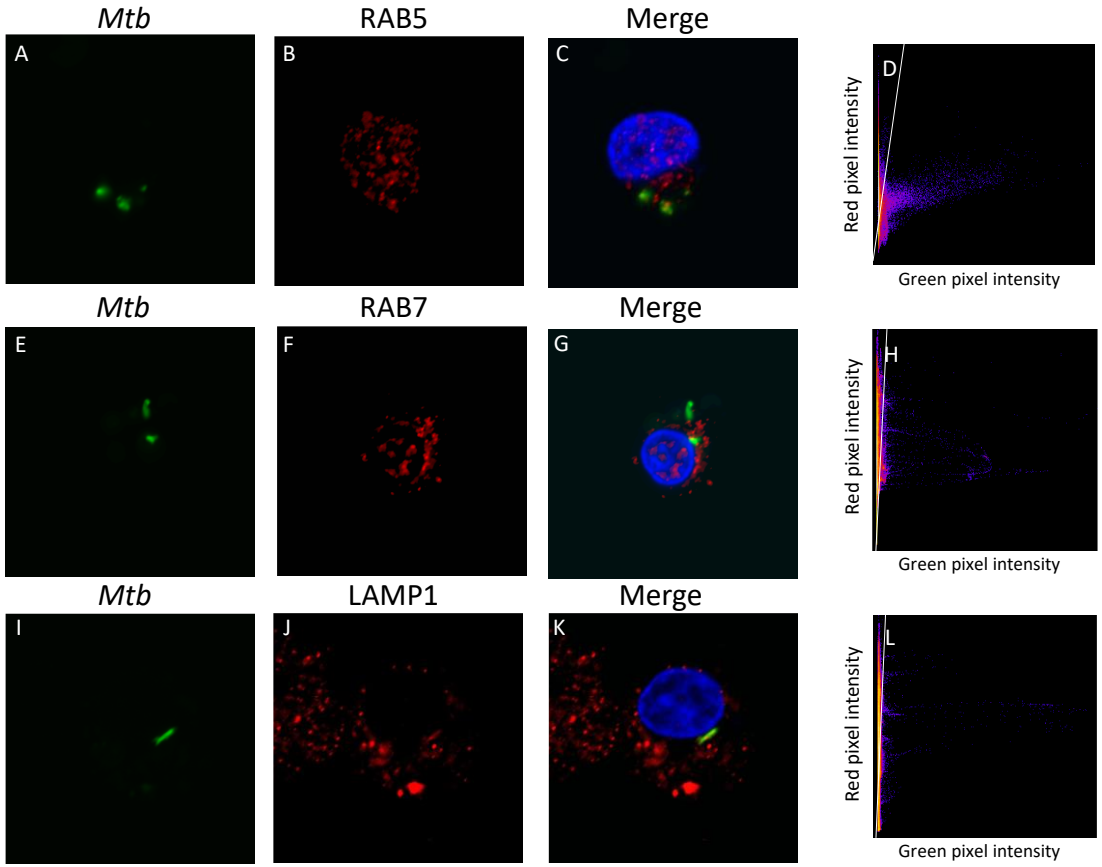

Figure 6.4 Confocal microscopy of U937-pBF2 cells over expressing RIN2 infected with M.tb H37Rv. Panels A,E and ,I, M.tb stained with FITC. Panels B, F, and J, stain endosomal markers (Rab5, Rab7 and Lamp1). Panels C, G, and K, merged images of the M.tb and endosomal marker. Panels D, H and L, co-localisation represented graphically in a scatterplot where the intensity of the red is plotted against the intensity of the green for each pixel.

6.3.3 Confocal microscopy of infected U937-pBF3 overexpressing OSBPL1a

Figure 6.4 shows representative images of the results of the fluorescence co-localisation studies for the cell line over-expressing OSBPL1a. As can be seen from the images in Figure 6.4c, the infected U937-pBF3 cells exhibit the same behaviour as native infected U937 cells (see Chapter 4, Figure 10), where the *M.tb* co-localise with Rab5. This is corroborated by the scatterplot (Figure 4 panel D), where two populations can be seen, one to the left and one along the straight line. The population on the left represents the Rab5 staining that does not co-localise with the FITC-stained *M.tb*, and the population on the straight line represents where the pixel is coloured both red and green, and thus co-localised. The statistical analysis confirmed this result; Pearson's R value was 0.58 and Manders' tM1 was 0.82.

Figure 6.4 panels G and K illustrate that there was no co-localisation between the *M.tb* and Rab7 or Lamp1. The graphical representation of *M.tb* and Rab7 (panel H) showed two populations, one adjacent to the Y axis and one adjacent to X axis. The statistical analysis corroborates this; Pearson's R value -0.49 and Manders' tM1 0.069. The statistical analysis of *M.tb* and Lamp1 also ratifies no localisation; the statistics were as follows (Table 6.3);

Table 6.3 Statistical analysis of the co-localisation results for U937-pBF2 overexpressing OSBPL1a

	Pearson's R Value	**Manders' tM1**
***M.tb* and Rab5**	0.58	0.82
***M.tb* and Rab7**	-0.49	0.069
***M.tb* and Lamp1**	-0.44	0.370

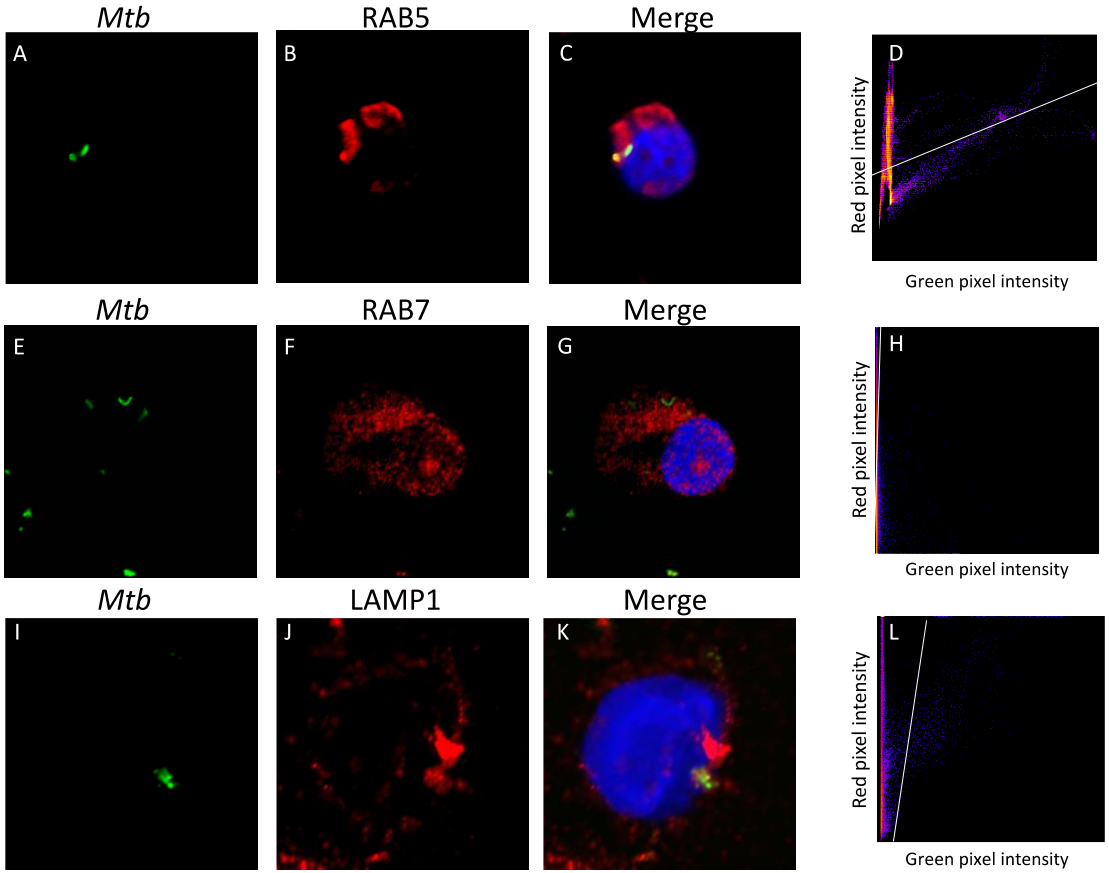

Figure 6.5 Confocal microscopy of U937-pBF3 cells over expressing OSBPL1a infected with M.tb H37Rv. Panels A,E and ,I, M.tb stained with FITC. Panels B, F, and J, stain endosomal markers (Rab5, Rab7 and Lamp1). Panels C, G, and K, merged images of the M.tb and endosomal marker. Panels D, H and L, co-localisation represented graphically in a scatterplot where the intensity of the red is plotted against the intensity of the green for each pixel.

6.4 Changes in mRNA expression levels in macrophage-derived *M.tb*

M.tb is one of the most successful pathogens at adaptation for long-term survival within host phagosomes. This adaptation results from the differential gene expression in response to their environment. With this is mind, published transcriptional data was the starting point for the selection of *M.tb* genes to study, during intracellular infection of the cell lines over expressing RILP, RIN2 and OSBPL1a. One comprehensive study by Schappinger et al. (2003) used global expression profiling to identify genes differentially expressed by intra-phagosomal *M.tb* compared with *M.tb* grown *in vitro* under standard conditions. The study identified 454 differentially regulated genes of which 21 were confirmed using qRT-PCR. Conclusions were made that defined the host-pathogen metabolism for different stages of *M.tb* -macrophage interactions.

6.4.1 Selection of the genes within the *M.tb*

The five *M.tb* genes identified to be studied for expression in response to over-expression of the host proteins RILP, RIN2 and OSBPL1a, were selected from this list (Schnappinger at al 2003) by the following criteria: i, they were specifically upregulated in response to macrophage activation, ii, identified by more than one publication, iii, had different functions (see Table 6.4 for further details). We hypothesise that these genes induced by the phagosomal environment may be impacted by the over-expression of the host proteins (RILP, RIN2 and OSBPL1a), if the suppression of these host proteins is indeed important for the survival of the *M.tb* within the macrophage. The selected genes and their probable functions are listed in Table 6.4.

RNA polymerase sigma factor (*sigA*) was selected as a reference gene to standardise the qRT-PCR to correct for variation in the amount of total mRNA in the sample. It is considered to be constitutively expressed under most conditions, as it is involved in the regulation of bacterial housekeeping genes (Manganelli et al., 1999).

Table 6.4 Selected M.tb genes

Gene	Accession number	Summary	References
mpt83	Rv2873	*mpt83* encodes the *M.tb* cell surface glycolipoprotein Mpt83 (lipoprotein P23), only small quantities of the protein are produced in vitro. However, this is strongly induced during adaptation to the phagosomal environment. It has been shown to induce macrophage apoptosis and necrosis. This increase in expression is regulated by sigma factor K (SigK).	(Charlet et al., 2005; Gold et al., 2001; Schnappinger et al., 2003b; Wang et al., 2017)
hrp1	Rv2626c	Hypoxic response protein 1 (hrp1) is a secreted protein with a cystathionine-beta-synthase (CBS) domain. The gene is part of the dormancy regulation and its expression is induced in the phagosomal environment. While the function of hrp1 is still unknown, there is evidence that its expression enhances the bacterial survival ability in macrophages.	(Aguilar-Ayala et al., 2017; Danelishvili et al., 2016; Schnappinger et al., 2003b; Sun et al., 2017)
hspX	Rv2031	α-crystallin (hspX) is a small heat-shock protein found in the mycobacterial cell wall, it is an ATP-independent chaperone and it is required for growth within macrophages. Induction of the gene begins on entry into macrophages, and after 4 hours, an induction of over 100-fold can be measured, and can be detected in patient sera.	(Castro-Garza et al., 2017; Dubnau et al., 2002; Schnappinger et al., 2003b; Yuan et al., 1998)
icl1	Rv0467	Isocitrate lyase (icl1) is a key enzyme of the glyoxylate pathway, catalysing the formation of succinate and glyoxylate from isocitrate. It allows the consumption of lipids in low oxygen environments, and has been found to be essential for *M.tb* persistence.	(Dubnau et al., 2002; Graham and Clark-Curtiss, 1999; McKinney et al., 2000; Schnappinger et al., 2003b; Sharma et al., 2000)
echA19	Rv3516	Enoyl-CoA hydratase (echA19) plays a role in lipid metabolism, particularly in the oxidation of the fatty acids. echA19 expression is increased after phagocytosis by macrophages and it has been suggested that it contributes to the mycobacteria ability to catabolise cholesterol (side-chain degradation), which is essential for survive in macrophages.	(Dubnau et al., 2002; Geize et al., 2007; Schnappinger et al., 2003b)

To test this hypothesis, infections with *M.tb* H37Rv (MOI 20:1) were set up in each of the over-expression cell lines; U937-pBF1, U937-pBF2 and U937-pBF3 over-expressing RILP, RIN2 and OSBPL1a, respectively. After 24 hours, RNA was extracted from the bacteria and cDNA was prepared. qRT-PCR was performed for all five genes listed in Table 6.1, plus *sigA*, which was used as a control to correct for differing amounts of mRNA. The gene expression was compared to a control which was *M.tb* that had been processed through empty vector transfected U937 (pBF0). The experiment was set up in biological duplicate with three technical replicates, and results are shown in Figure 6.6.

For the genes *hspX, echA19*, *hrp1* and *icl1*, a large induction of expression was seen in response to the over-expression of RILP, RIN2 and OSBPL1a. When compared to the control, there was as much as 64-fold in some cases (hrp1 Figure 6.6 panel C). For *hspX* (Panel A), *echA19* (Panel B) and *icl1* (Panel D) the induction was similar in response to all three over-expressed proteins RILP, RIN2 and OSBPL1a (P-value 0.14, 0.78, and 0.95 respectively). For *hrp1*, a stronger induction was seen in response for the over-expression of RILP compared to RIN2 (P-value 0.01) and OSBPL1a (P-value 0.02). No different was seen between the induction of *hrp1* in response to RIN2 and OSBPL1a (P-Value 0.95).

Expression of *mpt83* varied in response to each protein over-expressed (Panel E) (P-value 0.0075). Induction of *mpt83* was the highest in response to RILP with an induction of up to 55-fold, whereas the induction in response to OSBPL1a was only up to 4-fold. The only gene suppression was seen in *mpt83* in response to the over-expression of RIN2, when compared to the expression in *M.tb* processed through non-transfected U937s (P-value 0.0004).

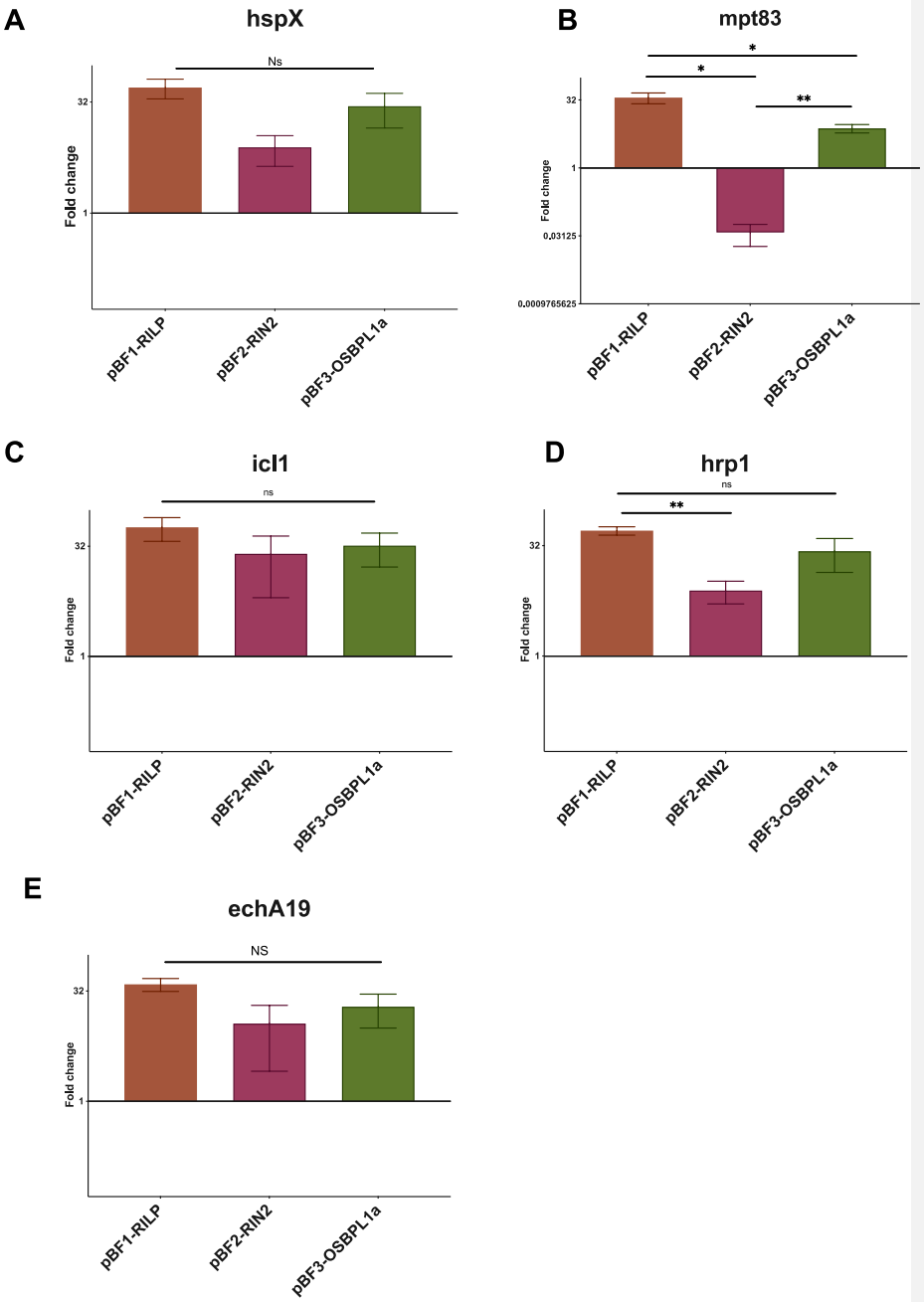

Figure 6.5 Fold change of gene expression from multiple qPCR assays using selected primers. Each panel is a different set of primers with M.tb from each cell line. Results presented a fold changes to sham transfected control cells. Values normalised to sigA.

6.5 Conclusion

In summary, this chapter covers the effect of overexpression of RILP, RIN2 and OSBPL1a on the infection of U937 macrophage-like cell line by *M.tb*. The survival rate, intracellular trafficking and changes in gene expression of the bacteria were all analysed. Viable counts demonstrated that over-expression of RILP, RIN2 and OSBPL1a had no effect on the ability of *M.tb* to survive within the macrophage (Figure 6.1).

Confocal microscopy revealed that over-expressing RILP or OSBPL1a did not alter the trafficking of the bacteria within the cell, as in both over-expressed cell lines the *M.tb* still co-localised with Rab5 (Figures 6.2C and 6.4C), as is expected in native macrophages. However, microscopy of the infected U937s over-expressing RIN2 suggested a change to the trafficking as the *M.tb* was not co-localised with Rab5 (early endosome), nor with Rab7 or Lamp1 (late endosome- phagosome). This suggests maybe some alternative trafficking compartment (see Discussion below).

The final part of the chapter addressed if there were changes in gene expression in *M.tb* in response to the over-expression of RILP, RIN2 and OSBPL1a. Five genes with different functions, known to be upregulated in the phagosome environment were selected (*hspX, echA19, hrp1, icl1* and *mpt83*) and qRT-PCR was performed. The qRT-PCR revealed that genes *hspX, echA19, hrp1* and *icl1* are all induced in response to the over-expression of the three proteins in the macrophages (Figure 6.6 A-D). The results for *mpt83* expression displayed a different pattern, although the expression was induced in response to the over-expression of RILP and OSBPL1a, a suppression was seen in reaction to the over-expression of RIN2 (Figure 6.6E).

6.6 Discussion

The aim of this chapter was to identify if over-expressing RILP, RIN2 and OSBPL1a in the macrophage restores phagosome maturation when the cells are infected with *M.tb.* With phagosome maturation restored, the *M.tb* would be trafficked to the lysosome and thus be killed. As previously discussed in section 6.3, these proteins are all involved in vesicular transport and suppressed in response to infection with *M.tb* in the host cell. It was hypothesised that reversing the suppression would restore the normal phagosome-lysosome pathway. The results of the bacterial viability assay however, did not reveal any killing of the *M.tb* (Figure 6.1). The over-expression of the host proteins RILP, RIN2 and

OSBPL1a did not appear to have any effect on the growth of the bacteria inside the macrophage. This is a relatively crude assay and may not be sensitive enough to detect subtle changes in viability of the bacteria. The small number of time points potentially masked the initial drop and the outgrowth of survivors that is often seen in publications, or the volume of cells and bacteria used to enable a large RNA harvest may have removed this effect. Also, the starting number of bacteria varied from $1x10^5$ to $5x10^5$ due to being counted by eye prior to plating; although in the same magnitude, this could explain why the cells over-expressing OSBPL1a (U937-pBF3) display more robust growth. Moreover, as the proteins were over-expressed individually in the cell lines, the other two proteins will still be supressed, so potentially just restoring one of the proteins is not enough to subvert the *M.tb* halt on phagosome maturation (manifested in the infection model used here as killing within the 48 hour time window).

To elucidate the effect of over-expressing RILP, RIN2 and OSBPL1a in more detail, confocal imaging was employed. Phagosomes containing virulent *M.tb* have been shown to stay within early endosomes retaining Rab5, and not acquiring Rab7 or the late lysosomal marker Lamp1 (section 6.4). And while over-expressing RILP, RIN2 and OSBPL1a did not have a killing effect on the bacteria, there was potential that this over-expression could allow for further or alternative maturation of the endosomes. To test this, immunofluorescence assays were set up for the three main markers, Rab5, Rab7 and Lamp1. This assay looked for co-localisation in the infected cells between the stained *M.tb* and the markers. RILP and OSBPL1a form a complex with Rab7. This complex is required for the assembly of microtubule motors, which in turn is essential for fusion of phago-lysosomes (Johansson et al., 2007a). The hypothesis was that *M.tb* actively suppresses RILP and OSBPL1a to disrupt this process, so by adding these proteins back in, this process could be restored. However, results of the co-localisation studies with either OSBPl1a or RILP (Figures 6.2 & 6.4) did not reveal any changes to the trafficking within the cell, instead the *M.tb* remained co-localised with Rab5. This means that the hypothesis is not proven, but there are other possibilities for why no change in trafficking was seen. One possibility is that the proteins need to be co-expressed, so both RILP and OSBPL1a are restored in the same cell, to see any effect. This could be tested by constructing a cell line over-expressing both genes at once, and the trafficking experiments repeated. Another possibility is that there

are other blocks on maturation before this process takes place; the suppression of RIN2 could be one such mechanism.

RIN2 forms a complex with Rab5 (Sandri et al., 2012), which is lost in normal P-L maturation. The hypothesis is that with RIN2 restored, Rab5 will be replaced by Rab7 as per the normal maturation. When the cells over-expressing RIN2 were infected, the confocal microscopy did indeed reveal alterations to the normal co-localisation pattern, no co-localisation with Rab5 was seen (Figure 6.3C). The obvious assumption is that Rab5 is lost because the endosome has maturated from an early to a late endosome. However, a late endosome would be discernible by the presence of Rab7, but no co-localisation with Rab7 was seen (Figure 6.3G). Moreover, results revealed no co-localisation with Lamp1 either, meaning that the bacteria were not trafficked to the phagolysosome. This theory is supported by the results of the viability assay, which failed to show any reduction in viability, and thus the *M.tb* is not being killed (or appropriately processed) by the cell within the time-frame studied. These results leave open the question of what is the fate of *M.tb* inside the cell. There are several hypotheses as to what could be happening to the *M.tb* upon the over-expression of RIN2 in the host cell.

One hypothesis is that the bacteria could still be in an early endosome but Rab5 has been lost, and the normal pathway has been disrupted by the over-expression of RIN2 so Rab7 has not been recruited.

Another is that the over-expression of RIN2 disrupts the normal trafficking events in such a way that the early endosome enters the “recycling pathway”. This pathway is normally reserved for returning membrane proteins and lipids to the cell surface. Recycling endosomes do not have Rab5 on their surface, instead they can be recognised by the presence of Rab11 (Goldenring, 2015). This remains to be tested.

A further hypothesis is that the *M.tb* containing phagosome has been sequestered within an autophagosome; this process is not uncommon for pathogens inside macrophages. Recent work has shown that autophagy not only functions to degrade cellular proteins but also as an antibacterial mechanism. Autophagy has been shown to target bacteria and transport them to lysosomes for degradation (Shahnazari and Brumell, 2011). Previously, Gutierrez et al has shown that if autophagy is artificially stimulated in a cell infected with *M.tb*, then the phagosome containing the bacteria can be engulfed by

autophagosomes, but this process is normally blocked as part of the mechanisms of survival employed by *M.tb* (Gutierrez et al., 2004).

A final hypothesis is that over-expressing RIN2 had damaged the phagosome membrane resulting in the loss of Rab5 and allowing the bacteria to escape the phagosome into the cytosol of the cell. Although this escape is a possibility, as discussed in the Introduction above, a recent study reported that some clinical strains escape from the phagosomes to reside in the cytoplasm (Jamwal et al., 2016). They hypothesise that this escape to the cytoplasm enables the bacteria to avoid some of the microbicidal mechanisms of the macrophage. This hypothesis is less likely, as it appears that the bacteria actively suppress the expression of RIN2, so its over-expression should not be advantageous for *M.tb*.

Further studies are needed to determine if any of these hypotheses are correct. Electron microscopy could be used to identify the location of the *M.tb* within the cell, to answer the question of if it's still within a phagosome or a double membrane vesical, for example an autophagosome, or if it has escaped to the cytosol. Rab5, Rab7 and LAMP1 are traditionally used for markers of early, late endosomes and lysosomes respectively (Bucci et al., 1992; Epp et al., 2011; Eskelinen, 2006; Gorvel et al., 1991; Rink et al., 2005). However, there are recent studies that suggest that these may not be as specific as once thought. Shearer and Petersen, (2019) found that some endosomes displayed these three markers simultaneously, and they hypothesise that the maturation and fusion process is not as linear as once thought; however, this also highlights the potential need for re-evaluation of the use of these markers. Other markers could be used for the co-localisation studies such as Early endosome antigen 1 (EEA1), an alternative marker for early endosomes, or light chain 3 (IC3) a biomarker of autophagosomes, or Rab11 a marker of a recycling endosome.

The effect of over-expression of RILP, RIN2 or OSBPL1a on *M.tb* gene expression has also been investigated in this chapter. Five genes known to be induced in the phagosomal environment were selected (Table 6.2), with the rationale that they would be most affected by the changes in host proteins resulting from or causing alterations to endosome trafficking pathways. For all five *M.tb* genes induced in the phagosomal environment, there was a further increase in expression in response to both RILP and OSBPL1a being over-expressed. One consideration is that the transfection agent could have an effect on the induction of host genes, resulting in the increase in the *M.tb* genes. Jacobsen et al (2009)

found that 48 hours post-transfection using FuGENE HD, 157 genes were differentially expressed in the transfected cells. To remove this potentially confounding effect, the expression in the empty vector control was used as the baseline for comparison. As all five *M.tb* genes showed a similar increase in expression irrespective of the over-expressed host gene, this would suggest that this increase is less likely to be a result of the specific gene being over-expressed. The five genes were expected to be induced in the phagosomal environment, this further induction could suggest a more hostile environment due to the replacement of RILP, RIN2 and OSBPL1a in the host cell. To test this, the hostility of the phagosomal environment could be assayed, using PH tracker for example.

The response to the over-expression of RIN2 showed a slightly different pattern. All the genes selected for study were induced in bacteria recovered from the cells over-expressing RIN2, except for *mpt83*. In fact, *mpt83* expression was significantly suppressed in response to over-expression of RIN2. *mpt83* encodes the *M.tb* cell surface glycolipoprotein MPT83 (lipoprotein P23). Despite many research studies involving MPT83 as an antigen and subunit vaccine candidate, very little is known about its function; it has been predicted to be a signalling protein (Målen et al., 2007). It has been found to induce apoptosis in macrophages, following recognition of MPT83 by TLR2 on the cell surface: a cascade of events triggered by the production of COX-2 led to apoptosis of the cell (Wang et al., 2017) The increase in the expression of mpt83 in the phagocytic environment appears to be counter-intuitive, as apoptotic cell death is seen as a host protective mechanism. Supporting this, Wang et al. (2017) also showed that over-expressing MPT83 in *M. smegmatis* reduced survival capacity although this work has yet to be done in *M.tb*. The downregulation of MPT83 in the presence of over-expressed RIN2 suggests that there is a change in the intracellular environment that results in a differential gene expression profile, possibly reflective of the bacteria's altered metabolic state or expression of virulence mediators, such as MPT83. This supports the finding of the co-localisation studies, which revealed changes in trafficking when RIN2 was over-expressed. While this remains to be resolved, identifying the location of the *M.tb* within the cell with the proposed further studies would give further insight.

Chapter 7 – Identification of *M.tb* genes involved in suppression of phagosome trafficking.

7.1 Introduction and aims

As previously discussed in Chapter 1, *M.tb* survives in the host cell in the phagosomes by arresting their maturation. Although some bacterial components have been shown to be involved in this arrest of maturation, (see Introduction), the mechanisms remain elusive despite the use of diverse experimental strategies. Multiple large scale studies have been undertaken using mutant libraries to identify mutants that fail to prevent phagolysosome fusion (Brodin et al., 2010; MacGurn and Cox, 2007; Pethe et al., 2004; Stewart et al., 2005). Such studies resulted in large lists of genes which could be mediators of the arrest of phagosome maturation; however, as many of the genes have no known function, extrapolating any useful mechanistic information is challenging. The aim of this chapter was to identify from the literature *M.tb* mutants known to be trafficked to the lysosome, thereby inferring a functional role of that gene in P-L arrest. Mutant strains were obtained (by request to published authors) then used to establish macrophage infections and host gene expression was subsequently analysed as a correlate of altered cellular responses and P-L maturation. Using this method, we hope to identify the *M.tb* genes associated with the downregulation of RILP, RIN2 and OSBPL1a, and altered vascular transport processes. It is hypothesised that if the genes knocked-out are involved in the evasion of phagolysosome fusion, these mutants will be unable to suppress the host genes RILP, RIN2 and OSBPL1a.

This chapter covers two main areas; i) selection and investigation of mutant stains of *M.tb* that are unable to arrest phagolysosome fusion and ii) assessment of the expression of the host genes *RILP*, *RIN2* and *OSBPL1a* in infections with known *M.tb* mutants.

7.2 Selection of transposon mutants

Brodin et al. (2010) developed a high throughput method for identifying mutant strains of *M.tb* that are unable to suppress phagolysosome fusion, and thus are rapidly trafficked into acidified compartments. In their paper entitled "High Content Phenotypic Cell-Based Visual Screen Identifies *Mycobacterium tuberculosis* Acyltrehalose-Containing Glycolipids Involved

in Phagosome Remodelling", over 11,000 transposon mutants were constructed by transposition of the IS1096-derived Tn5367 transposon into the *M.tb* strain GC1237, and were screened using automated confocal fluorescence microscopy. Of these 11,000, ten mutants were identified as being trafficked to the phago-lysosome. These ten mutants were analysed to identify the genes disrupted by the transposon, using PCR and sequencing (Brodin et al., 2010). Eight of these known mutants were provided for use in the study as a kind gift from Dr Olivier Neyrolles (French National Centre for Scientific Research) and Prof Graham Stewart (University of Surrey), following guidelines for safe and appropriate transfer of HG3 organisms to SGUL. The eight mutants are listed in Table 7.1 with the gene that is disrupted and a summary was then compiled of what is known about their function. The mutants will be referred to by the nomenclature Tn:: and the gene interrupted.

Table 7.1 summary of Tn mutants used for this study

Gene interrupted	Accession number	Summary	References
lppM	*Rv2171*	LppM is a lipoprotein whose molecular function is not well understood. It is found either anchored to the mycobacterial cell wall or secreted in a truncated form. It has been shown to be capable of binding phosphatidylinositol mannosides (PIM), which have been implicated in modulation of the host immune response. It has also been suggested that LppM hinders phagocytosis by macrophages of the bacteria. The transposon mutant was found to be trafficked to the lysosome.	(Barthe et al., 2016; Brodin et al., 2010; Deboosère et al., 2017)
moaC1	*Rv3111*	Molybdenum cofactor biosynthesis proteins C and D (MoaC1 & MoaD1) are part of a gene set involved in molybdenum cofactor biosynthesis, they are known to be induced in the phagosomal environment. Molybdenum is required by enzymes catalysing carbon, sulphur and nitrogen. MoaC1 has been shown to bind GTP and is secreted by the bacteria, and mutants have been shown to have reduced virulence in macrophages by multiple studies.	(Brodin et al., 2010; Dutta et al., 2010; Kanaujia et al., 2010; Levillain et al., 2017; MacGurn and Cox, 2007; Magalon and Mendel, 2015; Målen et al., 2007; Rosas-Magallanes et al., 2007; Wang and Behr, 2014)
moaD1	*Rv31112*		
pstS3	*Rv0928*	Periplasmic phosphate-binding lipoprotein (PstS3) is a component of the inorganic phosphate transport chain, it is predicted that it acts as cell surface signalling peptide. Studies have shown it is required for survival in primary murine macrophages, and the transposon mutant is trafficked to the lysosome.	(Brodin et al., 2010; Målen et al., 2007; Sassetti et al., 2003)
Rv1503c	*Rv1503c*	Rv1503c is a hypothetical protein with no known function, found in the cell wall and membrane. It is thought to be required for virulence, a number of studies have found transposon mutants grow poorly in macrophages and the mutant is unable to arrest phagosome-lysosome fusion.	(Brodin et al., 2010; Forrellad et al., 2013; Mawuenyega et al., 2005)
Rv1506c	*Rv1506c*	Rv1506c is a hypothetical protein with no known function encoded by the same operon as Rv1503c, it was recently identified as playing a role in virulence. As with RV1503c the mutant was unable to arrest phagosome-lysosome fusion.	(Brodin et al., 2010; Forrellad et al., 2013; Mawuenyega et al., 2005; Ru et al., 2017)
Rv2295	*Rv2295*	Rv2295 encodes a hypothetical protein not considered to be an essential gene, however, the transposon mutant has been shown to be trafficked to the lysosome in macrophages.	(Brodin et al., 2010; Mazandu and Mulder, 2012)
espL	*Rv3880c*	espL is an ESX-1 secretion-associated protein of unknown function, ESX-1 is required for virulence and for the secretion of protein ESAT-6. The gene shows increased expression in virulent strains inside macrophages, and the transposon mutant was found to be trafficked to the lysosome.	(Brodin et al., 2010; Li et al., 2010; McLaughlin et al., 2007)

7.3 Comparison of mutant parent strain and laboratory stain.

The *M.tb* transposon library was constructed using the parent strain GC1237. This strain differs from the laboratory strain used in our previous experiments. Thus, in order to know if any observed effect is due to the interrupted gene rather than the differences in the parent strains, comparisons between the two strains were performed (H37Rv and GC1237). These comparisons covered two aspects: i) viable counting of the intracellular growth of both strains to assess their survival and growth within U937 macrophages; and ii) comparison of the ability of the strains to downregulate the host genes of interest in this study, namely *RILP*, *RIN2* and *OSBPL1α*.

7.3.1 Comparison of intracellular growth and survival.

CFU counts were taken at 2, 6, 24, and 48 hours post-infection of U937 macrophage cell lines (MOI 20:1) for the two strains and plotted in Figure 7.1. The results showed that despite having a different inoculum size, the pattern of growth was the same (Figure 7.1). Both strains displayed a sharp increase in CFU over the first 6 hours., This is due to continuation of phagocytosis rather than bacterial growth: bacteria were washed off at 24 hours, so phagocytosis continued for the first 24 hours but the rate reduced as the numbers of free bacteria were depleted. After 24 hours, the increase in CFU is consistent with the growth after phagocytosis. Between 24 hours and 48 hours both stains saw equivalent rates of increases in CFU.

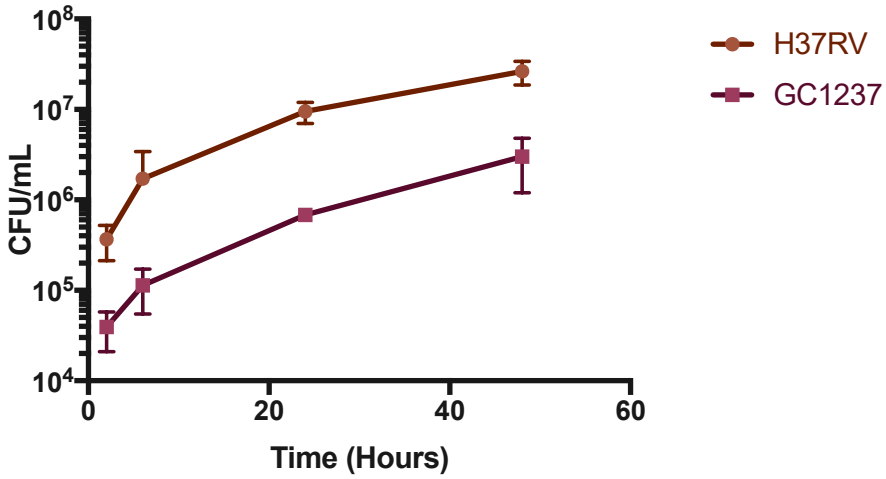

Figure 7.1 - Intracellular growth of M.tb strains H37Rv and GC1237 throughout a 20:1 infection in U937 cells. Each time point was performed in triplicate and plated in duplicate.

7.3.2. Modulation of host gene expression

In order to test the hypothesis that if the genes knocked-out are involved in the evasion of phagolysosome fusion, these mutants will be unable to suppress the host genes RILP, RIN2 and OSBPL1a (as is seen with wild-type). The ability of the parent strain GC1237 to downregulate the host genes of interest in this study, *RILP*, *RIN2* and *OSBPL1a,* required confirmation for valid comparison to data derived from using H37Rv used throughout the work in this thesis. This would confirm that any change in expression in response to the mutants is the effect of the transposon disputed gene in *M.tb* rather than the differences in the *M.tb* parent strains.

Figure 7.2, depicts these comparisons. For each gene, the fold change of expression in response to H37Rv is compared to the fold change of expression in response to GC1237 and plotted as a ratio, over 4 time points - 2, 6, 24 and 48 hours. The raw data after loading control correction is shown in Table 7.2, TATA binding protein (TBP) was used as the loading control as it is constitutionally expressed. It can clearly be seen that there is no difference in the strains' ability to suppress the expression of RILP, RIN2 and OSBPL1a.

7.3.3. Conclusion

These results confirm there are no differences in bacterial growth or effect on the suppression of host genes between the *M.tb* strains used in these studies (H37Rv and GC1237, the parental strain for the Tn-mutants used) and therefore, the use of Tn mutants represents a valid experimental approach from which data can be interpreted in the context of studies performed using H37Rv in previous chapters of this thesis. H37Rv is thus a valid wildtype comparison for the Tn mutants in subsequent studies, despite the different parental strains' background.

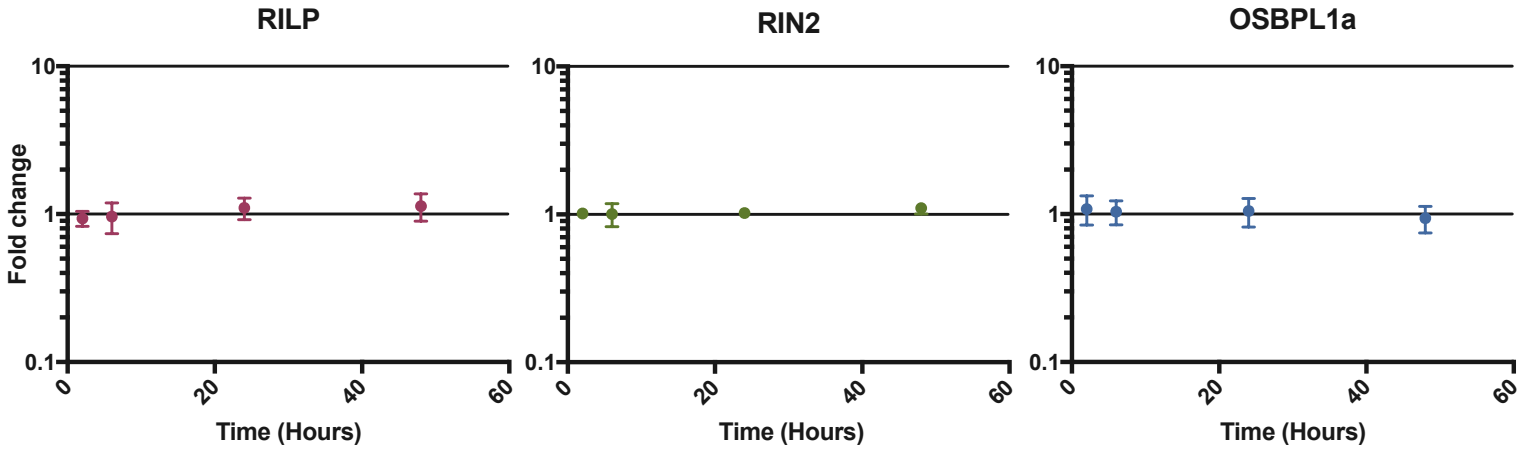

Figure 7.2 – Comparison of expression of RILP, RIN2 and OSBPL1a between H37Rv and GC1237 infected U937s, over the first 48 hours of infection. Moi 20:1, Biological triplicates with technical duplicates pooled with the mean plotted.

Table 7.2 Raw ΔCq data after correction to TBP for loading differences.

	RILP						**RIN2**						**OSBPL1a**					
Time (hours)	H37Rv ΔCq			GS1237 ΔCq			H37Rv ΔCq			GS1237 ΔCq			H37Rv ΔCq			GS1237 ΔCq		
2	-1.05	-1.46	-0.72	-0.74	-0.51	-0.73	4.07	3.72	3.62	3.5	3.61	3.57	0.31	0.42	0.44	0.39	0.5	0
6	-1.44	-1.32	-2.81	-1.22	-1.35	-3.03	2.72	3.16	2.28	2.92	2.89	2.38	-0.62	0.23	0.03	-0.72	0.26	-0.31
24	-2.56	-3.69	-2.36	-2.47	-1.97	-2.98	-0.72	0.11	-0.55	-0.68	-0.57	-0.45	0.2	-0.17	0.11	0.18	0.18	-0.15
48	-2.11	-2.44	-2.51	-2.6	-2.34	-2.66	1.01	1.67	1.77	1.02	1.51	1.52	-0.41	-0.61	-0.77	-0.6	-0.23	-0.62

7.4 Evaluation of the infection parameters for Tn mutant infection

7.4.1 Infection rates per cell

When looking at changes in host gene expression in response to *M.tb* infection, large numbers of cells are necessarily used to facilitate measurement. These cells can be in different stages of infection as the asynchronous infection progresses, as discussed in Chapter 4. In order for changes in gene expression to be comparable, the number of infected cells per assay need to be similar. A coverslip-based assay was employed to characterise the infection rates (measured by counting the number of bacteria per cell) of the Tn mutants compared to H37Rv infection in the U937 cells. U937 cells were set up on glass coverslips and infected (MOI 20:1) with the different mutants, and at each time point were fixed and stained using Kinyoun's cold stain.

Microscopy revealed a very similar infection pattern across all the strains. A selection of representative images for the infection of H37Rv and GC1237 (Tn::moaC1) is shown in Figure 7.3. Typically, only a very small number of cells had phagocytosed bacteria by 4 hours, and those that had, only contained a single bacillus. The number of bacteria increases in the cells over time, whereas the number of cells decreases, as previously seen in Chapter 4. A detailed analysis of the infection rate and intracellular counts was conducted for all the mutants and H37Rv for comparison. For each time-point, the number of intracellular *M.tb* were counted in a minimum of 100 U937 cells across two different coverslips. This allowed the calculation of the mean percentage of U937 cells infected (Figure 7.4A) and the mean number of *M.tb* per cell at each time-point throughout the infection (Figure 7.4B).

At 4 hours, the infection rate ranged from 26 % to 42 % with a mean rate of 36 %; there was no statistical difference between the infection rates of each of the mutant strains and the H37Rv, P-value 0.08. The percentage of infected cells increased significantly as phagocytosis continued up to 24 hours (P- value <0.0001), after which time the extracellular bacteria were washed off. At 24 and 48 hours there was no significant difference between the percentage of cells infected by the different Tn mutant strains (P-values 0.97 and 0.53 respectively), ranging from 49 % to 72 % with a mean of 61 % at 24 hours, and ranging from 60 % to 74 % with a mean of 65% at 48 hours. There was also no significant increase in the percentage of infected cells between 24 and 48 hours (P-value 0.16). This was to be expected after the initial inoculum was washed off. The slight increases could be due to the

incomplete removal of the initial bacterial inoculum, or the re-phagocytosis of the released bacteria from the lysed infected U937 cells.

Figure 7.4B details the average numbers of bacteria per cell. At 4 hours, the mean number of bacteria ranges from 0.39 to 0.99 bacteria per cell with a mean of 0.62. There was no statistical difference between the different strains of bacteria (P-value – 0.112). At 24 hours, the mean numbers of bacteria per cell ranged from 1.47 and 2.79 with a mean of 1.95 bacteria per cell. This was a significant increase from 4 hours (P value <0.0001), but again there was no significant difference of the numbers of bacteria between strains (P value 0.351). At 48 hours, the number of bacteria per cell ranged from 2.18 to 3.4 with a mean of 2.53. There was no significant difference between strains except GC1237 (Tn::moaC1) (P-value 0.552). For the GC1237 (Tn::moaC1) strain, the average number of bacteria per cell was slightly higher at 3.4 compared to the mean of the other strains of 2.53; this difference had slight statistical significance when compared with the numbers of H37Rv per cell (P value 0.0251).

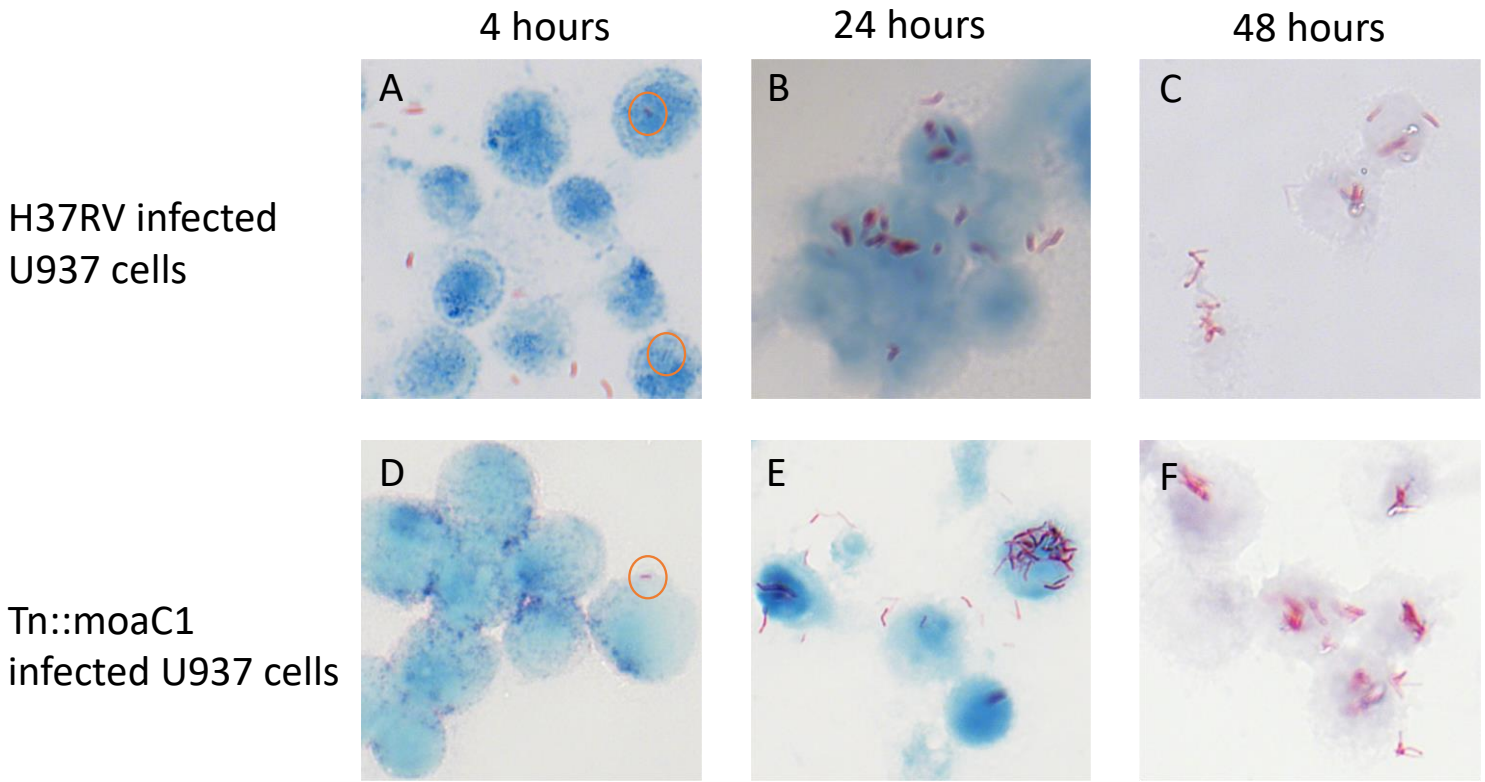

Figure 7.3 Representative images of H37Rv and Tn::moaC1 infected U937 cells after 4 hours, 24 hours and 48 hours, with a maximum infection period of 24 hours. Images were taken using a Zeiss Axioplan 2 upright microscope coupled with a Axiocam HR digital CCD camera. The cells were stained using Kinyoun's carbol fuchsin and counter-stained with 2% malachite green. Single infecting bacillus are circled in the 4 hour images (A&D) for the infected U937 cells.

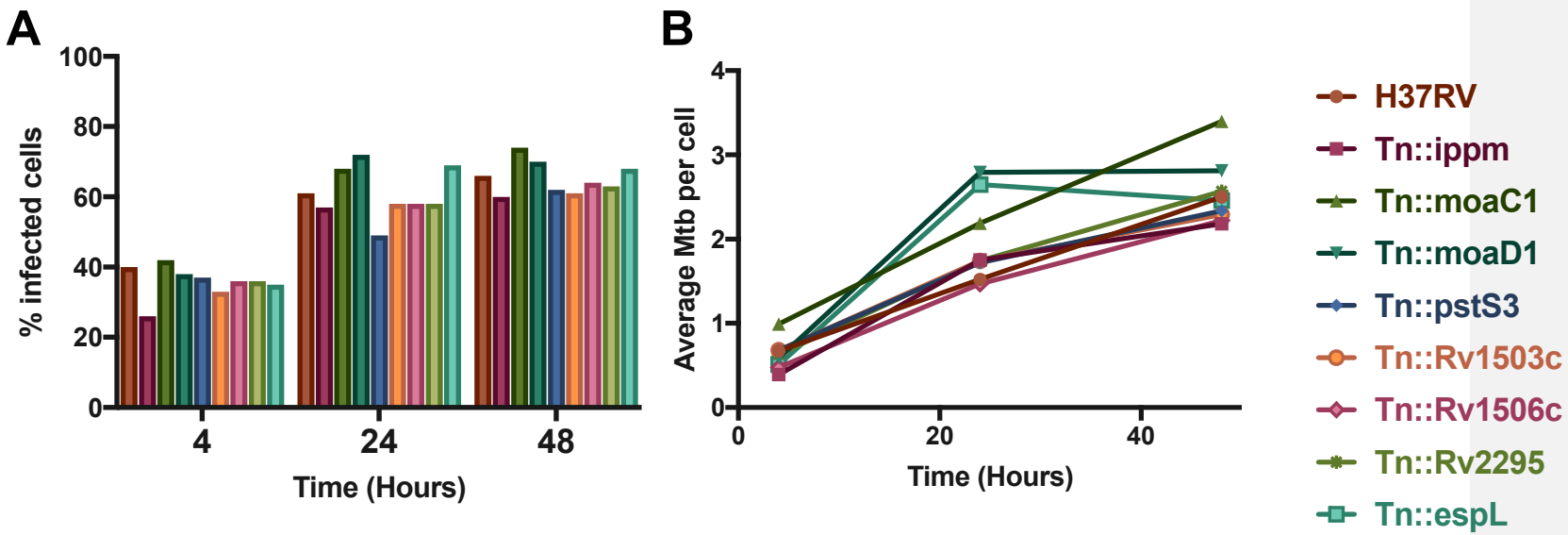

Figure 7.4 Graphical results of the coverslip assays: A- Infection rate assay, percentage of cells infected with H37Rv and the mutant strains at 4, 24 and 48 hours post-infection. B- assay of intracellular bacteria, the average number of bacteria per infected U937 cell at 4, 24 and 48 hours post-infection. The U937 cells were infected at a MOI of 20:1 and were washed at 24 hours.

7.4.2 Survival and intracellular growth of mutant strains

The coverslip assays, while useful, are limited to total counts of bacteria, whether they are viable or not. Hence, a further study was performed to assess the survival of the mutant strains after phagocytosis by the U937 cells. The U937 cells were infected as previously described, and at three different time points (4, 24 and 48 hours) the bacteria contained within the cells were plated in serial dilutions on 7H11 agar. After four weeks, the plates were counted and results are displayed in Figure 7.5.

Phagocytosis of the bacteria continued for 24 hours, after 24 hours the non-phagocytosed bacteria were washed off. Thus, the increase in CFU in the first 24 hours is not purely intracellular growth, but rather new bacteria being taken up by the cells. Between the 24th and 48th hour of infection, the number of H37Rv continued to increase as the bacteria grew within the cell, with a large increase of CFU, again re-phagocytosis of the released bacteria from the lysed infected U937 cells contributed to this increase. However, the mutant strains behaved differently, as would be expected: very little growth was observed after 24 hours. In fact, some strains (Tn::Rv2295, Tn::Rv1506c and Tn::ippM) saw a reduction of CFU, implying that the bacteria were being killed. The greatest decrease was seen in the *ippM* KO strain where there was a log decrease in CFU. The other five strains (Tn::moaC1, Tn::moaD1, Tn::pstS3, Tn::Rv1503c and Tn::espL) exhibited a small increase in CFU (less than half a log) compared with H37Rv. This could be due to growth within the cells, alternatively it could be continued phagocytosis of bacteria that has been released from other cells, or bacteria that remained after washing.

This data, in general, indicates either less growth, no growth or killing of Tn mutants. This was anticipated as the Tn mutants were selected as strains that are trafficked to the phagolysosome (as this was the basis of the initial Tn library screen by Brodin et al (2010)), and thus, expected to show lower survival rates compared to wildtype parental strains. This therefore confirms, using alternative methodologies (to the initial Tn screen), that these mutants are defective in their interactions with the host cell. Mechanisms underlying this are investigated further in subsequent sections of this chapter.

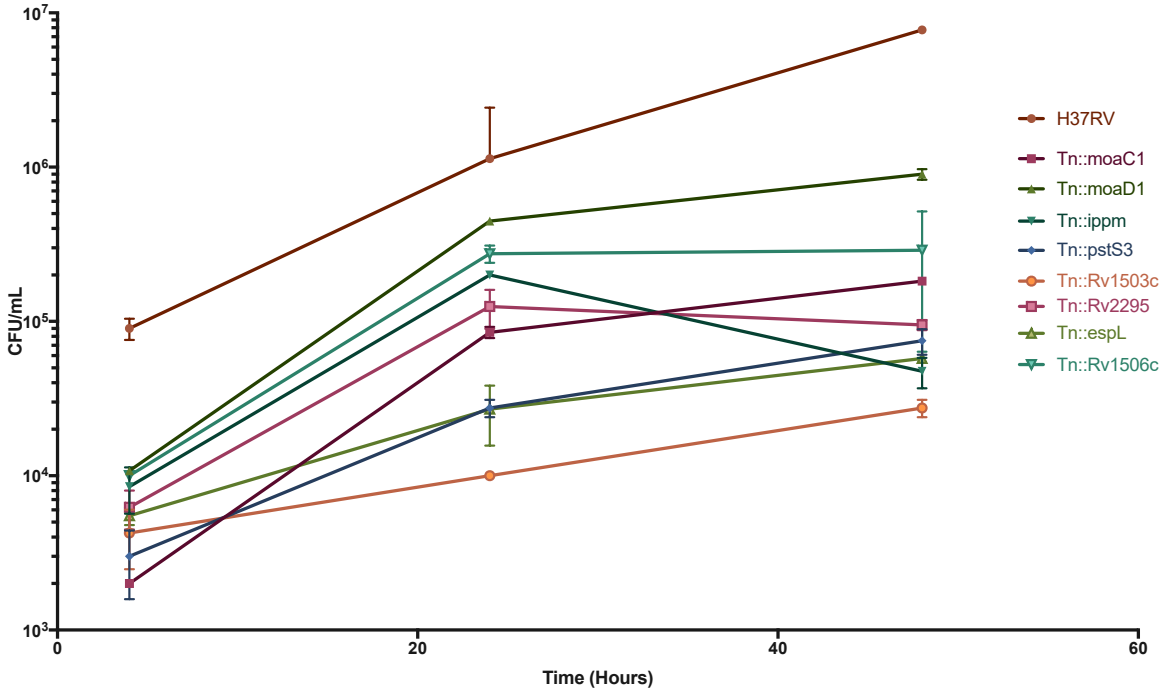

Figure 7.5 Graph of the growth of the mutant strains and H37Rv throughout a 20:1 infection in U937 macrophage like cell line, for the maximum time of 24 hours. Each time point was performed in triplicate and plated in duplicate. Errors bars represent standard deviation from the mean.

7.5 Host gene expression changes in response to infection with transposon mutants

In previous chapters, it was hypothesised that the downregulation of *RIN2, RILP and OSBPL1a* in the host cell after infection with *M.tb*, may have an important role in the arrest of phagosome maturation and survival of the bacteria within the cell. If this is the case, it could be predicted that the mutants which are trafficked to the phago-lysosome would be unable to impede the cellular processes of phagosome trafficking, for which the expression of *RILP, RIN2* and *OSPBL1a* have been identified as possible surrogate markers. To test this hypothesis, infections (MOI 20:1) were set up with each of the eight mutants and host RNA was extracted at 4, 24 and 48 hours. qRT-PCR was performed to identify if the mutants were still able to suppress the expression of *RILP, RIN2* and *OSBPL1a.* For each mutant, the expression of *RILP, RIN2* and *OSBPL1a* at 24 and 48 hours was compared to the expression at 4 hours and plotted as fold change in Figure 7.6. For statistical analysis, individual unpaired t tests were performed.

In Figure 7.6 the cells infected with H37Rv displayed the suppression of RILP, RIN2 and OSBPL1a that was previously described in Chapter 3. Figure 7.6C and 7. 6D show the expression of RIN2 in U937s infected with each of the mutant strains plus H37Rv, at 24 hours and 48 hours, respectively; at both time points the expression of RIN2 is downregulated. At 24 hours, the least amount of suppression is found with infection from strain Tn::Rv2295, but at 48 hours the downregulation is comparable with the other strains. Six out of the eight strains (Tn::Rv1503c, Tn::Rv1506c, Tn::Rv2295, Tn::Rv3880, Tn::pstS3, and Tn::ippM) caused a greater downregulation of host RIN2 at 48 hours than at 24 hours. However, infection with strains Tn::moaC1 and Tn::moaD1 showed a greater suppression at 24 hours than 48 hours.

Host transcriptional expression responses to infection with the Tn mutants for *RILP* and *OSPBL1a* was similar to that of *RIN2* with the exception of mutants Tn::moaC1 and Tn::moaD1. Cells infected with Tn::moaC1 did not display the same downregulation of RILP and OSBPL1a, in fact there is significant upregulation.

A greater than two-fold increase is seen in both host *RILP* and *OSBPL1a* 48 hours after infection with the mutant (Figure 7.6B and 7.6F) P-values 0.0287 and 0.001 respectively, with a smaller increase seen at 24 hours (Figure 7.6A and 7.6E) P-Values 0.0306 and 0.0207 respectively. This significant induction of both *RILP* and *OSBPL1a* expression has

not been seen in any other infections performed. Cells infected with the mutant strain Tn::moaD1 displayed an upregulation of *OSBPL1a* at 48 hours similar to the upregulation seen in response to Tn::moaC1 (P-value 0.0062), but suppression of *RIN2* and *RILP* was seen as with the wildtype strain. This suggests that the hypothesis that if the genes knocked-out are involved in the inhibition of phagolysosome fusion pathways, these mutants will be unable to suppress the host genes *RILP, RIN2* and *OSBPL1a*, appears to be true for *MoaC1* and possibly *MoaD1* to a lesser extent, in their inability to suppress *RILP* and *OSBPL1a*.

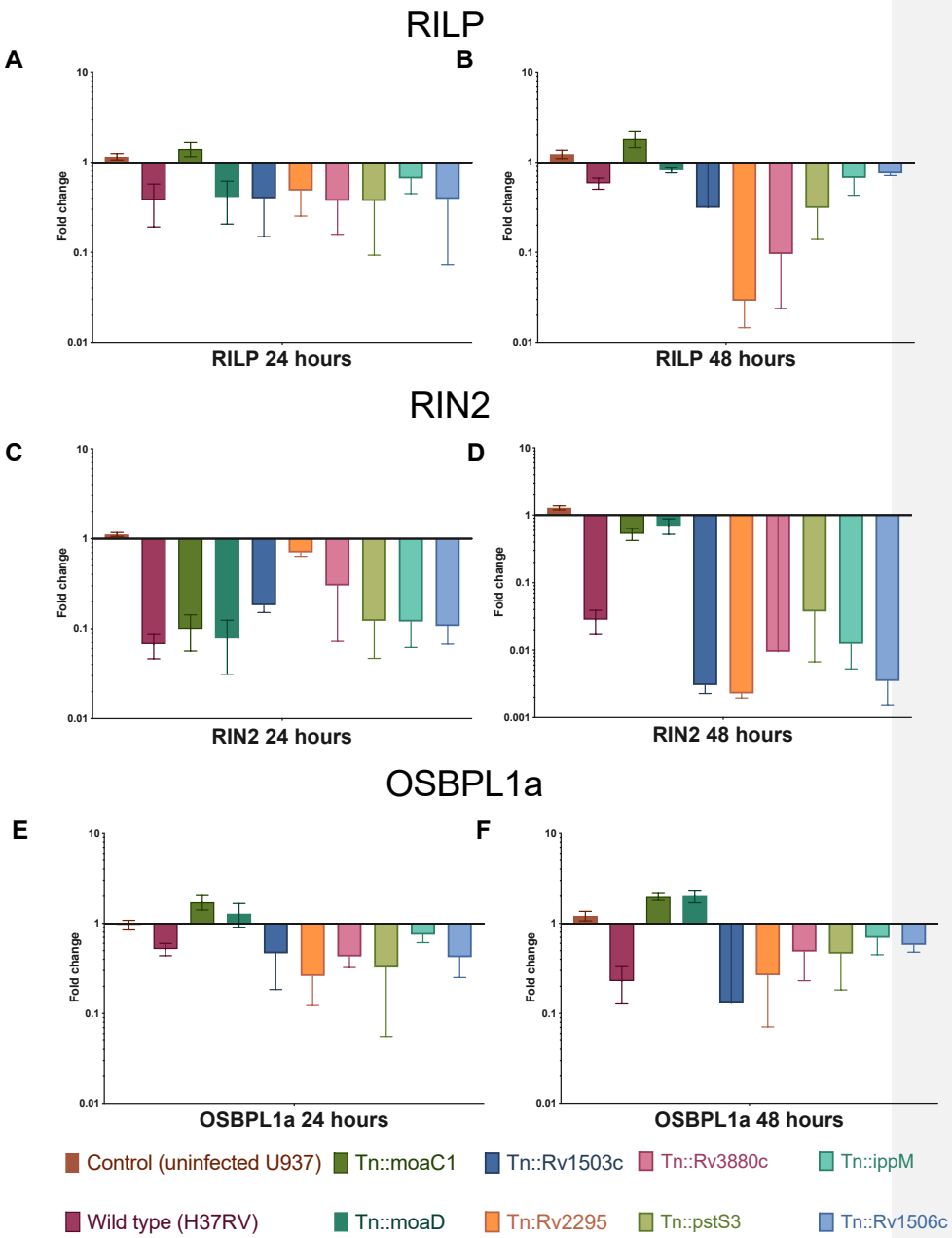

Figure 7.6 - Fold change of gene expression from qRT-PCR runs using primers for RILP (A & B), RIN2 (C & D), and OSBPL1a (E & F). RNA was extracted at 4, 24 and 48 hours from M. tuberculosis naive U937 cell (negative control), H37Rv infected U937s (positive control) and Tn mutant infected U937s. Each assay was set up in triplicate, the qRT-PCR was performed in duplicate. Individual t tests were used to compare the expression with the expression in infection with the wild type.

7.6 Confocal microscopy of infection with Tn::MoaC1

From the qRT-PCR data in the previous section it is clear that the strain Tn::moaC1 was an outlier: it lacked the ability to supress the expression of both *RILP* and *OSBPL1α* in the host cell. This suggests a role for MoaC1 in phago-lysosome maturation and this can be directly studied by fluorescent confocal microscopy and tracking dye analysis as a confirmatory experimental approach at the direct cellular host-pathogen interaction level . All the mutants chosen had previously been described as being trafficked to the phago-lysosome in mouse bone marrow-derived macrophages (Brodin et al., 2010). To confirm that this translates into the cell line used for this study (U937s), analysis of the intracellular trafficking of strain Tn::moaC1 assays were performed.

An immunofluorescence assay was set up to look for co-localisation of the bacteria with Lamp1 (the late stage P-L marker) as predicted by Brodin et al (2010). Figure 7.7 shows representative images of the results of the fluorescence co-localisation studies. The slides were set up in triplicate and all three coverslips were examined for the assay, totalling over 100 cells; representative images were taken for illustration purposes. While the bacteria were in different stages of phagocytosis at the point of fixation, there was a clear majority of co-localisation with Lamp1 in the host cells. Figure 7.7 panel C illustrates co-localisation of Tn::moaC1 with Lamp1: this is evident from the yellow colour which is a result of the merging of the green fluorescence stained bacteria (image 7A) and the red fluorescence stained Lamp1 (image 7B). Figure 7D is the result for the co-localisation represented graphically in a scatterplot, the points of the scatterplot cluster around a straight line, thus confirming the visually apparent co-localisation. For further confirmation, a statistical quantification of the co-localisation was also performed, giving a Pearsons R value of 0.84 and a Manders tM1 value of 0.918. This confirmed the expected trafficking to the P-L as described in the literature and now confirmed in U937 cells in this thesis for Tn::moaC1.

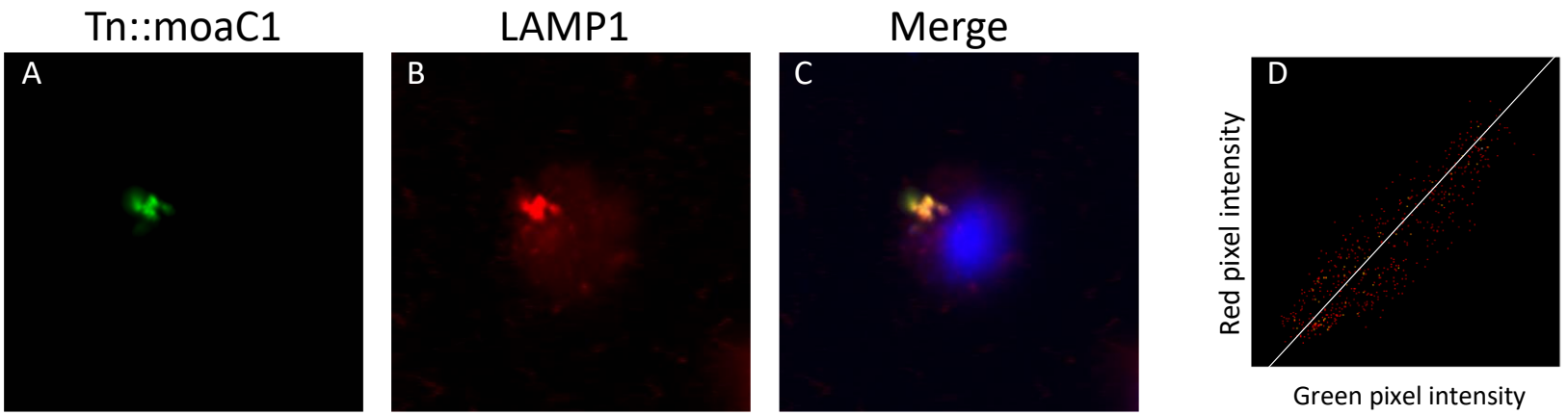

Figure 7.7 Confocal microscopy of U937 cells infected with mutant Tn::moaC1. Panel A, Tn::moaC1 stained with FITC. Panel B - stained lysosomal marker Lamp1. Panel C - merged images of the M.tb and endosomal marker. Panel D - co-localisation represented graphically in a scatterplot where the intensity of the red is plotted against the intensity of the green for each pixel

7.7 Expression analysis of moaC1: compensatory transcriptional responses

The above results have shown that Tn::moaC1 was unable to suppress the host genes as a result of the loss of a functional *moaC*1 gene. The mechanism underpinning the relationship between *moaC1* and the suppression of RILP and OSBPL1a can be tested by analysing *M.tb* expression of *moaC1* in response to the intracellular environment of the transfected cell lines constructed in Chapter 5, particularly the transfected cells over expressing RILP and OSBPL1a. It is hypothesised that if the *moaC1* has a direct relationship with the suppression of both *RILP* and *OSBPL1a*, then their over-expression will result in the increase in expression of *moaC1* in the *M.tb*.

To test this hypothesis, the two cell lines over-expressing RILP and OSBPL1a, respectively, were infected with H37Rv; the RNA from the bacteria was extracted, and qRT-PCR was used to measure *moaC1* expression. This had not previously been measured in the U937 experimental model. A number of published studies have shown the gene set moaA1-D1 to be strongly induced under hypoxia (Levillain et al., 2017) and they are required for nitrate assimilation (Williams et al., 2011). RNA polymerase sigma factor (*sigA*) was again used as a reference gene to standardise the qRT-PCR to correct for variation in the total amount of mRNA in the sample. The gene expression was compared to that of *M.tb* which had been processed through U937 transfected with the empty vector, pBF0 (Figure 7.8).

In both the cell line over-expressing RILP (U937-pBF1) and the cell line over-expressing OSBPL1a (U937-pBF3), a significant increase in *moaC1* expression was seen compared to control, P-values 0.0390 and 0.0214 respectively.

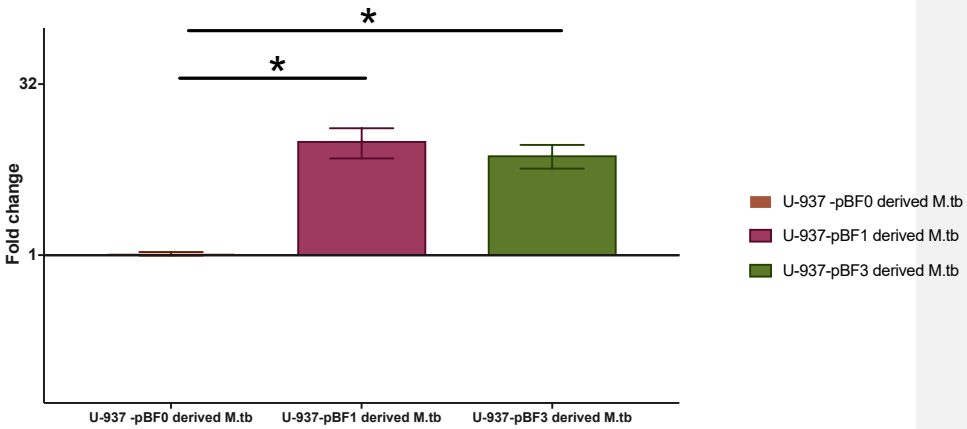

Figure 7.8 _Fold change of expression of moaC1 in response to the over-expression of RILP and OSBPL1a in U937 cells. The experiment was set up in biological duplicates with three technical replicates U937pBF0 derived M.tb = empty vector control, U937pBF1 derived M.tb = over-expressing RILP, U937pBF3 derived M.tb =over-expressing

7.8 Conclusion

In summary, this chapter investigated which *M.tb* mutants (Table 7.1) were trafficked to the phago-lysosome. The ability of the mutants to infect macrophages, their intracellular survival rate, and the host's response to them, were analysed. Intracellular counts revealed that the mutants were able to infect the macrophages similarly to the strain H37Rv (Figure 7.3 & 7.4). However, viable counts demonstrated that the mutant's growth was attenuated inside the macrophage as would be expected for defective vesicle trafficking mutants (Figure 7.5). The suppression of *RILP* and *OSBPL1a* in the host was not seen after infection with the Tn::*moaC1* (Figure 7.6) suggesting a role for *moaC1* in this process. Confocal microscopy confirmed that the mutant Tn::*moaC1* was trafficked to the phago-lysosome (Figure 7.7). Finally, qRT-PCR revealed an increase in expression of *moaC1* in response to the over-expression of *RLIP* and *OSBPL1a* in U937s (Figure 7.8).

7.10 Discussion

The aim of this chapter was to establish if host *RILP*, *RIN2*, and *OSBPL1a* are differentially expressed in infections with *M.tb* mutants which are known to be trafficked to the lysosome (Brodin 2010). This was to enable further elucidation of the involvement of the suppression of these host genes in survival of the bacteria. Preliminary experiments showed that in infections with the parent strain (GC1237), used to construct the transposon library,

suppression of *RILP, RIN2* and *OSBPL1a* in the host was seen, thus any differences seen in expression were due to the gene disrupted in the mutant rather than the differences in the parent strain compared to H37Rv. The Tn-mutants strains were similarly able to infect the U937s, however viability of the Tn-mutants within the cells was impaired. This impaired growth within macrophages corroborates the observation of Brodin et, al. (2010), that the mutants were trafficked to lysosomes.

The suppression of *RILP*, *RIN2* and *OSBPL1a* was still seen in response to the majority of the mutants. However, in both Tn::*moaC1* and Tn::*moaD1*, the expression of *OSBPL1a* and *RILP* was not suppressed and the expression of *OSBPL1a* was not suppressed, respectively. Analyses showed that bacteria enter the macrophages (Figure 7.3) and were trafficked to the phagolysosome (as shown by confocal microscopy and colocation analysis (Figure 7.7), confirming that the effect was not due to the inability of the bacteria to enter the cells. The genes *maoC1* and *moaD1* are part of the same genomic island (Cole et al., 1998) which was acquired by horizontal gene transfer and has been implicated in *M.tb* evolution towards pathogenicity (Levillain et al., 2017). *moaC1* and *moaD1* are predicted to encode enzymes involved in molybdenum cofactor biosynthesis which are required for nitrate respiration, thus allowing the bacteria to survive within hypoxic environments such as TB granulomas (Magalon and Mendel, 2015). Or indeed during intra-macrophage metabolism, where a switch to anaerobic electron transfer is indicated from differential gene expression responses (Williams et al., 2011) whereby nitrates act as the terminal electron acceptors.

Further work focused on MoaC1 as it is secreted from the bacteria, meaning it is more likely to be implicated in the observed suppression of host gene expression responses (Målen et al., 2007). The hypothesis is that since MoaC1 is able to bind GTP and since Rab7 is a GTPase, the presence of moaC1 likely blocks recruitment of the Rab7-RILP-OSBPL1a complex to the phagosome, in turn preventing the assembly of the microtubule motors, required for phago-lysosome fusion.

A number of studies have shown that MoaC1 expression is induced in the host infection (Roxas and Li, 2009; Schnappinger et al., 2003a; Yimer et al., 2017), supporting the hypothesis that it plays a role in virulence. Interestingly, *moaC1* expression was even further increased in response to the over-expression of both RILP and OSBPL1a in the host cells. However, it was previously shown in Chapter 6 (Figure 6.6) that *M.tb* genes upregulated in

the phagosome environment (*hspX, mpt83, icl1, hrp1 and echA19*) were even further induced when exposed to the over-expression of *RILP, RIN2 and OSBPL1a*. This suggests that the over-expression of these proteins causes the environment to be more hostile, as discussed in Chapter 6.6. Thus, the increase in expression of *moaC1* may not be directly related to the presence of RILP and OSBPL1a, but rather a response to the environment that their over-expression creates in the cell.

Further work is required to gain a better understanding of the precise mechanisms by which MoaC1 plays in bacterial survival in the host macrophage. To test the hypothesis that MoaC1 disrupts the formation of the microtubule motors by suppression of the RAB7-RILP-OSBPL1a complex, analyses of the protein-protein interactions could be employed. Co-immunoprecipitation or pull-down assays coupled with SDS-PAGE and Western blot analysis could identify where MoaC1 acts within the host. If no strong interactions are found, a label transfer protein interaction analysis could be performed, as this would identify proteins that interact, even transiently, with MoaC1 in the host. If MoaC1 does indeed play a role in the arrest of phagosome-lysosome fusion, then identifying the interaction of *MoaC1* within the host could potentially lead to a better understanding of the survival of the bacteria inside the host.

Chapter 8 – Concluding remarks and future work

The aim of this research was to explore the hypothesis that *M.tb* actively suppresses the expression of host genes that encode functional components involved in phagolysosome biogenesis and trafficking within macrophages as a consequence of infection. To answer this question the study began with the identification of genes of interest: these were first selected from the most down-regulated host genes following infection of macrophages, taken from the study by Tailleux et al., (2008) that used microarray transcriptional profiling. This list was narrowed by selection on the basis of function and then by recapitulation and reproducibility of the expression patterns in cell lines used in this thesis (Chapter 3). Three genes important in vesicular transport were found to be significantly down-regulated in *M.tb* infection, namely: *RIN2, RILP*, and *OSBPL1a.* The current understanding of the function of these gene products is displayed in Figure 8.1. To confirm suppression of these genes in cell infection models, qRT-PCR was used to measure host mRNA levels during infection with *M.tb* of the macrophage cell line U937. These studies showed and confirmed the suppression of the three genes. This reduction in expression occurred 24 hours post-infection (data presented in Chapter4). Many published studies focus on the involvement of Rab GTPases in the arrest of maturation of the lysosome (Mottola, 2014; Prashar et al., 2017; Sun et al., 2007) with little or no mention of the proteins that they interact with, nor their suppression during infection. The studies in this thesis therefore adds to this knowledge.

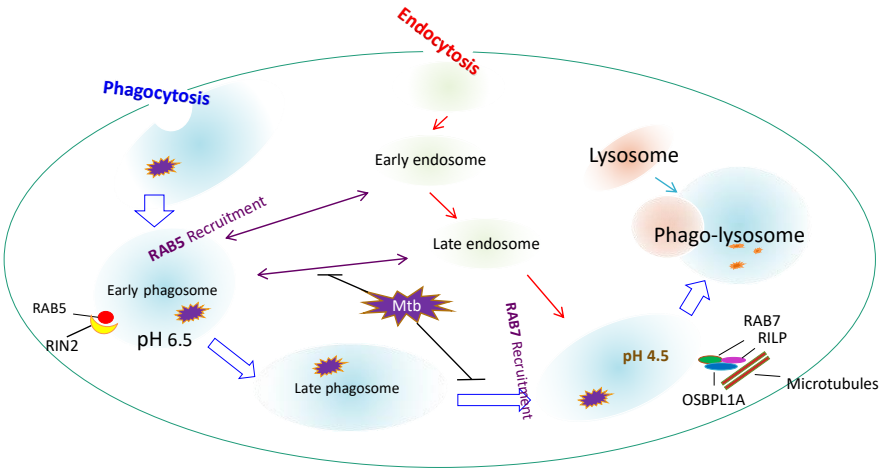

Figure 8.1 A simplified diagram of phagocytosis in a macrophage. The diagram shows that RIN2 associates with the early endosome-RAB5 complex. RILP and OSBPl1a associates with the late endosome-Rab7 containing complex that also involves interactions with cellular microtubules. It can be hypothesised from the data in the thesis that the M.tb-infection related down regulation of these host genes at the different stages of phagosome-lysosome maturation is part of the mechanism by which M.tb prevents P-L maturation and manipulation of the cell's vesicular trafficking homeostasis, thereby allowing for M.tb survival

Once the genes were selected and shown to be expressed correctly in *M.tb* infected experimental cell lines, cell lines over-expressing these 3 down-regulated genes were constructed using expression vectors transfected into U937 cells. These transfected cell lines were then shown to over-express the proteins of interest, OSBPL1a, RILP and RIN2 (data in Chapter 5) as demonstrated using both Western blotting and increased RNA expression. These cell lines were used for co-location studies using confocal microscopy and gene expression analysis of the macrophage derived *M.tb* to look for altered expression in response to the over-expressed proteins (Chapter 6). The co-location studies exhibited only differential trafficking for RIN2 in over-expression cells; the other transfected cell lines trafficked the bacteria similarly to that seen in control non-transfected U937s. The production of a cell line overexpressing both RILP and OSBPL1a was attempted multiple times but was eventually unsuccessful. As RILP and OSBPL1a are currently thought to function in a complex, it would have been necessary for both proteins to be expressed in co-transfected cell lines for any function to be investigated. Had this co- overexpression been

successfully achieved, conclusions as to a functional interference by *M.tb* infection could have been observed. Clearly this would be a necessary next step for further study. As both *RILP* and *OSBPL1a* are suppressed during *M.tb* infection, adding just one back by transfection may not have more enough to see the change in *M.tb* trafficking. With further work involving a different transfection reagent or cell line it may be possible to produce a cell line over expressing both RILP and OSBPL1a, allowing for this hypothesis to be tested. It is possible that a vector containing both genes could also be constructed giving a better chance of successful over-expression of both. For the co-localisation studies, a control of either BCG or zymogen beads should have been included to show the full maturation and acquisition of Lamp1 or Rab7, to show the vacuole trafficking pathways were functional in the cell lines used. Nevertheless, this appropriately functioning vacuole trafficking was indirectly indicated with the acquisition of Lamp1 in the infection using the mutant Tn::*moaC1* known to be trafficked to the phago-lysosome. As such, this finding acted as a control indicating correct functional trafficking.

Subsequent experiments then used *M.tb* gene expression as a marker for location within the P-L vacuole continuum post-infection. Gene expression in *M.tb* in response to the over-expression of *RILP, RIN2 and OSBPL1a*, was interrogated. Five genes with different functions, previously reported in the literature (Schnappinger et al., 2003b) and known to be up-regulated in the phagosome environment were selected (*hspX, echA19, hrp1, icl1* and *mpt83*) and qRT-PCR was performed. The qRT-PCR revealed that genes *hspX, echA19, hrp1* and *icl1* are all induced during infection of cells over-expressing *RILP, RIN2 and OSBPL1a.* Whereas mpt83 expression was suppressed in response to the over-expression of host *RIN2*; this change in expression supports the finding of co-localisation studies of altered trafficking. As little is known about MPT83 function this is an area that requires further research to understand the implication of its suppression.

As a final approach, eight *M.tb* mutants (Chapter 7, table 1) known to be trafficked to the lysosome were identified from the literature and sourced from the authors, with permission. U937 macrophage Infections were performed with these mutants and complemented mutants and wild type *M.tb* as controls. Host mRNA levels for *RILP, RIN2* and *OSBPL1a* were measured to look for the reversal of the ability of a gene knock out to suppress the host expression, thereby confirming a potential role in P-L trafficking inhibition of that *M.tb* gene as is seen with wildtype *M.tb*. One Tn mutant, with the *moaC1*

gene disrupted, was unable to suppress the expression of *RILP and OSBPL1a*. Confocal microscopy confirmed that this mutant *moaC1* was trafficked to the phago-lysosome and qRT-PCR revealed an increase in expression of *moaC1* in response to the over-expression of RLIP and OSBPL1a in U937s. Thus, these three lines of evidence suggest a role for MoaC1 in the process in the inhibition of P-L maturation leading to *M.tb* survival. Further studies would more clearly define the specific mechanisms for MoaC1 in bacterial survival and its site of action.

While the focus of this study was that the active suppression of *RIN2, RILP* and *OSBPL1a* by *M.tb* was advantageous due to the altered trafficking, recent work suggests that the suppression of *RILP* and *OSBPl1a* may have a dual purpose. Zhao and Ridgway, (2017) have implicated OSBPL1a involvement in the delivery of cholesterol from late endosomes to the endoplasmic reticulum (ER), to allow export from the cell, and in OSBPL1a knock-out cells they saw an accumulation of cholesterol enriched vesicles (Figure 8.2). This suggests that the suppression of OSBPL1a or both RILP and OSBPL1a in *M.tb* infection would also result in the accumulation of cholesterol.

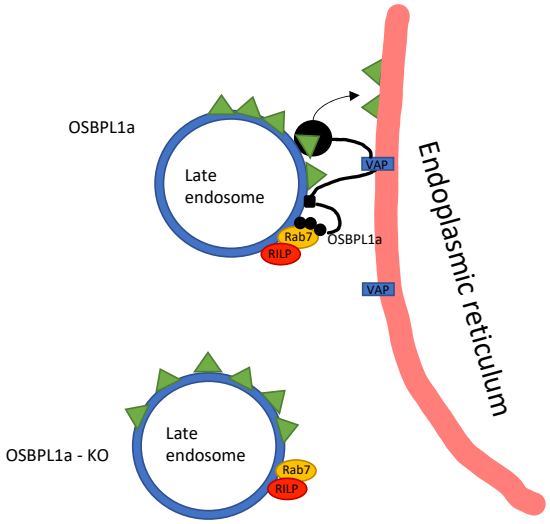

Figure 8.2 Graphical representation of OSBPL1a and RILP involvement in cholesterol export based on figure in Zhao and Ridgway, 2017. OSBPL1a in tethered to vesicle-associated membrane protein-associated protein (VAP) to assist the transfer of cholesterol to the endoplasmic reticulum.

While *M.tb*'s ability to accumulate cholesterol has been documented previously by a number of studies (Brzostek et al., 2009; Miner et al., 2009; Wipperman et al., 2014) the link between the suppression of OSBPL1a has not previously been made. This may be due to the well documented lack of acquisition of RAB7 during *M.tb* containing vacuole trafficking indicating retention within early endosomes as being the favoured area of study. The proteins that interact with RAB7, such as RILP and OSBPL1a, have been largely ignored. Such an accumulation of cholesterol is hugely advantageous for the bacteria, as it has been found to be essential for optimal growth and persistence in many studies (Garton et al., 2008; Nesbitt et al., 2010; Van der Geize et al., 2007; VanderVen et al., 2015). Also *M.tb* has been shown to upregulate the cholesterol catabolism gene locus, encoding the entire metabolic pathway for cholesterol utilisation, during macrophage infection models and recovered from infected human sputum (Tailleux et al., 2008)

A review by Wilburn et. al. in 2018, describes the current understanding of cholesterol usage of *M.tb*. The breakdown of cholesterol yields a number of products: acetyl-CoA, propionyl-CoA, succinyl-CoA and pyruvate, which are used as carbon precursors for intermediary metabolism pathways. One example of these contributing to virulence would be propionyl-CoA, which is involved in the synthesis of phthiocerol-dimycocerosate (PDIM), found on the outer cell wall of the *M.tb* and plays a role in pathogenesis (Cambier et al., 2014). PDIMs are also highly upregulated by *M.tb* inside macrophages (Tailleux et al., 2008). PDIM is involved in virulence in multiple ways including: the invasion of macrophages, resistance to immune-mediated stress and masking of cell wall antigens (Rens et al., 2021; Wilburn et al., 2018).

This newly described aspect of the suppression of *OSBPL1a* and *RILP* as defined and functionally explored in this thesis adds another dimension to the original hypothesis that *M.tb* actively suppresses the expression of genes involved in phagolysosome biogenesis and vacuolar trafficking to prevent phagolysosomal fusion, with the suppression also causing the accumulation of a carbon substrate required for intracellular survival and growth. This is also supported by the "fat and lazy" persistent bacteria phenotype (Garton et al., 2008; Maurya et al., 2019), in which all the genes for cholesterol import, degradation and regulation are upregulated, and moreover, may go some way towards explaining the foamy phenotype of *M.tb* infected macrophages which as yet remains unknown (Genoula et al.,

2018). This area requires much further study and highlights again the importance of considering not just up regulated genes but also down-regulated genes, as seen in this study.

References

Aderem, A., Underhill, D.M., 1999. Mechanisms of Phagocytosis in Macrophages. Annu. Rev. Immunol. 17, 593–623. https://doi.org/10.1146/annurev.immunol.17.1.593

Aguilar-Ayala, D.A., Tilleman, L., Van Nieuwerburgh, F., Deforce, D., Palomino, J.C., Vandamme, P., Gonzalez-Y-Merchand, J.A., Martin, A., 2017. The transcriptome of Mycobacterium tuberculosis in a lipid-rich dormancy model through RNAseq analysis. Sci. Rep. 7, 17665. https://doi.org/10.1038/s41598-017-17751-x

Allison, R., Edgar, J.R., Pearson, G., Rizo, T., Newton, T., Günther, S., Berner, F., Hague, J., Connell, J.W., Winkler, J., Lippincott-Schwartz, J., Beetz, C., Winner, B., Reid, E., 2017. Defects in ER–endosome contacts impact lysosome function in hereditary spastic paraplegia. J. Cell Biol. 216, 1337–1355. https://doi.org/10.1083/jcb.201609033

Amer, A.O., Swanson, M.S., 2002. A phagosome of one's own: a microbial guide to life in the macrophage. Curr. Opin. Microbiol. 5, 56–61. https://doi.org/10.1016/S1369-5274(02)00286-2

Andreu, N., Phelan, J., de Sessions, P.F., Cliff, J.M., Clark, T.G., Hibberd, M.L., 2017. Primary macrophages and J774 cells respond differently to infection with Mycobacterium tuberculosis. Sci. Rep. 7, 42225. https://doi.org/10.1038/srep42225

Apt, A., Kramnik, I., 2009. Man and mouse TB: contradictions and solutions. Tuberc. Edinb. Scotl. 89, 195–198. https://doi.org/10.1016/j.tube.2009.02.002

Armstrong, J.A., Hart, P.D., 1971. RESPONSE OF CULTURED MACROPHAGES TO MYCOBACTERIUM TUBERCULOSIS, WITH OBSERVATIONS ON FUSION OF LYSOSOMES WITH PHAGOSOMES. J. Exp. Med. 134, 713–740. https://doi.org/10.1084/jem.134.3.713

Ates, L.S., Ummels, R., Commandeur, S., Weerd, R. van der, Sparrius, M., Weerdenburg, E., Alber, M., Kalscheuer, R., Piersma, S.R., Abdallah, A.M., Ghany, M.A.E., Abdel-Haleem, A.M., Pain, A., Jiménez, C.R., Bitter, W., Houben, E.N.G., 2015. Essential Role of the ESX-5 Secretion System in Outer Membrane Permeability of Pathogenic Mycobacteria. PLOS Genet. 11, e1005190. https://doi.org/10.1371/journal.pgen.1005190

Balaji, K., French, C.T., Miller, J.F., Colicelli, J., 2014. The RAB5-GEF Function of RIN1 Regulates Multiple Steps During Listeria monocytogenes Infection. Traffic 15, 1206–1218. https://doi.org/10.1111/tra.12204

Barthe, P., Veyron-Churlet, R., de Visch, A., Gilleron, M., Saliou, J.-M., Tomavo, S., Nigou, J., Brodin, P., Cohen-Gonsaud, M., 2016. Mycobacterium tuberculosis LppM Displays an Original Structure and Domain Composition Linked to a Dual Localization. Struct. Lond. Engl. 1993 24, 1788–1794. https://doi.org/10.1016/j.str.2016.07.009

Beisiegel, M., Mollenkopf, H.-J., Hahnke, K., Koch, M., Dietrich, I., Reece, S.T., Kaufmann, S.H.E., 2009. Combination of host susceptibility and Mycobacterium tuberculosis virulence define gene expression profile in the host. Eur. J. Immunol. 39, 3369–3384. https://doi.org/10.1002/eji.200939615

Blondel, C.J., Jiménez, J.C., Leiva, L.E., Álvarez, S.A., Pinto, B.I., Contreras, F., Pezoa, D., Santiviago, C.A., Contreras, I., 2013. The Type VI Secretion System Encoded in Salmonella Pathogenicity Island 19 Is Required for Salmonella enterica Serotype Gallinarum Survival within Infected Macrophages. Infect. Immun. 81, 1207–1220. https://doi.org/10.1128/IAI.01165-12

Bogdan, C., Röllinghoff, M., Diefenbach, A., 2000. Reactive oxygen and reactive nitrogen intermediates in innate and specific immunity. Curr. Opin. Immunol. 12, 64–76. https://doi.org/10.1016/S0952-7915(99)00052-7

Both, U. von, Berk, M., Agapow, P.-M., Wright, J.D., Git, A., Hamilton, M.S., Goldgof, G., Siddiqui, N., Bellos, E., Wright, V.J., Coin, L.J., Newton, S.M., Levin, M., 2018. Mycobacterium tuberculosis Exploits a Molecular Off Switch of the Immune System for Intracellular Survival. Sci. Rep. 8, 661. https://doi.org/10.1038/s41598-017-18528-y

Brennan, P.J., 2003. Structure, function, and biogenesis of the cell wall of Mycobacterium tuberculosis. Tuberculosis 83, 91–97. https://doi.org/10.1016/S1472-9792(02)00089-6

Brignull, L.M., Czimmerer, Z., Saidi, H., Daniel, B., Villela, I., Bartlett, N.W., Johnston, S.L., Meira, L.B., Nagy, L., Nohturfft, A., 2013. Reprogramming of lysosomal gene expression by interleukin-4 and Stat6. BMC Genomics 14, 853. https://doi.org/10.1186/1471-2164-14-853

Brodin, P., Majlessi, L., Marsollier, L., de Jonge, M.I., Bottai, D., Demangel, C., Hinds, J., Neyrolles, O., Butcher, P.D., Leclerc, C., Cole, S.T., Brosch, R., 2006. Dissection of ESAT-6 System 1 of Mycobacterium tuberculosis and Impact on Immunogenicity and Virulence. Infect. Immun. 74, 88–98. https://doi.org/10.1128/IAI.74.1.88-98.2006

Brodin, P., Poquet, Y., Levillain, F., Peguillet, I., Larrouy-Maumus, G., Gilleron, M., Ewann, F., Christophe, T., Fenistein, D., Jang, J., Jang, M.-S., Park, S.-J., Rauzier, J., Carralot, J.-P., Shrimpton, R., Genovesio, A., Gonzalo-Asensio, J.A., Puzo, G., Martin, C., Brosch, R., Stewart, G.R., Gicquel, B., Neyrolles, O., 2010. High Content Phenotypic Cell-Based Visual Screen Identifies Mycobacterium tuberculosis Acyltrehalose-Containing Glycolipids Involved in Phagosome Remodeling. PLoS Pathog 6, e1001100. https://doi.org/10.1371/journal.ppat.1001100

Brozzi, A., Urbanelli, L., Luc Germain, P., Magini, A., Emiliani, C., 2013. hLGDB: a database of human lysosomal genes and their regulation. Database J. Biol. Databases Curation 2013. https://doi.org/10.1093/database/bat024

Brzostek, A., Pawelczyk, J., Rumijowska-Galewicz, A., Dziadek, B., Dziadek, J., 2009. Mycobacterium tuberculosis Is Able To Accumulate and Utilize Cholesterol. J. Bacteriol. 191, 6584–6591. https://doi.org/10.1128/JB.00488-09

Bucci, C., Parton, R.G., Mather, I.H., Stunnenberg, H., Simons, K., Hoflack, B., Zerial, M., 1992. The small GTPase rab5 functions as a regulatory factor in the early endocytic pathway. Cell 70, 715–728. https://doi.org/10.1016/0092-8674(92)90306-W

Bunduc, C.M., Bitter, W., Houben, E.N.G., 2020. Structure and Function of the Mycobacterial Type VII Secretion Systems. Annu. Rev. Microbiol. 74, 315–335. https://doi.org/10.1146/annurev-micro-012420-081657

Butler, R.E., Krishnan, N., Garcia-Jimenez, W., Francis, R., Martyn, A., Mendum, T., Felemban, S., Locker, N., Salguero, F.J., Robertson, B., Stewart, G.R., 2017. Susceptibility of Mycobacterium tuberculosis-infected host cells to phospho-MLKL driven necroptosis is dependent on cell type and presence of TNFα. Virulence 8, 1820–1832. https://doi.org/10.1080/21505594.2017.1377881

Büttner, D., 2012. Protein export according to schedule: architecture, assembly, and regulation of type III secretion systems from plant- and animal-pathogenic bacteria. Microbiol. Mol. Biol. Rev. MMBR 76, 262–310. https://doi.org/10.1128/MMBR.05017-11

Cai, Y., Dai, Y., Wang, Y., Yang, Q., Guo, J., Wei, C., Chen, W., Huang, H., Zhu, J., Zhang, C., Zheng, W., Wen, Z., Liu, H., Zhang, M., Xing, S., Jin, Q., Feng, C.G., Chen, X., 2020. Single-cell transcriptomics of blood reveals a natural killer cell subset depletion in tuberculosis. EBioMedicine 53, 102686. https://doi.org/10.1016/j.ebiom.2020.102686

Cambier, C.J., Takaki, K.K., Larson, R.P., Hernandez, R.E., Tobin, D.M., Urdahl, K.B., Cosma, C.L., Ramakrishnan, L., 2014. Mycobacteria manipulate macrophage recruitment through coordinated use of membrane lipids. Nature 505, 218–222. https://doi.org/10.1038/nature12799

Cappelli, G., Volpe, E., Grassi, M., Liseo, B., Colizzi, V., Mariani, F., 2006. Profiling of Mycobacterium tuberculosis gene expression during human macrophage infection: Upregulation of the alternative sigma factor G, a group of transcriptional regulators, and proteins with unknown function. Res. Microbiol. 157, 445–455. https://doi.org/10.1016/j.resmic.2005.10.007

Carbon, S., Ireland, A., Mungall, C.J., Shu, S., Marshall, B., Lewis, S., 2009. AmiGO: online access to ontology and annotation data. Bioinformatics 25, 288–289. https://doi.org/10.1093/bioinformatics/btn615

Carey, K.L., Newton, H.J., Lührmann, A., Roy, C.R., 2011. The Coxiella burnetii Dot/Icm System Delivers a Unique Repertoire of Type IV Effectors into Host Cells and Is Required for Intracellular Replication. PLOS Pathog. 7, e1002056. https://doi.org/10.1371/journal.ppat.1002056

Castro-Garza, J., García-Jacobo, P., Rivera-Morales, L.G., Quinn, F.D., Barber, J., Karls, R., Haas, D., Helms, S., Gupta, T., Blumberg, H., Tapia, J., Luna-Cruz, I., Rendon, A., Vargas-Villarreal, J., Vera-Cabrera, L., Rodríguez-Padilla, C., 2017. Detection of anti-HspX antibodies and HspX protein in patient sera for the identification of recent latent infection by Mycobacterium tuberculosis. PLOS ONE 12, e0181714. https://doi.org/10.1371/journal.pone.0181714

Chan, D.Y.L., Moralli, D., Khoja, S., Monaco, Z.L., 2017. Noncoding Centromeric RNA Expression Impairs Chromosome Stability in Human and Murine Stem Cells. Dis. Markers 2017. https://doi.org/10.1155/2017/7506976

Chandra, P., Ghanwat, S., Matta, S.K., Yadav, S.S., Mehta, M., Siddiqui, Z., Singh, A., Kumar, D., 2015. Mycobacterium tuberculosis Inhibits RAB7 Recruitment to Selectively Modulate Autophagy Flux in Macrophages. Sci. Rep. 5. https://doi.org/10.1038/srep16320

Chang, M.H.Y., Karageorgos, L.E., Meikle, P.J., 2002. CD107a (LAMP-1) and CD107b (LAMP-2). J. Biol. Regul. Homeost. Agents 16, 147–151.

Charlet, D., Mostowy, S., Alexander, D., Sit, L., Wiker, H.G., Behr, M.A., 2005. Reduced expression of antigenic proteins MPB70 and MPB83 in Mycobacterium bovis BCG strains due to a start codon mutation in sigK. Mol. Microbiol. 56, 1302–1313. https://doi.org/10.1111/j.1365-2958.2005.04618.x

Chomarat, P., Banchereau, J., Davoust, J., Palucka, A.K., 2000. IL-6 switches the differentiation of monocytes from dendritic cells to macrophages. Nat. Immunol. 1, 510–514. https://doi.org/10.1038/82763

Cianciola, N.L., Greene, D.J., Morton, R.E., Carlin, C.R., 2013. Adenovirus RIDα uncovers a novel pathway requiring ORP1L for lipid droplet formation independent of NPC1. Mol. Biol. Cell 24, 3309–3325. https://doi.org/10.1091/mbc.E12-10-0760

Clemens, D.L., Horwitz, M.A., 1995. Characterization of the Mycobacterium tuberculosis phagosome and evidence that phagosomal maturation is inhibited. J. Exp. Med. 181, 257–270. https://doi.org/10.1084/jem.181.1.257

Clemens, D.L., Lee, B.-Y., Horwitz, M.A., 2000. Deviant Expression of Rab5 on Phagosomes Containing the Intracellular Pathogens Mycobacterium tuberculosis andLegionella pneumophila Is Associated with Altered Phagosomal Fate. Infect. Immun. 68, 2671–2684. https://doi.org/10.1128/IAI.68.5.2671-2684.2000

Cole, S.T., Brosch, R., Parkhill, J., Garnier, T., Churcher, C., Harris, D., Gordon, S.V., Eiglmeier, K., Gas, S., Barry, C.E., Tekaia, F., Badcock, K., Basham, D., Brown, D., Chillingworth, T., Connor, R., Davies, R., Devlin, K., Feltwell, T., Gentles, S., Hamlin, N., Holroyd, S., Hornsby, T., Jagels, K., Krogh, A., McLean, J., Moule, S., Murphy, L., Oliver, K., Osborne, J., Quail, M.A., Rajandream, M.-A., Rogers, J., Rutter, S., Seeger, K., Skelton, J., Squares, R., Squares, S., Sulston, J.E., Taylor, K., Whitehead, S., Barrell, B.G., 1998. Deciphering the biology of Mycobacterium tuberculosis from the complete genome sequence. Nature 393, 537–544. https://doi.org/10.1038/31159

Costa, T.R.D., Felisberto-Rodrigues, C., Meir, A., Prevost, M.S., Redzej, A., Trokter, M., Waksman, G., 2015. Secretion systems in Gram-negative bacteria: structural and mechanistic insights. Nat. Rev. Microbiol. 13, 343–359. https://doi.org/10.1038/nrmicro3456

Daffé, M., Marrakchi, H., 2019. Unraveling the Structure of the Mycobacterial Envelope. Microbiol. Spectr. 7, 7.4.1. https://doi.org/10.1128/microbiolspec.GPP3-0027-2018

Danelishvili, L., Everman, J., Bermudez, L.E., 2016. Mycobacterium tuberculosis PPE68 and Rv2626c genes contribute to the host cell necrosis and bacterial escape from macrophages. Virulence 7, 23–32. https://doi.org/10.1080/21505594.2015.1102832

de Chastellier, C., 2009. The many niches and strategies used by pathogenic mycobacteria for survival within host macrophages. Immunobiology, Vesicular trafficking in immune cells 214, 526–542. https://doi.org/10.1016/j.imbio.2008.12.005

Deboosère, N., Iantomasi, R., Queval, C.J., Song, O., Deloison, G., Jouny, S., Debrie, A., Chamaillard, M., Nigou, J., Cohen-Gonsaud, M., Locht, C., Brodin, P., Veyron-Churlet, R., 2017. LppM impact on the colonization of macrophages by Mycobacterium tuberculosis. Cell. Microbiol. 19. https://doi.org/10.1111/cmi.12619

Denise, R., Abby, S.S., Rocha, E.P.C., 2020. The Evolution of Protein Secretion Systems by Co-option and Tinkering of Cellular Machineries. Trends Microbiol. 28, 372–386. https://doi.org/10.1016/j.tim.2020.01.005

Dubnau, E., Chan, J., Mohan, V.P., Smith, I., 2005. Responses of Mycobacterium tuberculosis to Growth in the Mouse Lung. Infect. Immun. 73, 3754–3757. https://doi.org/10.1128/IAI.73.6.3754-3757.2005

Dubnau, E., Fontán, P., Manganelli, R., Soares-Appel, S., Smith, I., 2002. Mycobacterium tuberculosis genes induced during infection of human macrophages. Infect. Immun. 70, 2787–2795.

Dutta, N.K., Mehra, S., Didier, P.J., Roy, C.J., Doyle, L.A., Alvarez, X., Ratterree, M., Be, N.A., Lamichhane, G., Jain, S.K., Lacey, M.R., Lackner, A.A., Kaushal, D., 2010. Genetic Requirements for the Survival of Tubercle Bacilli in Primates. J. Infect. Dis. 201, 1743–1752. https://doi.org/10.1086/652497

Epp, N., Rethmeier, R., Krämer, L., Ungermann, C., 2011. Membrane dynamics and fusion at late endosomes and vacuoles – Rab regulation, multisubunit tethering complexes and SNAREs. Eur. J. Cell Biol., SFB 431: Membrane proteins - Functional dynamics

and coupling to cellular networks 90, 779–785. https://doi.org/10.1016/j.ejcb.2011.04.007
Eskelinen, E.-L., 2006. Roles of LAMP-1 and LAMP-2 in lysosome biogenesis and autophagy. Mol. Aspects Med., Autophagy 27, 495–502. https://doi.org/10.1016/j.mam.2006.08.005
Feltcher, M.E., Sullivan, J.T., Braunstein, M., 2010. Protein export systems of Mycobacterium tuberculosis: novel targets for drug development? Future Microbiol. 5, 1581–1597. https://doi.org/10.2217/fmb.10.112
Ferrari, G., Langen, H., Naito, M., Pieters, J., 1999. A Coat Protein on Phagosomes Involved in the Intracellular Survival of Mycobacteria. Cell 97, 435–447. https://doi.org/10.1016/S0092-8674(00)80754-0
Flannagan, R.S., Cosío, G., Grinstein, S., 2009. Antimicrobial mechanisms of phagocytes and bacterial evasion strategies. Nat. Rev. Microbiol. 7, 355–366. https://doi.org/10.1038/nrmicro2128
Fontán, P., Aris, V., Ghanny, S., Soteropoulos, P., Smith, I., 2008. Global Transcriptional Profile of Mycobacterium tuberculosis during THP-1 Human Macrophage Infection. Infect. Immun. 76, 717–725. https://doi.org/10.1128/IAI.00974-07
Forrellad, M.A., Klepp, L.I., Gioffré, A., Sabio y García, J., Morbidoni, H.R., Santangelo, M. de la P., Cataldi, A.A., Bigi, F., 2013. Virulence factors of the Mycobacterium tuberculosis complex. Virulence 4, 3–66. https://doi.org/10.4161/viru.22329
Fratti, R.A., Backer, J.M., Gruenberg, J., Corvera, S., Deretic, V., 2001. Role of phosphatidylinositol 3-kinase and Rab5 effectors in phagosomal biogenesis and mycobacterial phagosome maturation arrest. J. Cell Biol. 154, 631–644. https://doi.org/10.1083/jcb.200106049
Fratti, R.A., Chua, J., Vergne, I., Deretic, V., 2003. Mycobacterium tuberculosis glycosylated phosphatidylinositol causes phagosome maturation arrest. Proc. Natl. Acad. Sci. U. S. A. 100, 5437–5442. https://doi.org/10.1073/pnas.0737613100
Garton, N.J., Waddell, S.J., Sherratt, A.L., Lee, S.-M., Smith, R.J., Senner, C., Hinds, J., Rajakumar, K., Adegbola, R.A., Besra, G.S., Butcher, P.D., Barer, M.R., 2008. Cytological and Transcript Analyses Reveal Fat and Lazy Persister-Like Bacilli in Tuberculous Sputum. PLOS Med. 5, e75. https://doi.org/10.1371/journal.pmed.0050075
Geize, R.V. der, Yam, K., Heuser, T., Wilbrink, M.H., Hara, H., Anderton, M.C., Sim, E., Dijkhuizen, L., Davies, J.E., Mohn, W.W., Eltis, L.D., 2007. A gene cluster encoding cholesterol catabolism in a soil actinomycete provides insight into Mycobacterium tuberculosis survival in macrophages. Proc. Natl. Acad. Sci. 104, 1947–1952. https://doi.org/10.1073/pnas.0605728104
Genoula, M., Marín Franco, J.L., Dupont, M., Kviatcovsky, D., Milillo, A., Schierloh, P., Moraña, E.J., Poggi, S., Palmero, D., Mata-Espinosa, D., González-Domínguez, E., León Contreras, J.C., Barrionuevo, P., Rearte, B., Córdoba Moreno, M.O., Fontanals, A., Crotta Asis, A., Gago, G., Cougoule, C., Neyrolles, O., Maridonneau-Parini, I., Sánchez-Torres, C., Hernández-Pando, R., Vérollet, C., Lugo-Villarino, G., Sasiain, M. del C., Balboa, L., 2018. Formation of Foamy Macrophages by Tuberculous Pleural Effusions Is Triggered by the Interleukin-10/Signal Transducer and Activator of Transcription 3 Axis through ACAT Upregulation. Front. Immunol. 9. https://doi.org/10.3389/fimmu.2018.00459

Gerrick, E.R., Barbier, T., Chase, M.R., Xu, R., François, J., Lin, V.H., Szucs, M.J., Rock, J.M., Ahmad, R., Tjaden, B., Livny, J., Fortune, S.M., 2018. Small RNA profiling in Mycobacterium tuberculosis identifies MrsI as necessary for an anticipatory iron sparing response. Proc. Natl. Acad. Sci. U. S. A. 115, 6464–6469. https://doi.org/10.1073/pnas.1718003115

Gill, W.P., Harik, N.S., Whiddon, M.R., Liao, R.P., Mittler, J.E., Sherman, D.R., 2009. A replication clock for Mycobacterium tuberculosis. Nat. Med. 15, 211–214. https://doi.org/10.1038/nm.1915

Gold, B., Rodriguez, G.M., Marras, S.A., Pentecost, M., Smith, I., 2001. The Mycobacterium tuberculosis IdeR is a dual functional regulator that controls transcription of genes involved in iron acquisition, iron storage and survival in macrophages. Mol. Microbiol. 42, 851–865.

Goldenring, J.R., 2015. Recycling endosomes. Curr. Opin. Cell Biol. 35, 117–122. https://doi.org/10.1016/j.ceb.2015.04.018

Goren, M.B., D'Arcy Hart, P., Young, M.R., Armstrong, J.A., 1976. Prevention of phagosome-lysosome fusion in cultured macrophages by sulfatides of Mycobacterium tuberculosis. Proc. Natl. Acad. Sci. U. S. A. 73, 2510–2514.

Gorvel, J.-P., Chavrier, P., Zerial, M., Gruenberg, J., 1991. rab5 controls early endosome fusion in vitro. Cell 64, 915–925. https://doi.org/10.1016/0092-8674(91)90316-Q

Graham, J.E., Clark-Curtiss, J.E., 1999. Identification of Mycobacterium tuberculosis RNAs synthesized in response to phagocytosis by human macrophages by selective capture of transcribed sequences (SCOTS). Proc. Natl. Acad. Sci. U. S. A. 96, 11554–11559.

Green, E.R., Mecsas, J., 2016. Bacterial Secretion Systems: An Overview. Microbiol. Spectr. 4. https://doi.org/10.1128/microbiolspec.VMBF-0012-2015

Guan, N., Liu, L., 2020. Microbial response to acid stress: mechanisms and applications. Appl. Microbiol. Biotechnol. 104, 51–65. https://doi.org/10.1007/s00253-019-10226-1

Gutierrez, M.G., 2013. Functional role(s) of phagosomal Rab GTPases. Small GTPases 4, 148–158. https://doi.org/10.4161/sgtp.25604

Gutierrez, M.G., Master, S.S., Singh, S.B., Taylor, G.A., Colombo, M.I., Deretic, V., 2004. Autophagy is a defense mechanism inhibiting BCG and Mycobacterium tuberculosis survival in infected macrophages. Cell 119, 753–766. https://doi.org/10.1016/j.cell.2004.11.038

Hamilton, H.L., Dillard, J.P., 2006. Natural transformation of Neisseria gonorrhoeae: from DNA donation to homologous recombination. Mol. Microbiol. 59, 376–385. https://doi.org/10.1111/j.1365-2958.2005.04964.x

Hamm, A., Krott, N., Breibach, I., Blindt, R., Bosserhoff, A.K., 2002. Efficient Transfection Method for Primary Cells. Tissue Eng. 8, 235–245. https://doi.org/10.1089/107632702753725003

Heim, V.J., Stafford, C.A., Nachbur, U., 2019. NOD Signaling and Cell Death. Front. Cell Dev. Biol. 7, 208. https://doi.org/10.3389/fcell.2019.00208

Jacobsen, L., Calvin, S., Lobenhofer, E., 2009. Transcriptional effects of transfection: the potential for misinterpretation of gene expression data generated from transiently transfected cells. BioTechniques 47, 617–624. https://doi.org/10.2144/000113132

Jacobsen, M., Repsilber, D., Gutschmidt, A., Neher, A., Feldmann, K., Mollenkopf, H.J., Ziegler, A., Kaufmann, S.H.E., 2007. Candidate biomarkers for discrimination

between infection and disease caused by Mycobacterium tuberculosis. J. Mol. Med. 85, 613–621. https://doi.org/10.1007/s00109-007-0157-6
Jakubzick, C.V., Randolph, G.J., Henson, P.M., 2017. Monocyte differentiation and antigen-presenting functions. Nat. Rev. Immunol. 17, 349–362. https://doi.org/10.1038/nri.2017.28
Jamwal, S.V., Mehrotra, P., Singh, A., Siddiqui, Z., Basu, A., Rao, K.V.S., 2016. Mycobacterial escape from macrophage phagosomes to the cytoplasm represents an alternate adaptation mechanism. Sci. Rep. 6, 23089. https://doi.org/10.1038/srep23089
Jayachandran, R., Sundaramurthy, V., Combaluzier, B., Mueller, P., Korf, H., Huygen, K., Miyazaki, T., Albrecht, I., Massner, J., Pieters, J., 2007. Survival of Mycobacteria in Macrophages Is Mediated by Coronin 1-Dependent Activation of Calcineurin. Cell 130, 37–50. https://doi.org/10.1016/j.cell.2007.04.043
Jin, J., Sundararaj, K.P., Samuvel, D.J., Zhang, X., Li, Y., Lu, Z., Lopes-Virella, M.F., Huang, Y., 2012. Different Signaling Mechanisms Regulating IL-6 Expression by LPS between Gingival Fibroblasts and Mononuclear Cells: Seeking the Common Target. Clin. Immunol. Orlando Fla 143, 188–199. https://doi.org/10.1016/j.clim.2012.01.019
Johansson, M., Rocha, N., Zwart, W., Jordens, I., Janssen, L., Kuijl, C., Olkkonen, V.M., Neefjes, J., 2007a. Activation of endosomal dynein motors by stepwise assembly of Rab7-RILP-p150Glued, ORP1L, and the receptor betalll spectrin. J. Cell Biol. 176, 459–471. https://doi.org/10.1083/jcb.200606077
Johansson, M., Rocha, N., Zwart, W., Jordens, I., Janssen, L., Kuijl, C., Olkkonen, V.M., Neefjes, J., 2007b. Activation of endosomal dynein motors by stepwise assembly of Rab7-RILP-p150Glued, ORP1L, and the receptor ?lll spectrin. J. Cell Biol. 176, 459–471. https://doi.org/10.1083/jcb.200606077
Kadlecova, Z., Spielman, S.J., Loerke, D., Mohanakrishnan, A., Reed, D.K., Schmid, S.L., 2017. Regulation of clathrin-mediated endocytosis by hierarchical allosteric activation of AP2. J. Cell Biol. 216, 167–179. https://doi.org/10.1083/jcb.201608071
Kanaujia, S.P., Jeyakanthan, J., Nakagawa, N., Balasubramaniam, S., Shinkai, A., Kuramitsu, S., Yokoyama, S., Sekar, K., 2010. Structures of apo and GTP-bound molybdenum cofactor biosynthesis protein MoaC from Thermus thermophilus HB8. Acta Crystallogr. D Biol. Crystallogr. 66, 821–833. https://doi.org/10.1107/S0907444910019074
Kang, P.B., Azad, A.K., Torrelles, J.B., Kaufman, T.M., Beharka, A., Tibesar, E., DesJardin, L.E., Schlesinger, L.S., 2005. The human macrophage mannose receptor directs Mycobacterium tuberculosis lipoarabinomannan-mediated phagosome biogenesis. J. Exp. Med. 202, 987–999. https://doi.org/10.1084/jem.20051239
Kanonenberg, K., Spitz, O., Erenburg, I.N., Beer, T., Schmitt, L., 2018. Type I secretion system—it takes three and a substrate. FEMS Microbiol. Lett. 365. https://doi.org/10.1093/femsle/fny094
Koh, H.-J., Kim, Y.-R., Kim, J.-S., Yun, J.-S., Kim, S., Kim, S.Y., Jang, K., Yang, C.-S., 2018. CD82 hypomethylation is essential for tuberculosis pathogenesis via regulation of RUNX1-Rab5/22. Exp. Mol. Med. 50, 1–15. https://doi.org/10.1038/s12276-018-0091-4
Koo, M.-S., Subbian, S., Kaplan, G., 2012. Strain specific transcriptional response in Mycobacterium tuberculosis infected macrophages. Cell Commun. Signal. CCS 10, 2. https://doi.org/10.1186/1478-811X-10-2
Kortüm, B., Campregher, C., Lang, M., Khare, V., Pinter, M., Evstatiev, R., Schmid, G., Mittlböck, M., Scharl, T., Kucherlapati, M.H., Edelmann, W., Gasche, C., 2015.

Mesalazine and thymoquinone attenuate intestinal tumour development in Msh2(loxP/loxP) Villin-Cre mice. Gut 64, 1905–1912. https://doi.org/10.1136/gutjnl-2014-307663
Koul, A., Herget, T., Klebl, B., Ullrich, A., 2004. Interplay between mycobacteria and host signalling pathways. Nat. Rev. Microbiol. 2, 189–202. https://doi.org/10.1038/nrmicro840
Koussounadis, A., Langdon, S.P., Um, I.H., Harrison, D.J., Smith, V.A., 2015. Relationship between differentially expressed mRNA and mRNA-protein correlations in a xenograft model system. Sci. Rep. 5, 10775. https://doi.org/10.1038/srep10775
Kühn, S., Bergqvist, J., Gil, M., Valenzuela, C., Barrio, L., Lebreton, S., Zurzolo, C., Enninga, J., 2020. Actin Assembly around the Shigella-Containing Vacuole Promotes Successful Infection. Cell Rep. 31, 107638. https://doi.org/10.1016/j.celrep.2020.107638
Lavarti, R., Ganugapati, J., Ratcha, S., Rao, L.S., SivaSai, K.S., 2016. Insights from the analysis of predicted Rv0679c protein peptide from Mycobacterium tuberculosis with Toll like Receptors in host. Bioinformation 12, 293–299. https://doi.org/10.6026/97320630012293
Lawe, D.C., Patki, V., Heller-Harrison, R., Lambright, D., Corvera, S., 2000. The FYVE Domain of Early Endosome Antigen 1 Is Required for Both Phosphatidylinositol 3-Phosphate and Rab5 Binding CRITICAL ROLE OF THIS DUAL INTERACTION FOR ENDOSOMAL LOCALIZATION. J. Biol. Chem. 275, 3699–3705. https://doi.org/10.1074/jbc.275.5.3699
Leake, E.S., Myrvik, Q.N., Wright, M.J., 1984. Phagosomal membranes of Mycobacterium bovis BCG-immune alveolar macrophages are resistant to disruption by Mycobacterium tuberculosis H37Rv. Infect. Immun. 45, 443–446.
Lee, B.-Y., Jethwaney, D., Schilling, B., Clemens, D.L., Gibson, B.W., Horwitz, M.A., 2010. The Mycobacterium bovis Bacille Calmette-Guérin Phagosome Proteome. Mol. Cell. Proteomics MCP 9, 32–53. https://doi.org/10.1074/mcp.M900396-MCP200
Lee, J., Lee, S.-G., Kim, K.K., Lim, Y.-J., Choi, J.-A., Cho, S.-N., Park, C., Song, C.-H., 2019. Characterisation of genes differentially expressed in macrophages by virulent and attenuated Mycobacterium tuberculosis through RNA-Seq analysis. Sci. Rep. 9, 4027. https://doi.org/10.1038/s41598-019-40814-0
Lesho, E., Forestiero, F.J., Hirata, M.H., Hirata, R.D., Cecon, L., Melo, F.F., Paik, S.H., Murata, Y., Ferguson, E.W., Wang, Z., Ooi, G.T., 2011. Transcriptional responses of host peripheral blood cells to tuberculosis infection. Tuberc. Edinb. Scotl. 91, 390–399. https://doi.org/10.1016/j.tube.2011.07.002
Levillain, F., Poquet, Y., Mallet, L., Mazères, S., Marceau, M., Brosch, R., Bange, F.-C., Supply, P., Magalon, A., Neyrolles, O., 2017. Horizontal acquisition of a hypoxia-responsive molybdenum cofactor biosynthesis pathway contributed to Mycobacterium tuberculosis pathoadaptation. PLoS Pathog. 13. https://doi.org/10.1371/journal.ppat.1006752
Li, A.H., Waddell, S.J., Hinds, J., Malloff, C.A., Bains, M., Hancock, R.E., Lam, W.L., Butcher, P.D., Stokes, R.W., 2010. Contrasting Transcriptional Responses of a Virulent and an Attenuated Strain of Mycobacterium tuberculosis Infecting Macrophages. PLoS ONE 5. https://doi.org/10.1371/journal.pone.0011066
Li, Q., Lau, A., Morris, T.J., Guo, L., Fordyce, C.B., Stanley, E.F., 2004. A Syntaxin 1, Gαo, and N-Type Calcium Channel Complex at a Presynaptic Nerve Terminal: Analysis by

Quantitative Immunocolocalization. J. Neurosci. 24, 4070–4081. https://doi.org/10.1523/JNEUROSCI.0346-04.2004
Lohmann-Matthes, M.L., Steinmuller, C., Franke-Ullmann, G., 1994. Pulmonary macrophages. Eur. Respir. J. 7, 1678–1689.
Lu, P., Vogel, C., Wang, R., Yao, X., Marcotte, E.M., 2007. Absolute protein expression profiling estimates the relative contributions of transcriptional and translational regulation. Nat. Biotechnol. 25, 117–124. https://doi.org/10.1038/nbt1270
Lübke, T., Lobel, P., Sleat, D.E., 2009. Proteomics of the lysosome. Biochim. Biophys. Acta 1793, 625–635. https://doi.org/10.1016/j.bbamcr.2008.09.018
Luca, M.D., Cogli, L., Progida, C., Nisi, V., Pascolutti, R., Sigismund, S., Fiore, P.P.D., Bucci, C., 2014. RILP regulates vacuolar ATPase through interaction with the V1G1 subunit. J Cell Sci 127, 2697–2708. https://doi.org/10.1242/jcs.142604
MacGurn, J.A., Cox, J.S., 2007. A genetic screen for Mycobacterium tuberculosis mutants defective for phagosome maturation arrest identifies components of the ESX-1 secretion system. Infect. Immun. 75, 2668–2678. https://doi.org/10.1128/IAI.01872-06
Maertzdorf, J., Ota, M., Repsilber, D., Mollenkopf, H.J., Weiner, J., Hill, P.C., Kaufmann, S.H.E., 2011. Functional Correlations of Pathogenesis-Driven Gene Expression Signatures in Tuberculosis. PLoS ONE 6, e26938. https://doi.org/10.1371/journal.pone.0026938
Magalon, A., Mendel, R.R., 2015. Biosynthesis and Insertion of the Molybdenum Cofactor. EcoSal Plus 6. https://doi.org/10.1128/ecosalplus.ESP-0006-2013
Målen, H., Berven, F.S., Fladmark, K.E., Wiker, H.G., 2007. Comprehensive analysis of exported proteins from Mycobacterium tuberculosis H37Rv. PROTEOMICS 7, 1702–1718. https://doi.org/10.1002/pmic.200600853
Manganelli, R., Dubnau, E., Tyagi, S., Kramer, F.R., Smith, I., 1999. Differential expression of 10 sigma factor genes in Mycobacterium tuberculosis. Mol. Microbiol. 31, 715–724.
Marshansky, V., Futai, M., 2008. The V-type H+-ATPase in vesicular trafficking: targeting, regulation and function. Curr. Opin. Cell Biol. 20, 415–426. https://doi.org/10.1016/j.ceb.2008.03.015
Martinet, W., Schrijvers, D.M., Kockx, M.M., 2003. Nucleofection as an efficient nonviral transfection method for human monocytic cells. Biotechnol. Lett. 25, 1025–1029.
Maurya, R.K., Bharti, S., Krishnan, M.Y., 2019. Triacylglycerols: Fuelling the Hibernating Mycobacterium tuberculosis. Front. Cell. Infect. Microbiol. 8. https://doi.org/10.3389/fcimb.2018.00450
Mawuenyega, K.G., Forst, C.V., Dobos, K.M., Belisle, J.T., Chen, J., Bradbury, E.M., Bradbury, A.R.M., Chen, X., 2005. Mycobacterium tuberculosis functional network analysis by global subcellular protein profiling. Mol. Biol. Cell 16, 396–404. https://doi.org/10.1091/mbc.E04-04-0329
Mazandu, G.K., Mulder, N.J., 2012. Function Prediction and Analysis of Mycobacterium tuberculosis Hypothetical Proteins. Int. J. Mol. Sci. 13, 7283–7302. https://doi.org/10.3390/ijms13067283
McDonough, K.A., Kress, Y., Bloom, B.R., 1993. Pathogenesis of tuberculosis: interaction of Mycobacterium tuberculosis with macrophages. Infect. Immun. 61, 2763–2773.
McKinney, J.D., Höner zu Bentrup, K., Muñoz-Elías, E.J., Miczak, A., Chen, B., Chan, W.T., Swenson, D., Sacchettini, J.C., Jacobs, W.R., Russell, D.G., 2000. Persistence of

Mycobacterium tuberculosis in macrophages and mice requires the glyoxylate shunt enzyme isocitrate lyase. Nature 406, 735–738. https://doi.org/10.1038/35021074
McLaughlin, B., Chon, J.S., MacGurn, J.A., Carlsson, F., Cheng, T.L., Cox, J.S., Brown, E.J., 2007. A Mycobacterium ESX-1–Secreted Virulence Factor with Unique Requirements for Export. PLoS Pathog. 3. https://doi.org/10.1371/journal.ppat.0030105
Miner, M.D., Chang, J.C., Pandey, A.K., Sassetti, C.M., Sherman, D.R., 2009. Role of cholesterol in Mycobacterium tuberculosis infection. IJEB Vol4706 June 2009.
Mitchell, G., Chen, C., Portnoy, D.A., 2016. Strategies used by bacteria to grow in macrophages. Microbiol. Spectr. 4. https://doi.org/10.1128/microbiolspec.MCHD-0012-2015
Mottola, G., 2014. The complexity of Rab5 to Rab7 transition guarantees specificity of pathogen subversion mechanisms. Front. Cell. Infect. Microbiol. 4. https://doi.org/10.3389/fcimb.2014.00180
Mukherjee, S., Ghosh, R.N., Maxfield, F.R., 1997. Endocytosis. Physiol. Rev. 77, 759–803.
Myrvik, Q.N., Leake, E.S., Wright, M.J., 1984. Disruption of phagosomal membranes of normal alveolar macrophages by the H37Rv strain of Mycobacterium tuberculosis. A correlate of virulence. Am. Rev. Respir. Dis. 129, 322–328.
Nesbitt, N.M., Yang, X., Fontán, P., Kolesnikova, I., Smith, I., Sampson, N.S., Dubnau, E., 2010. A Thiolase of Mycobacterium tuberculosis Is Required for Virulence and Production of Androstenedione and Androstadienedione from Cholesterol. Infect. Immun. 78, 275–282. https://doi.org/10.1128/IAI.00893-09
Newman, J.P., Wang, G.Y., Arima, K., Guan, S.P., Waters, M.R., Cavenee, W.K., Pan, E., Aliwarga, E., Chong, S.T., Kok, C.Y.L., Endaya, B.B., Habib, A.A., Horibe, T., Ng, W.H., Ho, I.A.W., Hui, K.M., Kordula, T., Lam, P.Y.P., 2017. Interleukin-13 receptor alpha 2 cooperates with EGFRvIII signaling to promote glioblastoma multiforme. Nat. Commun. 8. https://doi.org/10.1038/s41467-017-01392-9
Ng, B.Y.C., Xiao, W., West, N.P., Wee, E.J.H., Wang, Y., Trau, M., 2015. Rapid, Single-Cell Electrochemical Detection of Mycobacterium tuberculosis Using Colloidal Gold Nanoparticles. Anal. Chem. 87, 10613–10618. https://doi.org/10.1021/acs.analchem.5b03121
Nguyen, T.A., Croon, S., Rijkers, G., 2019. Mycobacterium tuberculosis: escape room world champion. Pneumonia 11, 1. https://doi.org/10.1186/s41479-019-0060-2
Nordenfelt, P., Grinstein, S., Björck, L., Tapper, H., 2012. V-ATPase-mediated phagosomal acidification is impaired by Streptococcus pyogenes through Mga-regulated surface proteins. Microbes Infect. 14, 1319–1329. https://doi.org/10.1016/j.micinf.2012.08.005
Ottenhoff, T.H.M., Dass, R.H., Yang, N., Zhang, M.M., Wong, H.E.E., Sahiratmadja, E., Khor, C.C., Alisjahbana, B., van Crevel, R., Marzuki, S., Seielstad, M., van de Vosse, E., Hibberd, M.L., 2012. Genome-wide expression profiling identifies type 1 interferon response pathways in active tuberculosis. PloS One 7, e45839. https://doi.org/10.1371/journal.pone.0045839
Patin, E.C., Geffken, A.C., Willcocks, S., Leschczyk, C., Haas, A., Nimmerjahn, F., Lang, R., Ward, T.H., Schaible, U.E., 2017. Trehalose dimycolate interferes with FcγR-mediated phagosome maturation through Mincle, SHP-1 and FcγRIIB signalling. PloS One 12, e0174973. https://doi.org/10.1371/journal.pone.0174973

Peddireddy, V., Doddam, S.N., Ahmed, N., 2017. Mycobacterial Dormancy Systems and Host Responses in Tuberculosis. Front. Immunol. 8. https://doi.org/10.3389/fimmu.2017.00084

Pethe, K., Swenson, D.L., Alonso, S., Anderson, J., Wang, C., Russell, D.G., 2004. Isolation of Mycobacterium tuberculosis mutants defective in the arrest of phagosome maturation. Proc. Natl. Acad. Sci. U. S. A. 101, 13642–13647. https://doi.org/10.1073/pnas.0401657101

Pfaffl, M.W., 2001. A new mathematical model for relative quantification in real-time RT-PCR. Nucleic Acids Res. 29, e45.

Prashar, A., Schnettger, L., Bernard, E.M., Gutierrez, M.G., 2017. Rab GTPases in Immunity and Inflammation. Front. Cell. Infect. Microbiol. 7, 435. https://doi.org/10.3389/fcimb.2017.00435

Price, J.V., Vance, R.E., 2014. The macrophage paradox. Immunity 41, 685–693. https://doi.org/10.1016/j.immuni.2014.10.015

Puhar, A., Sansonetti, P.J., 2014. Type III secretion system. Curr. Biol. 24, R784–R791. https://doi.org/10.1016/j.cub.2014.07.016

Queval, C.J., Song, O.-R., Carralot, J.-P., Saliou, J.-M., Bongiovanni, A., Deloison, G., Deboosère, N., Jouny, S., Iantomasi, R., Delorme, V., Debrie, A.-S., Park, S.-J., Gouveia, J.C., Tomavo, S., Brosch, R., Yoshimura, A., Yeramian, E., Brodin, P., 2017. Mycobacterium tuberculosis Controls Phagosomal Acidification by Targeting CISH-Mediated Signaling. Cell Rep. 20, 3188–3198. https://doi.org/10.1016/j.celrep.2017.08.101

Rachman, H., Strong, M., Schaible, U., Schuchhardt, J., Hagens, K., Mollenkopf, H., Eisenberg, D., Kaufmann, S.H.E., 2006. Mycobacterium tuberculosis gene expression profiling within the context of protein networks. Microbes Infect. 8, 747–757. https://doi.org/10.1016/j.micinf.2005.09.011

Rack, K., Huck, V., Hoore, M., Fedosov, D.A., Schneider, S.W., Gompper, G., 2017. Margination and stretching of von Willebrand factor in the blood stream enable adhesion. Sci. Rep. 7. https://doi.org/10.1038/s41598-017-14346-4

Ragno, S., Romano, M., Howell, S., Pappin, D.J., Jenner, P.J., Colston, M.J., 2001. Changes in gene expression in macrophages infected with Mycobacterium tuberculosis: a combined transcriptomic and proteomic approach. Immunology 104, 99–108.

Rajaram, M.V.S., Arnett, E., Azad, A.K., Guirado, E., Ni, B., Gerberick, A.D., He, L.-Z., Keler, T., Thomas, L.J., Lafuse, W.P., Schlesinger, L.S., 2017. M. tuberculosis-Initiated Human Mannose Receptor Signaling Regulates Macrophage Recognition and Vesicle Trafficking by FcRγ-Chain, Grb2, and SHP-1. Cell Rep. 21, 126–140. https://doi.org/10.1016/j.celrep.2017.09.034

Ravasi, T., Suzuki, H., Cannistraci, C.V., Katayama, S., Bajic, V.B., Tan, K., Akalin, A., Schmeier, S., Kanamori-Katayama, M., Bertin, N., Carninci, P., Daub, C.O., Forrest, A.R.R., Gough, J., Grimmond, S., Han, J.-H., Hashimoto, T., Hide, W., Hofmann, O., Kamburov, A., Kaur, M., Kawaji, H., Kubosaki, A., Lassmann, T., van Nimwegen, E., MacPherson, C.R., Ogawa, C., Radovanovic, A., Schwartz, A., Teasdale, R.D., Tegnér, J., Lenhard, B., Teichmann, S.A., Arakawa, T., Ninomiya, N., Murakami, K., Tagami, M., Fukuda, S., Imamura, K., Kai, C., Ishihara, R., Kitazume, Y., Kawai, J., Hume, D.A., Ideker, T., Hayashizaki, Y., 2010. An atlas of combinatorial transcriptional regulation in mouse and man. Cell 140, 744–752. https://doi.org/10.1016/j.cell.2010.01.044

Rens, C., Chao, J.D., Sexton, D.L., Tocheva, E.I., Av-Gay, Y., 2021. Roles for phthiocerol dimycocerosate lipids in Mycobacterium tuberculosis pathogenesis. Microbiol. Read. Engl. 167. https://doi.org/10.1099/mic.0.001042

Repasy, T., Lee, J., Marino, S., Martinez, N., Kirschner, D.E., Hendricks, G., Baker, S., Wilson, A.A., Kotton, D.N., Kornfeld, H., 2013. Intracellular Bacillary Burden Reflects a Burst Size for Mycobacterium tuberculosis In Vivo. PLoS Pathog 9, e1003190. https://doi.org/10.1371/journal.ppat.1003190

Riendeau, C.J., Kornfeld, H., 2003. THP-1 Cell Apoptosis in Response to Mycobacterial Infection. Infect. Immun. 71, 254–259. https://doi.org/10.1128/IAI.71.1.254-259.2003

Rink, J., Ghigo, E., Kalaidzidis, Y., Zerial, M., 2005. Rab conversion as a mechanism of progression from early to late endosomes. Cell 122, 735–749. https://doi.org/10.1016/j.cell.2005.06.043

Rivera-Calzada, A., Famelis, N., Llorca, O., Geibel, S., 2021. Type VII secretion systems: structure, functions and transport models. Nat. Rev. Microbiol. 19, 567–584. https://doi.org/10.1038/s41579-021-00560-5

Rosas-Magallanes, V., Stadthagen-Gomez, G., Rauzier, J., Barreiro, L.B., Tailleux, L., Boudou, F., Griffin, R., Nigou, J., Jackson, M., Gicquel, B., Neyrolles, O., 2007. Signature-Tagged Transposon Mutagenesis Identifies Novel Mycobacterium tuberculosis Genes Involved in the Parasitism of Human Macrophages. Infect. Immun. 75, 504–507. https://doi.org/10.1128/IAI.00058-06

Roxas, B.A., Li, Q., 2009. Acid stress response of a mycobacterial proteome: insight from a gene ontology analysis. Int. J. Clin. Exp. Med. 2, 309–328.

Ru, H., Liu, X., Lin, C., Yang, J., Chen, F., Sun, R., Zhang, L., Liu, J., 2017. The Impact of Genome Region of Difference 4 (RD4) on Mycobacterial Virulence and BCG Efficacy. Front. Cell. Infect. Microbiol. 7, 239. https://doi.org/10.3389/fcimb.2017.00239

Russell, A.B., Peterson, S.B., Mougous, J.D., 2014. Type VI secretion system effectors: poisons with a purpose. Nat. Rev. Microbiol. 12, 137–148. https://doi.org/10.1038/nrmicro3185

Saito, K., Murai, J., Kajiho, H., Kontani, K., Kurosu, H., Katada, T., 2002. A Novel Binding Protein Composed of Homophilic Tetramer Exhibits Unique Properties for the Small GTPase Rab5. J. Biol. Chem. 277, 3412–3418. https://doi.org/10.1074/jbc.M106276200

Sandri, C., Caccavari, F., Valdembri, D., Camillo, C., Veltel, S., Santambrogio, M., Lanzetti, L., Bussolino, F., Ivaska, J., Serini, G., 2012. The R-Ras/RIN2/Rab5 complex controls endothelial cell adhesion and morphogenesis via active integrin endocytosis and Rac signaling. Cell Res. 22, 1479–1501. https://doi.org/10.1038/cr.2012.110

Sarantis, H., Grinstein, S., 2012. Subversion of Phagocytosis for Pathogen Survival. Cell Host Microbe 12, 419–431. https://doi.org/10.1016/j.chom.2012.09.001

Sassetti, C.M., Boyd, D.H., Rubin, E.J., 2003. Genes required for mycobacterial growth defined by high density mutagenesis. Mol. Microbiol. 48, 77–84.

Schnappinger, D., Ehrt, S., Voskuil, M.I., Liu, Y., Mangan, J.A., Monahan, I.M., Dolganov, G., Efron, B., Butcher, P.D., Nathan, C., Schoolnik, G.K., 2003a. Transcriptional Adaptation of Mycobacterium tuberculosis within Macrophages Insights into the Phagosomal Environment. J. Exp. Med. 198, 693–704. https://doi.org/10.1084/jem.20030846

Schnappinger, D., Ehrt, S., Voskuil, M.I., Liu, Y., Mangan, J.A., Monahan, I.M., Dolganov, G., Efron, B., Butcher, P.D., Nathan, C., Schoolnik, G.K., 2003b. Transcriptional Adaptation of Mycobacterium tuberculosis within Macrophages: Insights into the Phagosomal Environment. J. Exp. Med. 198, 693–704. https://doi.org/10.1084/jem.20030846

Schröder, B.A., Wrocklage, C., Hasilik, A., Saftig, P., 2010. The proteome of lysosomes. Proteomics 10, 4053–4076. https://doi.org/10.1002/pmic.201000196

Shahnazari, S., Brumell, J.H., 2011. Mechanisms and consequences of bacterial targeting by the autophagy pathway. Curr. Opin. Microbiol. 14, 68–75. https://doi.org/10.1016/j.mib.2010.11.001

Sharma, V., Sharma, S., Hoener zu Bentrup, K., McKinney, J.D., Russell, D.G., Jacobs, W.R., Sacchettini, J.C., 2000. Structure of isocitrate lyase, a persistence factor of Mycobacterium tuberculosis. Nat. Struct. Biol. 7, 663–668. https://doi.org/10.1038/77964

Shearer, L.J., Petersen, N.O., 2019. Distribution and Co-localization of endosome markers in cells. Heliyon 5, e02375. https://doi.org/10.1016/j.heliyon.2019.e02375

Shen, P., Li, Q., Ma, J., Tian, M., Hong, F., Zhai, X., Li, J., Huang, H., Shi, C., 2017. IRAK-M alters the polarity of macrophages to facilitate the survival of Mycobacterium tuberculosis. BMC Microbiol. 17. https://doi.org/10.1186/s12866-017-1095-2

Shepelkova, G., Pommerenke, C., Alberts, R., Geffers, R., Evstifeev, V., Apt, A., Schughart, K., Wilk, E., 2013. Analysis of the lung transcriptome in Mycobacterium tuberculosis-infected mice reveals major differences in immune response pathways between TB-susceptible and resistant hosts. Tuberc. Edinb. Scotl. 93, 263–269. https://doi.org/10.1016/j.tube.2012.11.007

Shi, L., Sohaskey, C.D., Kana, B.D., Dawes, S., North, R.J., Mizrahi, V., Gennaro, M.L., 2005. Changes in energy metabolism of Mycobacterium tuberculosis in mouse lung and under in vitro conditions affecting aerobic respiration. Proc. Natl. Acad. Sci. U. S. A. 102, 15629–15634. https://doi.org/10.1073/pnas.0507850102

Simeone, R., Bobard, A., Lippmann, J., Bitter, W., Majlessi, L., Brosch, R., Enninga, J., 2012. Phagosomal rupture by Mycobacterium tuberculosis results in toxicity and host cell death. PLoS Pathog. 8, e1002507. https://doi.org/10.1371/journal.ppat.1002507

Spanò, S., Galán, J.E., 2018. Taking control: Hijacking of Rab GTPases by intracellular bacterial pathogens. Small GTPases 9, 182–191. https://doi.org/10.1080/21541248.2017.1336192

Stanley, S.A., Raghavan, S., Hwang, W.W., Cox, J.S., 2003. Acute infection and macrophage subversion by Mycobacterium tuberculosis require a specialized secretion system. Proc. Natl. Acad. Sci. U. S. A. 100, 13001–13006. https://doi.org/10.1073/pnas.2235593100

Stewart, G.R., Patel, J., Robertson, B.D., Rae, A., Young, D.B., 2005. Mycobacterial Mutants with Defective Control of Phagosomal Acidification. PLoS Pathog 1, e33. https://doi.org/10.1371/journal.ppat.0010033

Stockinger, W., Zhang, S.C., Trivedi, V., Jarzylo, L.A., Shieh, E.C., Lane, W.S., Castoreno, A.B., Nohturfft, A., 2006. Differential Requirements for Actin Polymerization, Calmodulin, and Ca2+ Define Distinct Stages of Lysosome/Phagosome Targeting. Mol. Biol. Cell 17, 1697–1710. https://doi.org/10.1091/mbc.E05-12-1140

Strausberg, R.L., Feingold, E.A., Grouse, L.H., Derge, J.G., Klausner, R.D., Collins, F.S., Wagner, L., Shenmen, C.M., Schuler, G.D., Altschul, S.F., Zeeberg, B., Buetow, K.H.,

Schaefer, C.F., Bhat, N.K., Hopkins, R.F., Jordan, H., Moore, T., Max, S.I., Wang, J., Hsieh, F., Diatchenko, L., Marusina, K., Farmer, A.A., Rubin, G.M., Hong, L., Stapleton, M., Soares, M.B., Bonaldo, M.F., Casavant, T.L., Scheetz, T.E., Brownstein, M.J., Usdin, T.B., Toshiyuki, S., Carninci, P., Prange, C., Raha, S.S., Loquellano, N.A., Peters, G.J., Abramson, R.D., Mullahy, S.J., Bosak, S.A., McEwan, P.J., McKernan, K.J., Malek, J.A., Gunaratne, P.H., Richards, S., Worley, K.C., Hale, S., Garcia, A.M., Gay, L.J., Hulyk, S.W., Villalon, D.K., Muzny, D.M., Sodergren, E.J., Lu, X., Gibbs, R.A., Fahey, J., Helton, E., Ketteman, M., Madan, Anuradha, Rodrigues, S., Sanchez, A., Whiting, M., Madan, Anup, Young, A.C., Shevchenko, Y., Bouffard, G.G., Blakesley, R.W., Touchman, J.W., Green, E.D., Dickson, M.C., Rodriguez, A.C., Grimwood, J., Schmutz, J., Myers, R.M., Butterfield, Y.S.N., Krzywinski, M.I., Skalska, U., Smailus, D.E., Schnerch, A., Schein, J.E., Jones, S.J.M., Marra, M.A., Mammalian Gene Collection Program Team, 2002. Generation and initial analysis of more than 15,000 full-length human and mouse cDNA sequences. Proc. Natl. Acad. Sci. U. S. A. 99, 16899–16903. https://doi.org/10.1073/pnas.242603899

Sturgill-Koszycki, S., Schlesinger, P.H., Chakraborty, P., Haddix, P.L., Collins, H.L., Fok, A.K., Allen, R.D., Gluck, S.L., Heuser, J., Russell, D.G., 1994. Lack of acidification in Mycobacterium phagosomes produced by exclusion of the vesicular proton-ATPase. Science 263, 678–681. https://doi.org/10.1126/science.8303277

Sun, C., Yang, G., Yuan, J., Peng, X., Zhang, C., Zhai, X., Luo, T., Bao, L., 2017. Mycobacterium tuberculosis hypoxic response protein 1 (Hrp1) augments the pro-inflammatory response and enhances the survival of Mycobacterium smegmatis in murine macrophages. J. Med. Microbiol. 66, 1033–1044. https://doi.org/10.1099/jmm.0.000511

Sun, J., Deghmane, A.-E., Soualhine, H., Hong, T., Bucci, C., Solodkin, A., Hmama, Z., 2007. Mycobacterium bovis BCG disrupts the interaction of Rab7 with RILP contributing to inhibition of phagosome maturation. J. Leukoc. Biol. 82, 1437–1445. https://doi.org/10.1189/jlb.0507289

Sun, J., Wang, X., Lau, A., Liao, T.-Y.A., Bucci, C., Hmama, Z., 2010. Mycobacterial Nucleoside Diphosphate Kinase Blocks Phagosome Maturation in Murine Raw 264.7 Macrophages. PLOS ONE 5, e8769. https://doi.org/10.1371/journal.pone.0008769

Sundström, C., Nilsson, K., 1976. Establishment and characterization of a human histiocytic lymphoma cell line (U-937). Int. J. Cancer 17, 565–577.

Tailleux, L., Waddell, S.J., Pelizzola, M., Mortellaro, A., Withers, M., Tanne, A., Castagnoli, P.R., Gicquel, B., Stoker, N.G., Butcher, P.D., Foti, M., Neyrolles, O., 2008. Probing Host Pathogen Cross-Talk by Transcriptional Profiling of Both Mycobacterium tuberculosis and Infected Human Dendritic Cells and Macrophages. PLoS ONE 3. https://doi.org/10.1371/journal.pone.0001403

Theus, S.A., Cave, M.D., Eisenach, K.D., 2004. Activated THP-1 Cells: an Attractive Model for the Assessment of Intracellular Growth Rates of Mycobacterium tuberculosis Isolates. Infect. Immun. 72, 1169–1173. https://doi.org/10.1128/IAI.72.2.1169-1173.2004

Tietz, S.M., Berghoff, M., 2012. Gene Silencing of MK2 in Hard-to-Transfect Human U937 Cells. J. Biomol. Tech. JBT 23, 47–50. https://doi.org/10.7171/jbt.12-2302-005

Tsuchiya, S., Kobayashi, Y., Goto, Y., Okumura, H., Nakae, S., Konno, T., Tada, K., 1982. Induction of maturation in cultured human monocytic leukemia cells by a phorbol diester. Cancer Res. 42, 1530–1536.

Tufariello, J.M., Chapman, J.R., Kerantzas, C.A., Wong, K.-W., Vilchèze, C., Jones, C.M., Cole, L.E., Tinaztepe, E., Thompson, V., Fenyö, D., Niederweis, M., Ueberheide, B., Philips, J.A., Jacobs, W.R., 2016. Separable roles for Mycobacterium tuberculosis ESX-3 effectors in iron acquisition and virulence. Proc. Natl. Acad. Sci. 113, E348–E357. https://doi.org/10.1073/pnas.1523321113

Uribe-Querol, E., Rosales, C., 2017. Control of Phagocytosis by Microbial Pathogens. Front. Immunol. 8. https://doi.org/10.3389/fimmu.2017.01368

Van der Geize, R., Yam, K., Heuser, T., Wilbrink, M.H., Hara, H., Anderton, M.C., Sim, E., Dijkhuizen, L., Davies, J.E., Mohn, W.W., Eltis, L.D., 2007. A gene cluster encoding cholesterol catabolism in a soil actinomycete provides insight into Mycobacterium tuberculosis survival in macrophages. Proc. Natl. Acad. Sci. U. S. A. 104, 1947–1952. https://doi.org/10.1073/pnas.0605728104

van der Wel, N., Hava, D., Houben, D., Fluitsma, D., van Zon, M., Pierson, J., Brenner, M., Peters, P.J., 2007. M. tuberculosis and M. leprae translocate from the phagolysosome to the cytosol in myeloid cells. Cell 129, 1287–1298. https://doi.org/10.1016/j.cell.2007.05.059

VanderVen, B.C., Fahey, R.J., Lee, W., Liu, Y., Abramovitch, R.B., Memmott, C., Crowe, A.M., Eltis, L.D., Perola, E., Deininger, D.D., Wang, T., Locher, C.P., Russell, D.G., 2015. Novel Inhibitors of Cholesterol Degradation in Mycobacterium tuberculosis Reveal How the Bacterium's Metabolism Is Constrained by the Intracellular Environment. PLOS Pathog. 11, e1004679. https://doi.org/10.1371/journal.ppat.1004679

Vergne, I., Chua, J., Lee, H.-H., Lucas, M., Belisle, J., Deretic, V., 2005. Mechanism of phagolysosome biogenesis block by viable Mycobacterium tuberculosis. Proc. Natl. Acad. Sci. U. S. A. 102, 4033–4038. https://doi.org/10.1073/pnas.0409716102

Vergne, I., Gilleron, M., Nigou, J., 2015. Manipulation of the endocytic pathway and phagocyte functions by Mycobacterium tuberculosis lipoarabinomannan. Front. Cell. Infect. Microbiol. 4. https://doi.org/10.3389/fcimb.2014.00187

Via, L.E., Deretic, D., Ulmer, R.J., Hibler, N.S., Huber, L.A., Deretic, V., 1997. Arrest of Mycobacterial Phagosome Maturation Is Caused by a Block in Vesicle Fusion between Stages Controlled by rab5 and rab7. J. Biol. Chem. 272, 13326–13331. https://doi.org/10.1074/jbc.272.20.13326

Vieira, O.V., Bucci, C., Harrison, R.E., Trimble, W.S., Lanzetti, L., Gruenberg, J., Schreiber, A.D., Stahl, P.D., Grinstein, S., 2003. Modulation of Rab5 and Rab7 recruitment to phagosomes by phosphatidylinositol 3-kinase. Mol. Cell. Biol. 23, 2501–2514.

Vogel, J.P., Andrews, H.L., Wong, S.K., Isberg, R.R., 1998. Conjugative transfer by the virulence system of Legionella pneumophila. Science 279, 873–876.

Volpe, E., Cappelli, G., Grassi, M., Martino, A., Serafino, A., Colizzi, V., Sanarico, N., Mariani, F., 2006. Gene expression profiling of human macrophages at late time of infection with Mycobacterium tuberculosis. Immunology 118, 449–460. https://doi.org/10.1111/j.1365-2567.2006.02378.x

Waddell, S.J., 2010. Reprogramming the Mycobacterium tuberculosis transcriptome during pathogenesis. Drug Discov. Today Dis. Mech., Mycobacterial infections 7, e67–e73. https://doi.org/10.1016/j.ddmec.2010.09.007

Wang, J., Behr, M.A., 2014. Building a better bacillus: the emergence of Mycobacterium tuberculosis. Front. Microbiol. 5. https://doi.org/10.3389/fmicb.2014.00139

Wang, L., Zuo, M., Chen, H., Liu, S., Wu, X., Cui, Z., Yang, H., Liu, H., Ge, B., 2017. Mycobacterium tuberculosis Lipoprotein MPT83 Induces Apoptosis of Infected

Macrophages by Activating the TLR2/p38/COX-2 Signaling Pathway. J. Immunol. 198, 4772–4780. https://doi.org/10.4049/jimmunol.1700030
Wang, M., Qazi, I.H., Wang, L., Zhou, G., Han, H., 2020. Salmonella Virulence and Immune Escape. Microorganisms 8, 407. https://doi.org/10.3390/microorganisms8030407
Weiss, G., Schaible, U.E., 2015. Macrophage defense mechanisms against intracellular bacteria. Immunol. Rev. 264, 182–203. https://doi.org/10.1111/imr.12266
Welin, A., Eklund, D., Stendahl, O., Lerm, M., 2011. Human Macrophages Infected with a High Burden of ESAT-6-Expressing M. tuberculosis Undergo Caspase-1- and Cathepsin B-Independent Necrosis. PLOS ONE 6, e20302. https://doi.org/10.1371/journal.pone.0020302
Welin, A., Lerm, M., 2012. Inside or outside the phagosome? The controversy of the intracellular localization of Mycobacterium tuberculosis. Tuberc. Edinb. Scotl. 92, 113–120. https://doi.org/10.1016/j.tube.2011.09.009
Westman, J., Grinstein, S., 2021. Determinants of Phagosomal pH During Host-Pathogen Interactions. Front. Cell Dev. Biol. 8, 1781. https://doi.org/10.3389/fcell.2020.624958
Wilburn, K.M., Fieweger, R.A., VanderVen, B.C., 2018. Cholesterol and fatty acids grease the wheels of Mycobacterium tuberculosis pathogenesis. Pathog. Dis. 76. https://doi.org/10.1093/femspd/fty021
Williams, M.J., Kana, B.D., Mizrahi, V., 2011. Functional analysis of molybdopterin biosynthesis in mycobacteria identifies a fused molybdopterin synthase in Mycobacterium tuberculosis. J. Bacteriol. 193, 98–106. https://doi.org/10.1128/JB.00774-10
Wipperman, M.F., Sampson, N.S., Thomas, S., T., 2014. Pathogen 'Roid Rage: Cholesterol Utilization by Mycobacterium tuberculosis. Crit. Rev. Biochem. Mol. Biol. 49, 269–293. https://doi.org/10.3109/10409238.2014.895700
Wong, K.-W., Jacobs, W.R., 2011. Critical role for NLRP3 in necrotic death triggered by Mycobacterium tuberculosis. Cell. Microbiol. 13, 1371–1384. https://doi.org/10.1111/j.1462-5822.2011.01625.x
Wu, K., Dong, D., Fang, H., Levillain, F., Jin, W., Mei, J., Gicquel, B., Du, Y., Wang, K., Gao, Q., Neyrolles, O., Zhang, J., 2012. An interferon-related signature in the transcriptional core response of human macrophages to Mycobacterium tuberculosis infection. PloS One 7, e38367. https://doi.org/10.1371/journal.pone.0038367
Wu, Z., Irizarry, R.A., Gentleman, R., Martinez-Murillo, F., Spencer, F., 2004. A Model-Based Background Adjustment for Oligonucleotide Expression Arrays. J. Am. Stat. Assoc. 99, 909–917. https://doi.org/10.1198/016214504000000683
Xu, Y., Xie, J., Li, Y., Yue, J., Chen, J., Chunyu, L., Wang, H., 2003. Using a cDNA microarray to study cellular gene expression altered by Mycobacterium tuberculosis. Chin. Med. J. (Engl.) 116, 1070–1073.
Yang, D., Fu, X., He, S., Ning, X., Ling, M., 2017. Analysis of Differentially Expressed Proteins in Mycobacterium avium-Infected Macrophages Comparing with Mycobacterium tuberculosis-Infected Macrophages. BioMed Res. Int. 2017. https://doi.org/10.1155/2017/5103803
Yimer, S.A., Birhanu, A.G., Kalayou, S., Riaz, T., Zegeye, E.D., Beyene, G.T., Holm-Hansen, C., Norheim, G., Abebe, M., Aseffa, A., Tønjum, T., 2017. Comparative Proteomic Analysis of Mycobacterium tuberculosis Lineage 7 and Lineage 4 Strains Reveals

Differentially Abundant Proteins Linked to Slow Growth and Virulence. Front. Microbiol. 8. https://doi.org/10.3389/fmicb.2017.00795

Yuan, Y., Crane, D.D., Simpson, R.M., Zhu, Y.Q., Hickey, M.J., Sherman, D.R., Barry, C.E., 1998. The 16-kDa alpha-crystallin (Acr) protein of Mycobacterium tuberculosis is required for growth in macrophages. Proc. Natl. Acad. Sci. U. S. A. 95, 9578–9583.

Zhang, J., 2013. Transcriptome Analysis Reveals Novel Entry Mechanisms and a Central Role of SRC in Host Defense during High Multiplicity Mycobacterial Infection. PloS One 8, e65128. https://doi.org/10.1371/journal.pone.0065128

Zhao, K., Ridgway, N.D., 2017. Oxysterol-Binding Protein-Related Protein 1L Regulates Cholesterol Egress from the Endo-Lysosomal System. Cell Rep. 19, 1807–1818. https://doi.org/10.1016/j.celrep.2017.05.028

Ziegenhain, C., Vieth, B., Parekh, S., Reinius, B., Guillaumet-Adkins, A., Smets, M., Leonhardt, H., Heyn, H., Hellmann, I., Enard, W., 2017. Comparative Analysis of Single-Cell RNA Sequencing Methods. Mol. Cell 65, 631-643.e4. https://doi.org/10.1016/j.molcel.2017.01.023